



The University of
Nottingham

UNITED KINGDOM • CHINA • MALAYSIA

Department of Chemical and Environmental Engineering

**Direct Online Monitoring and Control
of Chemical Reactions using Dielectric Spectroscopy**

Alexis Kalamiotis

Thesis submitted to the University of Nottingham
for the degree of Doctor of Philosophy.

April 2020

ABSTRACT

Over the last decades, the increasing demand for both the production of biobased products and the need for more sustainable material synthesis processes led to the development of novel techniques such as the Nitroxide Mediated Polymerization (NMP), Catalytic Chain Transfer Polymerisation (CCTP), and Ring-Opening Polymerisation (ROP). However, the commercial development of those techniques has been limited, with a key issue being the need to determine how far a particular reaction has progressed in order to continue to the next stage of the process (e.g., addition of other reactants) or terminate the reaction when the target conversion has been reached. Dielectric spectroscopy has been considered a promising technique for ‘in-situ’ monitoring since it is a non-invasive technique which can be applied to most industrial reactors.

The aims of this research were to investigate the use of dielectric spectroscopy for the ‘in-situ’ monitoring of chemical reactions at microwave frequencies and relate the dielectric properties with key reaction features such as the molecular weight and the level of conversion that has been achieved.

The thesis presents a detailed study of the tin octanoate mediated ROP of ϵ -caprolactone, and the para toluene sulfonic acid catalysed hydrolysis of sorbitol to sorbitan and isosorbide. Additionally, dielectric spectroscopy was utilised to differentiate the polymer architecture and molecular weight of Styrene–divinylbenzene copolymers synthesised by CCTP and NMP.

An open-ended coaxial line sensor was placed directly into the reaction medium and used to measure the dielectric properties of the mixture both “in-situ” and

with time. A swept signal (0.5 GHz–20 GHz) was then transmitted from a Vector Network Analyser (VNA), through the open-ended coaxial line, into the sample. Depending on the complex permittivity of the sample, a portion of that signal was reflected to the VNA and the reflection coefficient of the sample was used to calculate the complex permittivity. In addition to the measurements obtained by the sensor, samples of the medium were extracted at various time points for off-line analysis, using Gel Permeation Chromatography and Nuclear Magnetic Resonance spectroscopy to confirm key reaction features, e.g., molecular weight and the level of conversion that had been achieved.

The results demonstrated that in case of ϵ -caprolactone polymerisation and sorbitol dehydration the dielectric property values exhibited by the reaction medium could be correlated to both the progress of the reaction and the structure of the final product. Thus, the experimental data allowed the construction of a calibration curve which could be used to predict the level of conversion that has been achieved. The use of dielectric data also permitted the identification of key reaction parameters, such as the optimum point of termination for the reaction. Furthermore, the analysis of the dielectric data over a wide frequency spectrum enabled the identification of the most suitable frequencies for the practical operation of the sensor, in terms of linearity and sensitivity.

This study has demonstrated a method to determine the product properties or conversion during the reaction progress based on the real-time measurement of the dielectric properties during the ϵ -caprolactone polymerisation and sorbitol dehydration. This work provides a basis for developing process control strategies based on observing the change in the dielectric properties which can be applied to commercial manufacturing. The proposed method could improve product

quality (e.g., by terminating the reaction when the target conversion has been reached batch to batch repeatability can be improved) and reduce the production cost of materials, e.g., by optimising the amount of time that the reaction is kept at the required temperature, energy usage and waste generation can be minimised).

ACKNOWLEDGEMENTS

Firstly, I would like to thank my supervisors Dr. Georgios Dimitrakis and Professor Derek Irvine for their continuous support, patience and motivation through my research work and writing up periods. I would also like to thank the Faculty of Engineering for their funding support.

In addition, I would like to thank Dr. Chris Dodds and all the members of the former Microwave Process Engineering research group for all their help and support during my PhD research.

Special thanks to my family for the love, support, and encouragement during all these years of my study. Finally, I would like to thank all my friends in Nottingham who have been very supportive and made my time enjoyable.

PUBLICATIONS

Kalamiotis, A., Ilchev, A., Irvine, D. J. and Dimitrakis, G. (2019) Optimised use of dielectric spectroscopy at microwave frequencies for direct online monitoring of polymerisation reactions. *Sensors and Actuators B: Chemical* 290: pp.34–40.

Cot, S., Leu, M. K., **Kalamiotis, A.**, Dimitrakis, G., Sans, V., de Pedro, I. and Cano, I. (2019) An Oxalate-Bridged Binuclear Iron(III) Ionic Liquid for the Highly Efficient Glycolysis of Polyethylene Terephthalate under Microwave Irradiation. *ChemPlusChem* 84(7): pp.786–793.

Toolan, D. T. W., Adlington, K., Isakova, A., **Kalamiotis, A.**, Mokarian-Tabari, P., Dimitrakis, G., Dodds, C., Arnold, T., Terrill, N. J., Bras, W., Merino, D. H., Topham, P. D., Irvine, D. J. and Howse, J. R. (2017) Selective molecular annealing: in situ small angle X-ray scattering study of microwave-assisted annealing of block copolymers. *Physical Chemistry Chemical Physics* 19(31): pp.20412–20419.

CONFERENCES

Kalamiotis, A. N., Ilchev, A. A., Irvine, D. J. and Dimitrakis, G. A. (2018) Direct Online Monitoring of ϵ -caprolactone Polymerisation via Dielectric Property Measurement. *Proceedings IMCS 2018*: pp.763–764. Poster presentation at the 17th International Meeting on Chemical Sensors - IMCS 2018, Vienna, Austria.

TABLE OF CONTENTS

ABSTRACT	i
ACKNOWLEDGEMENTS	iv
PUBLICATIONS	v
TABLE OF CONTENTS	vi
LIST OF FIGURES	xi
LIST OF TABLES.....	xviii
ABBREVIATIONS AND SYMBOLS	xix
1 INTRODUCTION	1
References.....	5
2 REACTION MONITORING TECHNIQUES	8
2.1 Introduction.....	8
2.2 Ultraviolet-Visible Spectroscopy.....	9
2.3 Infrared Spectroscopy	13
2.3.1 Fourier Transform Infrared Spectroscopy	13
2.3.2 Near Infrared Spectroscopy	18
2.4 Raman Spectroscopy	22
2.5 Nuclear Magnetic Resonance Spectroscopy.....	27
2.6 Differential Scanning Calorimetry	31
2.7 Mass Spectrometry	35
2.8 Dielectric Spectroscopy	40
2.9 Comparison of reaction monitoring techniques.....	45
2.10 Conceptual framework and research hypothesis	62
2.11 Aims and objectives.....	62
2.12 Research methodology.....	63
2.13 Conclusions	63
References.....	65

3	DIELECTRIC THEORY.....	74
3.1	Introduction.....	74
3.2	Interaction between microwave radiation and matter.....	74
3.3	Fundamentals of Dielectric Theory.....	75
3.3.1	Polarisation mechanisms.....	76
3.3.2	Dielectric properties.....	78
3.3.3	Factors affecting the permittivity.....	80
3.4	Static Permittivity Theories.....	82
3.4.1	Debye's theory.....	82
3.4.2	Onsager's theory.....	82
3.4.3	Kirkwood's theory.....	83
3.4.4	Fröhlich's theory.....	84
3.5	Complex permittivity models.....	84
3.5.1	Debye Model.....	85
3.5.2	Cole-Cole Model.....	86
3.5.3	Cole-Davidson Model.....	87
3.5.4	Havriliak-Negami Model.....	88
3.6	Relaxation frequency and time.....	89
3.7	Dielectric mixture equations.....	91
3.8	Conclusions.....	94
	References.....	95
4	EXPERIMENTAL METHODS.....	97
4.1	Introduction.....	97
4.2	Dielectric property measurements.....	97
4.2.1	Open-ended coaxial line technique.....	98
4.2.2	Cavity Perturbation Technique.....	103
4.3	Nuclear Magnetic Resonance spectroscopy.....	105
4.4	Gel Permeation Chromatography.....	109
4.5	Conclusions.....	112
	References.....	113

5 ONLINE MONITORING OF THE ϵ-CAPROLACTONE POLYMERISATION	116
5.1 Introduction.....	116
5.2 Experimental.....	120
5.2.1 Materials.....	120
5.2.2 Ring Opening Polymerisation Procedure.....	121
5.2.3 Online Dielectric property measurement.....	123
5.2.4 Offline molecular analysis.....	123
5.2.5 Accuracy of Dielectric property measurements.....	125
5.3 Dielectric properties of ϵ -caprolactone monomer.....	126
5.3.1 Frequency dependence of ϵ -caprolactone monomer dielectric properties.....	126
5.3.2 Temperature dependence of ϵ -caprolactone monomer dielectric properties.....	128
5.4 Dielectric relaxation analysis of ϵ -caprolactone monomer.....	130
5.4.1 Relaxation frequency and time of ϵ -caprolactone.....	131
5.4.2 Debye permittivity model of ϵ -caprolactone.....	134
5.4.3 Cole-Cole permittivity model of ϵ -caprolactone.....	137
5.4.4 Cole-Davidson permittivity model of ϵ -caprolactone.....	139
5.5 Real time monitoring of the ϵ -caprolactone polymerisation using the dielectric properties.....	141
5.5.1 Dielectric properties of individual precursors and reaction mixtures.....	142
5.5.2 Relationship between the Dielectric Properties and Monomer to Polymer Conversion.....	144
5.5.3 Frequency dependence of Dielectric properties during polymerisation.....	147
5.5.4 Construction of a calibration curve for following the ϵ -caprolactone polymerisation.....	149
5.5.5 Effect of magnetic stirring compared to mechanical stirring ...	151
5.6 Conclusions.....	152
References.....	154

6	MONITORING OF THE CHEMICAL TRANSFORMATIONS OF SUGARS	157
6.1	Introduction.....	157
6.2	Experimental	159
6.2.1	Materials	160
6.2.2	Dielectric property measurement.....	160
6.2.3	Off-line molecular analysis	162
6.3	Dielectric property analysis of sugars.....	162
6.3.1	Temperature dependence of dielectric properties.....	163
6.3.2	Frequency dependence of dielectric properties	165
6.4	Dehydration of Sorbitol	166
6.4.1	Synthesis of 1,4-sorbitan and isosorbide from D-sorbitol.....	167
6.4.2	Frequency dependence of dielectric properties during the dehydration reaction	169
6.4.3	Relationship between the dielectric properties and isosorbide composition.....	173
6.5	Conclusions.....	177
	References.....	178
7	HYPERBRANCHED POLYMERS.....	180
7.1	Introduction.....	180
7.2	Experimental	182
7.2.1	Materials	182
7.2.2	Dielectric property measurement.....	182
7.2.3	Gel Permeation Chromatography	183
7.3	Free radical polymerisation of Styrene–divinylbenzene copolymers.....	184
7.3.1	Catalytic Chain Transfer Polymerisation	188
7.3.2	Nitroxide Mediated Polymerisation.....	189
7.4	Dielectric property assessment of styrene-co-divinylbenzene copolymers.....	191
7.4.1	Temperature dependence of dielectric properties.....	191

7.4.2	Relationship between dielectric properties and hyperbranched polymer structure	193
7.4.3	Relationship between polymer molecular weight and dielectric properties	198
7.5	Conclusions.....	200
	References.....	201
8	CONCLUSIONS AND FUTURE WORK.....	205
8.1	ϵ -caprolactone polymerisation	206
8.2	Dehydration of sorbitol to isosorbide	207
8.3	Synthesis of DVB-co-styrene hyperbranched polymers.....	208
8.4	Limitations of the application of dielectric spectroscopy to the monitoring of chemical transformations.....	209
8.5	Future work.....	209

LIST OF FIGURES

Figure 2.1: Online UV spectra of the of the pinacol formation reaction of benzophenone in isopropanol (Lu, Schmidt and Jensen, 2001)	11
Figure 2.2: Raman spectra (and original reaction spectra in the mini graph) of laccase-catalysed indigo carmine oxidation, as calculated with multivariate curve resolution (Kandelbauer, Kessler and Kessler, 2008).....	12
Figure 2.3: Typical structure of a Michelson interferometer (Tasumi, 2014)..	14
Figure 2.4: BA conversion (mol %) versus time (min) for BA solution homopolymerisation in toluene (Jovanovic and Dube, 2003).	15
Figure 2.5: Comparison of THF concentration determined by infrared and NMR versus time (Deng et al., 2014).....	17
Figure 2.6: NIR spectrometer configuration (Reich, 2005).....	18
Figure 2.7: Comparison of PLS and HPLC product concentration (Coffey, Cooley and Walker, 1999).....	20
Figure 2.8: Comparison of polystyrene weight fraction values calculated by NIR spectroscopy and gravimetry (Fontoura et al., 2003).	21
Figure 2.9: Raman estimations of conversion of four reactions with a smoothing-spline filter: (o) reaction R1; (□) reaction R2; (▲) reaction R3; (●) reaction R4 (Santos et al., 2004).	24
Figure 2.10: Monitoring of product conversion of salicylaldehyde and ethyl acetoacetate to 3-acetylcoumarin in a variety of reaction conditions (Hamlin and Leadbeater, 2013).	25
Figure 2.11: Raman spectra of the hydrolysis of 50% (w/w) acetonitrile in water at 300 °C and 500 bar (Venardou et al., 2004).	26
Figure 2.12: Conversion (%) of the cycloaddition reaction product as a function of reaction time for various temperatures (Gomez et al., 2010).	29

Figure 2.13: Reaction profile analysis of starting material (TAG), formation of product (FAME) and intermediates (DAGs) (Anderson and Franz, 2012).	30
Figure 2.14: Conversion and normalized fluorescence intensity versus polymerization time for various temperatures (Serrano et al., 1997).	32
Figure 2.15: (a) Isothermal DSC and (b) conversion curves as a function of time, during the vulcanization of elastomeric matrix (Vasilakos and Tarantili, 2017).	34
Figure 2.16: Mass spectra of the polymerisation of nanofilm products (NFP-1) on glass: (a) 1 min, and (b) 15 min after spraying on a glass surface (Nørgaard et al., 2010).	38
Figure 2.17: Mass spectra (A) and real time molar concentration changes and (B) of Michael addition reaction of Phenethylamine (Zhu et al., 2012).	39
Figure 2.18: Dielectric constant (ϵ') at 2450 MHz and number average molecular weight (M_n) over time for ring-opening polymerisation (Kamaruddin et al., 2014a).	42
Figure 2.19: (A): Conductance (G, Siemens) versus time and (B): Capacitance (B/ω) versus time during isothermal curing of neat cyanate ester (Pissis et al., 2015).	44
Figure 3.1: Electromagnetic wave propagation through a surface S (Muhibullah, Haleem and Ikuma, 2017).	75
Figure 3.2: Electric dipole moment	76
Figure 3.3: Polarisation types of normal dielectric materials under an external electric field (Guo et al., 2016).	78
Figure 3.4: Cole-Cole plot for an ideal and non-ideal Debye response (dashed and solid lines respectively) (Metaxas and Meredith, 1905).	86
Figure 3.5: : Cole-Cole plot of glycerine at -50°C (Davidson and Cole, 1950).	88
Figure 3.6: Cole-Cole plot of a pure polar material (solid line), and non-ideal Debye material (dashed line).	90

Figure 4.1: Schematic diagram of a coaxial probe (Gregory and Clarke, 2006).	99
Figure 4.2: Experimental setup and apparatus, b) Schematic diagram of experimental set up.....	100
Figure 4.3: Cavity apparatus.....	105
Figure 4.4: Energy levels of spin $\frac{1}{2}$ nucleus (Richards and Hollerton, 2010).	106
Figure 4.5: ^1H NMR spectrum of Sorbitol measured in Dimethyl sulfoxide.	108
Figure 4.6: Schematic representation of size separation and concentration elution curve versus retention time (Striegel et al., 2009).....	110
Figure 5.1: $\text{Sn}(\text{Oct})_2$ catalysed coordination-insertion ROP mechanism of CL (Raquez, Narayan and Dubois, 2008).....	122
Figure 5.2: : Comparison between measured and literature dielectric data (Kamaruddin, 2012) of ϵ -caprolactone at 30 °C.....	125
Figure 5.3: Dielectric constant versus frequency (GHz) of ϵ -caprolactone at 20 °C. Due to the small deviation, the error bars are indistinguishable. The maximum standard deviation of the measured data is: $[\epsilon' \pm 0.02]$	127
Figure 5.4: Dielectric loss and $\tan \delta$ versus frequency (GHz) of ϵ -caprolactone at 20 °C. The maximum standard deviation of the measured data is: $[\epsilon'' \pm 0.04]$; $[\tan\delta \pm 0.03]$	128
Figure 5.5: Dielectric constant versus frequency (GHz) for temperature 20 °C, 50 °C, 100 °C, 140 °C and 170 °C. The maximum standard deviations of the measured data are: 20 °C $[\epsilon' \pm 0.02]$; 50 °C: $[\epsilon' \pm 0.03]$; 100 °C: $[\epsilon' \pm 0.03]$; 140 °C: $[\epsilon' \pm 0.002]$; 170 °C: $[\epsilon' \pm 0.003]$	129
Figure 5.6: Dielectric loss versus frequency (GHz) at 20 °C, 50 °C, 100 °C, 140 °C and 170 °C. The maximum standard deviations of the measured data are: 20 °C $[\epsilon'' \pm 0.04]$; 50 °C: $[\epsilon'' \pm 0.2]$; 100 °C: $[\epsilon'' \pm 0.3]$; 140 °C: $[\epsilon'' \pm 0.2]$; 170 °C: $[\epsilon'' \pm 0.1]$	130

Figure 5.7: Dielectric loss versus frequency (GHz) of ϵ -caprolactone monomer at selected temperatures. The maximum standard deviations of the measured data are: 20 °C [$\epsilon'' \pm 0.04$]; 50 °C: [$\epsilon'' \pm 0.2$]; 80 °C: [$\epsilon'' \pm 0.3$]; 110 °C: [$\epsilon'' \pm 0.1$]; 140 °C: [$\epsilon'' \pm 0.2$]; 170 °C: [$\epsilon'' \pm 0.1$]. 132

Figure 5.8: Cole-Cole plot of ϵ -caprolactone at selected temperatures..... 133

Figure 5.9: Dielectric constant and loss versus log frequency of ϵ -caprolactone at 20 °C. The data points correspond to the measured data and the lines to the fitted Debye model. 136

Figure 5.10: Dielectric constant and loss versus log frequency of ϵ -caprolactone at 160 °C. The blue and green data points correspond to the measured data and the dashed lines to the fitted Debye model..... 136

Figure 5.11: Dielectric constant and loss versus log frequency of ϵ -caprolactone at 20 °C. The blue and green data points correspond to the measured data and the dashed lines to the fitted Cole-Cole model..... 138

Figure 5.12: Dielectric constant and loss versus log frequency of ϵ -caprolactone at 160 °C. The blue and green data points correspond to the measured data and the dashed lines to the fitted Cole-Cole model..... 138

Figure 5.13: Dielectric constant and loss versus log frequency of ϵ -caprolactone at 20 °C. The blue and green data points correspond to the measured data and the dashed lines to the fitted Cole-Davidson model. 140

Figure 5.14: Dielectric constant and loss versus log frequency of ϵ -caprolactone at 160 °C. The data points correspond to the measured data and the lines to the fitted Cole-Davidson model..... 141

Figure 5.15: Plot of the dielectric constant versus frequency (GHz) of ϵ -caprolactone monomer and polymer mixtures at 160 °C. The maximum standard deviations of the measured data are: ϵ -caprolactone monomer: [$\epsilon' \pm 0.3$]; 32% PCL: [$\epsilon' \pm 0.4$]; 99% PCL: [$\epsilon' \pm 0.3$]. 143

Figure 5.16: Plot of dielectric loss versus frequency (GHz) of ϵ -caprolactone monomer and polymer mixtures at 160 °C. The maximum standard deviations

of the measured data are: ϵ -caprolactone monomer: [$\epsilon'' \pm 0.2$]; 32% PCL: [$\epsilon'' \pm 0.2$]; 99% PCL: [$\epsilon'' \pm 0.1$].	144
Figure 5.17: Comparison plot of ϵ' (at 0.95 GHz) and M_n versus reaction time.	145
Figure 5.18: Dielectric constant versus time during the polymerisation of ϵ -caprolactone at 160 °C. The maximum standard deviations of the measured data are: 0 min: [$\epsilon' \pm 0.5$]; 2 min. [$\epsilon' \pm 0.6$]; 4 min. [$\epsilon' \pm 0.5$]; 6 min. [$\epsilon' \pm 0.4$]; 10 min: [$\epsilon' \pm 0.3$]; 15 min: [$\epsilon \pm 0.2$].	148
Figure 5.19: Dielectric loss versus time during the polymerisation of ϵ -caprolactone at 160 °C. The maximum standard deviations of the measured data are: 0 min: [$\epsilon'' \pm 0.2$]; 2 min. [$\epsilon'' \pm 0.2$]; 4 min. [$\epsilon'' \pm 0.2$]; 6 min. [$\epsilon'' \pm 0.2$]; 10 min: [$\epsilon'' \pm 0.1$]; 15 min: [$\epsilon'' \pm 0.1$].	148
Figure 6.1: Dielectric constant versus temperature at 2470 MHz.	163
Figure 6.2: Dielectric loss versus temperature at 2470 MHz.	164
Figure 6.3: Dielectric constant and loss of sorbitol versus frequency at 110 °C. Due to the small deviation, the error bars are indistinguishable. The maximum standard deviations of the measured data are: [$\epsilon' \pm 0.2$]; [$\epsilon'' \pm 0.4$].	165
Figure 6.4: Dielectric constant and loss of isosorbide versus frequency at 110 °C. The maximum standard deviations of the measured data are: [$\epsilon' \pm 0.1$]; [$\epsilon'' \pm 0.1$].	166
Figure 6.5: Mono- and double-dehydration products of sorbitol catalysed by pTSA.	168
Figure 6.6: Dielectric constant versus frequency (GHz). The maximum standard deviations of the measured data are: 20 min: [$\epsilon' \pm 0.2$]; 60 min: [$\epsilon' \pm 0.4$]; 100 min: [$\epsilon' \pm 0.4$]; 140 min: [$\epsilon' \pm 0.3$]; 180 min: [$\epsilon' \pm 0.2$].	170
Figure 6.7: Dielectric loss versus frequency (GHz). The maximum standard deviations of the measured data are: 20 min: [$\epsilon'' \pm 0.2$]; 60 min: [$\epsilon'' \pm 0.4$]; 100 min: [$\epsilon'' \pm 0.4$]; 140 min: [$\epsilon'' \pm 0.3$]; 180 min: [$\epsilon'' \pm 0.2$].	171

Figure 6.8: Dielectric constant (ϵ') versus frequency (GHz). The maximum standard deviations of the measured data are: 5 mol%: [$\epsilon' \pm 0.2$]; 10 mol%: [$\epsilon' \pm 0.3$]; 23 mol%: [$\epsilon' \pm 0.4$]; 40 mol%: [$\epsilon' \pm 0.4$]; 57 mol%: [$\epsilon' \pm 0.3$]; 100 mol%: [$\epsilon' \pm 0.1$].	172
Figure 6.9: Dielectric loss (ϵ'') versus frequency (GHz). The maximum standard deviations of the measured data are: 5 mol%: [$\epsilon'' \pm 0.2$]; 10 mol%: [$\epsilon'' \pm 0.4$]; 23 mol%: [$\epsilon'' \pm 0.4$]; 40 mol%: [$\epsilon'' \pm 0.3$]; 57 mol%: [$\epsilon'' \pm 0.2$]; 100 mol%: [$\epsilon'' \pm 0.1$].	173
Figure 6.10: Dielectric constant at 6 GHz and 19 GHz versus mol% Isosorbide composition.	175
Figure 6.11: Dielectric loss at 6 GHz and 19 GHz versus mol% Isosorbide composition.	175
Figure 7.1: Schematic representation of a linear polymer, dendrimer, and a hyperbranched polymer (Biron, 2013).	180
Figure 7.2: Mayo and Flory theory of the self-initiation of styrene (Khuong et al., 2005).	186
Figure 7.3: Controlled/living radical polymerisation mechanism (Nicolas et al., 2013).	190
Figure 7.4: Dielectric constant versus temperature at 2470 MHz of DVB:PS powder samples with variable DVB ratio.	192
Figure 7.5: Dielectric loss versus temperature at 2470 MHz of DVB:PS powder samples with variable DVB ratio.	192
Figure 7.6: Dielectric constant at 2.47 GHz versus DVB concentration at 150 °C.	194
Figure 7.7: Dielectric loss at 2.47 GHz versus DVB concentration at 150 °C.	194
Figure 7.8: Dielectric constant versus frequency of DVB:PS polymers with varied (%) DVB ratio, dissolved in cyclohexanone and measured at room temperature.	196

Figure 7.9: Dielectric loss versus frequency of DVB:PS samples with varied (%) DVB ratio, dissolved in cyclohexanone and measured at room temperature. 197

Figure 7.10: Dielectric constant versus frequency (MHz) for cyclohexanone, low and high molecular weight sample. 199

Figure 7.11: Dielectric loss versus frequency (MHz) for cyclohexanone, low and high molecular weight sample. 199

LIST OF TABLES

Table 2.1: Comparison of monitoring techniques.	49
Table 3.1: Complex permittivity of solid materials based on mixing formulas	93
Table 5.1: Temperature, static and infinite permittivity, relaxation frequency and time of ϵ -caprolactone at temperatures from 20 °C to 170 °C.	134
Table 5.2: Experimental conditions, theoretical and observed Mn and Dispersity values for the bulk polymerisation of ϵ -caprolactone using benzyl alcohol and tin octanoate at 160 °C.....	146
Table 6.1: Results of sorbitol dehydration in bulk, catalysed by 15 mol% pTSA at 110 °C.	169
Table 7.1: Styrene–divinylbenzene copolymers synthesis reaction conditions.....	189
Table 7.2: Styrene–divinylbenzene copolymers synthesis reaction conditions. *Sample no.2 gelled before gelation.	190

ABBREVIATIONS AND SYMBOLS

B	Magnetic field
C_f	Fringing capacitance inside the coaxial line
C_0	Fringing capacitance outside the probe (air part of the sensor)
<i>CCTP</i>	Catalytic Chain Transfer Polymerisation
$^{\circ}\text{C}$	Degree Celsius
D	Debye
<i>DSC</i>	Differential Scanning Calorimetry
<i>DS</i>	Dielectric Spectroscopy
<i>DVB</i>	Divinyl Benzene
E	Electric field
f	Frequency
f_c	Relaxation frequency
<i>FRP</i>	Free Radical Polymerisation
<i>FTIR</i>	Fourier Transform Infrared Spectroscopy
g	Correlation factor
<i>GPC</i>	Gel Permeation Chromatography
H	Magnetic field intensity
J	Current density
k	Boltzmann's constant
M_n	Number average molecular weight
M_w	Weight average molecular weight

MS	Mass Spectrometry
N	Avogadro's constant
n	Refractive index
NMR	Nuclear Magnetic Resonance Spectroscopy
NIR	Near Infrared Spectroscopy
Q	Quality factor
SEC	Size Exclusion Chromatography
T	Temperature
$\tan \delta$	Dissipation factor
a	Polarisability
∇	Del or nabla operator
ϵ^*	Complex permittivity
ϵ'	Dielectric constant
ϵ''	Dielectric loss
ϵ_s	Static permittivity
ϵ_∞	Infinite permittivity
μ	Dipole moment
σ	Conductivity
τ	Relaxation time
ω	Angular frequency

1 INTRODUCTION

Over the last few decades, there has been an ever increasing need to develop controlled and energy efficient chemical production techniques which allow much greater control over the final product structure to be achieved. These include the Ring-Opening Polymerisation (ROP) (Deng *et al.*, 2014a), Nitroxide Mediated Polymerization (NMP) (Hawker, Bosman and Harth, 2001), Atom Transfer Radical Polymerization (ATRP) (Matyjaszewski and Xia, 2001), and Catalytic Chain Transfer Polymerisation (CCTP) (Gridnev and Ittel, 2001). These techniques allow the synthesis of complex three-dimensional structures such as block, star (Deng *et al.*, 2013), branched and hyperbranched polymers to be achieved *via* multi-stage processes, that often require sequential addition of different monomer types (Wang *et al.*, 2007; Koh, Konkolewicz and Perrier, 2011). Additionally, the use of non-petrochemically derived starting materials, such as sugar-based bioproducts, have been reported for the production of sustainably sourced high-performance biopolymers (Aricò and Tundo, 2016). However, the commercial development of these materials has been limited by a number of practical factors, with a key issue being the need to determine how far a particular reaction has progressed in order to continue to the next stage of the process (e.g., addition of other reactants) or terminate the reaction when the target conversion has been reached (Zheng *et al.*, 2015). Additionally, the lack of real time feedback on batch processes can lead to batch to batch variability in industrial-scale production (Destarac, 2010).

To date, molecular analysis is mostly performed using off-line techniques such as Gel Permeation Chromatography (GPC) and Nuclear Magnetic Resonance

(NMR) spectroscopy. These techniques require sample extraction and preparation, thus normally cannot be easily adapted to perform measurements on-line within the process and in real time. Thus, there is a growing interest to develop a direct online method for real-time monitoring of reaction progress as well as measuring product properties, which can be easily incorporated in most industrial polymerisation reactor geometries.

Process Analytical Chemistry (PAC) is a subdiscipline of Analytical Chemistry aimed at monitoring and control of industrial chemical processes (Riebe and Eustace, 1990; McLennan and Kowalski, 1995). PAC techniques can be classified as off-line, at-line and on-line according to the type / level of sample extraction and preparation that is required (McLennan and Kowalski, 1995). Off-line and at-line analysis techniques, such as NMR and GPC, require sample extraction and transportation to a separate laboratory. By comparison, on-line analysis techniques, such as the Automated Continuous Online Monitoring of Polymerization Reactions (ACOMP), are performed within the process line and involve, at most, automated sampling and transport to an integrated analyser (Hassell and Bow, 1998; Alb, Drenski and Reed, 2007). Thus, they can deliver far more relevant information that enables greater control to be exercised over the process they are monitoring. During the last few decades, many off-line techniques, such as infrared and Raman spectroscopy, have been transformed into online in order to try and control chemical processes (Hergeth, 2000). However, when applying vibrational spectroscopic techniques, these efforts at industrial monitoring are met with limited success, with high background noise in the measurement and blackbody radiation and fluorescence in raman spectra being the most common issues (Lewis and Edwards, 2001; Bakeev, 2010).

Dielectric spectroscopy (DS) is a technique that involves the study of the response of a material to an external electric field. It is a non-destructive, non-intrusive technique that is used to measure the dielectric properties of materials, which consist of the dielectric constant (ϵ') and the dielectric loss (ϵ''), with temperature or frequency. Dielectric constant expresses the ability of the material to store energy by the motion of charged particles or by the realignment of polar groups within the molecules. The loss denotes the ability of the material to dissipate the stored energy into heat (Metaxas and Meredith, 1905). DS is a well-established technique with many applications in physics, chemistry, materials science and pharmacy such as the understanding of the effect of microwave heating (Durán-Jiménez et al., 2019), the investigation of polymer dynamics in nanocomposites (Malas, 2017), the non-destructive evaluation of composites (Pethrick, 2013), and the analysis of pharmaceutical systems (Craig, 1992). The application of dielectric spectroscopy in process monitoring provides a link between molecular spectroscopy, which monitors the properties of individual components, and techniques characterising the bulk properties of materials, such as viscosity. In particular, dielectric analysis provides a sensitive method to identify local motions along the chains of polar polymers, as polar bonds are affected by the electric stimulus (Menczel and Prime, 2009). Recently, the use of dielectric spectroscopy was reported as a technique for monitoring the progress of chemical reactions. Santos *et al.* (2001) used dielectric analysis for the in-line monitoring of monomer and overall conversion during methyl methacrylate/butyl acrylate (MMA/BuA) solution copolymerisations. Pissis *et al.* (2015) reported the use of broadband Dielectric Spectroscopy and electrical dc measurements in following the polymerisation and curing processes in

polymer/clay nanocomposites. Kamaruddin *et al.* (2011, 2014a) reported the use of dielectric property measurement as a technique for the “in situ” monitoring of the ϵ -caprolactone polymerisation. These studies showed that it would be possible to accurately follow the conversion of monomer to polymer by measuring the dielectric properties of the samples. However, the measurements were performed over a very limited frequency range and mainly on pre-prepared monomer to polymer concentrations. Therefore, they did not provide information to monitor, in real time, the progress of the polymerisation. Additionally, they did not consider investigating the optimum frequencies for the practical operation of the sensor, in terms of linearity and sensitivity, to enable the design and operation of dedicated sensors that can be employed as a part of a process control strategy. A detailed study of the factors that affect complex permittivity, especially the temperature and frequency is required for developing a device suitable for use in manufacturing processes. The aim of this work is to develop novel methods to follow the progress of chemical reactions using dielectric spectroscopy as the key monitoring technique. In detail, the tin octanoate mediated ROP of ϵ -caprolactone, and the para toluene sulfonic acid catalysed hydrolysis of sorbitol to sorbitan and isosorbide were monitored using dielectric property measurements. For each reaction, the effect of temperature and frequency on the dielectric properties was studied and a calibration curve was used to relate the dielectric data with the level of conversion that had been achieved. The level of conversion was validated using off-line molecular analysis by Proton Nuclear Magnetic Resonance spectroscopy (^1H NMR) and Gel Permeation Chromatography (GPC). The proposed method can be applied to any process that exhibits detectable changes in the dielectric properties over

the progress of the reaction and can be used in monitoring of processes without the need of expert knowledge on dielectric theory.

The thesis is structured into eight chapters. The current introductory chapter (Chapter 1) is followed by Chapter 2, where a literature overview of the most known techniques for reaction monitoring is presented. Chapter 3 is dedicated on the fundamental aspects of dielectric theory. In Chapter 4, the dielectric property measurement techniques used in this project are discussed. In Chapter 5, the application of dielectric spectroscopy to monitor the progress of the tin octanoate mediated ring-opening polymerisation of ϵ -caprolactone (CL) over a broad frequency range (0.5 GHz – 20 GHz) is presented. In Chapter 6, an open-ended coaxial line sensor utilised to monitor the dehydration of sorbitol to isosorbide is presented. The use of dielectric spectroscopy in molecular analysis and structural differentiation of hyperbranched polymers is investigated in Chapter 7. The conclusions of this study are presented in Chapter 8, along with recommendations for future work.

References

Alb, A. M., Drenski, M. F. and Reed, W. F. (2007) Automatic continuous online monitoring of polymerization reactions (ACOMP). **Polymer International** 57(3): pp.390–396.

Aricò, F. and Tundo, P. (2016) Isosorbide and dimethyl carbonate: a green match. **Beilstein Journal of Organic Chemistry** 12(1): pp.2256–2266.

Bakeev, K. A. (2010) **Process Analytical Technology: Spectroscopic Tools and Implementation Strategies for the Chemical and Pharmaceutical Industries**. John Wiley & Sons.

Craig, D. Q. M. (1992) Applications of low frequency dielectric spectroscopy to the pharmaceutical sciences. **Drug Development and Industrial Pharmacy** 18(11–12): pp.1207–1223.

- Deng, H., Shen, Z., Li, L., Yin, H. and Chen, J. (2014) Real-time monitoring of ring-opening polymerization of tetrahydrofuran via in situ Fourier Transform Infrared Spectroscopy. **Journal of Applied Polymer Science** 131(15): pp.n/a-n/a.
- Deng, Y., Zhang, S., Lu, G. and Huang, X. (2013) Constructing well-defined star graft copolymers. **Polymer Chemistry** 4(5): pp.1289–1299.
- Destarac, M. (2010) Controlled Radical Polymerization: Industrial Stakes, Obstacles and Achievements. **Macromolecular Reaction Engineering** 4(3–4): pp.165–179.
- Durán-Jiménez, G., Hernández-Montoya, V., Rodríguez Oyarzun, J., Montes-Morán, M. Á. and Binner, E. (2019) Pb(II) removal using carbon adsorbents prepared by hybrid heating system: Understanding the microwave heating by dielectric characterization and numerical simulation. **Journal of Molecular Liquids** 277: pp.663–671.
- Gridnev, A. A. and Ittel, S. D. (2001) Catalytic chain transfer in free-radical polymerizations. **Chemical Reviews** 101(12): pp.3611–3660.
- Hassell, D. C. and Bow, E. M. (1998) Process Analytical Chemistry for Spectroscopists. **Applied Spectroscopy** 52(1): pp.18A-29A. Available at: <https://www.osapublishing.org/abstract.cfm?uri=as-52-1-18A> (Accessed: 3 October 2017).
- Hawker, C. J., Bosman, A. W. and Harth, E. (2001) New Polymer Synthesis by Nitroxide Mediated Living Radical Polymerizations. **Chemical Reviews** 101(12): pp.3661–3688.
- Hergeth, W.-D. (2000) On-Line Monitoring of Chemical Reactions. in **Ullmann's Encyclopedia of Industrial Chemistry**. Wiley-VCH Verlag GmbH & Co. KGaA.
- Kamaruddin, M. J., Harfi, J. E., Dimitrakis, G., Nguyen, N. T., Kingman, S. W., Lester, E., Robinson, J. P. and Irvine, D. J. (2011) Continuous direct on-line reaction monitoring of a controlled polymerisation via dielectric measurement. **Green Chemistry** 13(5): pp.1147–1151.
- Kamaruddin, M. J., Nguyen, N. T., Dimitrakis, G. A., Harfi, J. E., Binner, E. R., Kingman, S. W., Lester, E., Robinson, J. P. and Irvine, D. J. (2014) Continuous and direct 'in situ' reaction monitoring of chemical reactions via dielectric property measurement: controlled polymerisation. **RSC Advances** 4(11): pp.5709–5717.
- Koh, M. L., Konkolewicz, D. and Perrier, S. (2011) A Simple Route to Functional Highly Branched Structures: RAFT Homopolymerization of Divinylbenzene. **Macromolecules** 44(8): pp.2715–2724.
- Lewis, I. R. and Edwards, H. (2001) **Handbook of Raman Spectroscopy: From the Research Laboratory to the Process Line**. CRC Press.

Malas, A. (2017) 6 - Rubber nanocomposites with graphene as the nanofiller. in Thomas, S. and Maria, H. J. (eds) **Progress in Rubber Nanocomposites**. Woodhead Publishing (Woodhead Publishing Series in Composites Science and Engineering) pp.179–229.

Matyjaszewski, K. and Xia, J. (2001) Atom Transfer Radical Polymerization. **Chemical Reviews** 101(9): pp.2921–2990.

McLennan, F. and Kowalski, B. R. (1995) **Process Analytical Chemistry**. Springer Science & Business Media.

Menczel, J. D. and Prime, R. B. (eds) (2009) **Thermal Analysis of Polymers: Fundamentals and Applications**. Hoboken, N.J: Wiley-Blackwell.

Metaxas, A. C. and Meredith, R. J. (1995) **Industrial Microwave Heating**. London, UK: The Institution of Engineering and Technology.

Pethrick, R. A. (2013) 8 - Non-destructive evaluation (NDE) of composites: dielectric methods for testing adhesive bonds in composites. in Karbhari, V. M. (ed.) **Non-Destructive Evaluation (NDE) of Polymer Matrix Composites**. Woodhead Publishing (Woodhead Publishing Series in Composites Science and Engineering) pp.185–219.

Riebe, M. T. and Eustace, D. J. (1990) Process analytical chemistry. An industrial perspective. **Analytical Chemistry** 62(2): pp.65A-71A.

Wang, W., Zheng, Y., Roberts, E., Duxbury, C. J., Ding, L., Irvine, D. J. and Howdle, S. M. (2007) Controlling Chain Growth: A New Strategy to Hyperbranched Materials. **Macromolecules** 40(20): pp.7184–7194.

Zheng, Y., Li, S., Weng, Z. and Gao, C. (2015) Hyperbranched polymers: advances from synthesis to applications. **Chemical Society Reviews** 44(12): pp.4091–4130.

2 REACTION MONITORING TECHNIQUES

2.1 Introduction

The growing demand for better quality products with reduced production cost and waste generation led to the development of a subdiscipline of analytical chemistry for the monitoring and control of industrial chemical processes. Process Analytical Chemistry (PAC) was first applied in 1950s to analyse the physical and chemical properties of petrochemical products (Riebe and Eustace, 1990; McLennan and Kowalski, 1995). PAC techniques can be classified as off-line, at-line and on-line according to sample extraction and preparation. Off-line analysis requires sample extraction and transportation to a remote or centralized laboratory. At-line analysis requires sample extraction and transportation to a closely located laboratory. On-line analysis is performed in the process line with automated sampling and transport to the analyser. Some authors reported inline and non-invasive analysis to further distinguish the methods which do not require sampling and sample contact (Hassell and Bow, 1998).

During the last few decades, many off-line techniques have been transformed into online (Hergeth, 2000). For example, near infrared spectroscopy was used as an in situ spectroscopic technique to monitor chemical reactions (Coffey, Cooley and Walker, 1999), raman spectroscopy was used for the online monitoring of polymerisation reactions (Santos *et al.*, 2004), and Nuclear Magnetic Resonance spectroscopy was used for the on-line monitoring of microliter continuous-flow microwave assisted organic reactions (Gomez *et al.*, 2010). As a result, significant gains in product quality and batch to batch

repeatability have been achieved as well as reduced energy consumption and waste generation (Reed and Alb, 2013).

The aim of this chapter is to present the most known techniques for reaction monitoring including UV-visible spectroscopy, Infrared spectroscopy, Raman spectroscopy, Nuclear Magnetic Resonance spectroscopy (NMR), Mass Spectrometry (MS), Differential Scanning Calorimetry (DSC), and Dielectric Spectroscopy (DS). A detailed description of the most widespread techniques is presented, followed by a review of previous studies in monitoring of chemical reactions. Finally, a comparison of the techniques assesses the advantages and limitations of each method.

2.2 Ultraviolet-Visible Spectroscopy

The ultraviolet (UV) – visible region is divided into three regions: far ultraviolet (10-200 nm), near ultraviolet (200 – 380 nm) and visible (380 – 780 nm). When a sample is subjected to UV or visible radiation, it undergoes electronic transitions. The development of sensitive and affordable array detectors, high-quality UV-grade optical fibers and chemometrics over the past 20 years opened up a variety of applications for the use of UV-visible spectroscopy for online monitoring of chemical reactions (Liauw, Baylor and O'Rourke, 2010). The emergence of photodiode-array detectors and charge coupled device detectors offered improved sensitivity and measurement capability in the UV-visible spectrophotometers. Additionally, the emergence of high-quality UV-grade optical fibers led to the development of fiber-optic probes capable of in-situ sampling of a process. Finally, the development of chemometrics allows the

analysis of large spectral data quantities as well as the analysis of residuals, which can help when something unexpected occurs in a process (Bakeev, 2010).

Lu, Schmidt and Jensen (2001) reported the design and fabrication of microreactors and detectors for photochemical reactions using silicon and related microfabrication technologies. In detail, two sets of microchip devices were fabricated: the first for demonstrating the detection of the photoinitiation of benzophenone in isopropanol and the second for on-line detection for shorter wavelength reactions. The variation of flow rate was used to control the extent of reaction and the results obtained from the on-line UV spectroscopy were confirmed with off-line analysis using HPLC. Figure 2.1 shows the UV absorbance spectra for the online detection of the reaction progress. The UV spectra of the unreacted solutions exhibited lower absorbance than reactive solutions, indicating the formation of highly absorbent intermediate species. The reaction devices presented in this work can be used for the on-line analysis of the reaction mixture in organic synthesis and photo-initiated polymerisation reactions in small scale reactors.

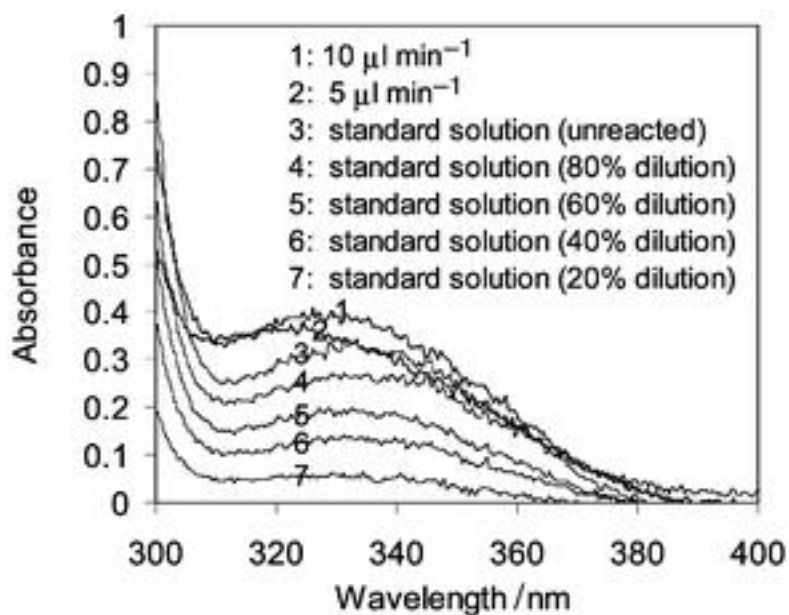


Figure 2.1: Online UV spectra of the of the pinacol formation reaction of benzophenone in isopropanol (Lu, Schmidt and Jensen, 2001)

Benito-Lopez *et al.* (2005) presented the use of UV/visible spectroscopy for high pressure online reaction monitoring. In brief, a nucleophilic aromatic substitution and an aza Diels-Alder reaction were monitored using a capillary microreactor. Therefore, p-halonitrobenzenes were reacted with a ten-fold excess of pyrrolidine, piperidine, and morpholine in THF at pressures 1, 200, 400, and 600 bar to give the p-N,N-dialkylamino-nitrobenzenes. The product formation and the reaction rate constants at different pressures were monitored by the increase of the absorbance at 391 nm. This study is the first application of a UV capillary system for the on-line monitoring of Diels-Alder reactions under high pressure.

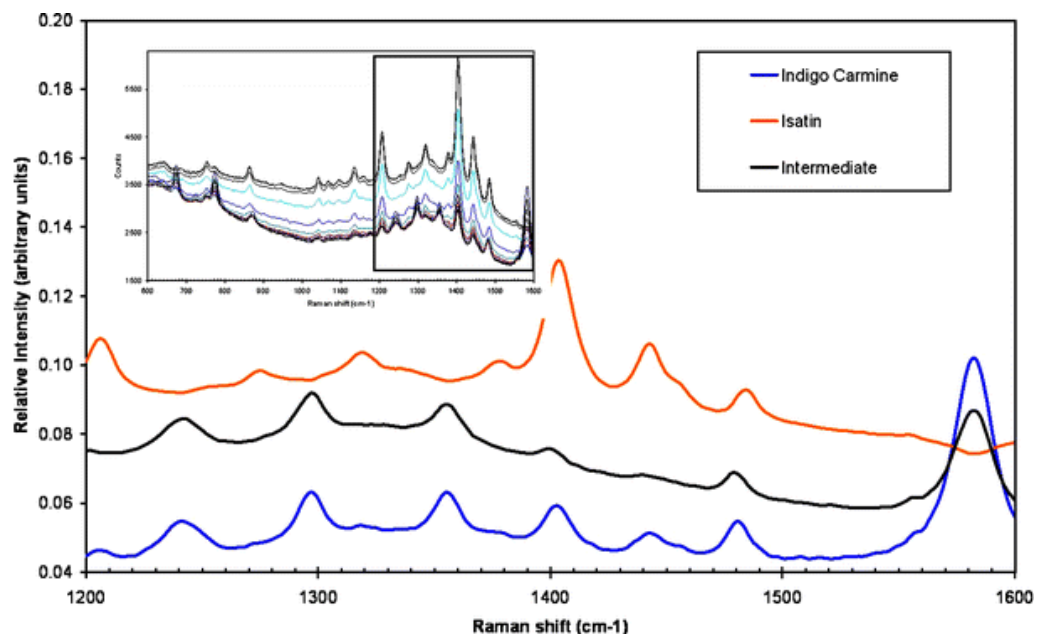


Figure 2.2: Raman spectra (and original reaction spectra in the mini graph) of laccase-catalysed indigo carmine oxidation, as calculated with multivariate curve resolution (Kandelbauer, Kessler and Kessler, 2008).

Kandelbauer, Kessler and Kessler (2008) demonstrated that the use of UV-visible spectroscopy combined with Multivariate Curve Resolution calculated by Alternating Least Squares (MCR-ALS) as a highly sensitive tool for online reaction monitoring. In brief, the laccase-catalysed oxidation of indigo carmine with and without redox active mediator was studied, and the MCR-ALS analysis enabled the identification of the participating species as well as derivation of kinetic characteristics. Figure 2.2 shows the real time and original reaction raman spectra. In brief, reaction precursors, such as indigo carmine (blue line) found to have the lowest relative intensity, while intermediates and the final product (isatine sulfonic acid) show a spectroscopic fingerprint with high relative intensity (black and red coloured lines). This study demonstrates the effectiveness of UV-visible spectroscopy in the real-time recording of spectral information of evolving mixtures. However, the presence of intermediates is

derived hypothetically by using the fit of ALS model and no structural characterization of the compound can be achieved.

2.3 Infrared Spectroscopy

Infrared spectroscopy is a widely used non-destructive reaction monitoring technique and referred to the interaction between a molecule and the infrared radiation. When a sample is subjected to IR radiation, a fraction of this radiation is absorbed and associated with the molecular vibrations and rotations. The absorbed IR radiation corresponds to selected frequencies (energies) related to the functional groups present in the sample (Rees, 2011).

The infrared is divided into three regions in the order from the highest to the lowest wavenumber¹: near infrared (14285 cm⁻¹ – 4000 cm⁻¹), mid infrared (4000 cm⁻¹ – 400 cm⁻¹) and far infrared (400 cm⁻¹ – 10 cm⁻¹). The mid-infrared spectrum can be divided into two regions: the functional group region (4000 cm⁻¹ – 1500 cm⁻¹) and the fingerprint region (1500 cm⁻¹ – 600 cm⁻¹) (Stuart, 2004). Fourier Transform Infrared spectroscopy and Raman spectroscopy can be used for reaction monitoring in the infrared region.

2.3.1 Fourier Transform Infrared Spectroscopy

Fourier Transform Infrared spectroscopy (FTIR) is based on interferometry, the interference of radiation between two beams. The most commonly used FTIR spectrometer is the Michelson interferometer, which consists of a beam splitter

¹ Wavenumber is the number of full cycles in a unit distance. The equation that relates the wavelength with the frequency of an electromagnetic waves is: $c = \lambda f$, where c is the speed of light, λ is the wavelength, and f is the frequency.

and two perpendicularly plane mirrors, as shown in Figure 2.3. The beam splitter, which is coated with an “infrared-transparent” substrate such as caesium iodide or potassium bromide, divides the incident IR radiation in two beams, the first one is reflected to a fixed mirror and the second is transmitted to a moving mirror. The two reflected beams are recombined at the beam splitter producing a modulated exit beam which is called the transmitted beam. The output from the interferometer, which include constructive/destructive interference patterns due to the optical path difference between the two components of the beam, reach a detector (Stuart, 2004; Rees, 2011; Tasumi, 2014).

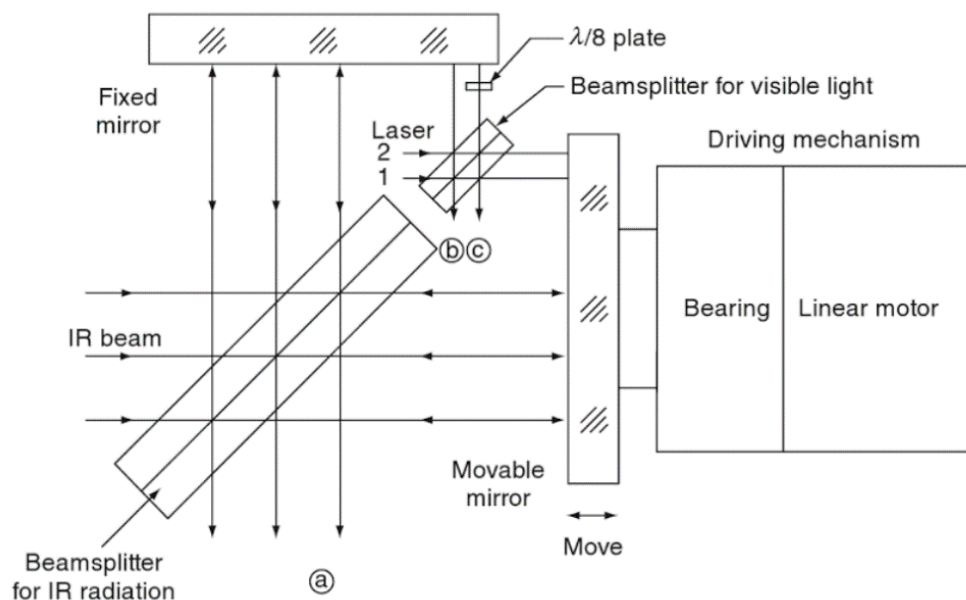


Figure 2.3: Typical structure of a Michelson interferometer (Tasumi, 2014).

FTIR analysis is non-destructive, can be performed in seconds and consequently, is an attractive reaction monitoring technique (Hergeth, 2000). Wolf, Leiberich and Seeba (1999) reported the use of horizontal Attenuated Total Reflectance (ATR) technique at pressures up to 200 bar and temperatures up to 300 °C for in-situ reaction monitoring. The addition reaction of n-butyl

isocyanate with butyric alcohol and the polycondensation reaction of bifunctional alcohols and carbonic acids were monitored with a use of an ATR crystal.

Jovanovic and Dube (2003) demonstrated the use of ATR-FTIR spectroscopy to monitor homogeneous and heterogeneous solution polymerisations. In brief, an ATR-FTIR probe was used for off-line and inline monitoring of butyl acrylate (BA) and vinyl acetate (VAc) solution polymerisations. As shown in Figure 2.4, the data obtained by ATR-FTIR were confirmed by gravimetry. The technique can also be used in real-time to identify the induction periods and an early catastrophic coagulation. However, the ATR-FTIR probe was found to be extremely sensitive to temperature variations.

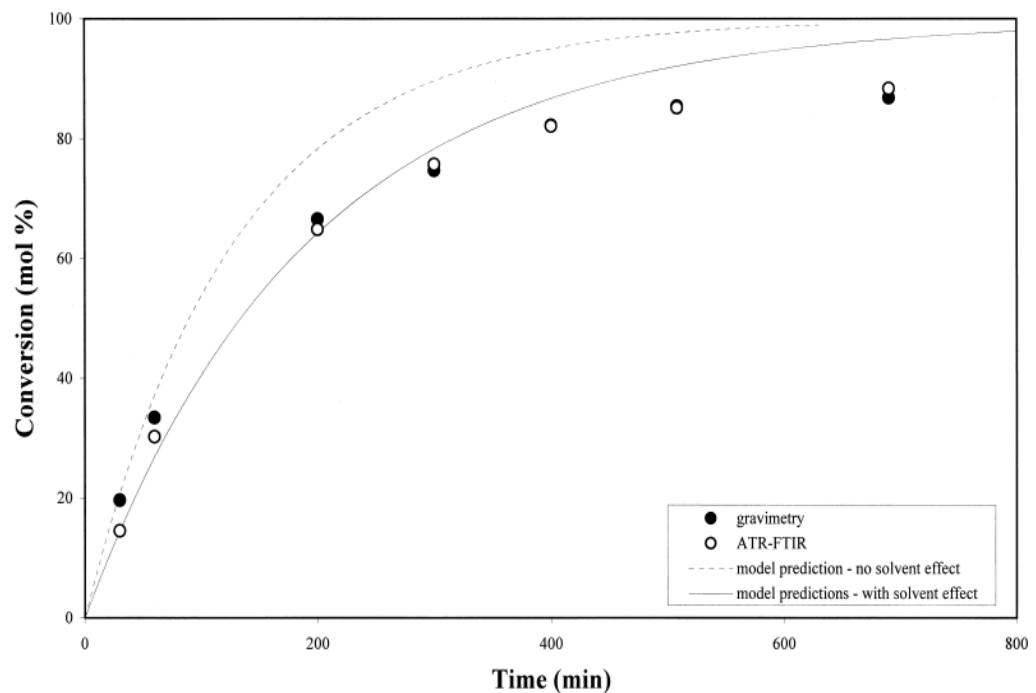


Figure 2.4: BA conversion (mol %) versus time (min) for BA solution homopolymerisation in toluene (Jovanovic and Dube, 2003).

Minnich *et al.* (2007) presented the use of an ATR-FTIR probe for the monitoring of solvent-free, highly air and oxygen sensitive reactions. In brief,

solvent-free synthesis of ionic liquids, organocatalyzed aza-Baylis-Hillman reaction and the transition metal-catalysed hydroamination were studied using a fibre optic ATR infrared probe inside an argon purged glove box connected to an FTIR spectrometer. The results obtained with the probe provide information about the reacting mixture and the change in molar fractions due to dilution and confirmed with measurements using offline techniques such as NMR spectroscopy and gas chromatography. An ATR-FTIR probe can also be used to monitor the concentration of hydroxyl groups in the step-growth polymerisation of glycerol (Salehpour and Dubé, 2012). The results were confirmed with offline techniques such as hydroxyl value calculation and water production monitoring.

Deng *et al.* (2014a) studied the ring-opening polymerisation of tetrahydrofuran (THF) with a silicon-attenuated total reflectance probe. The absorbance variation of two infrared peaks at approximately 1109 and 1068 cm^{-1} versus reaction time was monitored in-situ and utilized to determine the concentrations of the monomer and polymer in the reaction mixture, as shown in Figure 2.5.

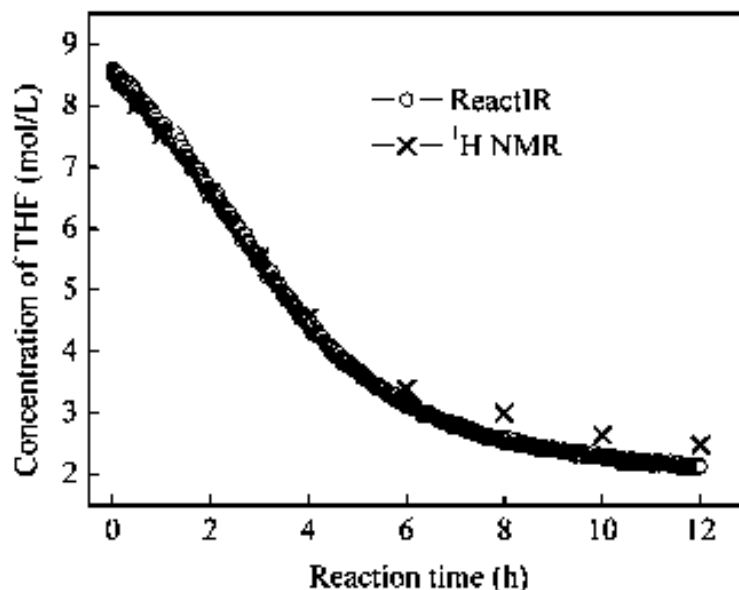


Figure 2.5: Comparison of THF concentration determined by infrared and NMR versus time (Deng et al., 2014).

Khanlari and Dubé (2015) reported the first application of ATR-FTIR spectroscopy for in-line monitoring of a polymerisation in the presence of nanofillers. The absorbance of various functional groups in the reaction mixture which correspond to either polymer or monomer was monitored versus time and the reaction conversion was predicted successfully and validated using off-line gravimetric data. A common issue of ATR-FTIR monitoring technique is that the presence of water can significantly affect the obtained spectra. This can be eliminated using spectral subtraction of the water absorbance (Khanlari and Dubé, 2015). Another limitation of FTIR spectrometers is the fact that FTIR is a single beam technique. As a result, the background spectrum, which includes the contribution of the environment and the instrument to the spectrum, is measured at a different time than the spectrum of the sample. Although the contribution from the environment and the instrument can be eliminated by minimizing the time between the background measurement and the sample measurement or by purging the light path with dry air or high-purity nitrogen, a change in the

instrument or the background between the two measurements can result in spectral artefacts in the sample spectrum, which could mask sample absorbances. A common example includes a water vapour or a carbon dioxide peak (Smith, 1995)

2.3.2 Near Infrared Spectroscopy

The Near Infrared region (NIR) was discovered in 1800 by William Herschel who separated the electromagnetic spectrum with a prism to identify which radiation was responsible for the heat of sunlight. Although a number of NIR spectroscopic techniques had been established since the nineteenth century, the first efficient NIR detectors become available in 1950s (Reed and Alb, 2013). A Near Infrared spectrometer generally consists of a light source, a monochromator, a sample holder and a detector, as shown in Figure 2.6. The light source is usually a tungsten halogen lamp. Detector types, allowing for transmittance or reflectance measurements, include lead sulphide (PbS), silicon, and indium gallium arsenide (InGaAs) (Reich, 2005).

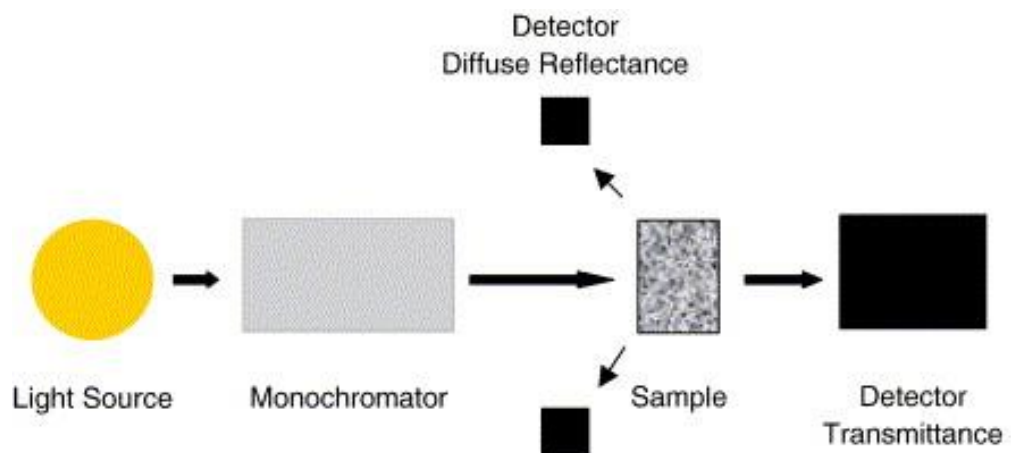


Figure 2.6: NIR spectrometer configuration (Reich, 2005).

Infrared radiation excites vibrational and rotational motions in molecules. The absorption of infrared light is characterised by the Beer-Lambert-Bouguer law:

$$A = a \cdot b \cdot c \quad (2.1)$$

where a is the molar absorptivity, b is the sample thickness and c the analyte concentration (Bakeev, 2010). Near Infrared spectroscopy has been used in the last few decades as a fast and non-destructive analytical technique to monitor polymer processing applications (Workman *et al.*, 2009). Selected studies are presented below to highlight the applications of the technique in reaction monitoring.

Coffey, Cooley and Walker (1999) demonstrated the use of fiber-optic near infrared spectroscopy as an in situ spectroscopic technique to monitor a chemical reaction. In detail, the preparation of methyl 2,3-O-isopropylidene- β -D-ribofuranoside was studied and the product formation and reaction end-point were determined with NIR spectroscopy. The proposed method was based on a calibration curve developed with a comparison of High-performance liquid chromatography (HPLC) data and IR spectra. A partial least squares (PLS) model was developed and successfully predicted the formation of the product, as shown in Figure 2.7.

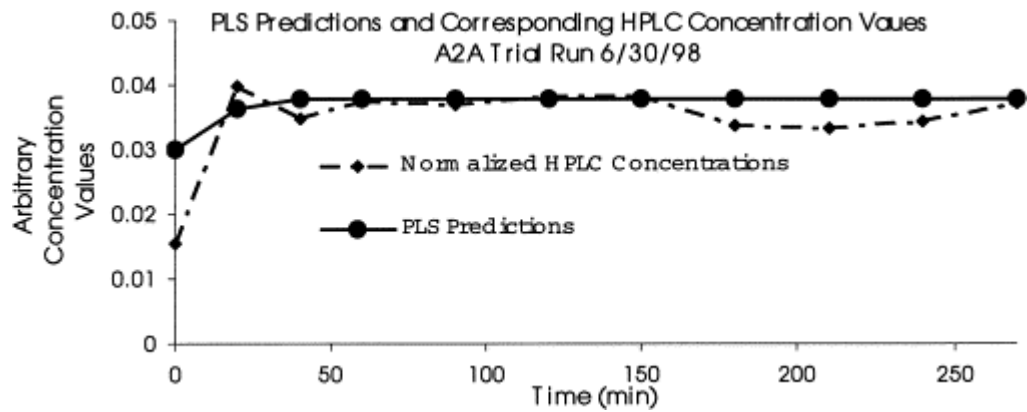


Figure 2.7: Comparison of PLS and HPLC product concentration (Coffey, Cooley and Walker, 1999).

Fontoura *et al.* (2003) presented the use of near infrared spectroscopy as a technique to in-line and in situ monitoring the styrene solution polymerisation, with the help of a Kalman filter estimator. In detail, monomer conversion and polymer average molecular weight were monitored using a combination of a calibration model and a first principle model. The combination of the near infrared spectroscopy and Kalman filter allowed the control of monomer conversion and polymer average molecular weight simultaneously. Figure 2.8 shows the correlation between the in-line and off-line values of the weight fraction values of polystyrene obtained with NIR spectroscopy and gravimetry accordingly.

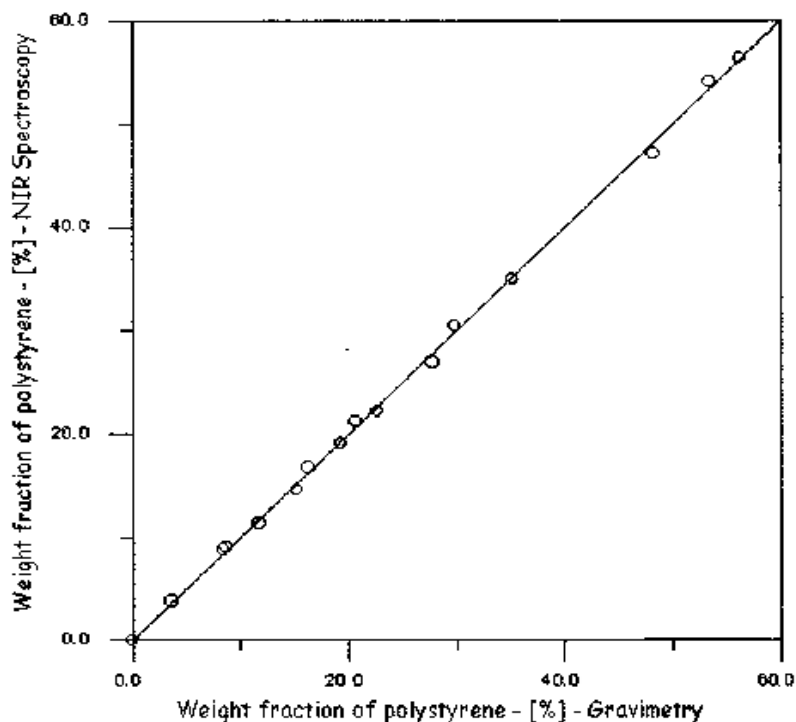


Figure 2.8: Comparison of polystyrene weight fraction values calculated by NIR spectroscopy and gravimetry (Fontoura *et al.*, 2003).

Sheibat-Othman, Peycelon and Févotte (2004) showed the use of a near infrared spectroscopy to monitor the monomer concentration in solution polymerization processes. In detail, the concentration of acrylic acid in solution polymerisation was monitored using a near infrared spectrometer, calibrated using the partial least-squares optimization technique. The results showed that the concentration of the monomer in the reactor can be maintained at a set value and help maximize the productivity of an industrial reactor.

Cervera-Padrell *et al.* (2012) reported the use of NIR spectroscopy as an inline tool for the monitoring and control of a continuous Grignard alkylation reaction of 2-chlorothioxantone (CTX) with allylmagnesium chloride (AllylMgCl) in tetrahydrofuran (THF). In detail, NIR transmission measurements, calibrated using High-performance liquid chromatography as a reference analytical

technique, was used to inline determine the CTX concentration. Additionally, at-line NIR spectroscopy measurements were used to create a chemometric model for the calculation of Grignard reagent concentration.

Despite the many advantages of infrared spectroscopy, there are also some limitations. A general limitation is that it cannot detect atoms or monoatomic ions, as single atoms do not contain chemical bonds, do not possess vibrational motion, and consequently do not absorb infrared radiation (Smith, 1995). Additionally, aqueous solutions are difficult to analyse using infrared spectroscopy, as water is a strong infrared absorber. Although water spectrum can be subtracted from the sample spectrum, the sensitivity of the technique in analysing aqueous systems is poor (Elfanso *et al.*, 2010). Furthermore, the application of infrared spectroscopy in analysing complex mixtures is challenging, as these mixtures give rise to complex spectra, and is hard to deconvolute them. To maximise the information contained in an infrared spectrum, it is advisable to obtain the spectra of individual molecules (Smith, 1995).

2.4 Raman Spectroscopy

Raman effect, which is discovered by C. V. Raman and K. S. Krishnan in 1928, is a light scattering effect based on the collisions of the molecules of the sample with the photons of the incident radiation. On these collisions, the photons may be elastically or inelastically scattered by the molecules of the material. In the second case, the scattered light has a slightly different frequency from that of the incident light. A fraction of this light interacts with the molecules and cause a

change in the polarization of the electron cloud. As a result, a change of atomic oscillation within the molecule occurs. We can use this effect to determine the molecular structure of a material and find the functional groups and the chemical bonds that are present in the molecules. The Raman effect occurs in the Infrared, visible and UV region and have been used to study liquid and solid phase reactions (Gauglitz and Moore, 2014; Kaur, 2014).

Raman spectroscopy has been used for the online monitoring of polymerisation reactions. Santos *et al.* (2004) verified the use of raman spectroscopy for the online monitoring of batch styrene suspension polymerisation reactions. In brief, a probe connected to the reactor was used to collect raman spectra during the progress of the reaction and the collected raman spectra allowed the estimation of conversion and identify any abnormal behaviour from the formation of unexpected particle size distributions. Samples were collected throughout the reaction progress for offline characterisation to measure the evolution of conversion along the reaction by gravimetry. Figure 2.9 shows Raman estimations of conversion for four polymerisations carried out at different temperatures. Reactions R2 and R3 presented similar polymerisation rates because the temperature was equal.

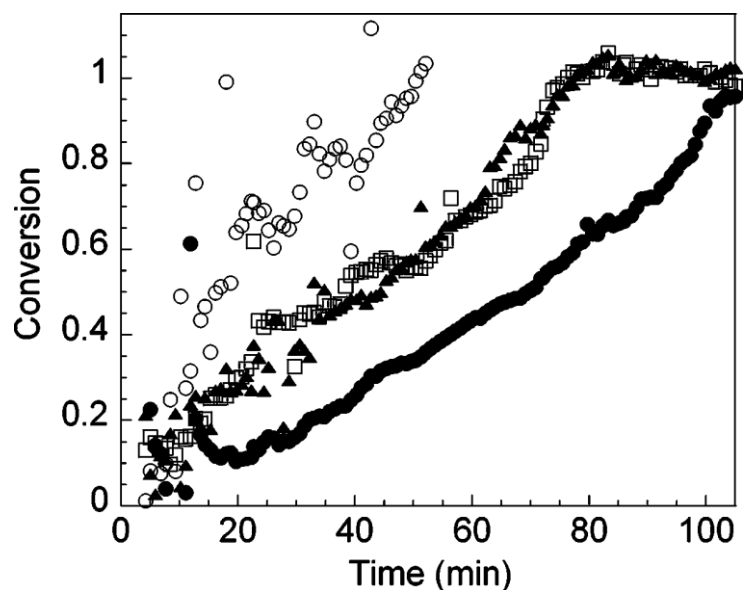


Figure 2.9: Raman estimations of conversion of four reactions with a smoothing-spline filter: (o) reaction R1; (\square) reaction R2; (\blacktriangle) reaction R3; (\bullet) reaction R4 (Santos et al., 2004).

Raman spectroscopy has been used for the in-situ reaction monitoring of microwave-assisted reactions. Pivonka and Empfield (2004) presented the use of a fiber-optic Raman spectrometer for the in situ, real time analysis of kinetics, yield and mechanisms in the imine formation and Knoevenagel condensation reaction. It was found that the formation of functional groups and the final product can be observed and the in-vivo performed kinetic analysis can be used to predict the reaction time even at the beginning of the reaction process. The main limitation of this method is that any change in temperature could affect the blackbody radiation which is detected. Leadbeater and Schmink (2008) showed the use of a commercially available Raman spectrometer to real time monitor the reaction progress and determine the end-point of the microwave-promoted base-catalysed reaction of salicylaldehyde with ethylacetoacetate. This study showed that in-situ Raman spectroscopy can be used to optimise reaction conditions and prevent decomposition. The author's previous work showed that it is also

possible to monitor esterification reactions and ligand substitution reactions in organometallic complexes using similar apparatus.

Hamlin and Leadbeater (2013) reported the use of Raman spectroscopy for real-time monitoring of continuous-flow processing reactions. In detail, four reactions were studied: the synthesis of 3-acetylcoumarin, the Knoevenagel condensation, the Claisen-Schmidt condensation and the Biginelli reaction. A calibration curve was made and the product conversion values for each reaction were measured. As shown in Figure 2.10, the set-up, which consists of a Raman spectrometer with a scientific microwave unit, monitored the product conversion of salicylaldehyde and ethyl acetoacetate to 3-acetylcoumarin in a variety of temperatures and flow rates. A calibration curve used to obtain the product conversion values in each temperature and flow rate.

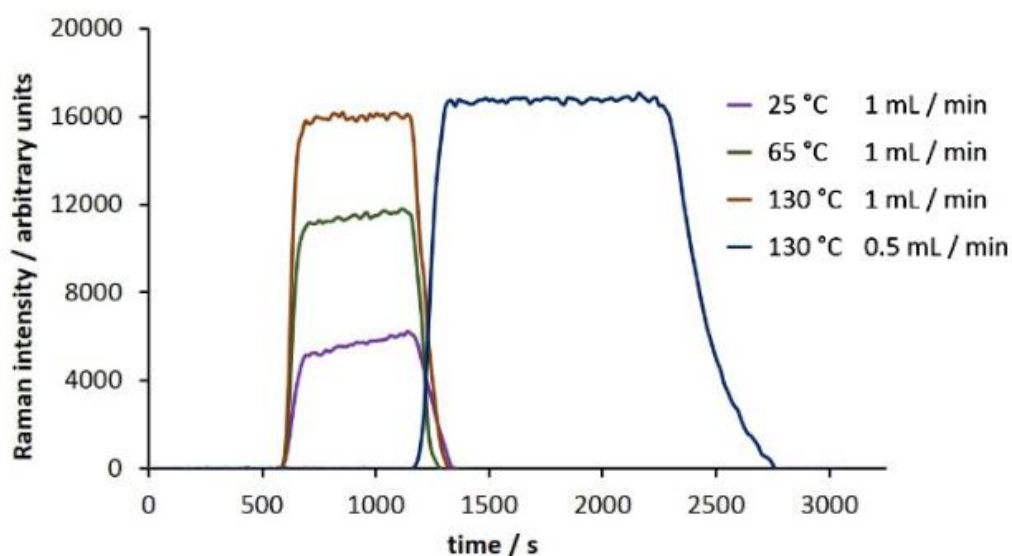


Figure 2.10: Monitoring of product conversion of salicylaldehyde and ethyl acetoacetate to 3-acetylcoumarin in a variety of reaction conditions (Hamlin and Leadbeater, 2013).

Raman spectroscopy can be successfully used for on-line reaction monitoring of hydrolysis reactions. Svensson, Josefson and Langkilde (1999) showed the use

of a Raman spectrometer with a 785 nm laser to monitor the synthesis and hydrolysis of ethyl acetate. The Raman spectra were used to determine first-order reaction and rate constants were determined with the use of multivariate techniques such as principal components analysis and partial least squares regression. Venardou *et al.* (2004) reported the use of on-line Raman spectroscopy to monitor the hydrolysis of acetonitrile in near-critical water. In situ spectroscopic data were obtained with the use of a high temperature high pressure (HTHP) Raman cell and allowed the calculation of activation energy and the pseudo-first-order rate constant. Figure 2.11 shows in situ IR spectra of the hydrolysis of 50% (w/w) acetonitrile in water, collected over a period of 1 h at pressure 500 bar and temperature 300 °C with the use of a HTHP IR cell.

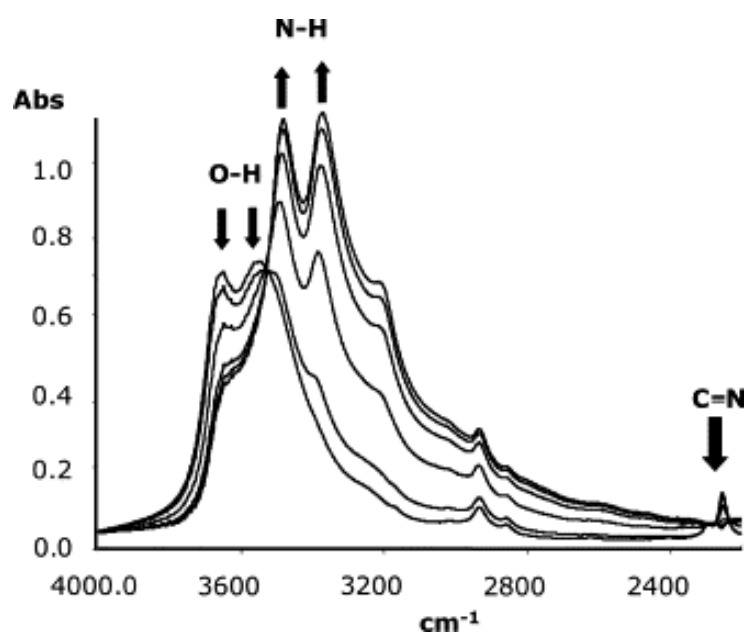


Figure 2.11: Raman spectra of the hydrolysis of 50% (w/w) acetonitrile in water at 300 °C and 500 bar (Venardou *et al.*, 2004).

Raman spectroscopy is more preferable than IR to monitor aqueous systems, since water is a poor Raman scatterer, and this allows the vibrations of organic functional groups to be detected (Elfanso *et al.*, 2010). The ability to obtain

resonance Raman spectra with good signal-to-noise ratio is the biggest challenge of the technique (Kneipp, Moskovits and Kneipp, 2006). Surface Enhanced Raman Scattering (SERS), which involves recording Raman scattering from an analyte adsorbed on a suitably roughened metal surface, offers improved sensitivity down to the single molecule level, enabling the use of the technique for in situ identification (Jeanmaire and Van Duyne, 1977; Littleford et al., 2019). However, the application of the technique in monitoring reactions at high temperatures and pressures is challenging and requires the use of expensive equipment to face issues, such as corrosion (Venardou *et al.*, 2004).

2.5 Nuclear Magnetic Resonance Spectroscopy

Nuclear Magnetic Resonance (NMR) is a very popular method for monitoring reaction processes. It is based on the interaction of the nucleus of an atom with an applied static or alternating radio frequency electromagnetic field. Nuclei can either align with or against the field depends on their energy state. We can observe either absorption or subsequent release of energy as the nucleus go back to a lower energy state. NMR can provide structural information about reaction components of complex fluid mixtures with similar compounds and is preferred instead of infrared spectroscopy (Gauglitz and Moore, 2014; Kaur, 2014).

There are four methods for NMR reaction monitoring: static NMR tube monitoring, online monitoring, stopped-flow and rapid injection NMR. Static NMR is the most used technique because there is no need for any modification of the setup and a standard spectrometer can be used. However, this method is offline and requires sample extraction. Online NMR can be used to real time

monitor complex multicomponent mixtures. It requires a custom tube or probe to be connected to the reaction vessel. Flow NMR can be used to real time monitor reaction kinetics. The sample is introduced in a custom designed probe as a flowing stream. Rapid injection NMR can be also used to determine reaction kinetics and reactive intermediates, but it lacks a flow system. As a result, the number of subsequent measurements is limited (Reed and Alb, 2013). The first commercial application of on-line time-domain (TD) NMR spectroscopy was applied into petrochemical plants in the 1990s (Bakeev, 2010).

Foley *et al.* (2015) compared online NMR, standard NMR tubes and NMR tubes with periodic inversion to understand how the different mixing in each method can influence the kinetic understanding of three reaction types: the L-proline-catalysed self-condensation of propionaldehyde, the homogenous coupling reaction of aniline and 4-fluorobenzaldehyde and the acid-catalysed transesterification of isopropanol and acetic anhydride. The results showed that reaction kinetics depends on the method selected because of the different amount of mixing in each method. Online NMR techniques can offer the most accurate results for kinetic studies because of continuous mixing.

Gomez *et al.* (2010) reported the use of a microfluidic NMR chip for the on-line monitoring of microliter continuous-flow microwave assisted organic reactions. In detail, the on-line monitoring and rapid optimisation of reaction conditions of the microwave activated Diels-Alder cycloaddition of 2,5-dimethylfuran and dimethyl-acetylene dicarboxylate was demonstrated. Figure 2.12 shows the conversion of the cycloaddition reaction product at three temperatures (125 °C, 135 °C and 150 °C) for different reaction times. In a more recent work, a microfluidic NMR chip hyphenated to a continuous-flow microreactor was used

to rapidly extract kinetic information from a chemical reaction. This approach allowed the extraction of the order, rate constant and Arrhenius parameters within a single nonisothermal on-flow experiment.

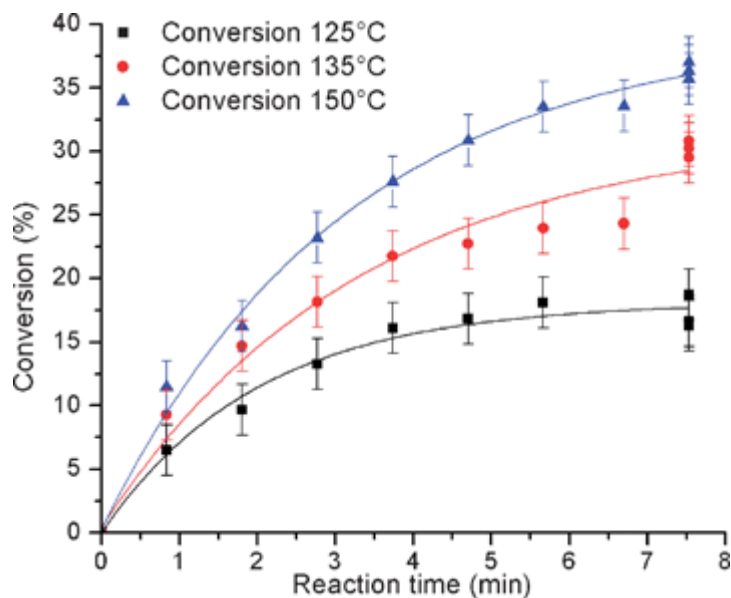


Figure 2.12: Conversion (%) of the cycloaddition reaction product as a function of reaction time for various temperatures (Gomez et al., 2010).

Anderson and Franz (2012) real-time monitored the consumption and formation of triacylglycerols, diacylglycerols and fatty methyl esters with the use of time-array H-NMR spectroscopy. As shown in Figure 2.13, the method can monitor the consumption of triacylglycerols (TAGs) which is the starting material, the formation of fatty acid methyl esters (FAMES) which is the product and indicate the presence of intermediates like diacylglycerols (DAGs). The real-time monitoring of reaction components can be used to optimize the reaction conditions.

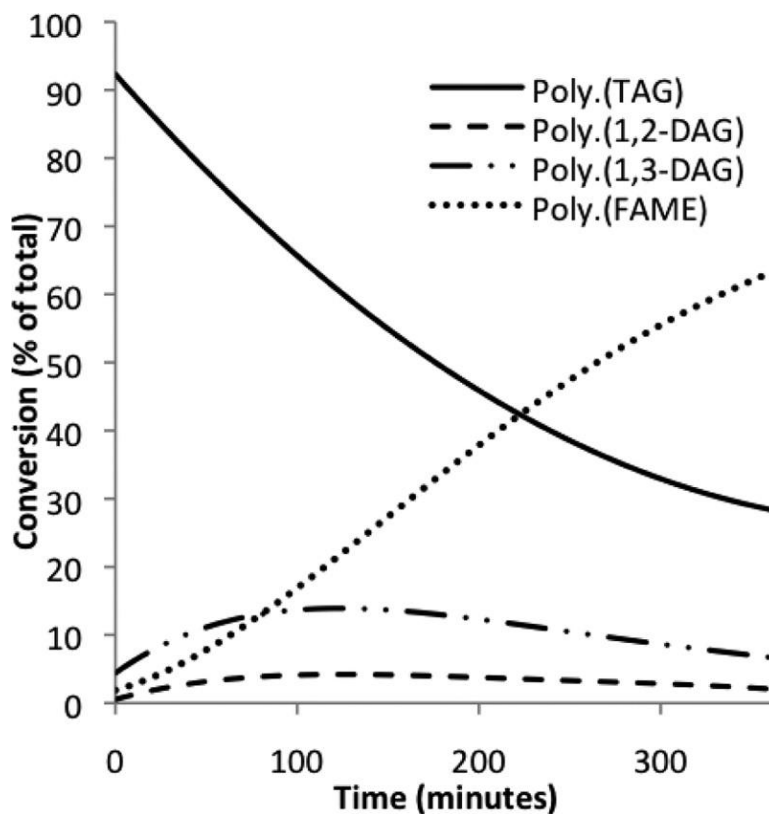


Figure 2.13: Reaction profile analysis of starting material (TAG), formation of product (FAME) and intermediates (DAGs) (Anderson and Franz, 2012).

NMR was proven to be a non-destructive monitoring technique which does not require prior knowledge of the analysed compounds and can deliver both structural and quantitative information. However, peak overlap is one of the major factors complicating the analysis of low resolution NMR spectra and has limited the application of the technique to reaction monitoring (Hefke, Schmucki and Güntert, 2013; Gouilleux et al., 2015). A proposed solution to the overlap problem in two-dimensional NMR spectroscopy is to introduce an additional evolution dimension to generate a three-dimensional spectrum (Kupče et al., 2005). Another common issue of NMR spectroscopy is magnetic field drift which, if not corrected, results in broadening of spectral peaks and distortion of lineshapes. In solution NMR spectroscopy, the issue is usually solved by tracking the field drift by detecting deuterium and correcting the magnetic field

while the measurement is recorded with the use of room temperature electromagnets (Najbauer and Andreas, 2019).

2.6 Differential Scanning Calorimetry

Differential Scanning Calorimetry (DSC) is the most commonly used thermal analysis method to measure the heat capacity of a process over a broad temperature range (Haynie, 2001). It is based in the difference in heat flow rate between a sample and a reference sample, monitored versus time. Two identical temperature sensors are used, one for measuring the sample temperature and the other for the reference temperature. The difference between the two sensors represents the thermal change present without any thermal effect that can affect both sensors (Haines, 2002). There are two main types of differential scanning calorimeters: heat-flux and power-compensated DSCs. In Heat-flux DSCs, the sample is enclosed in a pan, along with a reference pan are placed on a thermoelectric disk, which is placed in a furnace. The temperature (or power) difference between the reference and the sample is used to calculate the difference in the heat flow rate. In power-compensated DSCs separate furnaces heat the sample and reference pans. The sample and reference are heated at the same temperature and the difference in supplied power to maintain them at the same temperature is measured directly (Haines, Reading and Wilburn, 1998; Gill, Moghadam and Ranjbar, 2010).

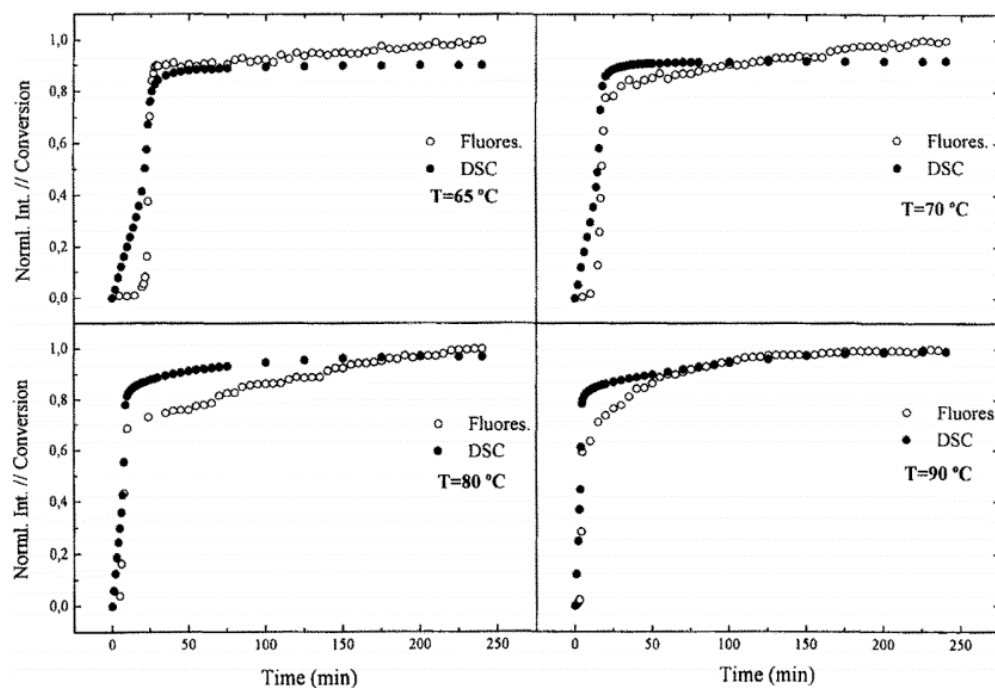


Figure 2.14: Conversion and normalized fluorescence intensity versus polymerization time for various temperatures (Serrano *et al.*, 1997).

Serrano *et al.* (1997) proposed a method to monitor the bulk polymerization of cyclohexyl methacrylate by using Differential Scanning Calorimetry coupled with fluorimetry. The proposed method can be used to detect vitrification phenomena by measuring the conversion change associated with the different behaviour of the intensity profile. Figure 2.14 shows the conversion and fluorescence intensity, normalized at their maximum values plotted against polymerisation time for cyclohexyl methacrylate at temperatures 65, 70, 80 and 90 °C. At temperatures above 70 °C, DSC and fluorimetry data are closer.

Several research groups have developed DSC techniques for the in-situ monitoring of chemical transformations. Swier and Mele (2003) reported the use of an in situ Modulated Temperature Differential Scanning Calorimeter (MTDSC) to study the reaction morphology and phase separation of two epoxy-amine based systems. Phase separation as well as the effect of cure temperature

to the morphology were studied by analysing the change in heat capacity signal for the cure of the reactive mixture. Hofmann *et al.* (2006) used isothermal differential calorimetry to monitor and determine the setting time of a fast-setting brushite-forming cement. The results showed that the technique can real time monitor the curing of the exothermic system of study over a wide range of powder to liquid ratio and citric acid retardant concentration. The drawback of this method is that it can only be used to monitor the reaction after the first 2-3 minutes which are needed for apparatus and sample preparation.

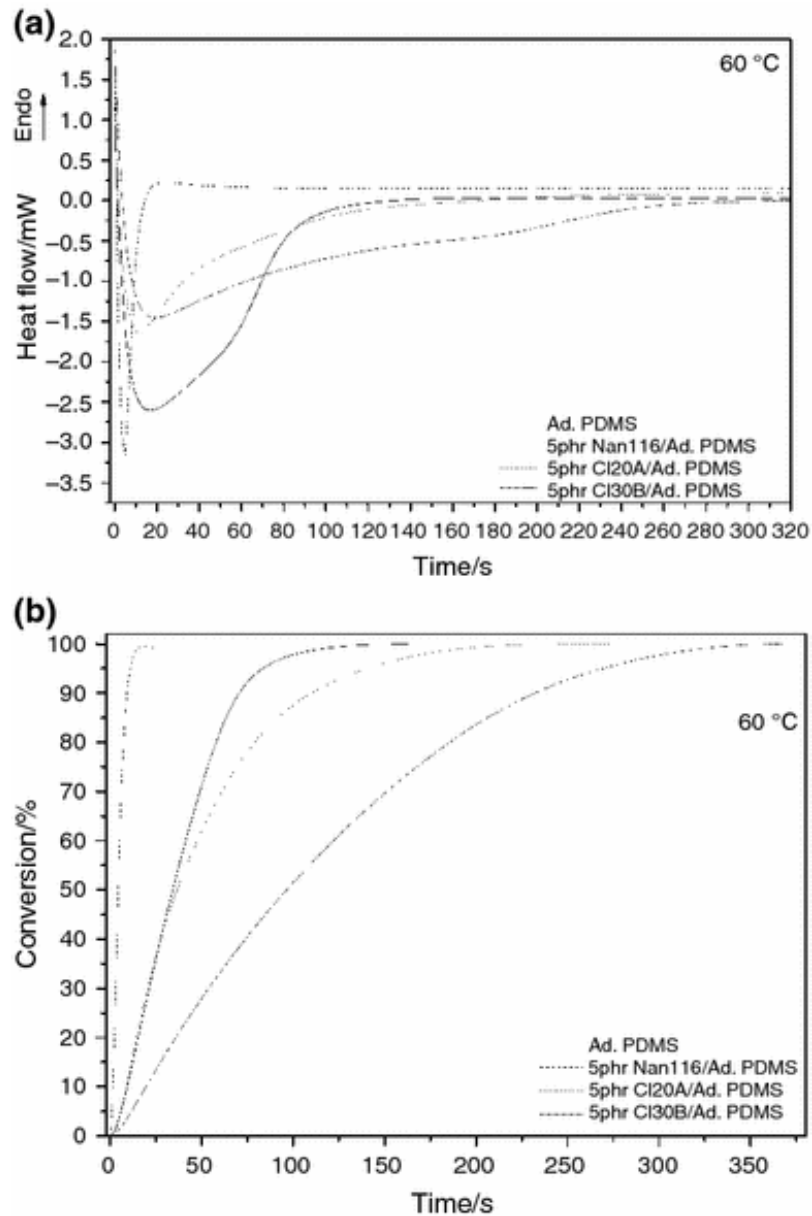


Figure 2.15: (a) Isothermal DSC and (b) conversion curves as a function of time, during the vulcanization of elastomeric matrix (Vasilakos and Tarantili, 2017).

Vasilakos and Tarantili (2017) studied the effect of organically modified and commercially unmodified clay nanoparticles in the curing mechanism on the vulcanization of Poly(dimethylsiloxane) (PDMS) elastomers. In this study, isothermal DSC runs were performed to monitor the vulcanization reaction of vinyl-terminated PDMS and was found that the degree of vulcanization can be correlated with the heat released during the reaction. Additionally,

non-isothermal DSC runs were performed to study the effect of the modified and unmodified montmorillonite clays on the vulcanization reaction. Figure 2.15 shows the effect of the addition of clay nanoparticles on the vulcanization of PDMS at 60 °C. It was found that Cloisite 30B and 20A nanoparticles increased the vulcanization time of vinyl-terminated PDMS.

Although, DSC has been proved to be a technique suitable to monitor chemical reactions, it has some limitations. Most modern DSC instruments have two or three samples cells with the sample size being only a few tens of milligrams. The small capillary cells make the cleaning more difficult, which may also result in bubble formation (Chiu and Prenner, 2011). Additionally, accurate specific heats² (with relative error of 1% or higher) are usually achieved at about 725 °C. Another important limitation of the technique is the potential reactivity of the sample with the container, which is the case when performing measurements with liquid metals (Yu, 2001).

2.7 Mass Spectrometry

Mass spectrometry is one of the most important analytical methods to obtain the molecular composition and unknown compound structure due to its sensitivity, speed, and detection limits. A typical mass spectrometer consists of three parts: the ion source where the sample is ionized, the mass analyser where the ions are separated according to their mass to charge ratio and the detector to measure the separated ions (Gauglitz and Moore, 2014; Kaur, 2014). Mass spectrometry

² Specific heat is the amount of heat per unit mass required to raise the temperature by one degree Celsius (Yu, 2001).

coupled with various ionization methods have been used to real-time monitor chemical and biochemical reactions. Conventional ionization methods such as electron ionization (EI) and chemical ionization (CI) are widely used to detect thermally stable compounds with a low boiling point. However, due to their thermal decomposition under heating and low ionization efficiency, they are preferred for the detection of large molecules. Matrix-assisted laser-desorption ionization (MALDI) and electrospray ionization (ESI) can reduce the fragmentation of target molecules and have been used for the monitoring of polymers, peptides and proteins. Atmospheric pressure ionization (API) can be used to monitor reactions with fast kinetics using ESI-based, plasma-based or other corresponding methods. ESI-based methods are widely used for the detection of polar compounds, biomacromolecules and small organic compounds. Plasma-based methods are generally applicable to monitor thermally unstable compounds (Chen and Lin, 2015).

The first application of mass spectrometry in online reaction monitoring was reported by Hambitzer and Heitbaum (Hambitzer and Heitbaum, 1986). In this work, an electrochemical cell was connected with a thermospray mass spectrometer to monitor the electrooxidation of N,N-dimethylaniline in an aqueous medium. Basic and acidic products of the reaction as well as the formation of dimers and trimers of N,N-dimethylaniline were identified directly from solution. Many research groups have developed various setups to study the mechanisms of solution-phase reactions such as electrochemical, photochemical, radical-initiated and organometallic reactions (Santos, Knaack and Metzger, 2005).

Many ionization methods have been developed ranging from conventional methods like electron and chemical ionization to matrix assisted laser desorption ionization and electrospray ionization. The development of atmospheric pressure ionization does not require vacuum and can be used for online reaction monitoring (Chen and Lin, 2015). Nørgaard *et al.* (2010) reported an ambient sonic spray ionization mass spectrometer that can be used for the direct online monitoring of polymerisation reactions. In detail, two nanofilm products consist of organosilicon compounds applied to glass, filter paper and cotton surfaces and the condensation polymerisation reaction was monitored by scanning the formed coating surface at an open atmosphere. The formation of oligomers and the consumption of monomers followed successfully in real time and polymerisation trends were observed. In Figure 2.16, the mass spectra produced by easy ambient sonic spray ionization technique (EASI-MS) was used to monitor the polymerisation of a nanofilm product (NFP) used for coating of floor materials. Figure 2.16 (b) shows the mass spectrum 15 min after spraying of the NFP on glass. Major changes can be observed such as the missing silane ion of m/z 509 as well as the increased tri and tetrasiloxane ions of m/z 1265 and 1715.

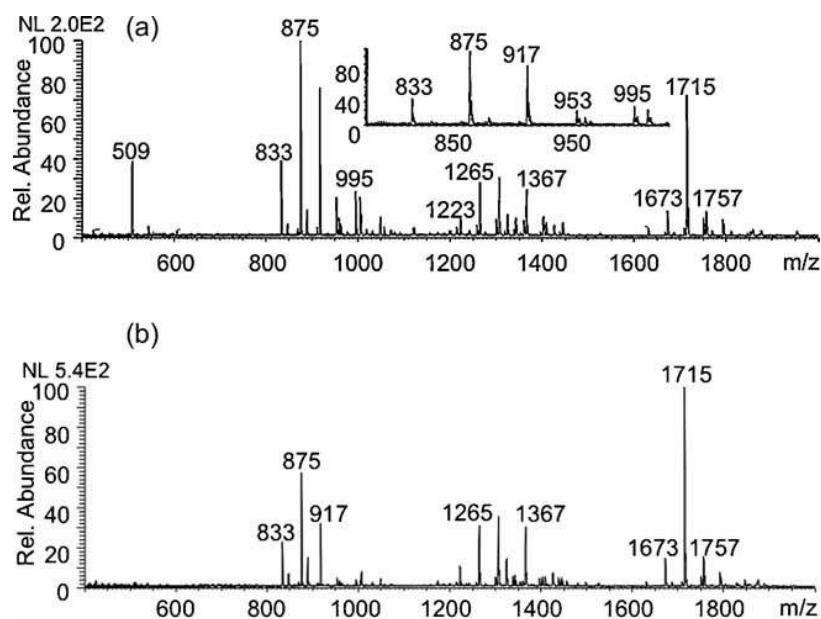


Figure 2.16: Mass spectra of the polymerisation of nanofilm products (NFP-1) on glass: (a) 1 min, and (b) 15 min after spraying on a glass surface (Nørgaard *et al.*, 2010).

Electrospray ion mobility coupled with mass spectrometry (ESI-IMMS) can be used to monitor the progress of pharmaceutical reactions in real-time. Roscioli *et al.* (2013) reported the use of ESI-IMMS for the monitoring of a reductive amination reaction. The consumption of starting materials and the production of products were monitored successfully in the same mobility experiment.

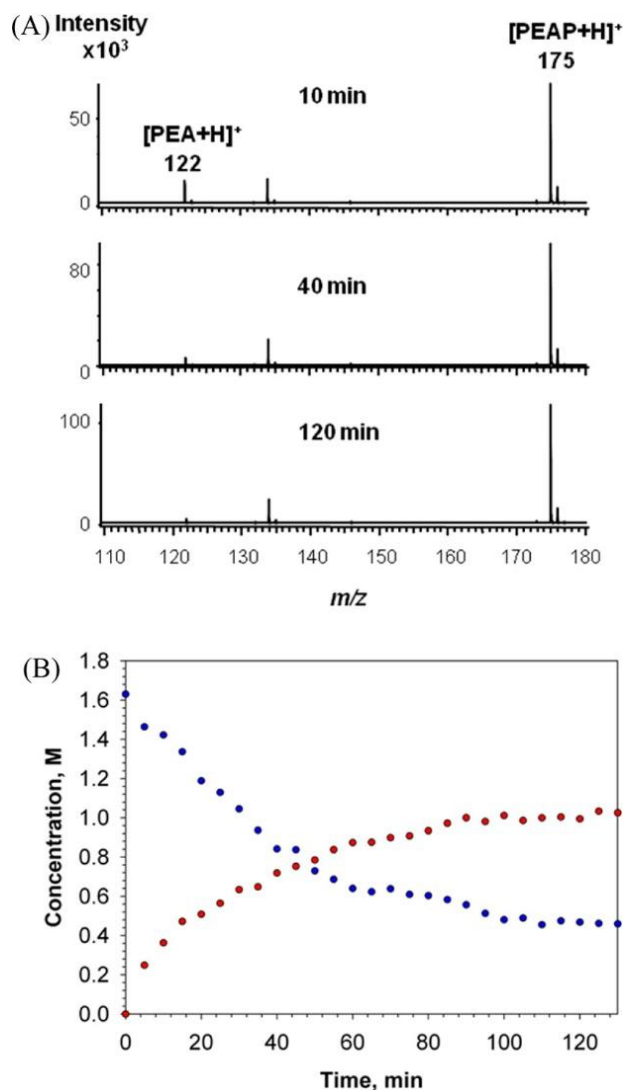


Figure 2.17: Mass spectra (A) and real time molar concentration changes and (B) of Michael addition reaction of Phenethylamine (Zhu *et al.*, 2012).

Zhu *et al.* (2012) developed a novel autosampling flow injection analysis coupled with an atmospheric pressure chemical ionization mass spectrometry (FIA/APCI-MS) system that can be used for real time monitoring of chemical/biochemical reactions. Different mass spectrometry techniques can be used to monitor the formation and consumption of reaction intermediates and products so that they can help in the optimisation of reaction conditions. The most accurate method depends on the type of reaction performed. Figure 2.17 (A) shows the mass spectra for a mass range (m/z) from 110 to 180

at 10 min, 40 min and 120 min reaction time for the Michael addition reaction of Phenethylamine and Acrylonitrile. Figure 2.17 (B) shows the concentration change of Phenethylamine (PEA) and 3-(Phenethylamino)propanenitrile (PEAP) during the reaction.

Although mass spectroscopy can be performed to monitor chemical reactions, the technique has some limitations in terms of the thermal-catalytic stability and volatility requirements of the compounds to be analysed, mass resolution, and mass accuracy. For example, the material under test must be stable under high-vacuum conditions as mass spectrometers involve the production of ions in a high-vacuum system (Hoffmann and Stroobant, 2007). Furthermore, the quality of mass spectra may be reduced in high molecular weight compounds and in cases where a large number of different low-abundance side-products occur (Desiderio, 1990). The addition of modern ionisation methods such as the electrospray ionisation (ESI) and atmospheric pressure chemical ionisation (APCI) are widely used in combination with liquid chromatography (LC) and desorption methods, such as the matrix-assisted laser desorption/ionisation (MALDI), to eliminate many of the above-mentioned limitations (Zaikin and Halket, 2009).

2.8 Dielectric Spectroscopy

UV/visible and infrared spectroscopy study the interaction of the electromagnetic radiation with molecular systems at frequencies above 1 THz (10^{12} Hz). Dielectric spectroscopy studies the dielectric dispersion and absorption phenomena that occurs in the frequency range, from 10^{-1} Hz to

10^{11} Hz (Gaiduk and McConnell, 1995). It is based on the tendency of ions and dipoles to orient under the presence of an external electric field. When a molecule with a permanent dipole moment is subjected to an external electric field, it undergoes orientation and generates an electric field which can interact with the external field. This interaction can lead to energy absorption or emission and can be described by the complex permittivity, ϵ^* . The real part is the dielectric constant (ϵ') and expresses the ability of the material to store energy through polarisation. The imaginary part, the loss (ϵ''), denotes the ability of the material to dissipate the stored energy into heat (Davies, 2007). A detailed analysis about dielectric theory is presented in chapter 3.

Dielectric Spectroscopy has become an effective process analytical technique due to its broad frequency range that allows the investigation of different characteristic relaxation processes. Additionally, it is a non-destructive monitoring technique that can be used “in-situ” to provide real-time process-related information. Santos *et al.* (2001) used dielectric analysis for the in-line monitoring of monomer and overall conversion during methyl methacrylate/butyl acrylate (MMA/BuA) solution copolymerisations. Samples were collected at set times during the polymerisation for off-line determination of monomer conversion by gravimetry. An empirical model was developed to relate monomer conversion with the dielectric loss. This technique allows the real-time evaluation of monomer conversion as well as the induction time. However, this method requires experiment-specific calibration.

Nahm (2006) reported the application of dielectric spectroscopy in real time monitoring the synthesis of three resins. The resins based on a variety of chemistries, had low molecular weight and are used as coating components.

A one-half inch diameter probe along with a thermocouple were used to real time monitoring impedance and temperature versus time during the synthesis of resins. The dielectric spectroscopy output data compared with ones from offline techniques such as gel permeation chromatography and attenuated total reflection Fourier transform infrared spectroscopy and a very good agreement was found. As a conclusion, dielectric spectroscopy is suitable to follow the progress of reactions and identify the reaction endpoints. The only drawback is that the technique is very sensitive to temperature changes and any variation in the reaction temperature can affect the dielectric properties.

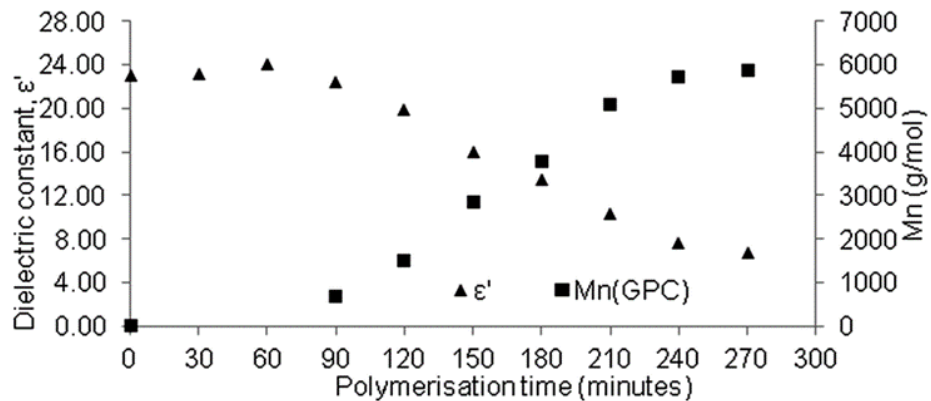


Figure 2.18: Dielectric constant (ϵ') at 2450 MHz and number average molecular weight (M_n) over time for ring-opening polymerisation (Kamaruddin *et al.*, 2014a).

Kamaruddin *et al.* (2014a) demonstrated the use of microwave dielectric spectroscopy in the monitoring of polymerisation reactions. In detail, the Ring Opening Polymerisation of ϵ -caprolactone was monitored online using a coaxial probe sensor. The results showed that the method can be used to predict the molecular weight of the polymer during the reaction with the help of a calibration curve. In Figure 2.18, the dielectric constant decreases with increasing molecular weight, indicating a dependence of the reaction mixture dielectric properties with

the concentration ratio of caprolactone monomer and polycaprolactone. In a later work, the authors verified the online dielectric property data with offline analysis using cavity perturbation method, Gel Permeation Chromatography, Nuclear Magnetic Resonance and Karl-Fisher titration. Key reaction features can also be identified such as reaction rates, the end points and induction periods (Kamaruddin *et al.*, 2014a).

Pissis *et al.* (2015) reported the use of broadband Dielectric Spectroscopy and electrical dc measurements in following the polymerisation and curing processes in polymer/clay nanocomposites. The reaction was followed in real time by Dielectric spectroscopy at 1, 10, 100, 500 and 1000 kHz using special comb electrodes as sensors. In Figure 2.19, conductance and capacitance versus time are plotted for neat cyanate ester at frequency of 1MHz and at 150 °C, 180 °C, 210 °C, 230 °C and 250 °C. The gelation and vitrification time as well as the degree of conversion were calculated for many polymer/carbon nanotubes nanocomposites with variable organic modification and fraction of clay. The results showed good agreement with the results using offline techniques such as Fourier Transform Infrared Spectroscopy and Differential Scanning Calorimetry.

Dielectric spectroscopy can be used for the real time monitoring of polymerisation reactions as well as the synthesis of resins and nanocomposite materials (Nahm, 2006; Kamaruddin *et al.*, 2014a; Pissis *et al.*, 2015). The main limitation of the technique is their sensitivity to temperature changes, which is a direct result of intermolecular interactions alteration with temperature. Additionally, most of dielectric spectroscopy apparatus require calibration (Gaiduk and McConnell, 1995).

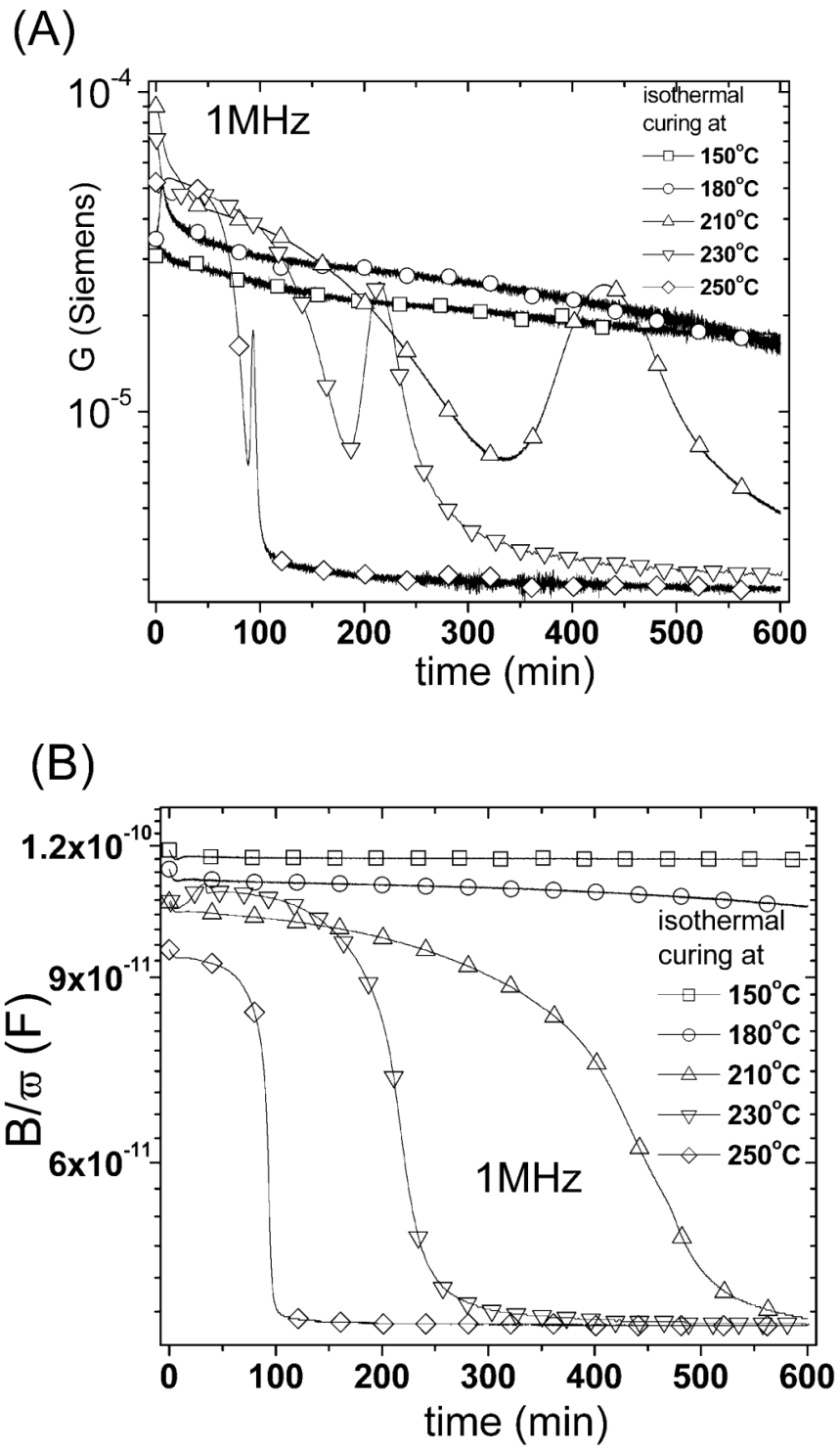


Figure 2.19: (A): Conductance (G , Siemens) versus time and (B): Capacitance (B/ω) versus time during isothermal curing of neat cyanate ester (Pissis et al., 2015).

2.9 Comparison of reaction monitoring techniques

During the last decades, many techniques for monitoring of chemical reactions have been developed. The use of UV-Visible spectroscopy to real time monitor chemical reactions is a relatively new development and is mainly used for the monitoring of liquid-phase reactions. It is also used in accordance to NIR, Raman and NMR for the in-line monitoring of the esterification of crotonic acid and butan-2-ol. In this case, NIR and NMR spectrometries found to be more precise in the prediction of the concentration of 2-butyl crotonate than Raman and UV-visible (McGill, Nordon and Littlejohn, 2002). The most common sources of error of UV-vis spectroscopy when it is used to extract kinetic parameters are the instrumental noise, the error in determining initial concentrations and error in the calibration of pure standards (Bakeev, 2010).

Infrared spectroscopy is one of the oldest techniques used to monitor chemical reactions in lab-based and industrial applications. In the form of mid-IR, NIR and Raman, vibrational spectroscopy is one of the most versatile techniques to study materials in any physical state. The physical form of the sample can be the deciding factor of the most suitable technique: for gas or vapour phase samples mid or near infrared methods are the most suitable, for liquid and solid samples a FTIR interferometer is the most suitable apparatus. For powder samples both Raman and NIR work well. The most common issues of vibrational spectroscopic techniques are the high background signals and stability. Fluorescence in raman spectra is the most common issue in Raman spectroscopy. Furthermore, black materials' spectra are usually degraded, burned, or damaged and it is difficult to collect Raman or mid and near infrared spectra because they are masked by the sample's blackbody radiation.

Additionally, the sample self-absorption, the phenomenon in which Raman scattering is absorbed by infrared absorption before it escapes the sample, affects the NIR region of the spectrum (Lewis and Edwards, 2001). However, IR and Raman spectra typically consist of sharper bands than UV-visible and can be used to identify specific compounds. NIR spectra can be obtained without sample preparation and along with FTIR have become a promising process monitoring technique in the pharmaceutical industry (Bakeev, 2010).

Nuclear Magnetic Resonance spectroscopy is one of the newest techniques that have been transformed from offline to online in industrial applications. Their applications in reaction monitoring were started from petroleum-related applications and expanded in other areas such as biofuels, food manufacturing and in the pharmaceutical area. The main limitation of NMR spectroscopy is that it can be greatly affected by the presence of paramagnetic materials such as iron. Furthermore, it is limited to the observation of proton nucleus chemistry. As a result, hetero and metallic chemistry cannot be observed directly. However, the combination of process NMR with other techniques such as electron spin resonance (ESR) helped to overcome those limitations and expand the applications of the technique in areas where paramagnetic metals or observation of free radicals is required. The relative sensitivity of NMR spectroscopy is lower than other analytical techniques such as UV-visible and FTIR spectroscopy and, consequently, limit its applications in areas where the observation of complex mixtures is required (Bakeev, 2010; Gomez and Hoz, 2017).

In the last decades, Differential Scanning Calorimetry have become a popular analytical method to follow reactions by continuous monitoring of the

temperature and heat flow during a process. Ulkowski *et al.* (2005) reported the use of DSC as a method to determine kinetic parameters in oxidation processes much faster than other techniques such as IR, NMR or Electron Spin Resonance. Recent advances in DSC techniques allowed the identification of structural thermodynamics of reaction intermediates as well as thermoanalytical parameters of biomolecules and nanomaterials and lead to applications in microfluidics, drug discovery, molecular biology and nanoscience (Gill, Moghadam and Ranjbar, 2010).

Mass spectrometry is another practical technique that can be used to real time determine reaction intermediates, products and investigate reaction mechanisms. The main limitation of the technique is the size, weight and complexity of instrumentation. The recent advancements in the instrumentation allowed the making of portable mass spectrometers (Llamas, Ojeda and Rojas, 2007). However, the major limitation of the method is the thermal stability and volatility of neutral compounds in gas-phase ion molecule reactions. Additionally, electrospray ionization mass spectrometry cannot be used to measure samples with high salt concentrations, due to the ESI emitter. Furthermore, the open-air environment used in some setups cannot be used for the online monitoring of air-sensitive reactions (Chen and Lin, 2015).

Dielectric Spectroscopy is a relatively new online reaction monitoring technique. Their non-invasive and non-destructive nature enabled the development of compact apparatus that can be implemented in the most common reactor geometries as a simple retrofit. Yang *et al.* (2014) reported the development of a dielectric sensor system for the on-line cure monitoring of composites. Dielectric spectroscopy is more flexible in terms of experimental setup and

configuration than other methods such as Dynamic Mechanical Analysis and Differential Scanning Calorimetry. Furthermore, it can be applied in large amounts of samples where DSC is not applicable. Dielectric spectroscopy methods have been successfully applied for the real time monitoring of polymerisation reactions as well as the synthesis of resins and nanocomposite materials (Nahm, 2006; Kamaruddin *et al.*, 2014a; Pissis *et al.*, 2015). The main limitations of the technique are that it is sensitive to temperature changes and requires calibration. The fundamentals of dielectric theory are discussed in chapter 3. In the following table (Table 1), a comparison of the techniques is presented, and the main advantages and limitations of each technique are highlighted.

Table 2.1: Comparison of monitoring techniques.

Technique	Advantages	Limitations	Type of sample	Commercial applications
UV-Visible spectroscopy	<ul style="list-style-type: none"> • High resolution UV spectrophotometers are suitable for use in on-line monitoring of chemical reactions (Gauglitz and Moore, 2014). • Fiber-optic probes are capable of in-situ sampling of a process (Bakeev, 2010). 	<ul style="list-style-type: none"> • The most common sources of error are the instrumental noise, the error in determining initial concentrations of the measured components, and the error in the calibration of pure standards (Bakeev, 2010). • Direct UV spectrophotometry cannot be easily applied to identify unknown 	<ul style="list-style-type: none"> • Gas and vapor analysis is possible through UV-visible absorption spectroscopy. For example, the use of optical fibres for the measurement of ozone concentration (O’Keeffe, Fitzpatrick and Lewis, 2007). • It has been used for liquid analysis, i.e. for measuring changes in concentration 	<ul style="list-style-type: none"> • Not yet fully entered industrial production for direct process analysis as spectra in this range are broader and less informative (Bakeev, 2010). • The introduction of ATR probes opened new possibilities for measurements on optically thick solutions (Reed and Alb, 2013).

Technique	Advantages	Limitations	Type of sample	Commercial applications
	<ul style="list-style-type: none"> The low cost and robustness of new UV spectrometers make them suitable to be applied in industrial processes (Gauglitz and Moore, 2014). 	<p>polymers/ additive mixtures and requires multivariate analysis to indicate the presence of more than one absorbing species (Bart, 2006).</p> <ul style="list-style-type: none"> Calibration of the absorbance measurements of the spectrophotometer is required (Clark, Frost and Russell, 1993). 	<p>and/or in composition of wastewater (Langergraber et al., 2006).</p> <ul style="list-style-type: none"> It has also been used for the in-situ characterisation of metal nanoparticles, such as gold nanoparticles (Salvati et al., 2005). 	

Technique	Advantages	Limitations	Type of sample	Commercial applications
Infrared spectroscopy	<ul style="list-style-type: none"> Infrared Spectroscopy is one of the oldest and most established analytical techniques. On-line techniques for process analysis are used in many laboratories (Bart, 2006) FTIR analysis can be performed in seconds, and can be used in high pressures and 	<ul style="list-style-type: none"> As most species have both UV and IR absorption spectra, UV and IR measurements are both necessary and complementary (Down and Lehr, 2005). NIR spectra can be affected by the sample self-absorption, the phenomenon in which raman scattering is absorbed by infrared absorption before it escapes 	<ul style="list-style-type: none"> Suitable for process analytical measurements for samples of all physical forms – solids, liquids, gases and mixed phase materials (Bakeev, 2010). It has a long history in polymerisation reaction monitoring such as in Free-Radical polymerisations and living radical polymerisations (Darcos, Monge and Haddleton, 	<ul style="list-style-type: none"> It is one of the oldest spectroscopic techniques for on-line or near-line monitoring in industrial applications (Bakeev, 2010). A variety of near and mid-IR in-situ probes are commercially available (Reed and Alb, 2013).

Technique	Advantages	Limitations	Type of sample	Commercial applications
	<p>temperatures for in-situ reaction monitoring (Hergeth, 2000).</p> <ul style="list-style-type: none"> • FTIR spectroscopy is a non-destructive, low cost and relatively simple technique which can be used to provide both qualitative and quantitative information (Bart, 2006). 	<p>the sample (Lewis and Edwards, 2001).</p> <ul style="list-style-type: none"> • FTIR spectroscopy requires sample preparation (grinding, pellet or film pressing) (Bart, 2006). • ATR-FTIR probe measurements are sensitive to temperature variations (Jovanovic and Dube, 2003). 	<p>2004; Sheibat-Othman, Peycelon and Févotte, 2004). However, it can present particular challenges in monitoring of homopolymerisations or copolymerisations due to the broad overlapping of bands for comonomers and associated copolymer (Reed and Alb, 2013)</p>	

Technique	Advantages	Limitations	Type of sample	Commercial applications
Raman spectroscopy	<ul style="list-style-type: none"> • It is a non-destructive, non-invasive technique which can be used for in-situ measurements (Bart, 2006). • It can be applied for the characterisation of almost any chemical substance (more universal than UV/ VIS spectroscopy) (Bart, 2006). 	<ul style="list-style-type: none"> • Fluorescence in raman spectra is the most common source of error. • Relatively high instrument cost. • Liquids or diluted solids show low sensitivity (Bart, 2006). 	<ul style="list-style-type: none"> • Raman spectroscopy performs well on compounds with double or triple bonds, isomers and sulfur-containing and symmetric species. It is also suitable for measurements of aqueous systems and polar solvents (Bakeev, 2010). • It is highly suitable for the analysis of solids. 	<ul style="list-style-type: none"> • The development of handheld Raman spectrometers allowed the measurements of samples through transparent packing such as glass or plastic (Gauglitz and Moore, 2014).

Technique	Advantages	Limitations	Type of sample	Commercial applications
			<ul style="list-style-type: none"> • It has been used for polymerisation reaction monitoring, i.e. in suspension polymerisation and emulsion copolymerisation (Brink et al., 2001; Santos et al., 2004). 	
Nuclear Magnetic Resonance Spectroscopy	<ul style="list-style-type: none"> • It is one of the most powerful non-destructive and non-invasive techniques for structural analysis of almost all type of 	<ul style="list-style-type: none"> • The two main problems encountered in high-resolution NMR techniques are line-broadening and low sensitive nuclei. 	<ul style="list-style-type: none"> • NMR spectroscopic techniques have proven useful for the monitoring of polymerisation reactions, especially for the determination of monomer 	<ul style="list-style-type: none"> • On-line coupling between a ¹H NMR spectrometer and a chemical reactor was first mentioned by BASF in 1986 (Neudert, Ströfer and Bremser, 1986). However,

Technique	Advantages	Limitations	Type of sample	Commercial applications
	<p>compounds (Bart, 2006).</p> <ul style="list-style-type: none"> • It can be used to study both the structure and dynamics of materials. 	<ul style="list-style-type: none"> • It requires sample extraction and usually preparation, i.e. by dissolving the sample in a solvent or pressing a polymer sample into a thin film (Reed and Alb, 2013). 	<p>composition and for providing insight into the sequence distribution of monomers in the polymer (Reed and Alb, 2013).</p>	<p>the requirements of process NMR analysers in a plant environment are quite different from those of laboratory instruments. For example, in a plant environment, NMR instrumentation needs to be robust and able to operate continuously in harsh environments, including automated sample introduction/removal, autotuning, temperature</p>

Technique	Advantages	Limitations	Type of sample	Commercial applications
				control, etc. For this reason the use of low-resolution NMR instrumentation is well-established in the polymer industry (Bart, 2006).
Differential Scanning Calorimetry	<ul style="list-style-type: none"> • It can be used to identify substances by reference to a characteristic transition temperature. • It is a powerful technique for structural 	<ul style="list-style-type: none"> • In general, thermal analysis is a powerful secondary technique. • DSC measurements are used for the interpretation of Dynamic Mechanical Analysis curves and provide 	<ul style="list-style-type: none"> • DSC has numerous applications in polymers, such as in determining the melting temperature, glass transition temperature, and transition temperatures (Bart, 2006). 	<ul style="list-style-type: none"> • Temperature modulated differential scanning calorimetry (MTDSC) was introduced commercially as an extension of DSC in which the linear or isothermal temperature

Technique	Advantages	Limitations	Type of sample	Commercial applications
	<p>analysis of polymeric materials, reflecting structural changes unique to substances composed of large extended chain molecules.</p> <ul style="list-style-type: none"> • A wide range of thermal analysis instruments are available that offer automation and are easy to use. 	<p>limited information regarding identification/quantification in polymer analysis.</p> <ul style="list-style-type: none"> • It requires sample preparation and a temperature calibration of thermobalance. 	<ul style="list-style-type: none"> • It has also been used for the detection of exothermic oxidation of plastics, such as of Acrylonitrile-butadiene-styrene (ABS) Resin Powder (Duh et al., 2010). 	<p>program is overlaid by temperature perturbation (Bart, 2006; Crompton, 2012)</p>

Technique	Advantages	Limitations	Type of sample	Commercial applications
Mass Spectrometry	<ul style="list-style-type: none"> • It is a highly sensitive analytical technique, capable of providing qualitative and quantitative analytical data on nanomolar to attomolar amounts of analyte (Mellon, 2003). • It has been successfully applied to a very wide range of analytical problems in the food and nutrition sciences. 	<ul style="list-style-type: none"> • Ion source contamination is the biggest limitation of the technique. • It is not suitable for multicomponent analysis of unknown compounds (Bart, 2006). 	<ul style="list-style-type: none"> • It is a powerful tool for the structural characterization of various biomolecules including proteins, nucleic acids, and carbohydrates (Vandell and Limbach, 2017). • Various MS methods have been used in macromolecular analysis to determine the absolute molar masses of homo- and copolymers and to detect 	<ul style="list-style-type: none"> • Mass spectrometry (MS) applications of an industrial or technical nature were first developed in the early 1940's for deducing the composition of a particular sample from its mass spectrum (Berry and Walker, 1955). • Nowadays it has many applications in the pharmaceutical and biomedical field i.e. for

Technique	Advantages	Limitations	Type of sample	Commercial applications
			<p>polymer structures (Cotter, 1997).</p> <ul style="list-style-type: none"> Matrix-assisted laser desorption/ionisation (MALDI) mass spectrometry is an established technique for measuring the molecular weight distribution of low molecular weight polymers and biopolymers (Reed and Alb, 2013). 	<p>structure elucidation of unknown compounds (Baghel et al., 2017).</p>

Technique	Advantages	Limitations	Type of sample	Commercial applications
Dielectric Spectroscopy	<ul style="list-style-type: none"> • A non-destructive, non-intrusive technique which can be used in-situ without any need for sample extraction and preparation. • It can be applied to the most common reactor geometries as a simple retrofit, e.g., by placing an open-ended coaxial line sensor directly into the reaction mixture. 	<ul style="list-style-type: none"> • It requires calibration prior to any measurement. The quality of calibration can significantly affect the results (Metaxas and Meredith, 1905). • The technique is sensitive to temperature changes. As the dielectric properties are temperature dependent, any change in the temperature can affect the measurements (Hill, 1969). 	<ul style="list-style-type: none"> • It can be used for determining the molecular structure (i.e. transitional mobility of ions and rotational mobility of dipoles in the presence of an electric field) of materials in liquid, amorphous, solid, crystalline and liquid-crystalline state (Bart, 2006). • Dielectric Spectroscopy is a powerful technique for 	<ul style="list-style-type: none"> • Dielectric Spectroscopy has been used to measure the octane number of gasoline (Gauglitz and Moore, 2014). • It has also been used in drug discovery processes which involves the measurement of the dielectric properties of biological particles in fluid suspension, i.e. the pharmacological evaluation of cell surface receptors in

Technique	Advantages	Limitations	Type of sample	Commercial applications
		<ul style="list-style-type: none"> • Reflectance methods such as an open ended coaxial line sensor require sufficient sample size and flat surface for proper contact (Huynh and Augustin, 2004). 	<p>studying heterogeneous materials. For example, if a heterogeneous material contains components with varied electrical conductivity, strong dielectric effects are detected (Bart, 2006).</p> <ul style="list-style-type: none"> • It can be applied in the monitoring of polymerisation reactions (Kalamiotis <i>et al.</i>, 2019a). 	<p>living cells (Leung <i>et al.</i>, 2005; Morgan <i>et al.</i>, 2006).</p>

2.10 Conceptual framework and research hypothesis

During the last few years, many off-line Process Analytical Chemistry techniques have been transformed into online to monitor and control chemical processes. However, the commercial applications of these techniques have been limited by a number of practical factors, with the key issue being the difficulty of the instrumentation to be installed in commercial reactors (Reed and Alb, 2013). Dielectric spectroscopy is a non-destructive technique which can be used “in-situ”, without any need of sample extraction and preparation. An open-ended coaxial line sensor can be easily incorporated into most industrial reactor geometries as a simple retrofit. The focus of this project is to develop methods to successfully follow the progress of chemical reactions using dielectric spectroscopy as the key monitoring technique.

2.11 Aims and objectives

The aim of this research is to investigate the use of dielectric spectroscopy as a method to follow the progress of chemical reactions in-situ in order to provide direct process control to modern continuous manufacturing techniques. Specific objectives to be achieved include:

- To understand the applicability of the technique in various chemical reactions. In detail, the ring opening polymerisation of ϵ -caprolactone was studied followed by the dehydration of sorbitol to sorbitan and isosorbide. Off-line measurements of styrene–divinylbenzene copolymers were carried out as a preliminary study to investigate the applicability of the technique in the monitoring of hyperbranched polymers.

- To analyse the dielectric data over a wide frequency and temperature spectrum, understand their effect on the dielectric properties and identify the most suitable frequency window for the practical operation of the sensor, in terms of linearity and sensitivity.
- To study the correlation between dielectric properties and key reaction parameters, such as identifying the optimum point to terminate the reaction to prevent the formation of by-products.

2.12 Research methodology

Key chemical reactions were studied to investigate the application of dielectric spectroscopy in monitoring of chemical reactions. The ring opening polymerisation ϵ -caprolactone was selected as the primary reaction to investigate the applicability of the technique in the monitoring of a typical chain-growth polymerisation. Findings in previous studies highlighted the potential use of dielectric spectroscopy in the monitoring of ϵ -caprolactone polymerisation. This reaction was used as the pilot reaction to develop the experimental setup and data collection techniques. The developed technique was then applied in the dehydration reaction of sorbitol to investigate the applicability of the technique in the monitoring of more rigid structures. Finally, hyperbranched polymers were studied to investigate the applicability of dielectric spectroscopy in differentiating materials with a three-dimensional shape with multiple chain end groups and dendritic architecture.

2.13 Conclusions

In this chapter, the most popular techniques for monitoring of chemical reactions have been presented. These methods – spectroscopic techniques cover a wide

region of the electromagnetic spectrum. Each method has its limitations and can be applicable in specific type of reactions. For example, the use of UV-Visible spectroscopy in monitoring of chemical reactions is mainly used for the monitoring of liquid-phase reactions. However, the presence of intermediates can be derived only hypothetically by using the fit of a model, such as the Alternating Least Squares model and no structural characterization of the compound can be achieved. Infrared spectroscopy is a widely used non-destructive analytical technique to monitor chemical reactions. It can be used in situ to monitor the progress of the reaction in real time. However, it is not the preferred technique to analyse aqueous solutions, as water is strong infrared absorber. Raman spectroscopy is more preferable than IR to monitor aqueous systems, since water is a poor Raman scatterer. NMR is one of the most powerful non-destructive and non-invasive techniques for off-line reaction monitoring. However, it requires expensive equipment and so far it has been mainly used at laboratory-level. DSC is a powerful secondary technique which can be used for the structural analysis of polymeric materials. Mass spectrometry is a powerful technique for the structural analysis of various biomolecules. However, ion source contamination is the biggest limitation of the technique the main limitation of the technique along with the fact that is not suitable for multicomponent analysis of unknown compounds. Dielectric spectroscopy is a non-invasive, non-destructive technique suitable for the monitoring of chemical transformations. Their main limitations are: (i) the need for sensor calibration, (ii) the fact that is sensitive to temperature changes, and (iii) reflectance methods require sufficient sample size and flat surface for good contact. It can be applied to the most common reactor geometries as a simple retrofit and is capable for

“in-situ” monitoring of key reaction parameters. In this study, dielectric spectroscopy was selected as the key monitoring technique for the in-situ monitoring of chemical reactions.

References

Anderson, L. A. and Franz, A. K. (2012) Real-Time Monitoring of Transesterification by ¹H NMR Spectroscopy: Catalyst Comparison and Improved Calculation for Biodiesel Conversion. **Energy & Fuels** 26(10): pp.6404–6410.

Baghel, U. S., Singh, A., Singh, D. and Sinha, M. (2017) Application of Mass Spectroscopy in Pharmaceutical and Biomedical Analysis. **Spectroscopic Analyses - Developments and Applications**.

Bakeev, K. A. (2010) **Process Analytical Technology: Spectroscopic Tools and Implementation Strategies for the Chemical and Pharmaceutical Industries**. John Wiley & Sons.

Bart, J. C. J. (2006) **Plastics Additives: Advanced Industrial Analysis**. IOS Press.

Benito-Lopez, F., Verboom, W., Kakuta, M., Gardeniers, J. (Han) G. E., Egberink, R. J. M., Oosterbroek, E. R., Berg, A. van den and Reinhoudt, D. N. (2005) Optical fiber-based on-line UV/Vis spectroscopic monitoring of chemical reaction kinetics under high pressure in a capillary microreactor. **Chemical Communications** 0(22): pp.2857–2859.

Brink, M. van den, Pepers, M., Herk, A. M. van and German, A. L. (2001) ON-LINE MONITORING AND COMPOSITION CONTROL OF THE EMULSION COPOLYMERIZATION OF VeoVA 9 AND BUTYL ACRYLATE BY RAMAN SPECTROSCOPY. **Polymer Reaction Engineering** 9(2): pp.101–133.

Cervera-Padrell, A. E., Nielsen, J. P., Jøneh Pedersen, M., Müller Christensen, K., Mortensen, A. R., Skovby, T., Dam-Johansen, K., Kiil, S. and Gernaey, K. V. (2012) Monitoring and Control of a Continuous Grignard Reaction for the Synthesis of an Active Pharmaceutical Ingredient Intermediate Using Inline NIR spectroscopy. **Organic Process Research & Development** 16(5): pp.901–914.

Chen, C.-C. and Lin, P.-C. (2015) Monitoring of chemical transformations by mass spectrometry. **Analytical Methods** 7(17): pp.6947–6959.

Chiu, M. H. and Prenner, E. J. (2011) Differential scanning calorimetry: An invaluable tool for a detailed thermodynamic characterization of macromolecules and their interactions. **Journal of Pharmacy and Bioallied Sciences** 3(1): pp.39–59.

Clark, B. J., Frost, T. and Russell, M. A. (1993) **UV Spectroscopy: Techniques, instrumentation and data handling**. Springer Science & Business Media.

Coffey, C., Cooley, B. E. and Walker, D. S. (1999) Real time quantitation of a chemical reaction by fiber optic near-infrared spectroscopy. **Analytica Chimica Acta** 395(3): pp.335–341.

Cotter, R. J. (1997) **Time-of-flight Mass Spectrometry: Instrumentation and Applications in Biological Research**. American Chemical Society.

Crompton, T. R. (2012) **Practical Polymer Analysis**. Springer Science & Business Media.

Darcos, V., Monge, S. and Haddleton, D. M. (2004) In situ Fourier transform near infrared spectroscopy monitoring of copper mediated living radical polymerization. **Journal of Polymer Science Part A: Polymer Chemistry** 42(19): pp.4933–4940.

Davies, M. (2007) **Dielectric and Related Molecular Processes**. Royal Society of Chemistry.

Deng, H., Shen, Z., Li, L., Yin, H. and Chen, J. (2014) Real-time monitoring of ring-opening polymerization of tetrahydrofuran via in situ Fourier Transform Infrared Spectroscopy. **Journal of Applied Polymer Science** 131(15): pp.n/a-n/a.

Desiderio, D. M. (1990) **Mass Spectrometry of Peptides**. CRC Press.

Down, R. D. and Lehr, J. H. (2005) **Environmental Instrumentation and Analysis Handbook**. John Wiley & Sons.

Duh, Y.-S., Ho, T.-C., Chen, J.-R. and Kao, C.-S. (2010) Study on Exothermic Oxidation of Acrylonitrile-butadiene-styrene (ABS) Resin Powder with Application to ABS Processing Safety. **Polymers** 2(3): pp.174–187.

Elfanso, E., Garland, M., Loh, K. C., Talukder, M. M. R. and Widjaja, E. (2010) In situ monitoring of turbid immobilized lipase-catalyzed esterification of oleic acid using fiber-optic Raman spectroscopy. **Catalysis Today**. (Recent Developments in Operando Spectroscopy) 155(3): pp.223–226.

Foley, D. A., Dunn, A. L. and Zell, M. T. (2015) Reaction monitoring using online vs tube NMR spectroscopy: seriously different results. **Magnetic Resonance in Chemistry** pp.n/a-n/a.

Fontoura, J. M. R., Santos, A. F., Silva, F. M., Lenzi, M. K., Lima, E. L. and Pinto, J. C. (2003) Monitoring and control of styrene solution polymerization using NIR spectroscopy. **Journal of Applied Polymer Science** 90(5): pp.1273–1289.

Gaiduk, V. I. and McConnell, J. R. (1995) **Dielectric Relaxation and Dynamics of Polar Molecules**. Singapore; River Edge, N.J.: World Scientific Publishing Co Pte Ltd.

Gauglitz, G. and Moore, D. S. (eds) (2014) **Handbook of Spectroscopy, 4 Volume Set**. John Wiley & Sons.

Gill, P., Moghadam, T. T. and Ranjbar, B. (2010) Differential Scanning Calorimetry Techniques: Applications in Biology and Nanoscience. **Journal of Biomolecular Techniques: JBT** 21(4): pp.167–193. Available at: <https://www.ncbi.nlm.nih.gov/pmc/articles/PMC2977967/> (Accessed: 12 April 2018).

Gomez, M. V. and Hoz, A. de la (2017) NMR reaction monitoring in flow synthesis. **Beilstein Journal of Organic Chemistry** 13(1): pp.285–300.

Gomez, M. V., Verputten, H. H. J., Díaz-Ortíz, A., Moreno, A., Hoz, A. de la and Velders, A. H. (2010) On-line monitoring of a microwave-assisted chemical reaction by nanolitre NMR-spectroscopy. **Chemical Communications** 46(25): pp.4514–4516.

Gouilleux, B., Charrier, B., Danieli, E., Dumez, J.-N., Akoka, S., Felpin, F.-X., Rodriguez-Zubiri, M. and Giraudeau, P. (2015) Real-time reaction monitoring by ultrafast 2D NMR on a benchtop spectrometer. **Analyst** 140(23): pp.7854–7858.

Haines, P. (ed.) (2002) **Principles of Thermal Analysis and Calorimetry**. Cambridge: Royal Society of Chemistry (RSC Paperbacks). Available at: <http://ebook.rsc.org/?DOI=10.1039/9781847551764> (Accessed: 21 April 2016).

Haines, P. J., Reading, M. and Wilburn, F. W. (1998) Chapter 5 - Differential Thermal Analysis and Differential Scanning Calorimetry. in Brown, M. E. (ed.) **Handbook of Thermal Analysis and Calorimetry**. Elsevier Science B.V. (Principles and Practice) pp.279–361.

Hambitzer, Guenther. and Heitbaum, Joachim. (1986) Electrochemical thermospray mass spectrometry. **Analytical Chemistry** 58(6): pp.1067–1070.

Hamlin, T. A. and Leadbeater, N. E. (2013) Raman spectroscopy as a tool for monitoring mesoscale continuous-flow organic synthesis: Equipment interface and assessment in four medicinally-relevant reactions. **Beilstein Journal of Organic Chemistry** 9: pp.1843–1852.

Hassell, D. C. and Bow, E. M. (1998) Process Analytical Chemistry for Spectroscopists. **Applied Spectroscopy** 52(1): pp.18A-29A. Available at: <https://www.osapublishing.org/abstract.cfm?uri=as-52-1-18A> (Accessed: 3 October 2017).

Haynie, D. T. (2001) **Biological Thermodynamics**. Cambridge University Press.

Hefke, F., Schmucki, R. and Güntert, P. (2013) Prediction of peak overlap in NMR spectra. **Journal of Biomolecular NMR** 56(2): pp.113–123.

Hergeth, W.-D. (2000) On-Line Monitoring of Chemical Reactions. in **Ullmann's Encyclopedia of Industrial Chemistry**. Wiley-VCH Verlag GmbH & Co. KGaA.

Hill, N. (1969) **Dielectric Properties and Molecular Behaviour**. London, New York: Van Nostrand Reinhold Inc., U.S.

Hoffmann, E. de and Stroobant, V. (2007) **Mass Spectrometry: Principles and Applications**. John Wiley & Sons.

Hofmann, M. P., Nazhat, S. N., Gbureck, U. and Barralet, J. E. (2006) Real-time monitoring of the setting reaction of brushite-forming cement using isothermal differential scanning calorimetry. **Journal of Biomedical Materials Research Part B: Applied Biomaterials** 79B(2): pp.360–364.

Huynh, J. and Augustin, D. (2004) Advances in probe development and calibration procedure enhance material measurements. in **Infrared and Millimeter Waves, Conference Digest of the 2004 Joint 29th International Conference on 2004 and 12th International Conference on Terahertz Electronics, 2004**. *Infrared and Millimeter Waves, Conference Digest of the 2004 Joint 29th International Conference on 2004 and 12th International Conference on Terahertz Electronics, 2004*. pp.215–216.

Jeanmaire, D. L. and Van Duyne, R. P. (1977) Surface raman spectroelectrochemistry: Part I. Heterocyclic, aromatic, and aliphatic amines adsorbed on the anodized silver electrode. **Journal of Electroanalytical Chemistry and Interfacial Electrochemistry** 84(1): pp.1–20.

Jovanovic, R. and Dube, M. A. (2003) Polymerization reaction monitoring for PSA production using an ATR-FTIR probe. **Adhesives & Sealants Industry**. Available at: <https://www.highbeam.com/doc/1G1-105476668.html> (Accessed: 5 April 2016).

Kalamiotis, A., Ilchev, A., Irvine, D. J. and Dimitrakis, G. (2019) Optimised use of dielectric spectroscopy at microwave frequencies for direct online monitoring of polymerisation reactions. **Sensors and Actuators B: Chemical** 290: pp.34–40.

Kamaruddin, M. J., Nguyen, N. T., Dimitrakis, G. A., Harfi, J. E., Binner, E. R., Kingman, S. W., Lester, E., Robinson, J. P. and Irvine, D. J. (2014) Continuous and direct 'in situ' reaction monitoring of chemical reactions via dielectric property measurement: controlled polymerisation. **RSC Advances** 4(11): pp.5709–5717.

Kandelbauer, A., Kessler, W. and Kessler, R. W. (2008) Online UV–visible spectroscopy and multivariate curve resolution as powerful tool for model-free investigation of laccase-catalysed oxidation. **Analytical and Bioanalytical Chemistry** 390(5): pp.1303–1315.

Kaur, H. (2014) **Spectroscopy**. Pragati Prakashan.

Khanlari, S. and Dubé, M. A. (2015) Reaction Monitoring of in Situ Formation of Poly(sodium acrylate)-Based Nanocomposites Using ATR-FTIR Spectroscopy. **Industrial & Engineering Chemistry Research** 54(21): pp.5598–5603.

Kneipp, K., Moskovits, M. and Kneipp, H. (2006) **Surface-Enhanced Raman Scattering: Physics and Applications**. Springer Science & Business Media.

Kupče, E., Nishida, T., Widmalm, G. and Freeman, R. (2005) Resolving overlap in two-dimensional NMR spectra: nuclear Overhauser effects in a polysaccharide. **Magnetic Resonance in Chemistry** 43(10): pp.791–794.

Langergraber, G., van den Broeke, J., Lettl, W. and Weingartner, A. (2006) Real-time detection of possible harmful events using UV/vis spectrometry. **Spectroscopy Europe** 18: pp.19–22.

Leadbeater, N. E. and Schmink, J. R. (2008) Use of Raman spectroscopy as a tool for in situ monitoring of microwave-promoted reactions. **Nature Protocols** 3(1): pp.1–7.

Leung, G., Tang, H. R., McGuinness, R., Verdonk, E., Michelotti, J. M. and Liu, V. F. (2005) Cellular Dielectric Spectroscopy: A Label-Free Technology for Drug Discovery. **JALA: Journal of the Association for Laboratory Automation** 10(4): pp.258–269.

Lewis, I. R. and Edwards, H. (2001) **Handbook of Raman Spectroscopy: From the Research Laboratory to the Process Line**. CRC Press.

Liauw, M. A., Baylor, L. C. and O'Rourke, P. E. (2010) UV-Visible Spectroscopy for On-Line Analysis. in **Process Analytical Technology**. John Wiley & Sons, Ltd pp.81–106.

Littleford, R. E., Graham, D., Smith, W. E. and Khan, I. (2019) Raman Spectroscopy | Surface-Enhanced☆. in Worsfold, P., Poole, C., Townshend, A., and Miró, M. (eds) **Encyclopedia of Analytical Science (Third Edition)**. Oxford: Academic Press pp.76–84.

Llamas, A. M., Ojeda, C. B. and Rojas, F. S. (2007) Process Analytical Chemistry—Application of Mass Spectrometry in Environmental Analysis: An Overview. **Applied Spectroscopy Reviews** 42(4): pp.345–367.

Lu, H., Schmidt, M. A. and Jensen, K. F. (2001) Photochemical reactions and on-line UV detection in microfabricated reactors. **Lab on a Chip** 1(1): pp.22–28.

McGill, C. A., Nordon, A. and Littlejohn, D. (2002) Comparison of in-line NIR, Raman and UV-visible spectrometries, and at-line NMR spectrometry for the monitoring of an esterification reaction. **Analyst** 127(2): pp.287–292.

McLennan, F. and Kowalski, B. R. (1995) **Process Analytical Chemistry**. Springer Science & Business Media.

Mellon, F. A. (2003) MASS SPECTROMETRY | Principles and Instrumentation. in Caballero, B. (ed.) **Encyclopedia of Food Sciences and Nutrition (Second Edition)**. Oxford: Academic Press pp.3739–3749.

Metaxas, A. C. and Meredith, R. J. (1905) **Industrial Microwave Heating**. London, UK: The Institution of Engineering and Technology.

Minnich, C. B., Buskens, P., Steffens, H. C., Bäuerlein, P. S., Butvina, L. N., Küpper, L., Leitner, W., Liauw, M. A. and Greiner, L. (2007) Highly Flexible Fibre-Optic ATR-IR Probe for Inline Reaction Monitoring. **Organic Process Research & Development** 11(1): pp.94–97.

Morgan, H., Sun, T., Holmes, D., Gawad, S. and Green, N. G. (2006) Single cell dielectric spectroscopy. **Journal of Physics D: Applied Physics** 40(1): pp.61–70.

Nahm, S. H. (2006) Use of dielectric spectroscopy for real-time in-situ reaction monitoring. **JCT Research** 3(4): pp.257–265.

Najbauer, E. E. and Andreas, L. B. (2019) Correcting for magnetic field drift in magic-angle spinning NMR datasets. **Journal of Magnetic Resonance** 305: pp.1–4.

Neudert, R., Ströfer, E. and Bremser, W. (1986) On-line NMR in process engineering. **Magnetic Resonance in Chemistry** 24(12): pp.1089–1092.

Nørgaard, A. W., Vaz, B. G., Lauritsen, F. R. and Eberlin, M. N. (2010) Real-time monitoring of the progress of polymerization reactions directly on surfaces at open atmosphere by ambient mass spectrometry. **Rapid Communications in Mass Spectrometry** 24(23): pp.3441–3446.

O’Keeffe, S., Fitzpatrick, C. and Lewis, E. (2007) An optical fibre based ultra violet and visible absorption spectroscopy system for ozone concentration monitoring. **Sensors and Actuators B-chemical - SENSOR ACTUATOR B-CHEM** 125: pp.372–378.

Pissis, P., Pandis, C., Maroulas, P., Kyritsis, A. and Kontou, E. (2015) Electrical/Dielectric Measurements for Monitoring Polymerization, Morphology and Mechanical Integrity in Polymer Nanocomposites. **Procedia Engineering**. (ICSI 2015 The 1st International Conference on Structural Integrity Funchal, Madeira, Portugal 1st to 4th September, 2015) 114: pp.598–605.

Pivonka, D. E. and Empfield, J. R. (2004) Real-time in situ Raman analysis of microwave-assisted organic reactions. **Applied Spectroscopy** 58(1): pp.41–46.

Reed, W. F. and Alb, A. M. (eds) (2013) **Monitoring Polymerization Reactions: From Fundamentals to Applications**. John Wiley & Sons.

Rees, O. J. (2011) **Fourier Transform Infrared Spectroscopy: Developments, Techniques & Applications**. New York: Nova Science Publishers Inc.

Reich, G. (2005) Near-infrared spectroscopy and imaging: Basic principles and pharmaceutical applications. **Advanced Drug Delivery Reviews**. (Non-Invasive Spectroscopic and Imaging Techniques in Drug Delivery) 57(8): pp.1109–1143.

Riebe, M. T. and Eustace, D. J. (1990) Process analytical chemistry. An industrial perspective. **Analytical Chemistry** 62(2): pp.65A-71A.

Roscioli, K. M., Zhang, X., Li, S. X., Goetz, G. H., Cheng, G., Zhang, Z., Siems, W. F. and Hill Jr., H. H. (2013) Real time pharmaceutical reaction monitoring by electrospray ion mobility-mass spectrometry. **International Journal of Mass Spectrometry** 336: pp.27–36.

Salehpour, S. and Dubé, M. A. (2012) Reaction Monitoring of Glycerol Step-Growth Polymerization Using ATR-FTIR Spectroscopy. **Macromolecular Reaction Engineering** 6(2–3): pp.85–92.

Salvati, R., Longo, A., Carotenuto, G., De Nicola, S., Pepe, G. P., Nicolais, L. and Barone, A. (2005) UV–vis spectroscopy for on-line monitoring of Au nanoparticles size during growth. **Applied Surface Science**. (4th International Conference on Photo-Excited Processes and Applications) 248(1): pp.28–31.

Santos, A., Cherfi, A., McKenna, T., Seytre, G., L. Lima, E., C. Pinto, J. and Fevotte, G. (2001) Inline Dielectric Monitoring of MMA/BuA Copolymerization Reactions. **CHIMIA International Journal for Chemistry** 55: pp.251–253.

Santos, J. C., Reis, M. M., Machado, R. A. F., Bolzan, A., Sayer, C., Giudici, R. and Araújo, P. H. H. (2004) Online Monitoring of Suspension Polymerization Reactions Using Raman Spectroscopy. **Industrial & Engineering Chemistry Research** 43(23): pp.7282–7289.

Santos, L. S., Knaack, L. and Metzger, J. O. (2005) Investigation of chemical reactions in solution using API-MS. **International Journal of Mass Spectrometry** 246(1–3): pp.84–104.

Serrano, B., Cabanelas, J. C., González-Benito, J., Baselga, J. and Bravo, J. (1997) Pyrene Fluorescence as a Probe for the Monitoring of Polymerization Processes: Simultaneous DSC and Fluorescence Study. **Journal of Fluorescence** 7(4): pp.341–345.

Sheibat-Othman, N., Peycelon, D. and Févotte, G. (2004) Monitoring and Control of Free-Radical Polymerizations Using Near-Infrared Spectroscopy. **Industrial & Engineering Chemistry Research** 43(23): pp.7383–7391.

Smith, B. C. (1995) **Fundamentals of Fourier Transform Infrared Spectroscopy**. CRC Press.

Stuart, B. H. (2004) **Infrared Spectroscopy: Fundamentals and Applications**. John Wiley & Sons.

Svensson, O., Josefson, M. and Langkilde, F. W. (1999) Reaction monitoring using Raman spectroscopy and chemometrics. **Chemometrics and Intelligent Laboratory Systems** 49(1): pp.49–66.

Swier, S. and Van Mele, B. (2003) In situ monitoring of reaction-induced phase separation with modulated temperature DSC: comparison between high-T_g and low-T_g modifiers. **Polymer** 44(9): pp.2689–2699.

Tasumi, M. (2014) **Introduction to Experimental Infrared Spectroscopy: Fundamentals and Practical Methods**. John Wiley & Sons.

Ulkowski, M., Musialik, M. and Litwinienko, G. (2005) Use of Differential Scanning Calorimetry To Study Lipid Oxidation. 1. Oxidative Stability of Lecithin and Linolenic Acid. **Journal of Agricultural and Food Chemistry** 53(23): pp.9073–9077.

Vandell, V. E. and Limbach, P. A. (2017) Overview of Biochemical Applications of Mass Spectrometry. in Lindon, J. C., Tranter, G. E., and Koppenaal, D. W. (eds) **Encyclopedia of Spectroscopy and Spectrometry (Third Edition)**. Oxford: Academic Press pp.514–516.

Vasilakos, S. P. and Tarantili, P. A. (2017) In situ monitoring by DSC and modeling of curing of vinyl polysiloxanes in layered silicate nanocomposites. **Journal of Thermal Analysis and Calorimetry** 127(3): pp.2049–2058.

Venardou, E., Garcia-Verdugo, E., Barlow, S. J., Gorbaty, Y. E. and Poliakoff, M. (2004) On-line monitoring of the hydrolysis of acetonitrile in near-critical water using Raman spectroscopy. **Vibrational Spectroscopy** 35(1–2): pp.103–109.

Wolf, U., Leiberich, R. and Seeba, J. (1999) Application of infrared ATR spectroscopy to in situ reaction monitoring. **Catalysis Today** 49(4): pp.411–418.

Workman, J., Koch, M., Lavine, B. and Chrisman, R. (2009) Process Analytical Chemistry. **Analytical Chemistry** 81(12): pp.4623–4643.

Yang, Y., Chiesura, G., Luyckx, G., Vervust, T., Bossuyt, F., Kaufmann, M., Degrieck, J. and Vanfleteren, J. (2014) Development of a Dielectric Sensor System for the On-line Cure Monitoring of Composites. **Procedia Technology**. (2nd International Conference on System-Integrated Intelligence: Challenges for Product and Production Engineering) 15: pp.631–637.

Yu, K.-O. (2001) **Modeling for Casting and Solidification Processing**. CRC Press.

Zaikin, V. and Halket, J. M. (2009) **A Handbook of Derivatives for Mass Spectrometry**. IM Publications.

Zhu, Z., Bartmess, J. E., McNally, M. E., Hoffman, R. M., Cook, K. D. and Song, L. (2012) Quantitative Real-Time Monitoring of Chemical Reactions by Autosampling Flow Injection Analysis Coupled with Atmospheric Pressure

Chemical Ionization Mass Spectrometry. **Analytical Chemistry** 84(17):
pp.7547–7554.

3 DIELECTRIC THEORY

3.1 Introduction

In order to understand the dielectric behaviour of materials, it is essential to go through the conceptual background of dielectric theory. The aim of this chapter is to describe the fundamentals of dielectric theory which will be used for the dielectric characterisation of the materials under study. The mechanism of interaction between microwave radiation and matter will be explained, followed by the fundamentals of dielectric theory including polarisation mechanisms, the complex permittivity and their frequency, temperature, humidity, and density dependence. Finally, the principal theories for the calculation of static permittivity of an isotropic polar material under a constant or very slowly changing field will be presented followed by the models for complex permittivity when the applied field alternates with frequency.

3.2 Interaction between microwave radiation and matter

An electromagnetic wave consists of an electric (E) and a magnetic field (H) which are perpendicular to each other and to the direction of propagation, as shown in Figure 3.1. Microwaves are electromagnetic waves in the frequency range from 300 MHz to 300 GHz which correspond to wavelengths from 1 millimeter to 1 meter (Metaxas and Meredith, 1905; Sorrentino, Bianchi and Chang, 2010).

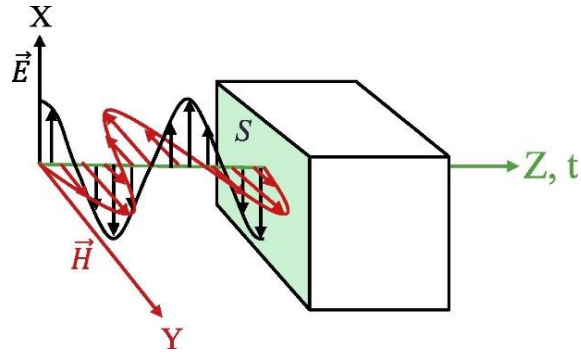


Figure 3.1: Electromagnetic wave propagation through a surface S (Muhibbullah, Haleem and Ikuma, 2017)

Materials can be classified into conductors, insulators, magnetic compounds and dielectrics, depending on the way they interact with electromagnetic waves (Mujumdar, 2014). Conductors are materials with free electrons that reflect electromagnetic waves, such as metals. Insulators, such as glass, ceramics and air are materials which absorb the electromagnetic waves. Magnetic compounds are materials that interact only with the magnetic component of the electromagnetic wave. Dielectrics are materials that have very few free charge carriers and their atoms or molecules exhibit a dipole movement (Jones *et al.*, 2002).

3.3 Fundamentals of Dielectric Theory

Dielectrics are insulating materials such that their charges are polarized when they are subjected to a high frequency electromagnetic field. The theory of polarisation was first introduced by P. J. W. Debye (1929). His book refers to polar molecules, the molecules which have a permanent electric dipole moment. An electric dipole consists of a positive (+q) and a negative charge (-q),

separated by a short distance (l), as shown in Figure 3.2. The electric dipole moment (μ) can be defined as (Riande and Diaz-Calleja, 2004):

$$\mu = ql \quad (3.1)$$

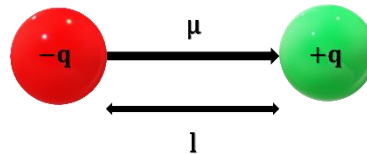


Figure 3.2: Electric dipole moment

3.3.1 Polarisation mechanisms

The interaction of a dielectric material with an alternating electric field, has its origin in the response of bound charge particles to the applied field. In detail, the bound charged particles tend to leave their equilibrium positions, rotate, align with the applied field, and form induced dipoles. There are four main mechanisms of such induced polarisation: electronic, atomic, dipolar and interfacial polarisation (Metaxas and Meredith, 1905).

Electronic polarisation occurs when the center of the electron cloud around the nuclei, under the presence of an electric field, is displaced leading to a dipole moment. Due to their small inertia, electrons can follow the applied electric field up to frequencies close to the visible light, as shown in Figure 3.3 (Mitchell, 2004).

Atomic polarisation is caused by the relative displacement of atomic nuclei relative to another nuclei in a molecule, due to an external electric field. This

polarisation mechanism occurs predominantly at frequencies around 10¹² Hz, in the infrared frequency region (Choudhary and Patri, 2009).

Dipolar or orientation polarisation is the most important mechanism in the microwave frequency range and is found in polar dielectrics. Polar dielectrics are materials with molecules having a permanent dipole moment such as water, and alcohols. When such a material is subjected to an alternating electric field, the permanent dipoles tend to reorientate parallel to the field (Cravotto and Carnaroglio, 2017).

Interfacial or space charge or Maxwell-Wagner polarisation is common in heterogeneous systems and is associated with trapped and mobile charges. It occurs when free charges located in interfaces between components, due to the application of an electric field, displaced where the discontinuity occur. As a result of the movement and charge build-up of free charges, the polarisation occurs at low frequencies below the radiofrequency region of the electromagnetic spectrum (Metaxas and Meredith, 1905).

The ability of the material to undergo each mechanism of polarisation is called polarisability (α). The total polarisability of the medium is:

$$a = a_e + a_a + a_d + a_{MW} \quad (3.2)$$

where $\alpha_e, \alpha_a, \alpha_d, \alpha_{MW}$ are the electronic, atomic, dipole and Maxwell-Wagner polarisabilities respectively (Mitchell, 2004).

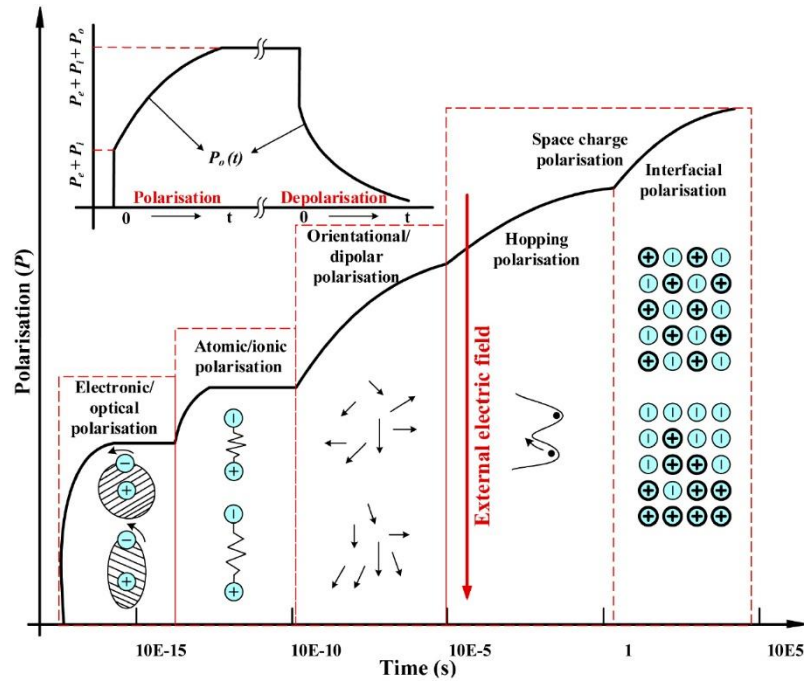


Figure 3.3: Polarisation types of normal dielectric materials under an external electric field (Guo et al., 2016).

Figure 3.3 shows the polarisation types of a dielectric material under an external electric field. In microwave heating applications, dipolar polarisation is the dominant mechanism present because the decay of the polarisation is similar to the oscillation periods of the field (Choudhary and Patri, 2009). Additionally, ionic conductivity is the main heating mechanism even for materials with small amounts of free charge carriers. Free charge carriers such as ions can move and collide with each other generating heat by ohmic effects (Metaxas and Meredith, 1905).

3.3.2 Dielectric properties

The dielectric properties describe the interaction of materials with an applied electromagnetic field. An elementary analysis to demonstrate the nature of

complex permittivity is presented in this section. Ampere's law, as described in equation 3.3 contains all the necessary components needed for this analysis.

$$\nabla \times \mathbf{H} = \mu_0 \mathbf{J} \quad 3.3$$

where μ_0 is the permeability of free space and \mathbf{J} is the total current per unit area. Maxwell modified Ampere's law for static fields by including a displacement current density term caused by the rate of change of the total electric flux passing through a surface S' bounded by l (Metaxas and Meredith, 1905). According to Maxwell's modification in Ampere's circuital law, the total current in a medium is:

$$\oint \frac{\mathbf{B}}{\mu_a} dl = \int_{S'} J_c dS' + \int_{S'} \frac{d}{dt} (\epsilon_0 \epsilon' \mathbf{E}) dS' \quad (3.4)$$

where B is the magnetic flux density, J_c is the current density due to ohmic effects and μ_a is the medium's permeability.

If we have a sinusoidal electromagnetic field, the electric field can be expressed as $E_{max} e^{j\omega t}$ and the total current density is:

$$\nabla \times \mathbf{H} = \sigma \mathbf{E} + j\omega \epsilon_0 \epsilon' \mathbf{E} \quad (3.5)$$

where σ is the conductivity of the medium, ϵ_0 is the dielectric constant of free space and ϵ' is the relative dielectric constant.

By combining equations 3.3 and 3.5 the total current per unit area is:

$$\mathbf{J} = j\omega \epsilon_0 \epsilon_c^* \mathbf{E} \quad (3.6)$$

where ϵ_c^* is the effective permittivity of the medium:

$$\epsilon_c^* = \epsilon' - \frac{j\sigma}{\omega \epsilon_0} = \epsilon' - j\epsilon_c'' \quad (3.7)$$

Equation 3.7 considers only ohmic loss. However, we can include all forms of losses:

$$\varepsilon'' = \varepsilon_e'' + \varepsilon_a'' + \varepsilon_d'' + \varepsilon_{MW}'' + \varepsilon_c'' \quad (3.8)$$

where ε'' is the loss factor, ε_e'' , ε_a'' , ε_d'' , ε_{MW}'' , ε_c'' are the electronic, atomic, dipolar, Maxwell-Wagner and ohmic loss forms respectively. Therefore, from equations 3.7 and 3.8 the complex permittivity (ε^*) is:

$$\varepsilon^* = \varepsilon' - j\varepsilon'' \quad (3.9)$$

where the real part is the dielectric constant (ε') and expresses the ability of the material to store energy under the presence of an external electric field and the imaginary part, the loss (ε''), includes all forms of losses and denotes the ability of the material to dissipate the stored energy into heat. The ratio of dielectric loss to dielectric constant is called loss tangent or dissipation factor. It is the ratio of the energy lost to the energy stored and determines the ability of the material to absorb and convert the applied electromagnetic energy into heat:

$$\tan\delta = \frac{\varepsilon''}{\varepsilon'} \quad (3.10)$$

3.3.3 Factors affecting the permittivity

The dielectric properties of materials depend on several factors. The frequency of the applied field and the temperature of the material are two of the most important parameters and will be extensively discussed in the following chapters. In hygroscopic materials, the moisture content can significantly affect the dielectric properties. In granular or particulate materials, the bulk density of the air-particle mixture can affect the permittivity and dielectric mixture

equations can be used to estimate the dielectric properties (Nelson, 1994; Komarov, 2012).

As it has been previously discussed, when a material is subjected to an electric field, the polarisation mechanism is dependent on the frequency of the field. As a result, the complex permittivity will be dependent on the frequency of the applied field. Dipolar or orientation polarisation is the dominant mechanism in the microwave region (Metaxas and Meredith, 1905). In heterogenous materials, when more than one polarisation mechanisms exist, a more complex behaviour of material's dielectric properties is observed, which is discussed in section 3.5.

The temperature dependency of permittivity is based on the influence of temperature in molecular mobility and intermolecular forces which affect the ability of the material to store and dissipate energy. When heat is applied, the increased molecular mobility result to a weakening of material's intermolecular forces (Nelson, 1994). As the temperature increases, the loss peak and the relaxation frequency shift to higher frequencies while the relaxation time decreases, as shown in Figure 3.5. In this figure, the dielectric constant and loss are plotted against log frequency at temperatures T_1 and T_2 , where $T_2 > T_1$.

The amount of water absorbed in a material can significantly influence the dielectric properties at low temperatures. In general, the water content of a material can be in free or bound state. Bound water can be physically absorbed to the surface of a dry material or chemically combined with other molecules and gives rise to losses at much lower frequencies than free water which exhibit in cavities and capillaries (Metaxas and Meredith, 1905).

3.4

3.4 Static Permittivity Theories

When a material is subjected to a constant or very slowly changing electric field, all types of polarization remain in equilibrium with it (Hill, 1969). In this section, the theories for the calculation of static permittivity of an isotropic polar material under a constant field will be presented.

3.4.1 Debye's theory

Debye's theory of static permittivity was the first model based on molecular considerations. It suggests that dielectric materials contain polar molecules and every molecule is spherical with constant electric dipole moment μ situated at the center. The normalised permittivity obtained by Debye's Model is:

$$\left(\frac{\epsilon_s - 1}{\epsilon_s + 2}\right) \left(\frac{M}{\rho}\right) = \frac{4\pi N}{3\epsilon} \left(\alpha + \frac{\mu^2}{3kT}\right) \quad (3.11)$$

where ϵ_s is the static permittivity, M is the molecular weight of the sample, ρ is the density, N is Avogadro's constant, α is the polarizability, μ is the dipole moment, k is the Boltzmann's constant and T is the temperature.

Debye's theory specifies the molar polarizability for non-polar materials and defines that it should be dependent on the density of the material but independent of temperature and pressure changes (Debye, 1929; Hill, 1969; Gaiduk and McConnell, 1995).

3.4.2 Onsager's theory

Onsager reported that the molecule can be assumed as a polarizable point dipole at the center of a spherical cavity with a radius α . As a result, this theory can be

applied in fluids without the dependence of Debye's equation in density (Hill, 1969). The static permittivity will be:

$$\frac{(\varepsilon_s - n^2)(2\varepsilon_s + n^2)}{\varepsilon_s(n^2 + 2)^2} = \frac{4\pi N\mu^2}{9kT\varepsilon} \quad (3.12)$$

where n is the refractive index. Onsager theory is based on the assumption that there are no interactions between the molecules or dipoles. However, it can be applied to liquids and organic compounds with weak intermolecular interactions.

Kirkwood and Fröhlich developed fully statistical theories to determine the short-range dipole-dipole interactions (Kao, 2004; Riande and Diaz-Calleja, 2004).

3.4.3 Kirkwood's theory

The Kirkwood's theory includes the distortion polarization by attributing a polarizability to each dipole and approximating the local field acting on a dipole by Onsager's cavity field (Hill, 1969). According to Kirkwood's equation for non-polarizable dipoles, the permittivity can be obtained as follows:

$$\frac{(\varepsilon_s - 1)(2\varepsilon_s + 1)}{3\varepsilon_s} = \frac{4\pi N}{\varepsilon V} \frac{g\mu^2}{3kT} \quad (3.13)$$

Where N/V is the number of atoms, molecules or unit cells per unit volume, and g is the correlation factor which is a measure of the local ordering of the material.

If the material has a known structure, the calculation of g is possible. Otherwise it can be roughly estimated from the permittivity and dipole moment of the material (Kao, 2004).

3.4.4 Fröhlich's theory

Fröhlich's theory for static permittivity can be compared to Debye's theory but it takes into account a non-polarizable continuum of permittivity. The static permittivity is given by

$$\frac{(\varepsilon_s - n^2)(2\varepsilon_s + n^2)}{\varepsilon_s(n^2 + 2)^2} = \frac{4\pi N g \mu_g^2}{9kTV\varepsilon} \quad (3.14)$$

where μ_g is the external moment of a non-polarizable dipole, and n^2 is the permittivity. In Fröhlich's model both deformational polarization and short-range intermolecular interactions are considered.

Kirkwood and Fröhlich's theories can be applied to liquids with strong interactions between molecules or dipoles. The main limitation is that a detailed knowledge of the liquid structure is required for the calculation of correlation factor (Riande and Diaz-Calleja, 2004).

3.5 Complex permittivity models

In the previous section, the permittivity was calculated for the case where the external field is constant or slowly changing. In this section, the frequency dependence of permittivity is taken into account for applied fields which alternate with frequency. The complex permittivity models can be applied to predict the dielectric properties of a material at frequencies higher or lower than the measured frequency range. As a result, the values of static and infinite permittivity as well as the relaxation frequency and time can be extracted. In chapter 5, the ε -caprolactone monomer data are fitted to the models described

below to identify the most suitable model to describe the dielectric behaviour of the material.

3.5.1 Debye Model

Peter Josef William Debye (1929) formed a theory for polar liquids, which is also applicable for most homogeneous materials. The complex permittivity according to Debye's equation is:

$$\varepsilon^* = \varepsilon_\infty + \frac{\varepsilon_s - \varepsilon_\infty}{1 + j\omega\tau} \quad (3.15)$$

where ε_s , ε_∞ is the dielectric constant at low and very high frequencies, also called static and infinite permittivity respectively, τ is the relaxation time and ω the angular frequency.

Separating the real and imaginary parts of equation 3.17 we obtain (Metaxas and Meredith, 1905):

$$\varepsilon' = \varepsilon_\infty + \frac{\varepsilon_s - \varepsilon_\infty}{1 + \omega^2\tau^2} \quad (3.16)$$

$$\varepsilon'' = \frac{(\varepsilon_s - \varepsilon_\infty)\omega\tau}{1 + \omega^2\tau^2} \quad (3.17)$$

Figure 3.4 shows the dielectric response of a real dielectric material compared to the ideal Debye response. S. Cole, R. H. Cole and D. W. Davidson formed models to describe the permittivity of complex molecules, as described below.

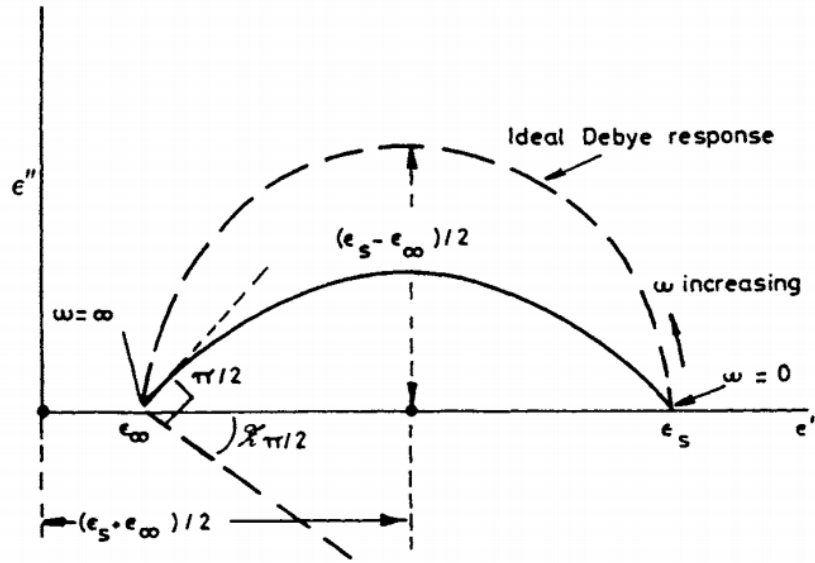


Figure 3.4: Cole-Cole plot for an ideal and non-ideal Debye response (dashed and solid lines respectively) (Metaxas and Meredith, 1905).

3.5.2 Cole-Cole Model

Debye's model for complex permittivity is suitable for simple molecules. Long chain molecules and polymers show a distribution of relaxation times compared to the Debye's single relaxation time. As a result, the representation of dielectric loss over constant differs compared to the Debye's semicircle. In brief, the maximum loss is lower, and the curve is broader than a semicircle. K. S. Cole and R. H. Cole (1941) described the behaviour of complex permittivity according to the following equation:

$$\epsilon^* = \epsilon_{\infty} + \frac{\epsilon_s - \epsilon_{\infty}}{1 + (j\omega\tau)^{1-a}} \quad (3.18)$$

where τ is the relaxation time and a is a constant, $0 \leq a \leq 1$. For $a = 0$, equation 3.18 becomes the Debye's equation.

Separating the real and imaginary parts of equation 3.18 we obtain (Cole and Cole, 1941):

$$\varepsilon'(\omega) = \varepsilon_{\infty} + (\varepsilon_s - \varepsilon_{\infty}) \frac{1 + (\omega\tau)^{1-\alpha} \sin \frac{1}{2} a\pi}{1 + 2(\omega\tau)^{1-\alpha} \sin \frac{1}{2} a\pi + (\omega\tau)^{2(1-\alpha)}} \quad (3.19)$$

$$\varepsilon''(\omega) = (\varepsilon_s - \varepsilon_{\infty}) \frac{(\omega\tau)^{1-\alpha} \cos \frac{1}{2} a\pi}{1 + 2(\omega\tau)^{1-\alpha} \sin \frac{1}{2} a\pi + (\omega\tau)^{2(1-\alpha)}} \quad (3.20)$$

3.5.3 Cole-Davidson Model

D. W. Davidson and R. H. Cole (1950) suggested a model which describes the behaviour of certain materials such as glycerine. This behaviour, compared to Cole-Cole arc, is like a skewed ark, as shown in Figure 3.5. The complex permittivity according to Cole-Davidson model is:

$$\varepsilon^* = \varepsilon_{\infty} + \frac{\varepsilon_s - \varepsilon_{\infty}}{1 + (j\omega\tau)^{\beta}} \quad (3.21)$$

where β is a constant, $0 \leq \beta \leq 1$. For $\beta = 1$ equation 3.21 will reduce to Debye equation. For values $\beta < 1$ the Cole-Cole arc will become asymmetrical. Figure 3.5 shows the dielectric response of glycerine at -50°C .

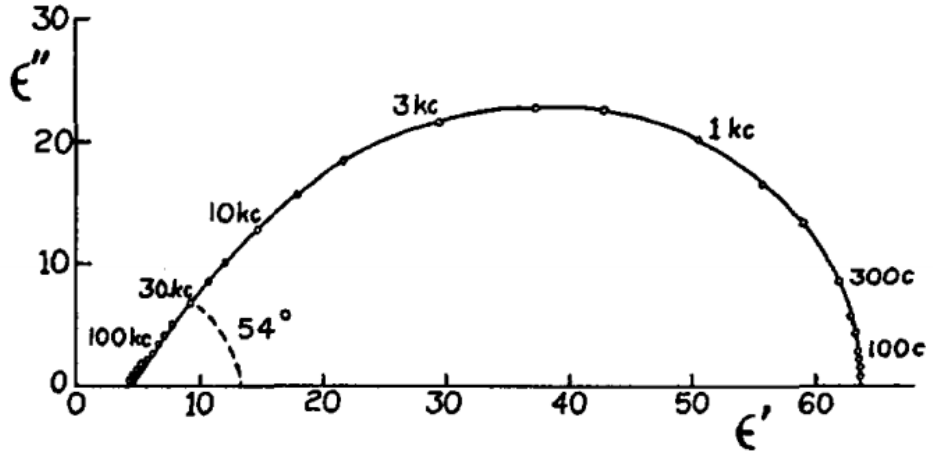


Figure 3.5: : Cole-Cole plot of glycerine at -50°C (Davidson and Cole, 1950).

Separating the real and imaginary parts of equation 3.24 we obtain:

$$\varepsilon'(\omega) = \varepsilon_{\infty} + (\varepsilon_s - \varepsilon_{\infty}) \cos\varphi^{\beta} \cos\beta\varphi \quad (3.22)$$

$$\varepsilon''(\omega) = (\varepsilon_s - \varepsilon_{\infty}) \cos\varphi^{\beta} \sin\beta\varphi \quad (3.23)$$

3.5.4 Havriliak-Negami Model

S. Havriliak and S. Negami (1969) proposed a generalised form of Cole-Cole and Cole-Davidson dielectric models:

$$\varepsilon^* = \varepsilon_{\infty} + \frac{\varepsilon_0 - \varepsilon_{\infty}}{(1 + (i\omega\tau)^{1-\alpha})^{\beta}} \quad (3.24)$$

where α , β are constants uniquely related to the distribution of relaxation times, $0 \leq \alpha \leq 1$ and $0 \leq \beta \leq 1$. For $\beta = 1$ equation 3.24 is reduced to Cole-Cole model equation. For $\alpha = 0$ we obtain the Cole-Davidson model and if $\alpha = 0$ and $\beta = 1$, equation 3.24 will be reduced to the Debye's equation. The constants α , β determines the shape of the relaxation and the relaxation time τ the angular frequency of the relaxation, where $\omega = 2\pi f = 1/\tau$. The Havriliak-

Negami model can give a much better fit to many experimental results if α and β parameters are properly determined (Kao, 2004).

3.6 Relaxation frequency and time

When an electric field is present, the dipoles of the material tend to reorientate and align with the direction of the field. The time that it takes for the dipoles to become 63% oriented with an applied electromagnetic field or vice versa the time required to return to disorder after the external field is removed is called dielectric relaxation time, τ (Kingston and Jassie, 1988). The maximum loss due to dipole rotation for many materials will occur at the relaxation frequency, $\omega = 1/\tau$, where ω is the angular frequency ($\omega = 2\pi f_c$). As a result, the relaxation time, τ (sec), is inversely related with the relaxation frequency, f (Hz):

$$\tau = \frac{1}{2\pi f_c} \quad (3.25)$$

The relaxation time is dependent on the molecular size and the viscosity of the medium. According to Debye, by using the Stokes' theorem, the relaxation time of a spherical molecule rotating in a viscous medium is:

$$\tau = \frac{4\pi r^3 \eta}{k_b T} \quad (3.26)$$

where r is the radius of the dipoles, η is the viscosity of the medium and k_b is the Boltzmann constant (Gabriel *et al.*, 1998). If the Mossotti local field is taken into account, the relaxation time can be calculated as follows:

$$\tau_e = \frac{\epsilon_s + 2}{\epsilon_\infty + 2} \tau \quad (3.27)$$

where τ_e is the effective relaxation time.

Pure polar materials exhibit a single relaxation time and can be represented by a semicircle in a ϵ'' versus ϵ' diagram, as shown in Figure 3.6. This representation is known as Cole-Cole diagram and the points of intersection with the horizontal axis, where $\epsilon'' = 0$, are the infinite and static permittivities accordingly. Infinite permittivity represents the dielectric constant at very high frequencies, where there is no contribution of molecular orientation to the polarisation. Static permittivity represents the dielectric constant in a static field (Nelson, 1994).

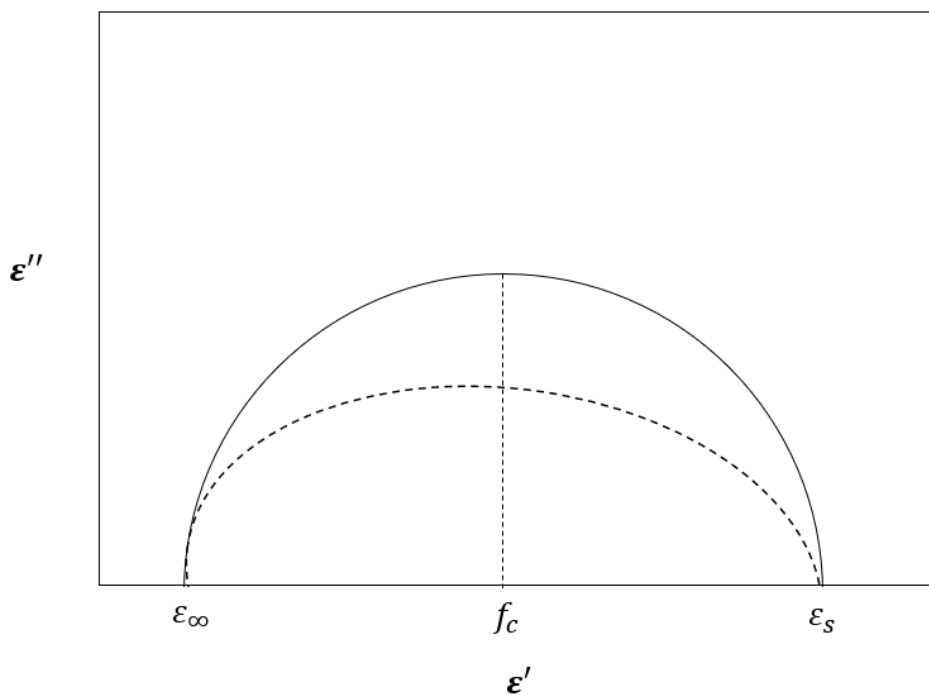


Figure 3.6: Cole-Cole plot of a pure polar material (solid line), and non-ideal Debye material (dashed line).

In Figure 3.6 the Cole-Cole plot for liquids with simple structure (solid line) is a semicircle and can be described by Debye model. For materials with a distribution of relaxation times such as glycerol (dashed line), Cole-Cole plot is a skewed arc and is described by Cole-Davidson model. The difference of arc

shape is a result of co-operative effects within the dielectric (Choudhary and Patri, 2009).

3.7 Dielectric mixture equations

The amount of mass interacting with the electric field can influence the dielectric properties. Granular or pulverised materials can be considered as a solid and air-particle mixture and the permittivity is dependent on the mass per unit volume or density. As a result, a sample with high packing density, which is the ratio of the total volume of the sample to the volume of containers, will exhibit high permittivity (Wu, Fan and Lu, 2003; Nelson and Trabelsi, 2012). For these materials, several dielectric mixture equations have been developed to estimate the permittivity of a mixture with two or more compounds. Dielectric mixture equations can be used to calculate the relationship between the permittivity of a solid material and the air-particle mixture of the pulverised particles of the solid (Nelson, Kraszewski and You, 1991). Several mixture equations have been reported in the literature to estimate the dielectric properties of an air-particle mixture. In this section, equations for two-component mixtures are discussed. In the annotation used here, particles with a complex permittivity of ϵ_2 are dispersed in a medium with complex permittivity ϵ_1 and v_1, v_2 are the volume fractions of the respective components.

The Complex Refractive Index mixture equation provide a reliable method to estimate the complex permittivity of granular and powdered materials with characteristics like grain products (Nelson and Trabelsi, 2012):

$$(\epsilon)^{\frac{1}{2}} = v_1(\epsilon_1)^{\frac{1}{2}} + v_2(\epsilon_2)^{\frac{1}{2}} \quad (3.28)$$

The Landau, Lifshitz, Looyenga equation implies the additivity of the cube roots of the permittivities of the two mixture components, each one multiplied by their volume fraction, and provide a closer estimation of the dielectric properties of pulverized materials such as pulverized coal, kernel wheat and ground wheat (Nelson, 1983):

$$(\varepsilon)^{\frac{1}{3}} = v_1(\varepsilon_1)^{\frac{1}{3}} + v_2(\varepsilon_2)^{\frac{1}{3}} \quad (3.29)$$

The Lichtenecker mixture equation has been used to estimate the permittivity of mixtures with particles of arbitrary shape such as compressed bread samples (Nelson, 1988; Liu, Tang and Mao, 2009):

$$\ln \varepsilon = v_1 \ln \varepsilon_1 + v_2 \ln \varepsilon_2 \quad (3.30)$$

One of the most commonly used equations to provide the dielectric properties of two-phase mixtures is the Rayleigh mixing formula (Robinson and Friedman, 2003; Behari, 2006):

$$\frac{\varepsilon - \varepsilon_1}{\varepsilon + 2 \varepsilon_1} = v_2 \frac{\varepsilon_2 - \varepsilon_1}{2 \varepsilon_1 + \varepsilon_2} \quad (3.31)$$

Böttcher's formula is another equation correlating the dielectric properties of powder and bulk materials, which found to give good results for low permittivity samples with particle sizes in the range 50 μm – 150 μm (Dube and Parshad, 1970):

$$\frac{\varepsilon - \varepsilon_1}{3 \varepsilon} = v_2 \frac{\varepsilon_2 - \varepsilon_1}{\varepsilon_2 + 2\varepsilon} \quad (3.32)$$

Another dielectric mixture equation applicable to a two-phase mixture is the Bruggeman-Hanai formula, in which there is no difference between the two phases of the mixture (Sihvola, 1999):

$$\frac{\varepsilon - \varepsilon_2}{\varepsilon_1 - \varepsilon_2} \left(\frac{\varepsilon_1}{\varepsilon} \right)^{\frac{1}{3}} = 1 - v_2 \quad (3.33)$$

In Table 3.1, the complex permittivity of the solid material is calculated using the above mixing formulas by substituting the complex permittivity of air ($1 - i0$).

Table 3.1: Complex permittivity of solid materials based on mixing formulas

Mixing rule	Equation
Complex Refractive Index:	$\varepsilon_2 = \left(\frac{\varepsilon^{1/2} + v_2 - 1}{v_2} \right)^2$
Landau, Lifshitz, Looyenga:	$\varepsilon_2 = \left(\frac{\varepsilon^{1/3} + v_2 - 1}{v_2} \right)^3$
Lichtenecker:	$\varepsilon_2 = \exp\left(\frac{\ln \varepsilon}{v_2}\right)$
Rayleigh:	$\varepsilon_2 = \frac{v_2(\varepsilon + 2) + 2(\varepsilon - 1)}{v_2(\varepsilon + 2) - (\varepsilon - 1)}$
Böttcher:	$\varepsilon_2 = \frac{\varepsilon[3v_2 + 2(\varepsilon - 1)]}{3v_2\varepsilon - (\varepsilon - 1)}$
Bruggeman-Hanai:	$\varepsilon_2 = \frac{1 - v_2 - \varepsilon^{2/3}}{1 - v_2 - \varepsilon^{-1/3}}$

3.8 Conclusions

The principles of dielectric theory have been discussed. A dielectric material, when subjected to an external electric field, becomes polarised. The type of this induced polarisation depends on the type of charges excited and can be electronic, atomic, dipolar, or interfacial. The dielectric properties of materials consist of the dielectric constant and loss, which includes all forms of losses according to the existing types of polarisation. The frequency, temperature, pressure, moisture, and density dependence of dielectric properties have been discussed. A detailed study of the effect of temperature and frequency on the dielectric properties for each chemical reaction is presented on the following chapters.

The frequency dependence of permittivity was described by empirical dielectric relaxation models as well as the graphic representation of ϵ'' versus ϵ' , which is called Cole - Cole plot. For materials with polar molecules which exhibit a single relaxation time, Debye model is the most suitable and the Cole - Cole plot is a semicircle. For long chain molecules, such as polymers, Cole-Cole model is the most suitable and the ϵ'' versus ϵ' curve falls inside the Debye semicircle. Cole-Davidson and Havriliak-Negami models can be used to describe the permittivity of complex materials with a distribution of relaxation times. In this case the Cole - Cole plot is a circular skewed arc. In Chapter 5, Debye, Cole-Cole and Cole-Davidson models are used to describe the complex permittivity of ϵ -caprolactone by iteratively fitting the measured complex permittivity values to a modelled counterpart.

References

- Behari, J. (2006) **Microwave Dielectric Behaviour of Wet Soils**. Springer Science & Business Media.
- Choudhary, R. N. P. and Patri, S. K. (2009) **Dielectric Materials: Introduction, Research and Applications**. New York: Nova Science Pub Inc.
- Cole, K. S. and Cole, R. H. (1941) Dispersion and Absorption in Dielectrics I. Alternating Current Characteristics. **The Journal of Chemical Physics** 9(4): pp.341–351.
- Cravotto, G. and Carnaroglio, D. (2017) **Microwave Chemistry**. Walter de Gruyter GmbH & Co KG.
- Davidson, D. W. and Cole, R. H. (1950) Dielectric Relaxation in Glycerine. **The Journal of Chemical Physics** 18(10): pp.1417–1417.
- Debye, P. J. W. (1929) **Polar Molecules**. Re Issue edition. Dover.
- Dube, D. C. and Parshad, R. (1970) Study of Böttcher's formula for dielectric correlation between powder and bulk. **Journal of Physics D: Applied Physics** 3(5): pp.677.
- Gabriel, C., Gabriel, S., Grant, E. H., Grant, E. H., Halstead, B. S. J. and Mingos, D. M. P. (1998) Dielectric parameters relevant to microwave dielectric heating. **Chemical Society Reviews** 27(3): pp.213–224.
- Gaiduk, V. I. and McConnell, J. R. (1995) **Dielectric Relaxation and Dynamics of Polar Molecules**. Singapore; River Edge, N.J.: World Scientific Publishing Co Pte Ltd.
- Guo, J., Bamber, T., Chamberlain, M., Justham, L. and Jackson, M. (2016) Optimization and experimental verification of coplanar interdigital electroadhesives. **Journal of Physics D: Applied Physics** 49(41): pp.415304.
- Hill, N. (1969) **Dielectric Properties and Molecular Behaviour**. London, New York: Van Nostrand Reinhold Inc., U.S.
- Jones, D. A., Lelyveld, T. P., Mavrofidis, S. D., Kingman, S. W. and Miles, N. J. (2002) Microwave heating applications in environmental engineering—a review. **Resources, Conservation and Recycling** 34(2): pp.75–90.
- Kao, K.-C. (2004) **Dielectric Phenomena in Solids: With Emphasis on Physical Concepts of Electronic Processes**. Academic Press.
- Kingston, H. M. and Jassie, L. B. (1988) **Introduction to Microwave Sample Preparation: Theory and Practice**. American Chemical Society.
- Komarov, V. V. (2012) **Handbook of Dielectric and Thermal Properties of Materials at Microwave Frequencies**. Artech House.

- Liu, Y., Tang, J. and Mao, Z. (2009) Analysis of bread dielectric properties using mixture equations. **Journal of Food Engineering** 93(1): pp.72–79.
- Metaxas, A. C. and Meredith, R. J. (1905) **Industrial Microwave Heating**. London, UK: The Institution of Engineering and Technology.
- Mitchell, B. S. (2004) **An Introduction to Materials Engineering and Science for Chemical and Materials Engineers**. John Wiley & Sons.
- Mujumdar, A. S. (2014) **Handbook of Industrial Drying, Fourth Edition**. CRC Press.
- Nelson, S., Kraszewski, A. and You, T. (1991) Solid and particulate material permittivity relationships. **Journal of Microwave Power and Electromagnetic Energy** 26(1): pp.45–51. Available at: https://www.researchgate.net/publication/292864342_Solid_and_particulate_material_permittivity_relationships (Accessed: 24 May 2016).
- Nelson, S. O. (1983) Observations on the Density Dependence of Dielectric Properties of Particulate Materials. **Journal of Microwave Power** 18(2): pp.143–152.
- Nelson, S. O. (1988) Estimating the Permittivity of Solids from Measurements on Granular or Pulverized Materials. **MRS Online Proceedings Library Archive** 124.
- Nelson, S. O. (1994) Measurement of microwave dielectric properties of particulate materials. **Journal of Food Engineering** 21(3): pp.365–384.
- Nelson, S. O. and Trabelsi, S. (2012) Factors Influencing the Dielectric Properties of Agricultural and Food Products. **Journal of Microwave Power and Electromagnetic Energy** 46(2): pp.93–107.
- Riande, E. and Diaz-Calleja, R. (2004) **Electrical Properties of Polymers**. CRC Press.
- Robinson, D. A. and Friedman, S. P. (2003) A method for measuring the solid particle permittivity or electrical conductivity of rocks, sediments, and granular materials. **Journal of Geophysical Research** 108.
- Sihvola, A. H. (1999) **Electromagnetic Mixing Formulas and Applications**. IET.
- Sorrentino, R., Bianchi, G. and Chang, K. (2010) **Microwave and RF Engineering**. New York, UNITED KINGDOM: John Wiley & Sons, Incorporated.
- Wu, Y., Fan, Z. and Lu, Y. (2003) Bulk and interior packing densities of random close packing of hard spheres. **Journal of Materials Science** 38(9): pp.2019–2025.

4 EXPERIMENTAL METHODS

4.1 Introduction

This chapter details the experimental methods used for the monitoring of chemical reactions presented in this thesis. Dielectric spectroscopy was used as the key monitoring technique for the dielectric characterization of precursors, reaction mixtures and products. Additionally, it was used to follow the reaction progress, target conversion and the end-point through a comparison of the real time measurements with off line techniques. Proton nuclear magnetic resonance spectroscopy (^1H NMR) and Gel Permeation Chromatography (GPC) were used for the off-line molecular analysis of reaction mixtures and products in order to determine the number and weight average molecular weight, dispersity (Đ), and level of conversion.

4.2 Dielectric property measurements

Various techniques were used for the measurement of the dielectric properties of materials. The choice of the most appropriate technique for a specific application depends on a number of factors such as the required accuracy, frequency, temperature, destructive or non-destructive, cost of the measurement system, material size, nature and its physical and electrical properties (Jilani, Khan and Ali, 2012). The most commonly used methods for dielectric property measurements in the microwave and radio frequency region are: the open-ended coaxial line, the cavity perturbation technique, waveguide, coaxial line, and the free space transmission method (Clarke *et al.*, 2003). In this thesis, the open-

ended coaxial line and the cavity perturbation technique were selected as the most appropriate methods for the online and offline measurement of the dielectric properties of precursors, reaction mixtures and products but also to follow the reaction progress, level of conversion and identify the reaction end point when the target conversion have reached. The open-ended coaxial line (probe) was selected as the optimum method for online monitoring as it can be fitted into any of the existing reactors eliminating the need for setup modification. The probe is submerged into the reaction mixture, without any need for sample extraction. Additionally, the probe is suitable for small reactors as it requires a small sample size (minimum 5 mm insertion and 5 mm around the tip of probe) (Keysight Technologies).

4.2.1 Open-ended coaxial line technique

The open-ended coaxial line technique is a common reflectometric method which is based on the measurement of complex reflection coefficient from which the dielectric properties of lossy materials can be determined at a broad frequency and temperature range (Gregory and Clarke, 2006). It was selected as the most suitable technique for the monitoring of chemical reactions because of its unique advantages as listed below:

- A non-destructive technique that allows the direct measurement of the dielectric properties by placing a coaxial sensor directly into the reaction mixture without any need for sample extraction and preparation (Kamaruddin *et al.*, 2011).
- It is the preferable method for measuring polar liquids with high accuracy (Nelson and Bartley Jr, 1997).

- A broadband method that covers a broad range of radio frequencies and allows the calculation of complex permittivity at low and high frequencies. As a result, the best frequency for the monitoring of each reaction can be determined (Kremer and Schönhals, 2002).

A coaxial sensor, also referred to as an open-ended coaxial line or just coaxial probe consists of a coaxial line and a flanged end, as shown in Figure 4.1 (Gregory and Clarke, 2007).

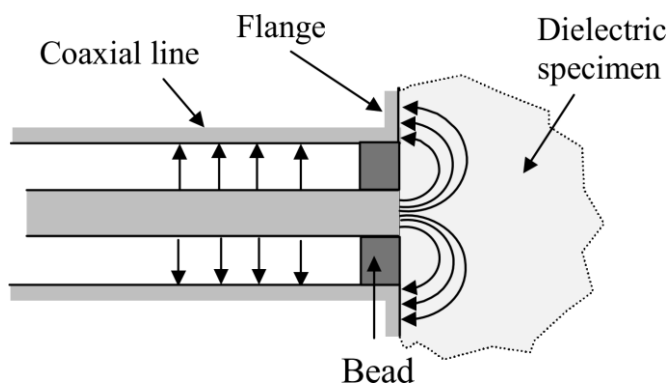


Figure 4.1: Schematic diagram of a coaxial probe (Gregory and Clarke, 2006).

The determination of the dielectric response of the reaction mixture was conducted with the use of an Agilent 85070E open ended coaxial probe sensor connected to an Agilent N4691B electronic calibration module. The electronic calibration module was connected with a Keysight N5232A PNA-L Vector Network Analyser (VNA) through a flexible cable. Figure 4.2 shows the experimental set up and apparatus, along with a schematic diagram where the coaxial line sensor and the electric field configuration is shown. A magnetic stirrer bar was used for mixing during the reaction progress. The probe was made of stainless steel (T316L body and T304L tip) and the dielectric insert of the

probe was made of borosilicate glass. The construction of the sensor took the form of a 9.5 mm coaxial line with an inner nickel-plated tungsten center conductor of 1.6 mm and was capable of operating in the frequency range from -40 °C up to 200 °C. The (typical) accuracy of the probe at 23 ± 3 °C is:

$$\varepsilon' = \varepsilon' \pm 0.05|\varepsilon^*| \quad (4.1)$$

$$\varepsilon'' = \varepsilon'' \pm 0.05|\varepsilon^*| \quad (4.2)$$

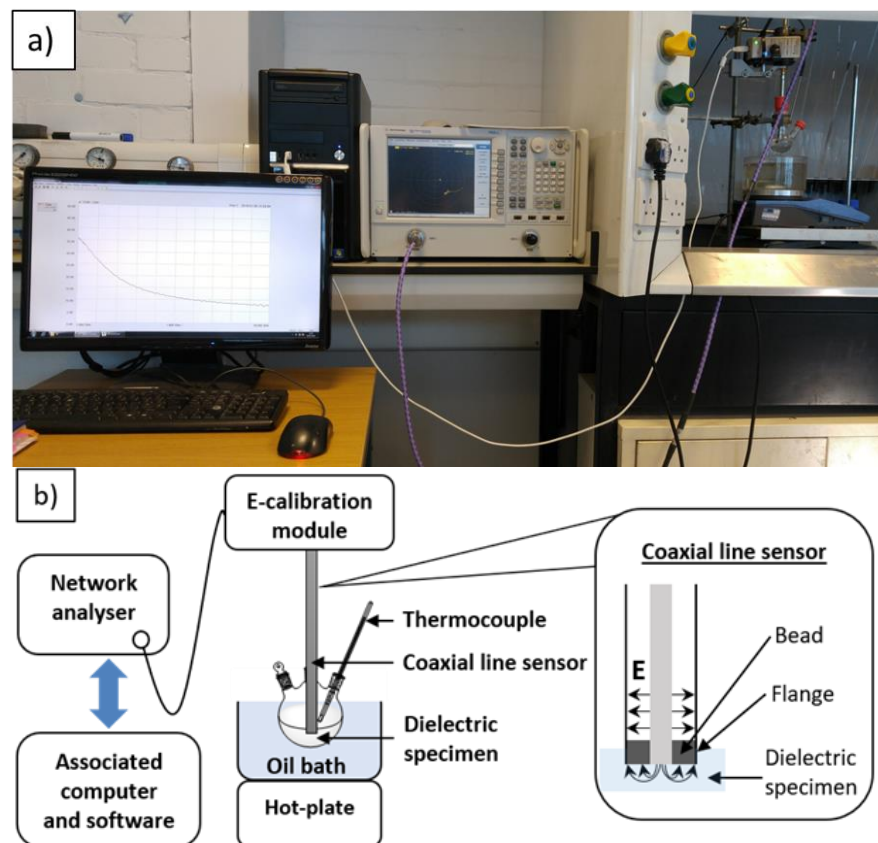


Figure 4.2: Experimental setup and apparatus, b) Schematic diagram of experimental set up.

The probe was immersed into the reaction mixture and a sweeping signal (0.5 GHz - 20 GHz) transmitted from the VNA, through the probe, into the reaction mixture. Depending on the dielectric properties of the sample, a portion

of that signal was reflected back and the VNA was used to measure the reflection coefficient. The true reflection coefficient is related to the measured reflection coefficient as follows (Kraszewski, Stuchly and Stuchly, 1983):

$$\Gamma = \frac{\rho_m - S_{11}}{S_{22}\rho_m + S_{12}S_{21} - S_{11}S_{22}} \quad 4.3$$

$$S_{11} = \frac{\Gamma_1\Gamma_2\rho_3(\rho_1 - \rho_2) + \Gamma_1\Gamma_3\rho_2(\rho_3 - \rho_1) + \Gamma_2\Gamma_3\rho_1(\rho_2 - \rho_3)}{\Gamma_1\Gamma_2(\rho_1 - \rho_2) + \Gamma_1\Gamma_3(\rho_3 - \rho_1) + \Gamma_2\Gamma_3(\rho_2 - \rho_3)} \quad 4.4$$

$$S_{22} = \frac{\Gamma_1(\rho_2 - S_{11}) + \Gamma_2(S_{11} - \rho_1)}{\Gamma_1\Gamma_2(\rho_2 - \rho_1)} \quad 4.5$$

$$S_{12}S_{21} = \frac{(\rho_1 - S_{11})(1 - S_{22}\Gamma_1)}{\Gamma_1} \quad 4.6$$

where Γ is the true complex reflection coefficient, $S_{11}, S_{12}, S_{21}, S_{22}$ are the scattering parameters of the network, $\Gamma_1, \Gamma_2, \Gamma_3$ are the reflection coefficients of the three standards used for calibration, ρ_m is the measured reflection coefficient, and ρ_1, ρ_2, ρ_3 are the measured reflection coefficients corresponding to the calibration standards.

Three calibration standards with known electrical properties (complex permittivity) were used to improve the accuracy of the measurements obtained with the probe; open line (air), short-circuited line (calibration short tool) and a reference liquid of known dielectric response (water). The reflection coefficients of the three standards are:

$$\Gamma_1 = -1 \quad 4.7$$

$$\Gamma_2 = e^{-j^2 \arctan(\omega C_T Z_0)} \quad 4.8$$

$$\Gamma_3 = \frac{1 - j\omega C_0 Z_0 \varepsilon' - j\omega C_f Z_0}{1 + j\omega C_0 Z_0 \varepsilon' + j\omega C_f Z_0} \quad 4.9$$

where Γ_1 is the reflection coefficient of short-circuited line, Γ_2 is the reflection coefficient of the open line and Γ_3 is the one for the reference liquid, ω is the angular frequency ($\omega = 2\pi f$), C_f is the capacitance due to the fringing fields inside the coaxial line, C_0 is the capacitance associated with the air part of the sensor, Z_0 is the characteristic capacitance of the coaxial line, and ε' is the complex permittivity of the reference liquid.

By using dimensional analysis, the relationship between the admittance of the probe scaled by the frequency is a function of a single dimensionless variable (Bartley *et al.*, 2004)

$$wy = \mathbf{F}(w\sqrt{\varepsilon}) \quad 4.10$$

where w is the measurement angular frequency, y is the admittance of the probe, ε is the material permittivity, and \mathbf{F} is the functional relationship between wy and $w\sqrt{\varepsilon}$.

The quality of calibration and short-circuit measurements were assessed by plotting the residual calibration errors for the whole frequency range investigated (Gregory and Clarke, 2007). The calibration was repeated if the residual errors were larger than 2%. As an additional step to ensure the quality of calibration, water and methanol samples were measured and their dielectric properties were compared with the literature (Gregory and Clarke, 2012).

4.2.2 Cavity Perturbation Technique

The cavity perturbation technique is a popular method to measure the dielectric properties of low loss materials (Metaxas and Meredith, 1905). It is based on the measurements of the shift in the resonant frequency and quality factor when a material is placed inside a resonant cavity. This method was selected to off-line measure the dielectric properties of samples according to the following criteria:

- It is the preferred method to measure low loss materials such as polymers.
- It is the most preferable method for measuring powders and pulverised samples.
- It is the preferred method for materials in which the total volume of the available sample is too small to be measured with the probe.

The method is based on the measurement of the frequency and quality factor shift caused by the insertion of the sample into the cavity. The quality factor is a dimensionless parameter which refers to the ratio of stored energy in a resonator to the dissipated energy to the resonator in one period of a cyclic process (Horner *et al.*, 1946; Smith, 1986):

$$Q = 2\pi \frac{\text{energy stored}}{\text{energy lost per cycle}} \quad (4.3)$$

The change in the resonant frequency is used in the calculation of the dielectric constant and the quality factor shift is used for loss calculation according to the following equations (Li, Akyel and Bosisio, 1981; Al-Harashseh *et al.*, 2009):

$$\varepsilon' = 1 + 2 J_1^2(X_{l,m}) \frac{\bar{V}_o}{\bar{V}_s} \frac{f_o - f_s}{f_o} \quad (4.4)$$

$$\varepsilon'' = J_1^2(X_{l,m}) \frac{\bar{V}_o}{\bar{V}_s} \left(\frac{1}{Q_s} - \frac{1}{Q_0} \right) \quad (4.5)$$

where $X_{l,m}$ is the m^{th} root of the first order Bessel function J_1 ($J_1(x)=0$), \bar{V}_s is the volume of the sample in mm^3 , \bar{V}_o is the volume of the cavity (mm^3), f_0 and f_s are the resonance frequencies of the empty and loaded with the sample cavity in Hz, Q_0 and Q_s are the quality factors of the empty and loaded cavity.

The experimental setup, as shown in Figure 4.3, consists of a cylindrical copper cavity of height 5 cm and diameter 57 cm resonating in the transverse magnetic modes (TM_{0n0}) occurring at 400 MHz, 912 MHz, 1429 MHz, 1949 MHz and 2470 MHz. Those operating modes were selected according to the industrial, scientific and medical (ISM) frequencies permissible in the UK (ITU, 2016). A Carbolite® tube furnace, capable of operating at temperatures up to 1300 °C is placed above the cavity to allow measurements at elevated temperatures. A step motor with a clamp is used to move the sample holder between the cavity and furnace.

The cavity is connected to a HP 8753B Vector Network Analyser to record the quality factor and frequency shift. A computer with a customized program was used to control the system and record the data. The samples were placed into quartz tubes.

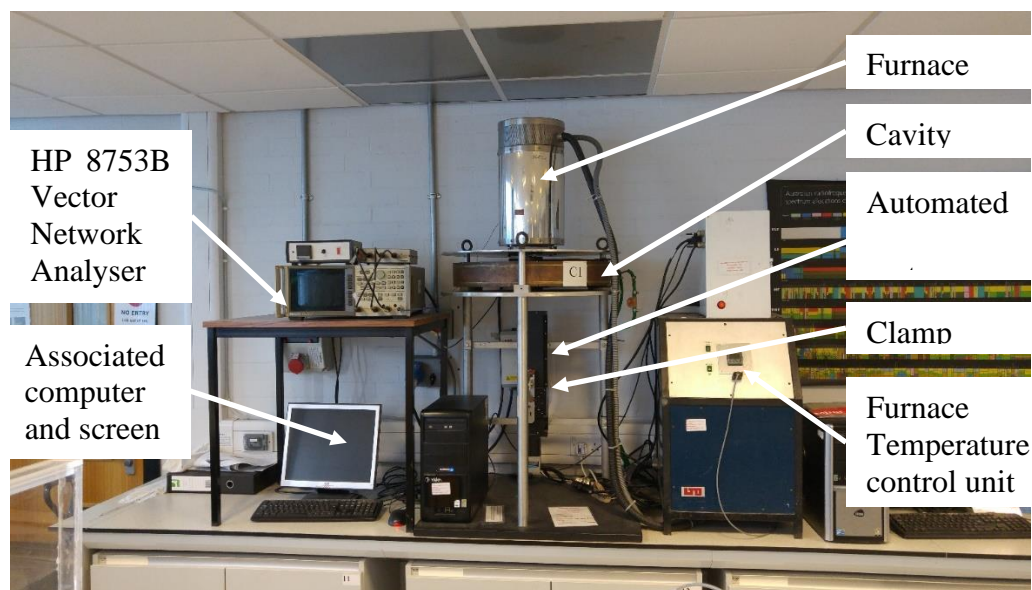


Figure 4.3: Cavity apparatus

4.3 Nuclear Magnetic Resonance spectroscopy

Nuclear Magnetic Resonance spectroscopy (NMR) is a very popular technique for the determination of the chemical structure of molecules (Bower, 2002). The NMR signal arises from a quantum mechanical property of nuclei called ‘spin quantum number (I)’. NMR spectroscopy utilises nuclei with an I equal to $\frac{1}{2}$, such as ^1H , ^{13}C , ^{19}F , and ^{31}P . ^1H and ^{13}C NMR spectra are the most commonly used for the analysis of organic compounds (Silverstein *et al.*, 2014). When protons are placed in a magnetic field, they can adopt two possible spin states where the energy difference between them is shown in Figure 4.4. The energy difference between the two states is dependent of the nucleus, the gyromagnetic ratio (γ) and the strength (B) of the external magnetic field. NMR spectroscopy observes the transition between these spin states and interprets this behaviour for different protons in frequency shift signal (Stuart, 2002).

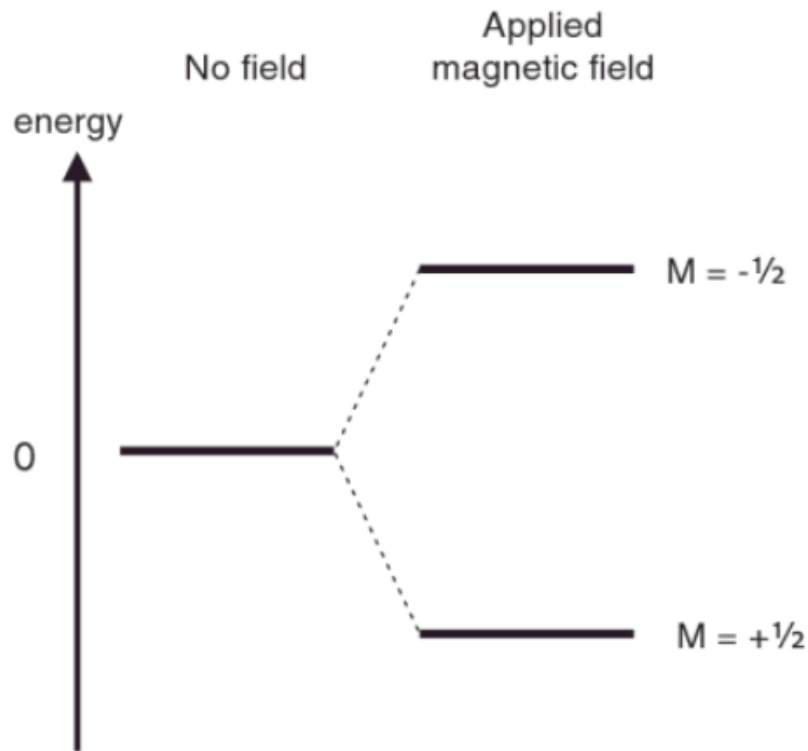


Figure 4.4: Energy levels of spin $\frac{1}{2}$ nucleus (Richards and Hollerton, 2010).

The relationship of the energy level of proton with the magnetic field strength and the frequency of radiation required to effect a transition between the energy states are shown in equations 4.6 and 4.6:

$$\Delta E = \frac{\gamma h B}{2\pi} \quad (4.5)$$

$$\nu = \frac{\gamma B}{2\pi} \quad (4.6)$$

where ΔE is the energy difference between spin states, γ is the nucleus gyromagnetic ratio, h is the Planck's constant, B is the magnetic field strength and ν is the resonance frequency (Richards and Hollerton, 2010). The two main technologies used to measure the NMR signal are: continuous wave (CW) and Fourier Transform (FT). Most modern NMR spectrometers are using Fourier

Transform technology to acquire the signal. In this case, the sample is exposed to a pulse of radio frequencies, where all of the signals of interest are excited simultaneously. Thus, a spectrum can be acquired in a few seconds in one go. After the pulse, a few microseconds wait are required to let the pulse ebb away, and the radio frequency signals emitted from the nuclei are acquired by a spectrometer in form of free induction decay with time domain. Then the time domain signal is converted to a frequency domain using Fourier transformations (Richards and Hollerton, 2010)

In this work, ^1H NMR was selected as the primary offline molecular analysis technique to provide an insight into the chemical, structural and electronic properties of molecules. ^1H NMR spectra were recorded at 25 °C on a Bruker AVIIIHD 400 (400 MHz) spectrometer, equipped with cryoprobe to prevent further reaction during analysis. The chemical shifts were recorded in δ (ppm), while coupling constants (J) were recorded to the nearest 0.5 Hz. In a typical ^1H NMR experiment, the sample is dissolved in a deuterated solvent in order to minimize background signals. For the analysis of the samples collected during ϵ -caprolactone polymerisation, the samples were dissolved in deuterated chloroform (CDCl_3) to which the chemical shifts were referenced (7.26 ppm). For sorbitol dehydration, the samples were dissolved in dimethyl sulfoxide (chemical shift referenced at 2.5 ppm) to ensure good stability and solubility (Tay et al., 2011). Sample preparation and analysis was performed with the assistance of Dr. Alexander Ilchev. The analysis of NMR spectra was performed using Mnova® software package from Mestrelab Research.

An NMR spectrum is a plot of intensity of absorption (or emission) versus chemical shift. The chemical shift scale is a relative scale for the absorption

frequency of a nucleus of interest to the frequency of absorption of a molecular standard (Keeler, 2011). Figure 4.4 presents a typical ^1H NMR spectrum of sorbitol.

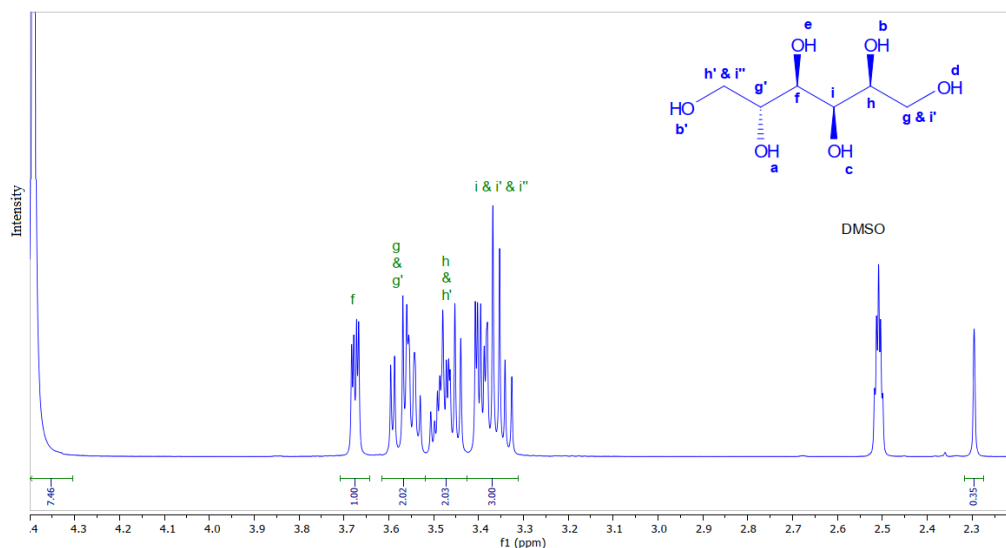


Figure 4.5: ^1H NMR spectrum of Sorbitol measured in Dimethyl sulfoxide.

As it has been discussed in section 2.5, NMR spectroscopy is a technique that can be used in monitoring reaction processes by determining key reaction features, such as conversion and molecular weight. In this study, NMR was used to determine conversion and the number average molecular weight in ϵ -caprolactone ring opening polymerisation. Conversion was determined by comparing the integral of the proton resonance of the methylene moiety adjacent to oxygen of the carbonyl group for both the monomer and polymer. The number average molecular weight was determined by comparing the integral of methylene proton resonance adjacent to the carbonyl group to that of methylene proton belonging to the benzyl ester end group. Additionally, NMR analysis was used in monitoring sorbitol dehydration to sorbitan and isosorbide. In this case, both conversion of raw material into products and relative product concentrations were determined by comparing the integrations of the methylene

resonances for sorbitol (at 3.35 ppm), with those for sorbitan at 3.90 ppm and for isosorbide at 4.05 ppm.

4.4 Gel Permeation Chromatography

Size Exclusion Chromatography (SEC), also called Gel Permeation Chromatography (GPC), is a popular method for determining the whole molar-mass distribution of polymers. It has its roots in conventional liquid chromatography and employs porous non-ionic gel beads to separate polymers in a solution. The beads are commonly made of glass or cross-linked polystyrene and containing pores of various sizes and distributions. A solvent is pumped through the column followed by a polymer dissolved in the same solvent (Stuart, 2002; Striegel et al., 2009). By measuring the concentration of polymer versus the time it needs to pass the column we can calculate the molar-mass distribution. A schematic diagram of size separation inside a column along with a chromatogram of concentration elution curve versus retention time is shown in Figure 4.6. Retention time refers to the length of time that a particular fraction remains in the column (Sperling, 2015). As shown in Figure 4.6, larger molecules spend less time in the column and elute faster than smaller molecules as they have less penetration into the pores of the packing. The chromatogram shows the peaks of solutes of two distinct sizes. The elution peak is broader than expected from the finite injected sample volume even for solutes of only one size due to mixing effect in the column, detector and connecting peak. Column band broadening of a pure component can be used to measure the accuracy of the chromatographic apparatus (Striegel et al., 2009). The molecular size distribution of a polymer can be measured by plotting the concentration of

elution as a function of retention time or eluted volume. To validate the data and enable relative sample comparison, calibration of the column is required. The calibration can be performed using mono-disperse samples of polymers with known molar masses and narrow molecular weight distributions, such as polystyrene (PS) (Bower, 2002).

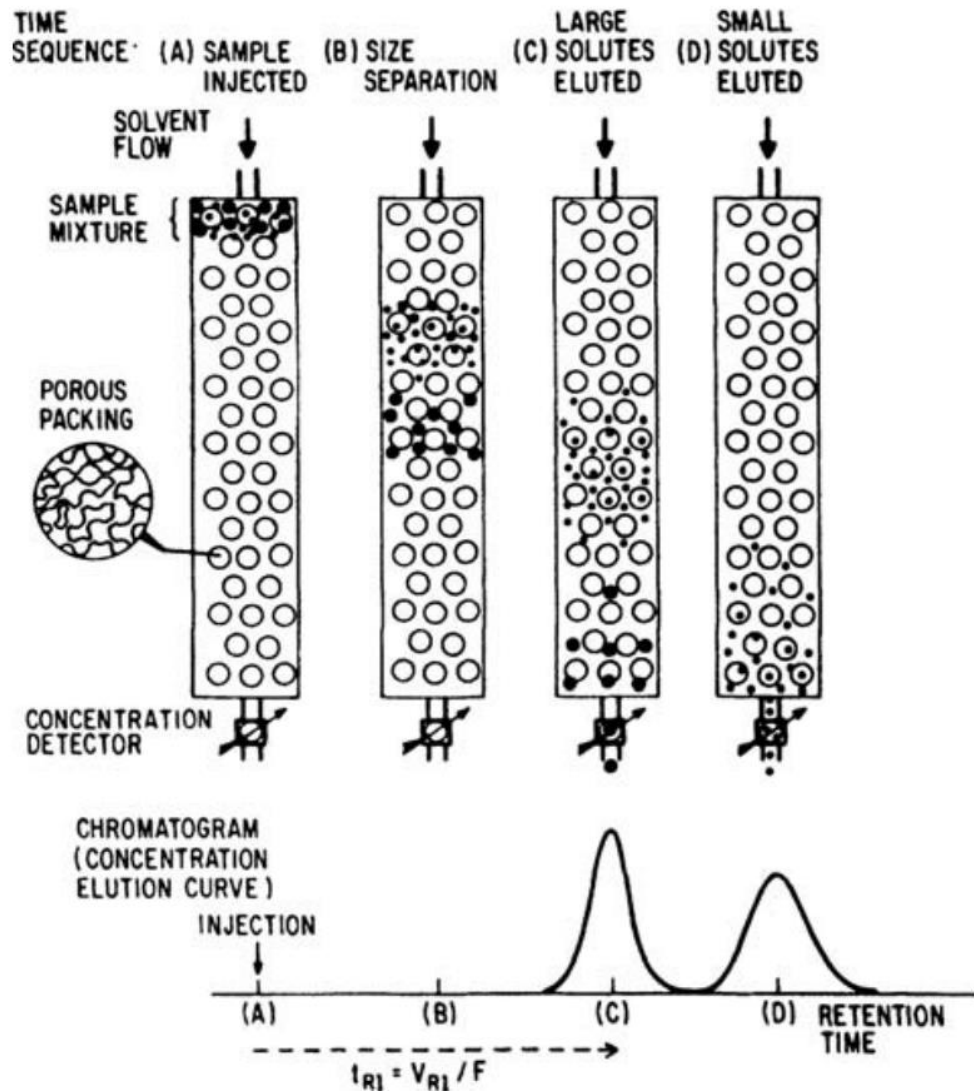


Figure 4.6: Schematic representation of size separation and concentration elution curve versus retention time (Striegel et al., 2009).

In this thesis, GPC analysis was performed on an Agilent 1260 infinity series HPLC with an online vacuum degasser, an Agilent online differential

refractometer (DRI) and a Wyatt Dawn Heleos II Multi-Angle Light Scattering detector (MALS.) Two Agilent 5 μm PLgel Mixed C columns (7.5 x 300 mm) were connected in series with an Agilent PLgel 5 μm Guard column (7.5 x 50 mm.). The column oven, DRI and MALS temperature were set to 35 $^{\circ}\text{C}$ and the flow rate was set to 1 mL per minute. Sample preparation and analysis was performed with the assistance of Dr. Alexander Ilchev. Each sample was dissolved in HPLC grade tetrahydrofuran (THF), at a concentration of 1 mg/mL. DRI calibration was performed using 30 kDa and 200 kDa linear polystyrene narrow dispersity standards dissolved in THF at a concentration of 1 mg/mL. MALS calibration was performed using HPLC grade toluene, filtered through a 0.02 μm PTFE filter and normalisation was performed in THF using a 30 kDa linear polystyrene narrow dispersity GPC calibration standard. The columns were calibrated using narrow dispersity polystyrene standards ranging from 580 Da to 1000 kDa.

GPC was used to determine monomer to polymer conversion, the number average molecular weight and polydispersity index values in the ring opening polymerisation of ϵ -caprolactone. The number average molecular weight (M_n) is an average of molecular weights of individual macromolecules, as shown in equation 4.7:

$$M_n = \frac{\sum n_i M_i}{\sum n_i} \quad (4.7)$$

where n_i is the number of molecules and M_i is the molecular weight of the molecules (Odian, 2004). The weight average molecular weight (M_w) is expressed by equation 4.8:

$$M_w = \frac{\sum n_i M_i^2}{\sum n_i} \quad (4.8)$$

The polydispersity index value (\mathcal{D}) is a measure of the molecular weight distribution and can be determined by dividing the weight average molecular weight by the number average molecular weight, as shown in equation 4.9 (Odian, 2004).

$$\mathcal{D} = \frac{M_w}{M_n} \quad (4.9)$$

GPC was also used to measure the M_n of two polymer homologous divinylbenzene samples. Column calibration using linear samples, such as PS, can affect the calculation of calibration curves when used to characterise branched polymers and lead to incorrect results. However, there are several methods in which the data can be treated correctly if combined with extra experimental information, such as the use of Drott-Mendelson method using viscosity data of the eluent or the polymer sample (Scholte and Meijerink, 1977).

4.5 Conclusions

In this chapter, the methods for dielectric property characterisation as well as off-line molecular analysis were presented. In detail, an open-ended coaxial line method and the cavity perturbation technique were used for online and offline dielectric property measurements. Nuclear magnetic resonance spectroscopy and gel permeation chromatography were used to determine material properties such as the number average molecular weight, dispersity, and the mole ratio between monomer and polymer (i.e. level of conversion). Details of the equipment for

each of the used techniques were discussed as well as the sample preparation and analysis procedures.

References

Al-Harahsheh, M., Kingman, S., Saeid, A., Robinson, J., Dimitrakis, G. and Alnawafleh, H. (2009) Dielectric properties of Jordanian oil shales. **Fuel Processing Technology** 90(10): pp.1259–1264.

Bartley, P. G., Nelson, S. O., McClendon, R. W. and Potter, W. D. (2004) Modeling permittivity measurement probes by using a genetic algorithm. in **Proceedings of the 21st IEEE Instrumentation and Measurement Technology Conference (IEEE Cat. No.04CH37510)**. *Proceedings of the 21st IEEE Instrumentation and Measurement Technology Conference (IEEE Cat. No.04CH37510)* pp.52-55 Vol.1.

Bower, D. I. (2002) **An Introduction to Polymer Physics**. Cambridge University Press.

Clarke, R. N., Gregory, A. P., Cannell, D., Patrick, M., Wylie, S., Youngs, I. and Hill, G. (2003) **Guide to Characterisation of Dielectric Materials at RF Microwave Frequencies**. National Physical Laboratory.

Gregory, A. P. and Clarke, R. N. (2006) A review of RF and microwave techniques for dielectric measurements on polar liquids. **IEEE Transactions on Dielectrics and Electrical Insulation** 13(4): pp.727–743.

Gregory, A. P. and Clarke, R. N. (2007) Dielectric metrology with coaxial sensors. **Measurement Science and Technology** 18(5): pp.1372.

Gregory, A. P. and Clarke, R. N. (2012) **Tables of the Complex Permittivity of Dielectric Reference Liquids at Frequencies Up to 5 GHz**. National Physical Laboratory.

Horner, F., Taylor, T. A., Dunsmuir, R., Lamb, J. and Jackson, W. (1946) Resonance Methods of Dielectric Measurement at Centimetre Wavelengths. **Journal of the Institution of Electrical Engineers - Part III: Radio and Communication Engineering** 93(21): pp.53–68.

ITU (2016) **Radio Regulations**. 1. Available at: <http://search.itu.int/history/HistoryDigitalCollectionDocLibrary/1.43.48.en.101.pdf>.

Jilani, M. T., Khan, M. T. and Ali, S. M. (2012) A Brief Review of Measuring Techniques for Characterization of Dielectric Materials. **International Journal of Information Technology and Electrical Engineering** 1(1): pp.5.

Kamaruddin, M. J., Harfi, J. E., Dimitrakis, G., Nguyen, N. T., Kingman, S. W., Lester, E., Robinson, J. P. and Irvine, D. J. (2011) Continuous direct on-line reaction monitoring of a controlled polymerisation via dielectric measurement. **Green Chemistry** 13(5): pp.1147–1151.

Keeler, J. (2011) **Understanding NMR Spectroscopy**. John Wiley & Sons.

Keysight Technologies (no date) **Agilent 85070E Dielectric Probe Kit 200 MHz to 50 GHz Technical Overview**. Available at: <http://literature.cdn.keysight.com/litweb/pdf/5989-0222EN.pdf>.

Kraszewski, A., Stuchly, M. A. and Stuchly, S. S. (1983) ANA Calibration Method for Measurements of Dielectric Properties. **IEEE Transactions on Instrumentation and Measurement** 32(2): pp.385–387.

Kremer, F. and Schönhals, A. (2002) **Broadband Dielectric Spectroscopy**. Springer Science & Business Media.

Li, S., Akyel, C. and Bosisio, R. G. (1981) Precise Calculations and Measurements on the Complex Dielectric Constant of Lossy Materials Using TM₀₁₀ Cavity Perturbation Techniques. **IEEE Transactions on Microwave Theory and Techniques** 29(10): pp.1041–1048.

Metaxas, A. C. and Meredith, R. J. (1995) **Industrial Microwave Heating**. London, UK: The Institution of Engineering and Technology.

Nelson, S. and Bartley Jr, P. G. (1997) Open-ended coaxial probe permittivity measurements on pulverized materials. in pp.653–657 vol.1.

Odian, G. (2004) **Principles of Polymerization**. John Wiley & Sons.

Richards, S. A. and Hollerton, J. C. (2010) **Essential Practical NMR for Organic Chemistry**. John Wiley & Sons.

Scholte, T. G. and Meijerink, N. L. J. (1977) Gel permeation chromatography on branched polymers. **British Polymer Journal** 9(2): pp.133–139.

Silverstein, R. M., Webster, F. X., Kiemle, D. J. and Bryce, D. L. (2014) **Spectrometric Identification of Organic Compounds**. John Wiley & Sons.

Smith, K. L. (1986) On the Origins of the Quality Factor Q 27: pp.695. Available at: <http://adsbit.harvard.edu/full/1986QJRAS..27..695S> (Accessed: 24 September 2018).

Sperling, L. H. (2015) **Introduction to Physical Polymer Science**. John Wiley & Sons.

Striegel, A., Yau, W. W., Kirkland, J. J. and Bly, D. D. (2009) **Modern Size-Exclusion Liquid Chromatography: Practice of Gel Permeation and Gel Filtration Chromatography**. John Wiley & Sons.

Stuart, B. H. (2002) **Polymer Analysis**. John Wiley & Sons.

Tay, B.-Y., Wang, C., Stubbs, L. P., Jacob, C. and van Meurs, M. (2011) Deuterated dimethyl sulfoxide as a good NMR solvent for the characterization of alkali metal cyclopentadienides, amides, alkoxides and phenoxides. **Journal of Organometallic Chemistry** 696(21): pp.3431–3435.

5 ONLINE MONITORING OF THE E-CAPROLACTONE POLYMERISATION

5.1 Introduction

Over the last few decades, the development of novel polymer synthesis techniques, such as the Nitroxide Mediated Polymerization (NMP) (Hawker, Bosman and Harth, 2001), Catalytic Chain Transfer Polymerisation (CCTP) (Gridnev and Ittel, 2001), and Ring-Opening Polymerisation (ROP) (Deng *et al.*, 2014b), allowed much greater control of the molecular structure of the produced polymers to be achieved. These techniques enabled the synthesis of complex three-dimensional polymer structures such as star, block, branched and hyperbranched polymers to be achieved via multi-stage processes, that often require sequential addition of different monomer types (Wang *et al.*, 2007; Koh, Konkolewicz and Perrier, 2011). For example, polycaprolactone (PCL) is a biodegradable polymer obtained by the ring opening polymerisation of ϵ -caprolactone (Mascia, 2012). PCL has received much attention especially in biomedical applications such as in tissue engineering, drug delivery, and medical devices due to its high flexibility and biodegradability as well as its hydrophobic nature. However, the high production cost of PCL appears to limit its commercial applications (Wu, Wu and Chang, 2007; Ghavimi *et al.*, 2015). Additionally, the lack of availability of control agents can lead to batch to batch variability in industrial-scale production (Destarac, 2010). These limitations could be overcome by an online process monitoring technique capable to follow the reaction progress in real time.

To date, most industrial polymerisation processes involve the use of off-line techniques for molecular analysis (e.g. calculation of monomer to polymer molecular weight and/or conversion) such as Gel Permeation Chromatography (GPC) and Nuclear Magnetic Resonance (NMR) spectroscopy. These techniques require sample extraction and preparation. These difficulties limit the application of those techniques to perform measurements on-line within the process and in real time. Consequently, there is a growing interest to develop a direct online method for real-time monitoring the conversion of monomer to polymer, which can be easily incorporated in most industrial polymerisation reactor geometries. As discussed in Chapter 2, during the last few decades, many off-line techniques, such as infrared and Raman spectroscopy, have been transformed into online in order to try and control chemical processes (Hergeth, 2000). However, when applying vibrational spectroscopic techniques, these efforts at industrial monitoring have met with limited success, with high background noise in the measurement and blackbody radiation and fluorescence in raman spectra being the most common issues (Lewis and Edwards, 2001; Bakeev, 2010). Recently, the use of dielectric spectroscopy for the “offline” monitoring of chemical reactions was reported. There are few published studies on using dielectric spectroscopy to real time follow polymerisation reactions such as the methyl methacrylate/butyl acrylate (MMA/BuA) solution copolymerisation (Santos *et al.*, 2001), the ϵ -caprolactone polymerisation (Kamaruddin *et al.*, 2014b) and the polymerisation of polymer/clay nanocomposites (Pissis *et al.*, 2015).

Santos *et al.* (2001) used dielectric analysis for the in-line monitoring of monomer and overall conversion during methyl methacrylate/butyl acrylate

(MMA/BuA) solution copolymerisations. They develop an empirical model to relate the dielectric loss with MMA conversion. The technique can be used to investigate the effects of MMA concentration on the dielectric properties and to calculate the induction time of the polymerisation.

Kamaruddin *et al.* (2014b) and Nguyen *et al.* (2014) studied the use of microwave dielectric spectroscopy in the monitoring of the Ring Opening Polymerisation of ϵ -caprolactone using a coaxial probe sensor. The dielectric property data were compared with data from off-line techniques such as cavity perturbation method, Gel Permeation Chromatography, Nuclear Magnetic Resonance and Karl-Fisher titration. In brief, the dielectric properties were related with the molar ratio of polycaprolactone in the polymerisation mixture and the polymerisation time. The results showed that the measurement of the dielectric properties can be used to identify specific reaction features such as the reaction rate, end-point, and induction periods with the help of a calibration curve.

Pissis *et al.* (2015) reported the use of broadband Dielectric Spectroscopy and electrical dc measurements in following the polymerisation and curing processes in polymer/clay nanocomposites. In brief, the degree of conversion, the gelation time and the vitrification time during isothermal curing of neat cyanate ester were related with the dielectric data. The results showed that Dielectric Spectroscopy can real time follow the state of polymerization and curing process and provide information about morphology and mechanical integrity of polymer systems.

Only in the last few decades there are few published reports on following polymerisation reactions using dielectric spectroscopy. These studies have shown that the “in situ” measurement of the dielectric properties during a polymerisation can be used to follow the progress of the reaction and estimate key reaction features such as induction periods and the conversion of reactants to the final product. However, some of the above-mentioned studies do not include details about the temperature dependency of the dielectric properties (Santos *et al.*, 2001) or investigate a limited frequency and temperature range (Kamaruddin *et al.*, 2014b; Pissis *et al.*, 2015), and mainly on pre-prepared monomer to polymer concentrations (Kamaruddin *et al.*, 2014b; Nguyen *et al.*, 2014). Therefore, they did not provide information on the use of the technique during the progress of a polymerisation reaction and did not consider investigating the frequencies that can potentially provide an optimum between measurement sensitivity and linearity and therefore utilised to inform the design and operation of dedicated sensors that can be employed as a part of a process control strategy.

In the present study, dielectric spectroscopy utilised to monitor, “in-situ”, the progress of the ring opening polymerisation of ϵ -caprolactone. A systematic study of the dielectric behaviour of ϵ -caprolactone will be presented in a broad frequency (500 MHz – 20 GHz) and temperature (20 °C – 170 °C) range. The analysis of the dielectric data with frequency will enable the identification of the most suitable strategy for the online monitoring of the polymerisation. Additionally, a detailed study on how the dielectric properties of the monomer change with frequency and temperature will be discussed by comparing the measured ϵ' and ϵ'' with the modelled ones using curve fitting with Debye, Cole-

Cole and Cole-Davidson relaxation models. Finally, the real time dielectric data during the ring opening polymerisation of ϵ -caprolactone have been compared with conversion of monomer to polymer. The construction of a calibration curve for following the polymerisation and the effect of magnetic stirring will be discussed in the final section of the chapter.

5.2 Experimental

An open-ended coaxial line sensor utilised to monitor the ring opening polymerisation of ϵ -caprolactone. The sensor was placed directly into the reaction medium and used to characterise the dielectric properties of the polymerisation mixture both 'in-situ' and with time at microwave frequencies. In addition to measurements obtained by the sensor, samples of the medium were extracted at various time points for off-line molecular analysis, to confirm the polymer molecular weights that had been achieved, level of conversion, and dispersity. The experimental results are presented together with their error bars. The maximum standard deviation was used to estimate the error. For results with small deviation, the error bars are omitted for clarity and the measurement error is presented in the label in terms of standard deviation, i.e. $\epsilon' \pm \sigma(\epsilon')$, where σ is the maximum standard deviation.

5.2.1 Materials

ϵ -caprolactone (99%) (CL), tin(II) 2-ethylhexanoate (96%) (Sn(Oct)₂) and benzyl alcohol (99%) (BzOH) were purchased from Alfa Aesar and used as

received without any purification. ϵ -caprolactone was dried with the use of molecular sieves for 48h at room temperature.

5.2.2 Ring Opening Polymerisation Procedure

All experiments were conducted with a constant [CL]:[Sn(Oct)₂]:[BzOH] molar ratio of 800:1:10. Sn(Oct)₂ was chosen as the preferable catalyst because it is used in the industrial production of polycaprolactone (Liao *et al.*, 2002). The most favoured mechanism for the ROP of CL using Sn(Oct)₂ that is reported in the literature is the coordination-insertion mechanism (Figure 5.1), in which the catalyst adds to the hydroxyl groups of the initiator and forms an alkoxide bond (Labet and Thielemans, 2009). All reactants were in liquid form and no bubble formation was observed during reaction progress. The final product (polycaprolactone) was in a viscous liquid form at the target reaction temperature (160 °C).

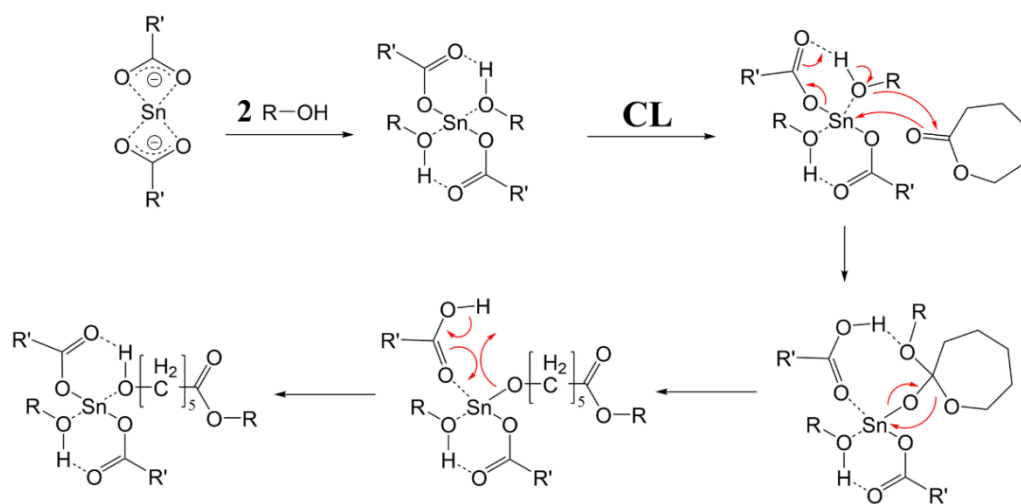


Figure 5.1: *Sn(Oct)₂ catalyzed coordination-insertion ROP mechanism of CL (Raquez, Narayan and Dubois, 2008).*

The reaction mixture tin(II) 2-ethylhexanoate (0.13 g, 0.32 mmol), ϵ -caprolactone (29.52 g, 260 mmol), and benzyl alcohol (0.35 g, 3.24 mmol) was placed into a 50 mL flask and pre-purged with nitrogen for 15 minutes. The mixture was then heated to the target reaction temperature (160 °C) with the use of a preheated oil bath and the mixture was mechanically stirred throughout the reaction progress. An open-ended coaxial line sensor was used to monitor the dielectric properties during the polymerisation progress. The sensor was introduced to the flask through a rubber septum, such that the end was immersed into the reaction mixture. At set times during the polymerisation progress, samples were extracted using a Hamilton syringe and needle and placed in a refrigerator, for further off-line analysis with NMR and GPC. At the end of the reaction, the flask was removed, and crude product was also analysed with NMR and GPC.

5.2.3 Online Dielectric property measurement

The determination of the dielectric response of the reaction mixture was conducted with the use of an Agilent 85070E open ended coaxial line sensor and a Keysight N5232A PNA-L Vector Network Analyser (VNA). The probe was immersed into the reaction mixture and a swept signal (0.5 GHz - 20 GHz) transmitted from the VNA, through the probe, into the reaction mixture. Depending on the complex permittivity of the sample, a portion of that signal was reflected to the VNA and the reflection coefficient (S_{11}) of the sample was collected and stored on a dedicated PC. The complex permittivity of the sample was determined using the reflection coefficient according to the method referred by Misra, Blackham, and Pollard (Misra, 1995; Blackham and Pollard, 1997). In order to account for systematic errors/experimental variation, a least-squares calibration algorithm was selected, and three standards were used: open line (air), short-circuited line (calibration short tool) and a reference liquid of known dielectric response (water). The quality of calibration and short-circuit measurements were assessed by plotting the residual calibration errors for the whole frequency range investigated. The calibration was repeated at least three times to ensure that the residual errors were less than 2%. The open-ended coaxial line technique is detailed in Section 4.2.1.

5.2.4 Offline molecular analysis

Samples were extracted at set times during the polymerisation. The extracted samples were subjected to off-line analysis by Proton Nuclear Magnetic Resonance spectroscopy (^1H NMR) and Gel Permeation Chromatography (GPC). Sample preparation and analysis was performed with the assistance of

Dr. Alexander Ilchev. This analysis enabled the number average molecular weight (M_n), dispersity (\mathcal{D}), and the mole ratio between monomer and polymer (i.e. level of conversion) to be calculated.

^1H NMR spectra were recorded in deuterated chloroform on a Bruker AVIIIHD 400 (400 MHz) spectrometer equipped with cryoprobe to prevent further reaction during analysis. The samples were dissolved in deuterated chloroform (CDCl_3) to which the chemical shifts were referenced (7.26 ppm). The analysis of the results was performed using the Mnova® software package from Mestrelab Research. Conversion was determined by comparing the integral of the proton resonance of the methylene moiety adjacent to oxygen of the carbonyl group for both the monomer and polymer. The number average molecular weight was determined by comparing the integral of methylene proton resonance adjacent to the carbonyl group to that of methylene proton belonging to the benzyl ester end group.

GPC analysis was performed on an Agilent 1260 infinity series HPLC with an online vacuum degasser, an Agilent online differential refractometer (DRI) and a Wyatt Heleos II Multi-Angle Light Scattering detector (MALS). Each sample was dissolved in HPLC grade tetrahydrofuran (THF), at a concentration of 1 mg/mL. DRI calibration was performed using 30 kDa and 200 kDa linear polystyrene narrow dispersity standards dissolved in THF at a concentration of 1.0 mg/mL. MALS calibration was performed using HPLC grade toluene, filtered through a 0.02 μm PTFE filter and normalisation was performed in THF using a 30 kDa linear polystyrene narrow dispersity GPC calibration standard. The columns were calibrated using narrow dispersity polystyrene standards ranging from 580 Da to 1000 kDa.

5.2.5 Accuracy of Dielectric property measurements

Considering the factors that contribute the error of the measurements obtained with the coaxial probe, these are as follows (Gregory *et al.*, 2008):

- Calibration errors that can occurred from the short-circuit and the reference liquid.
- Air bubbles that are formed on the flange of the probe.
- Temperature deviation during the measurements.

In order to confirm the accuracy of the measurements, a comparison between literature data reported by Kamaruddin *et al.* (2014b) and measured dielectric properties of ϵ -caprolactone at 30 °C was performed. Figure 5.2 shows the dielectric constant and loss data at frequencies ranging from 1 GHz to 5 GHz. The measured ϵ' and ϵ'' data in Figure 5.2 found to be in good agreement with the literature data.

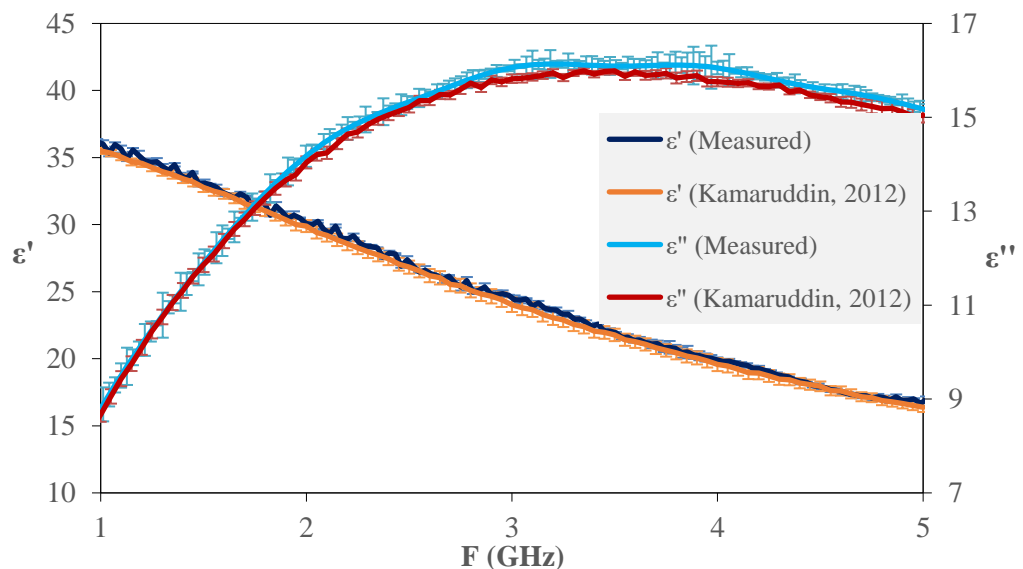


Figure 5.2: : Comparison between measured and literature dielectric data (Kamaruddin, 2012) of ϵ -caprolactone at 30 °C.

5.3 Dielectric properties of ϵ -caprolactone monomer

Previous studies showed that the dielectric properties of the polycaprolactone polymerisation mixture mostly follow the dielectric properties of the monomer (Kamaruddin *et al.*, 2014b). A study of the dielectric properties of ϵ -caprolactone monomer was performed in order to understand the effect of temperature and frequency on the dielectric properties. A broad frequency (500 MHz – 20 GHz) and temperature (20 °C – 170 °C) range was investigated. The measurements were repeated six times and the maximum standard deviation was found to be less than 4% which indicates good measurement repeatability. Each data point in the following figures is the average of at least five measurements. The standard deviation of each data point is shown as an error bar.

5.3.1 Frequency dependence of ϵ -caprolactone monomer dielectric properties

The dielectric properties of ϵ -caprolactone monomer at any target temperature found to be dependent on the frequency. Figure 5.3 shows the dielectric constant versus frequency at room temperature (20 °C). The ϵ' value of the monomer at 20 °C decreased from 39,6 at 500 MHz to 6.7 at 20 GHz which indicates the reduced ability of the material to store energy at high frequencies.

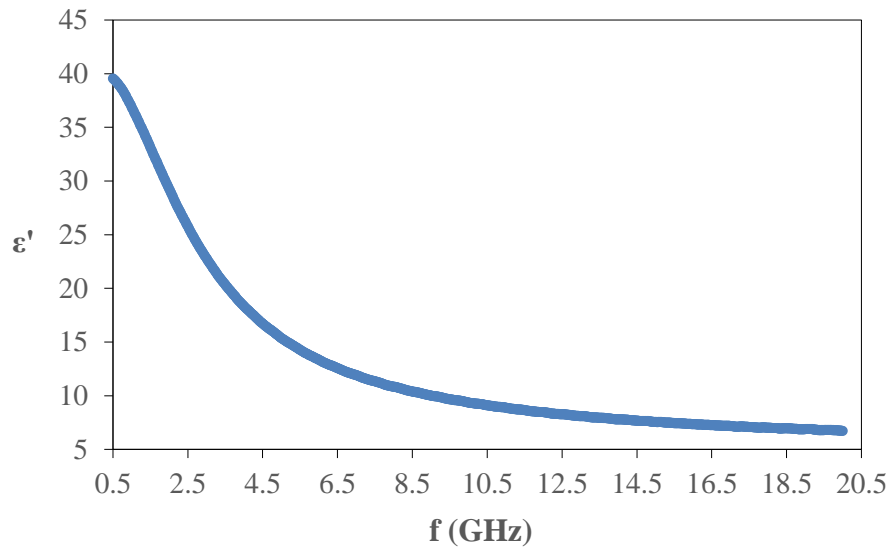


Figure 5.3: Dielectric constant versus frequency (GHz) of ϵ -caprolactone at 20 °C. Due to the small deviation, the error bars are indistinguishable. The maximum standard deviation of the measured data is: $[\epsilon' \pm 0.02]$.

In Figure 5.4, the dielectric loss and $\tan \delta$ values of ϵ -caprolactone at 20 °C are plotted against frequency. The dielectric loss shows an absorption peak, which is called relaxation frequency and is associated with the dipole polarization mechanism, will be discussed later in this chapter.

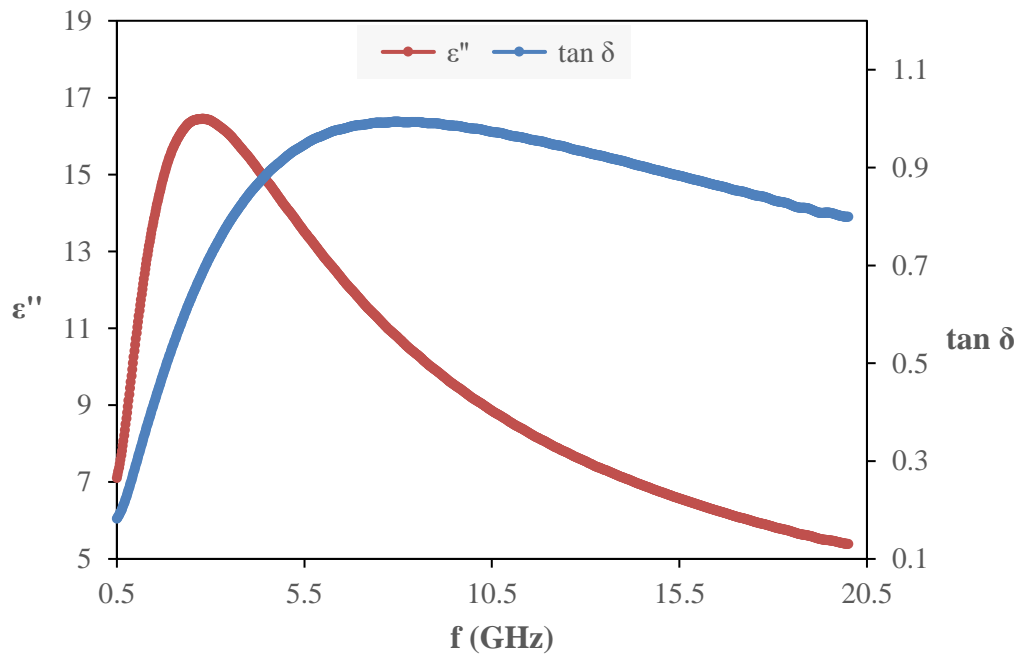


Figure 5.4: Dielectric loss and $\tan \delta$ versus frequency (GHz) of ϵ -caprolactone at 20 °C. The maximum standard deviation of the measured data is: [$\epsilon'' \pm 0.04$]; [$\tan \delta \pm 0.03$]

Tan δ values increase as the frequency increases up to 7.9 GHz and denote the increased ability of the material to absorb and convert the applied electromagnetic energy into heat as the frequency increases. At very high frequencies the ability of the material to dissipate energy as heat is reduced. As a result, ϵ'' and $\tan \delta$ values decrease.

5.3.2 Temperature dependence of ϵ -caprolactone monomer dielectric properties

Both dielectric constant and loss found to be strongly and non-linearly dependent with the temperature. Figure 5.5 illustrates the changes of dielectric constant versus frequency at temperatures 20 °C, 50 °C, 100 °C, 140 °C and 170 °C. In this graph, a decrease of the dielectric constant with increasing frequency can be observed at any of the selected temperatures. However, at high temperatures,

above 100 °C, ϵ' values observed to decrease less as the frequency increases. At 170 °C, the ϵ' value of the monomer decreased from 25.9 at 1 GHz to 13.9 at 20 GHz while at 20 °C decreased from 36.8 at 1 GHz to 6.7 at 20 GHz. This trend reflects the reduced ability of the material to store energy as the temperature increases.

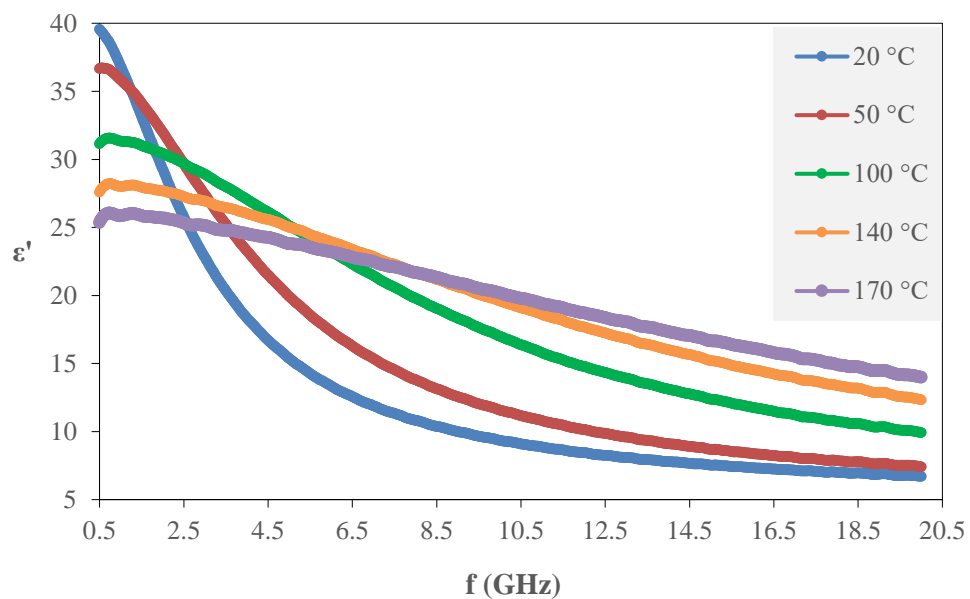


Figure 5.5: Dielectric constant versus frequency (GHz) for temperature 20 °C, 50 °C, 100 °C, 140 °C and 170 °C. The maximum standard deviations of the measured data are: 20 °C [$\epsilon' \pm 0.02$]; 50 °C: [$\epsilon' \pm 0.03$]; 100 °C: [$\epsilon' \pm 0.03$]; 140 °C: [$\epsilon' \pm 0.002$]; 170 °C: [$\epsilon' \pm 0.003$].

Figure 5.6 shows the dielectric loss values versus frequency at selected temperatures. In this graph, the peaks in the ϵ'' , which denote the relaxation frequency, shifts to higher frequencies as the temperature increases. Additionally, the relaxation frequency at high temperatures correspond to lower ϵ'' values as the ability of dipoles to convert electromagnetic energy into heat is reduced at high temperatures. Furthermore, the decreased ϵ'' values at high

temperature could be attributed to effects of conductivity (Metaxas and Meredith, 1905).

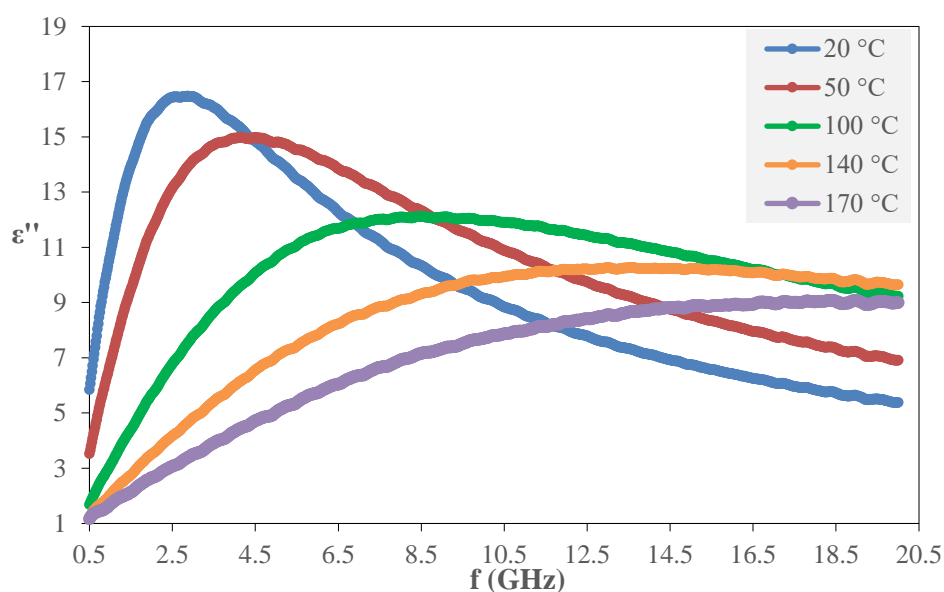


Figure 5.6: Dielectric loss versus frequency (GHz) at 20 °C, 50 °C, 100 °C, 140 °C and 170 °C. The maximum standard deviations of the measured data are: 20 °C [$\epsilon'' \pm 0.04$]; 50 °C: [$\epsilon'' \pm 0.2$]; 100 °C: [$\epsilon'' \pm 0.3$]; 140 °C: [$\epsilon'' \pm 0.2$]; 170 °C: [$\epsilon'' \pm 0.1$].

5.4 Dielectric relaxation analysis of ϵ -caprolactone monomer

It is possible to describe the experimental results of complex permittivity by iteratively fitting the measured complex permittivity values to a modelled counterpart. This will enable the estimate/analysis of complex permittivity values without the need for measurement of the material (Jol, 2008). The analysis of the dielectric properties of ϵ -caprolactone monomer will be performed by comparing the measured dielectric data with the fitted data based on Debye, Cole-Cole and Cole-Davidson model. A review of the empirical models was presented in section 3.4. The application of the above-mentioned models is based on the following assumptions:

1. ϵ -caprolactone is a homogenous material.
2. The high frequency permittivity (ϵ_∞) value was obtained from the extrapolated Cole-Cole plot and ignores molecular resonance phenomena and microwave relaxations that occur in the infrared region and as a result is higher than the square of refractive index (n_D^2) (Gregory, Clarke and Cox, 2009).
3. The value for the static permittivity (ϵ_∞) obtained from the lowest frequency dielectric constant measurement (500 MHz) since ϵ' values found to vary linearly with frequency and therefore can be interpolated with sufficient accuracy (Gregory and Clarke, 2012).

5.4.1 Relaxation frequency and time of ϵ -caprolactone

The relaxation frequency of ϵ -caprolactone monomer can be determined either from the dielectric loss curve or from Cole-Cole plot. Figure 5.7 shows the dielectric loss versus log frequency for temperature 20 °C, 50 °C, 80 °C, 110 °C, 140 °C and 170 °C. The maximum of ϵ'' , which corresponds to the relaxation frequency of ϵ -caprolactone shifts to higher frequencies as the temperature increases. In detail, from 2.82 GHz at 20 °C shifts to 18.38 GHz at 170 °C. Consequently, the relaxation time, which is inversely related to frequency ($\tau = 1/2\pi f_c$), decreases as temperature increases. The dielectric relaxation time is the time that it takes for the dipoles to become 63% oriented with an applied electromagnetic field or vice versa the time required to return to disorder after the external field is removed (Kingston and Jassie, 1988).

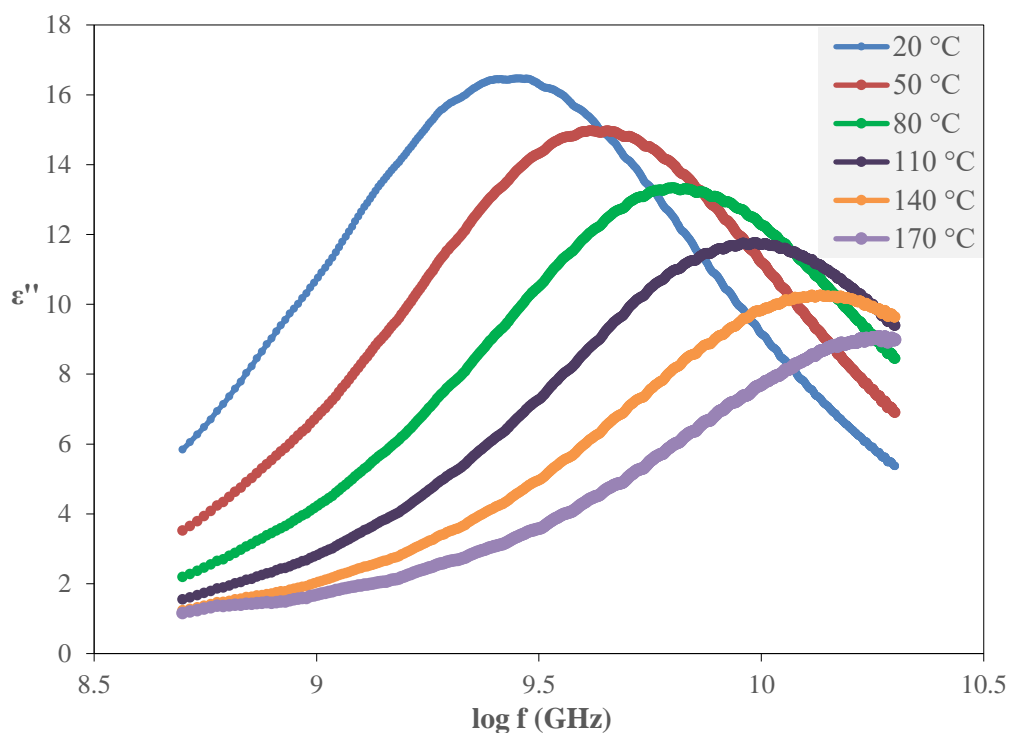


Figure 5.7: Dielectric loss versus frequency (GHz) of ϵ -caprolactone monomer at selected temperatures. The maximum standard deviations of the measured data are: 20 °C [$\epsilon'' \pm 0.04$]; 50 °C: [$\epsilon'' \pm 0.2$]; 80 °C: [$\epsilon'' \pm 0.3$]; 110 °C: [$\epsilon'' \pm 0.1$]; 140 °C: [$\epsilon'' \pm 0.2$]; 170 °C: [$\epsilon'' \pm 0.1$].

Figure 5.8 shows the Cole-Cole plot of ϵ -caprolactone at temperature 20 °C, 50 °C, 80 °C, 110 °C, 140 °C and 170 °C. ϵ -caprolactone exhibits a single relaxation time and can be represented by the Debye semicircle, in which the maximum value of ϵ'' provides the relaxation frequency and the points of intersection of the arc with the horizontal axis provide the static and infinite permittivities.

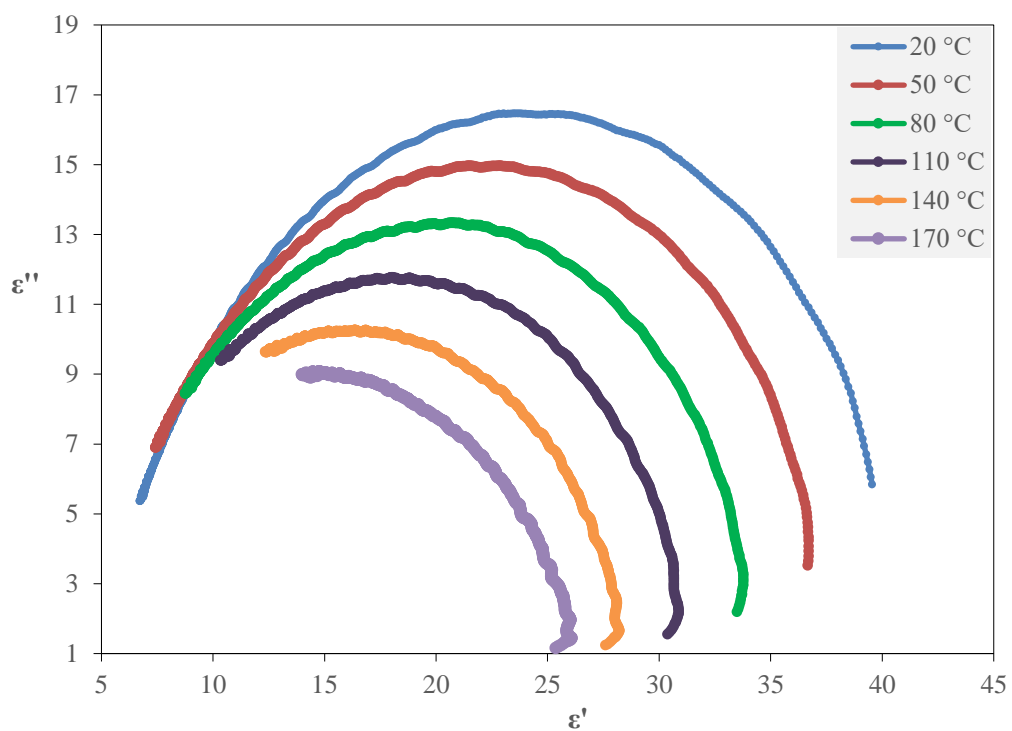


Figure 5.8: Cole-Cole plot of ϵ -caprolactone at selected temperatures.

Table 5.1 shows the values of static and infinite permittivity as well as the relaxation frequency and time for temperatures from 20 °C to 170 °C. Relaxation time decreases from 54.89 picoseconds (ps) at room temperature to 12.49 ps at 170 °C. The decrease of relaxation time is related with the increase of molecular collisions which occurs at high temperatures (Hill, 1969).

Table 5.1: Temperature, static and infinite permittivity, relaxation frequency and time of ϵ -caprolactone at temperatures from 20 °C to 170 °C.

T (°C)	ϵ_{∞}	ϵ_s	f_s (GHz)	τ (ps)
20	6.532611	38.85741	2.8205	54.89
30	6.502972	38.39884	2.996	49.13
40	6.427972	37.2223	3.9515	39.81
50	6.381479	36.66342	4.4975	35.84
60	6.330158	35.24568	5.2385	28.65
70	6.341169	34.32422	6.2135	25.66
80	6.360243	33.76746	6.3305	23.91
90	6.337021	32.62975	7.4225	20.90
100	6.472431	31.54344	8.4365	18.64
110	6.483421	30.82943	9.6455	17.20
120	6.885051	29.53824	11.3225	15.34
130	7.107004	28.67625	12.9995	14.17
140	7.394791	27.9595	13.565	13.42
150	7.757987	27.28291	14.6765	12.80
160	8.502251	26.58545	16.6655	12.49
170	9.237246	25.62357	18.3815	12.19

5.4.2 Debye permittivity model of ϵ -caprolactone

In order to analyse the dielectric properties using the Debye model, the experimental data were fitted to the Debye equation:

$$\epsilon' = \epsilon_{\infty} + \frac{\epsilon_s - \epsilon_{\infty}}{1 + \omega^2\tau^2} \quad (5.1)$$

$$\varepsilon'' = \frac{(\varepsilon_s - \varepsilon_\infty)\omega\tau}{1 + \omega^2\tau^2} \quad (5.2)$$

where ε_s , ε_∞ is the dielectric constant at low and very high frequencies, τ is the relaxation time ($\tau = \frac{1}{2\pi f_c}$, where f_c is the relaxation frequency) and ω the angular frequency ($\omega = 2\pi f_c$). The relaxation time was calculated by the relaxation frequency which was obtained from the dielectric loss curve. The values of static and infinite permittivity were obtained from Cole-Cole plot and presented in Table 5.1.

Figures 5.9 and 5.10 show a comparison between the measured dielectric properties and Debye relaxation model results. The results show that Debye model is accurate for the calculation of the dielectric constant. The modelled dielectric constant values are in good agreement with the measured values at both selected temperatures (20 °C and 160 °C). The highest deviation between measured ε' and model ε' values is about 5% at 20 °C and 2% at 160 °C. However, a comparison between the measured and modelled dielectric loss values produces a higher deviation with a maximum of about 20% at 20 °C and 40% at 160 °C. It is confirmed that when the measurements of permittivity are made over a wide frequency range, the results do not agree with the predictions from the Debye model (Brown *et al.*, 1998). Cole and Cole (1941) introduced an empirical modification which can be used to describe the complex permittivity of polymers.

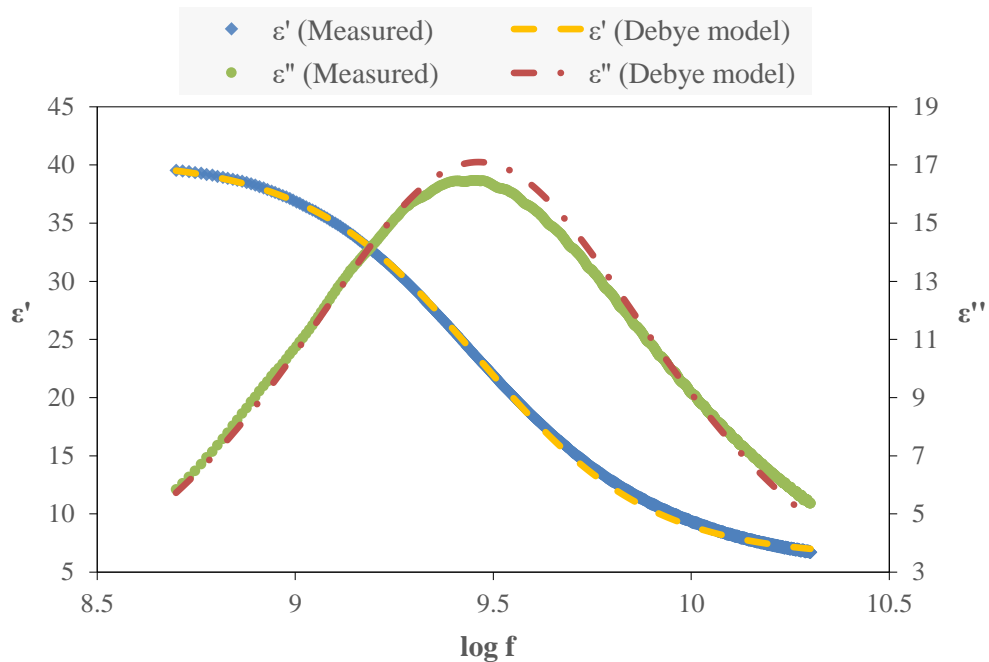


Figure 5.9: Dielectric constant and loss versus log frequency of ϵ -caprolactone at 20 °C. The data points correspond to the measured data and the lines to the fitted Debye model.

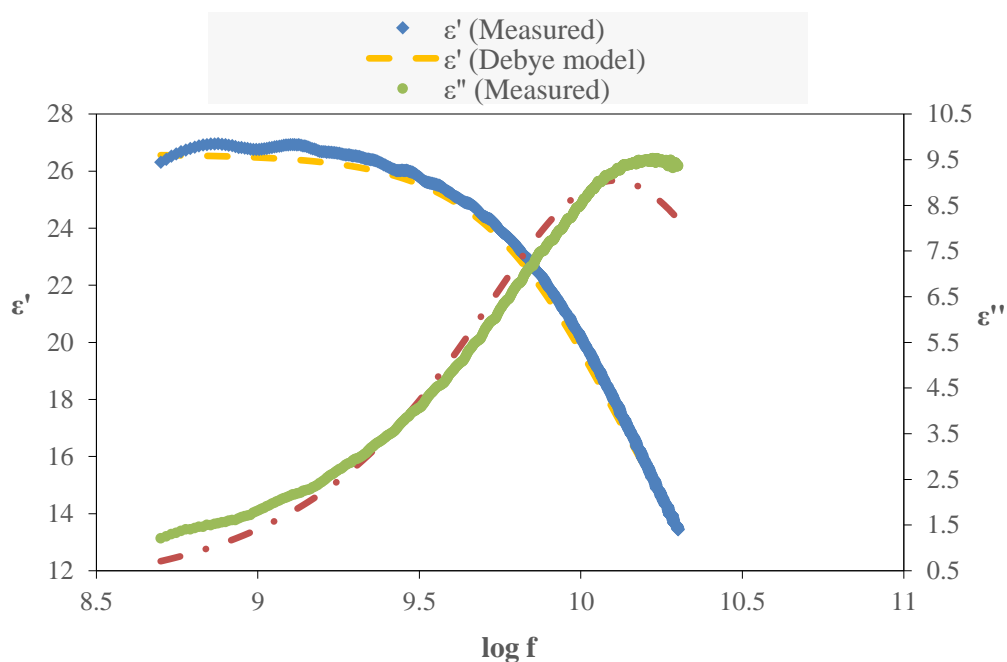


Figure 5.10: Dielectric constant and loss versus log frequency of ϵ -caprolactone at 160 °C. The blue and green data points correspond to the measured data and the dashed lines to the fitted Debye model.

5.4.3 Cole-Cole permittivity model of ϵ -caprolactone

It is confirmed that long-chain molecules, such as polymers, have a much broader and asymmetric distribution of relaxation times than a single Debye process (Mittal, 2012). Cole-Cole relaxation model is suitable to model the dielectric behaviour of materials that exhibit a distribution of relaxation times (Hill, 1969). In order to confirm this hypothesis for the ϵ -caprolactone, the dielectric properties were calculated using the Cole-Cole model equations:

$$\epsilon'(\omega) = \epsilon_{\infty} + (\epsilon_s - \epsilon_{\infty}) \frac{1 + (\omega\tau)^{1-\alpha} \sin \frac{1}{2} a\pi}{1 + 2(\omega\tau)^{1-\alpha} \sin \frac{1}{2} a\pi + (\omega\tau)^{2(1-\alpha)}} \quad (5.3)$$

$$\epsilon''(\omega) = (\epsilon_s - \epsilon_{\infty}) \frac{(\omega\tau)^{1-\alpha} \cos \frac{1}{2} a\pi}{1 + 2(\omega\tau)^{1-\alpha} \sin \frac{1}{2} a\pi + (\omega\tau)^{2(1-\alpha)}} \quad (5.4)$$

where ϵ_s , ϵ_{∞} is the dielectric constant at low and high frequency, τ is the relaxation time, ω the angular frequency and a is a constant, $0 \leq a \leq 1$. Figures 5.11 and 5.12 show the modelled dielectric properties compared to the experimental results for temperatures 20 °C and 160 °C. The highest deviation between the modelled and measured dielectric properties at room temperature is about 6% for ϵ' and 7% for ϵ'' . However, at high temperature (160 °C) the comparison between the measured and modelled dielectric constant and loss produces a maximum of about 4% for ϵ' and 40% for ϵ'' . It is reported that Cole-Davidson model is more accurate to describe the complex permittivity of materials with a long chain structure (Meurant, 2012).

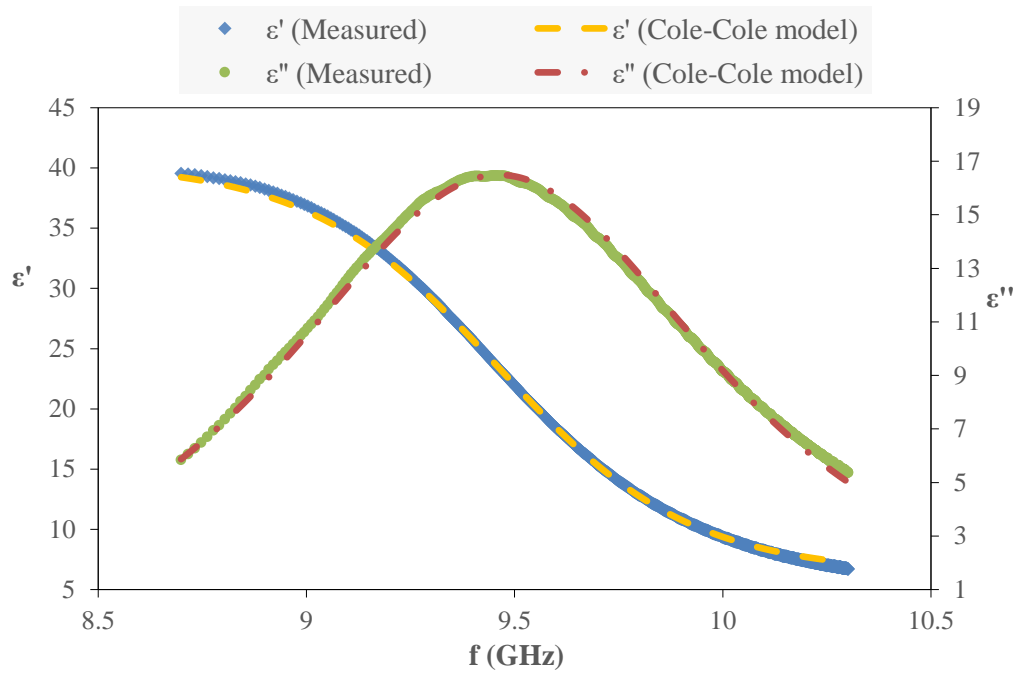


Figure 5.11: Dielectric constant and loss versus log frequency of ϵ -caprolactone at 20 °C. The blue and green data points correspond to the measured data and the dashed lines to the fitted Cole-Cole model.

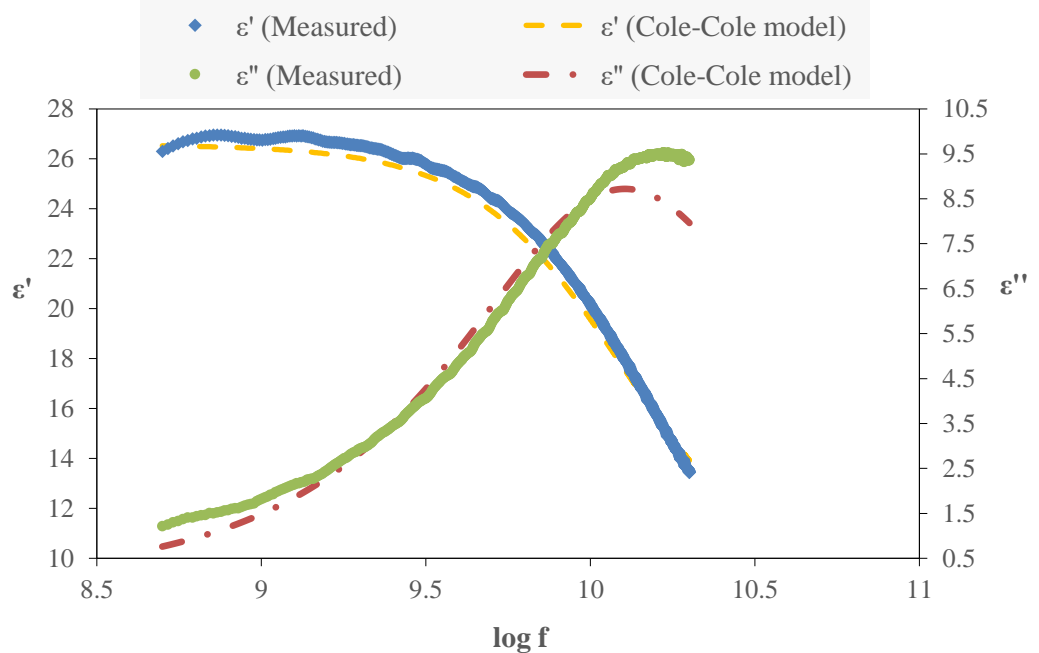


Figure 5.12: Dielectric constant and loss versus log frequency of ϵ -caprolactone at 160 °C. The blue and green data points correspond to the measured data and the dashed lines to the fitted Cole-Cole model.

5.4.4 Cole-Davidson permittivity model of ϵ -caprolactone

The Cole-Davidson model describes the behaviour of materials in which the Cole-Cole arc is similar to a skewed arc. To confirm if ϵ -caprolactone can be described by the Cole-Davidson model, the experimental data were fitted to the Cole-Davidson equation:

$$\epsilon'(\omega) = \epsilon_{\infty} + (\epsilon_s - \epsilon_{\infty}) \cos\varphi^{\beta} \cos\beta\varphi \quad (5.5)$$

$$\epsilon''(\omega) = (\epsilon_s - \epsilon_{\infty}) \cos\varphi^{\beta} \sin\beta\varphi \quad (5.6)$$

where ϵ_s , ϵ_{∞} is the dielectric constant at low and high frequency, τ is the relaxation time, ω the angular frequency and β is a constant, $0 \leq \beta \leq 1$. Figures 5.13 and 5.14 show the modelled dielectric properties compared to the experimental results for temperatures 20 °C and 160 °C.

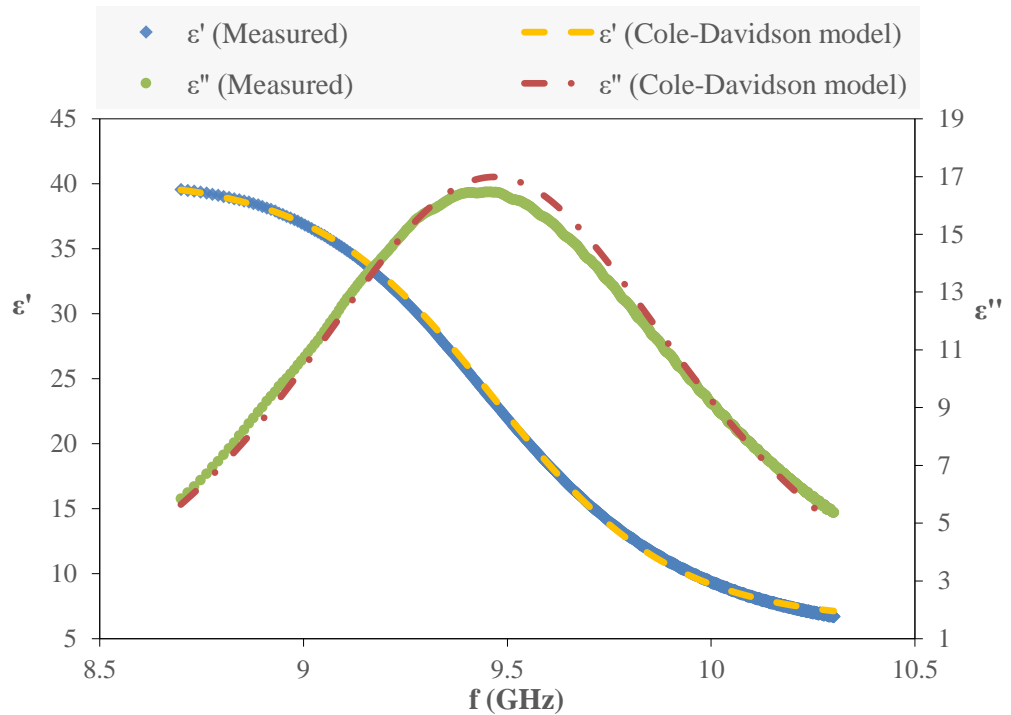


Figure 5.13: Dielectric constant and loss versus log frequency of ϵ -caprolactone at 20 °C. The blue and green data points correspond to the measured data and the dashed lines to the fitted Cole-Davidson model.

The highest deviation between measured ϵ' and modelled ϵ' values is about 3% at 20 °C and 6% at 160 °C. Meanwhile, the comparison between measured ϵ'' and modelled ϵ'' values is ~20% at 20 °C and ~40% at 160 °C. The position of maximal loss mainly depends on parameter β . The justification of β results in bigger differentiation between the modelled and experimental loss values.

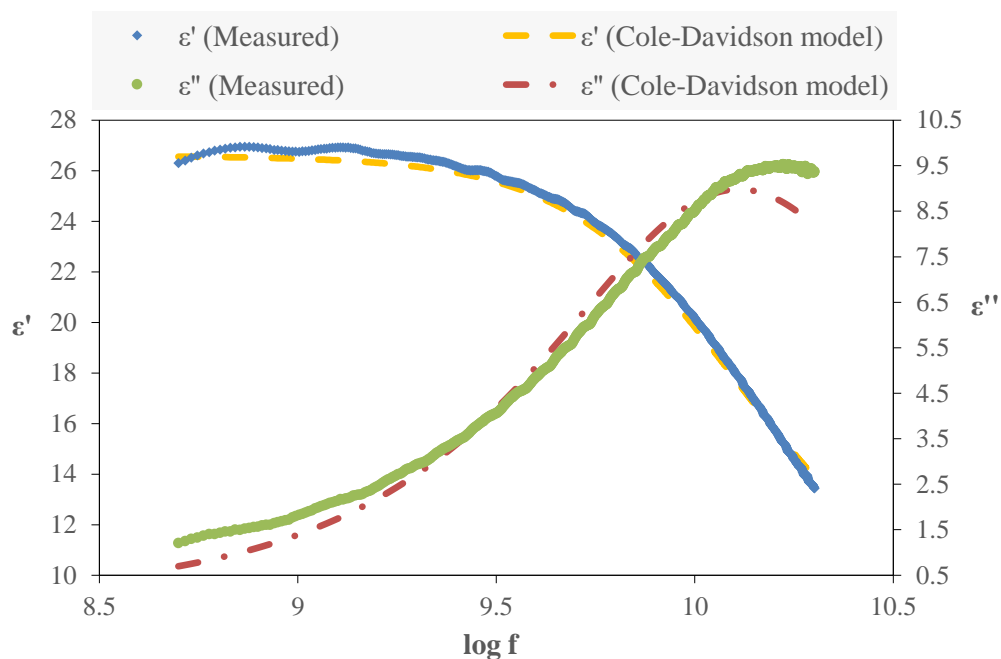


Figure 5.14: Dielectric constant and loss versus log frequency of ϵ -caprolactone at 160 °C. The data points correspond to the measured data and the lines to the fitted Cole-Davidson model.

In this section, the measured complex permittivity values were fitted to Debye, Cole-Cole, and Cole-Davidson model to estimate the complex permittivity based on basic material properties. Unfortunately, there is no single model to describe the permittivity of ϵ -caprolactone in the entire temperature and frequency range investigated due to the complex structure of the material. The addition of extra parameters is needed for the accurate estimation of complex permittivity values.

5.5 Real time monitoring of the ϵ -caprolactone polymerisation using the dielectric properties

Dielectric spectroscopy was utilised to monitor the progress of the ring opening polymerisation of ϵ -caprolactone in real time. A series of polymerisations were conducted with a constant [CL]:[Sn(Oct)₂]:[BzOH] molar ratio of 800:1:10. The reaction mixture was placed into a 50 mL flask, pre-purged with nitrogen, and

heated to the target reaction temperature (160 °C) with the use of a preheated oil bath. The mixture was mechanically stirred throughout the reaction progress. A coaxial probe sensor was used to monitor the dielectric properties during the polymerisation progress and samples were extracted at set times for off-line analysis with NMR and GPC.

5.5.1 Dielectric properties of individual precursors and reaction mixtures

The dielectric properties of the monomer (CL), catalyst (Sn(Oct)₂), initiator (BzOH), and polymer (PCL) were measured using the described open ended coaxial line sensor to highlight the differences between the dielectric response of the individual precursors and the final product. The dielectric properties of the monomer were found to be higher than that of its related polymer, as it has been previously reported (Kamaruddin *et al.*, 2014b). The dielectric properties of catalyst and initiator were assessed and found to have only minor contribution to the polymerisation mixture at the target reaction temperature (160 °C) and concentration that they are present in the reaction mixture, i.e. the selected monomer:catalyst:initiator molar ratio (800:1:10), which is consistent with previous studies (Nguyen *et al.*, 2014). Furthermore, the tin mediated ROP polymerisation is a chain growth polymerisation which exhibits pseudo living features (i.e. linear increase of molecular weight with conversion) (Dubois, Coulembier and Raquez, 2009). As the chain forms, the number of degrees of molecular freedom within each repeat unit is reduced compare to those of the monomer. Thus, the dielectric properties of the mixture have been found to decrease as the reaction progresses and this could be possibly attributed to the

consumption of the high dielectric properties monomer during its conversion to the low dielectric properties polymer as has been previously suggested (Nguyen *et al.*, 2014).

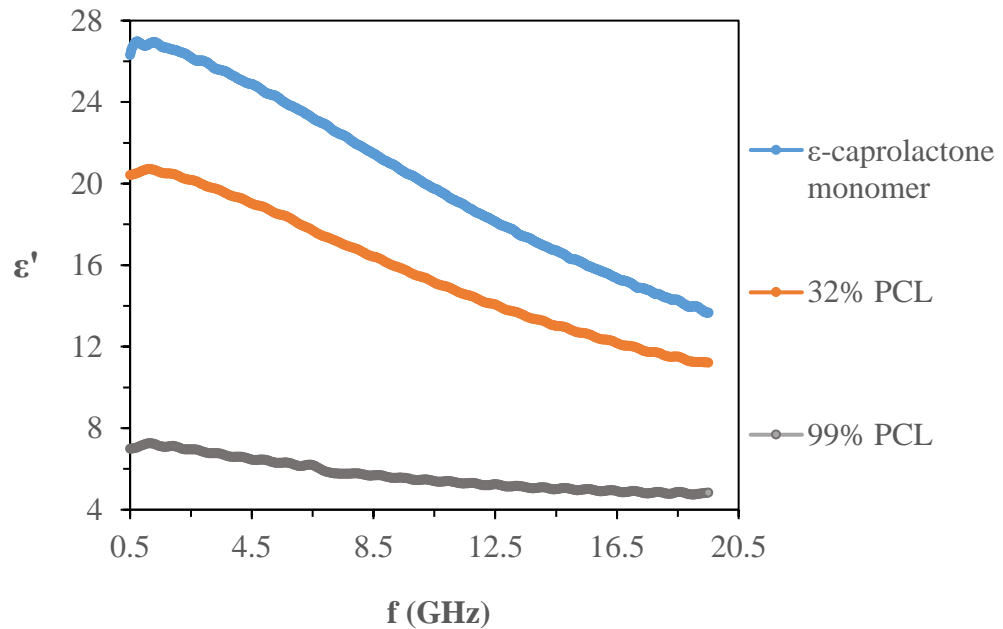


Figure 5.15: Plot of the dielectric constant versus frequency (GHz) of ϵ -caprolactone monomer and polymer mixtures at 160 °C. The maximum standard deviations of the measured data are: ϵ -caprolactone monomer: $[\epsilon' \pm 0.3]$; 32% PCL: $[\epsilon' \pm 0.4]$; 99% PCL: $[\epsilon' \pm 0.3]$.

The data in Figure 5.15 and 5.16 shows how the dielectric constant and loss of ϵ -caprolactone monomer and polymer mixtures vary with frequency when measured by the coaxial probe method. Both dielectric constant and loss drop significantly with the increasing amount of polymer, which is in agreement with previously published cavity perturbation data (Kamaruddin, 2012; Kamaruddin *et al.*, 2014b; Nguyen *et al.*, 2014).

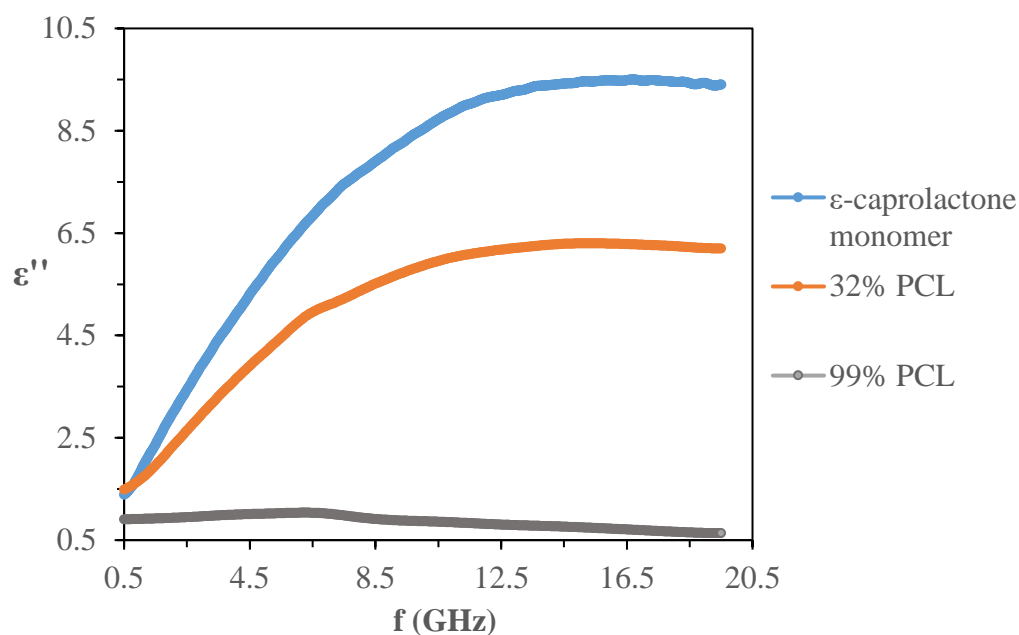


Figure 5.16: Plot of dielectric loss versus frequency (GHz) of ϵ -caprolactone monomer and polymer mixtures at 160 °C. The maximum standard deviations of the measured data are: ϵ -caprolactone monomer: $[\epsilon'' \pm 0.2]$; 32% PCL: $[\epsilon'' \pm 0.2]$; 99% PCL: $[\epsilon'' \pm 0.1]$.

5.5.2 Relationship between the Dielectric Properties and Monomer to Polymer Conversion

It has been reported that this reaction mechanism exhibits pseudo living characteristics i.e. a linear conversion of monomer to polymer with time (Kamaruddin *et al.*, 2014b; Nguyen *et al.*, 2014). Figure 5.17 shows a comparison of ϵ' and M_n versus monomer to polymer conversion. Each data point represents the average of 5 measurements and the standard deviation was used to estimate the error.

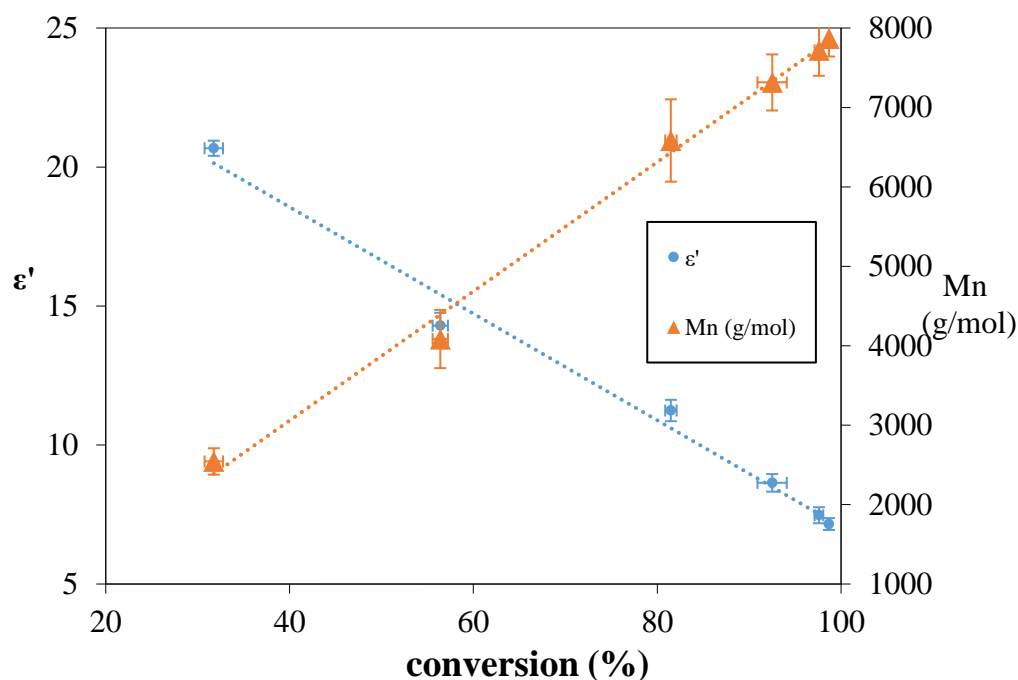


Figure 5.17: Comparison plot of ϵ' (at 0.95 GHz) and M_n versus reaction time.

In Figure 5.17, the dielectric data has been generated by “on-line” probe measurements, whilst the conversion data was determined with “off-line” NMR spectroscopy. As the M_n increases during the progress of the polymerisation, the dielectric properties exhibit a mirrored linear decrease. In detail, ϵ' decreases from 20.7 to 7.1 after 15 minutes of polymerisation time while the M_n increases from 2543 to 7869 g mol⁻¹. This relates to a monomer to polymer conversion from 32 % to 99 % which was also determined by NMR. As the monomer consumption is directly proportional to polymer growth a theoretical molecular weight can be predicted from the initial relative concentration of the monomer and the initiator (Odian, 2004). Table 5.2 details the conversion, theoretical and measured M_n values, and dispersity determined with NMR and GPC. The conversion corrected M_n values for this polymer were found to be in close agreement with the calculated, theoretical M_n values. Thus, this demonstrated that the polymerisation was exhibiting high levels of control with the probe

inserted in the reaction mixture. Therefore, the data in Figure 5.14 demonstrates that:

- the dielectric probe data can be used to record the loss of monomer during the polymerisation (Nguyen *et al.*, 2014), and
- a well-controlled polymerisation can be conducted with the probe in place. As a result, it was concluded that an open-ended coaxial line sensor can be used to monitor the progress of the ϵ -caprolactone ROP polymerisation.

Table 5.2: Experimental conditions, theoretical and observed M_n and Dispersity values for the bulk polymerisation of ϵ -caprolactone using benzyl alcohol and tin octanoate at 160 °C.

Time (min)	Conversion^a (%)	$M_{n,Theory}$ (g/mol)	$M_{n,NMR}^a$ (g/mol)	$M_{n,GPC}^b$ (g/mol)	\overline{D}^b	ϵ' (0.95GHz)
0.2	32	3000	2500	2700	1.16	20.7
2.2	56	5200	4100	4000	1.29	14.3
4.3	82	7500	6600	6300	1.48	11.2
6.3	93	8500	7300	6800	1.71	8.6
10.3	98	9100	7700	7100	1.91	7.5
15	99	9100	7900	6800	2.14	7.1

^a Determined using 1H NMR (400 MHz, $CDCl_3$, 25 °C).

^b Determined using GPC calibrated with polystyrene standards.

As Table 5.2 demonstrates, there was good agreement between the NMR and GPC generated molecular weight data showing that there was a clear evidence of growth with time that was in line with the predicted growth that was predicted by the theoretically calculated values. This is an evidence that a well-controlled polymerisation had been achieved. The difference between the theoretical and experimental values were as a result of water present in the monomer acting as an initiator. Drying of the monomer should result in reduction/removal of this offset.

5.5.3 Frequency dependence of Dielectric properties during polymerisation

Figures 5.18 and 5.19 show the dielectric constant and loss plotted versus frequency for selected times during the polymerisation. It was observed that both ϵ' and ϵ'' decreased during the polymerisation across the frequency range investigated (0.5 GHz - 20 GHz).

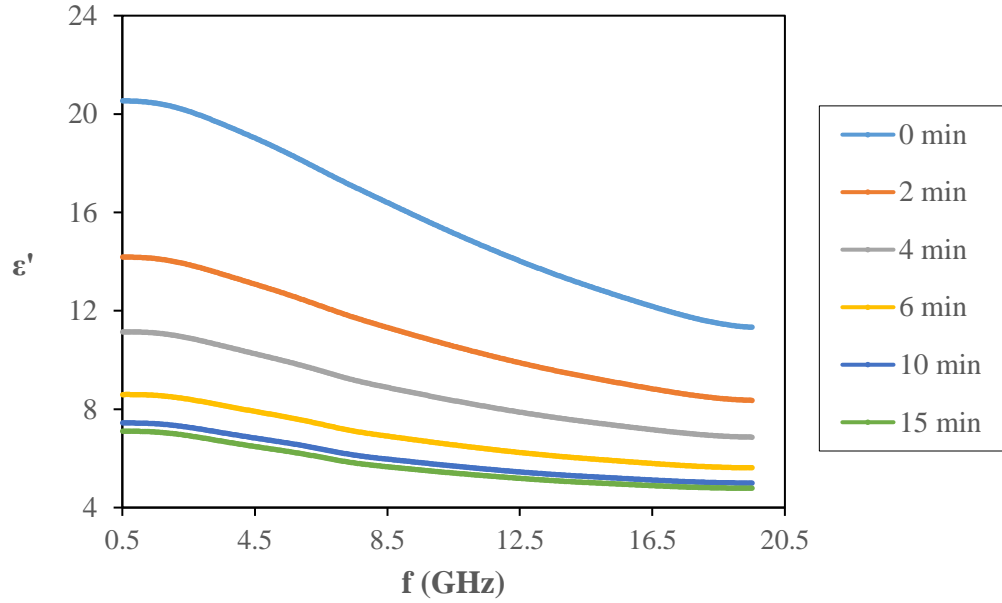


Figure 5.18: Dielectric constant versus time during the polymerisation of ϵ -caprolactone at 160 °C. The maximum standard deviations of the measured data are: 0 min: $[\epsilon' \pm 0.5]$; 2 min. $[\epsilon' \pm 0.6]$; 4 min. $[\epsilon' \pm 0.5]$; 6 min. $[\epsilon' \pm 0.4]$; 10 min: $[\epsilon' \pm 0.3]$; 15 min: $[\epsilon \pm 0.2]$.

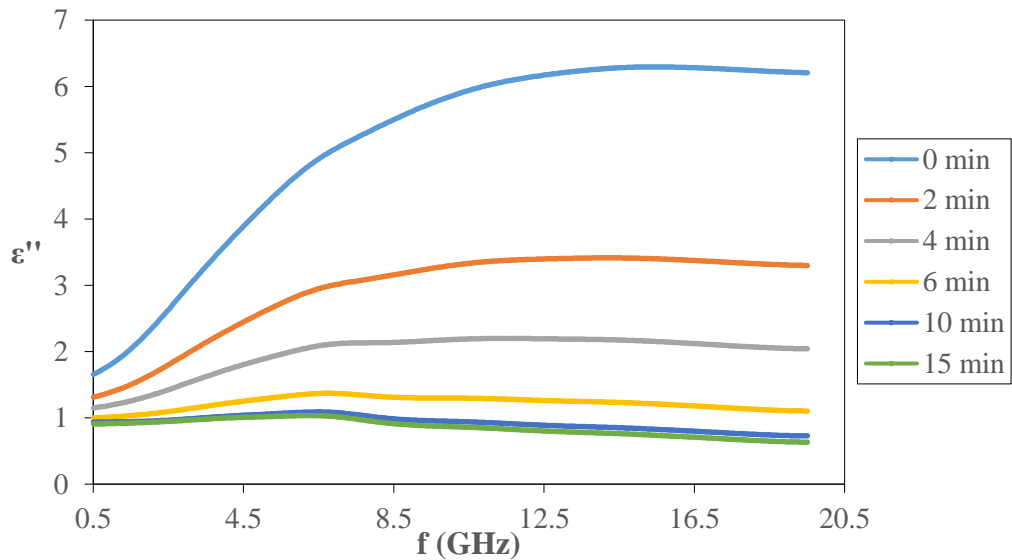


Figure 5.19: Dielectric loss versus time during the polymerisation of ϵ -caprolactone at 160 °C. The maximum standard deviations of the measured data are: 0 min: $[\epsilon'' \pm 0.2]$; 2 min. $[\epsilon'' \pm 0.2]$; 4 min. $[\epsilon'' \pm 0.2]$; 6 min. $[\epsilon'' \pm 0.2]$; 10 min: $[\epsilon'' \pm 0.1]$; 15 min: $[\epsilon'' \pm 0.1]$.

Figures 5.18 and 5.19 denote that there is a significant difference in the dielectric constant and loss values between the monomer and polymer mixtures. Polycaprolactone exhibits lower dielectric response than its monomer. The functional groups (ester groups), which tends to rotate as the chain is built, contribute to the dielectric properties of polymer. As a result, the overall dipolar moment of the molecule is affected as well as their dielectric properties (Kamaruddin *et al.*, 2014b).

5.5.4 Construction of a calibration curve for following the ϵ -caprolactone polymerisation

As it has been previously discussed, the dielectric properties decreased linearly as they are recording the loss of monomer to polymer. The optimum frequencies based on linearity and sensitivity were found at 0.95 GHz and 18.35 GHz. The most suitable type of sensor can be selected based on the optimum frequency to monitor the conversion of monomer to polymer.

In figures 5.20 and 5.21, the dielectric constant and loss are plotted against conversion. The ϵ'' data at high frequencies, such as 18.35 GHz, exhibited high values (see figure 5.21). As a result, a contact method such as a coaxial probe is the most suitable type of sensor. Low frequencies, such as 0.95 GHz, will provide low loss values. Consequently, resonant methods are more accurate for measuring low loss materials. However, the high ϵ' values at low frequencies (see figure 5.20) will affect the sensitivity of the monitoring system if a resonator method is the selected type of sensor.

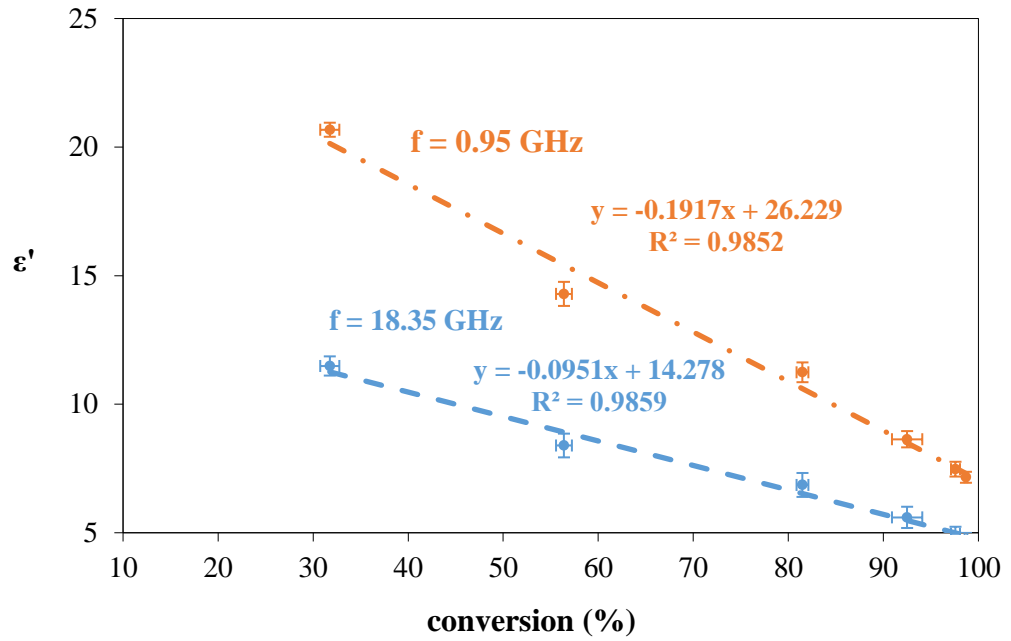


Figure 5.20: Dielectric constant versus conversion for frequency 0.95 GHz and 18.35 GHz

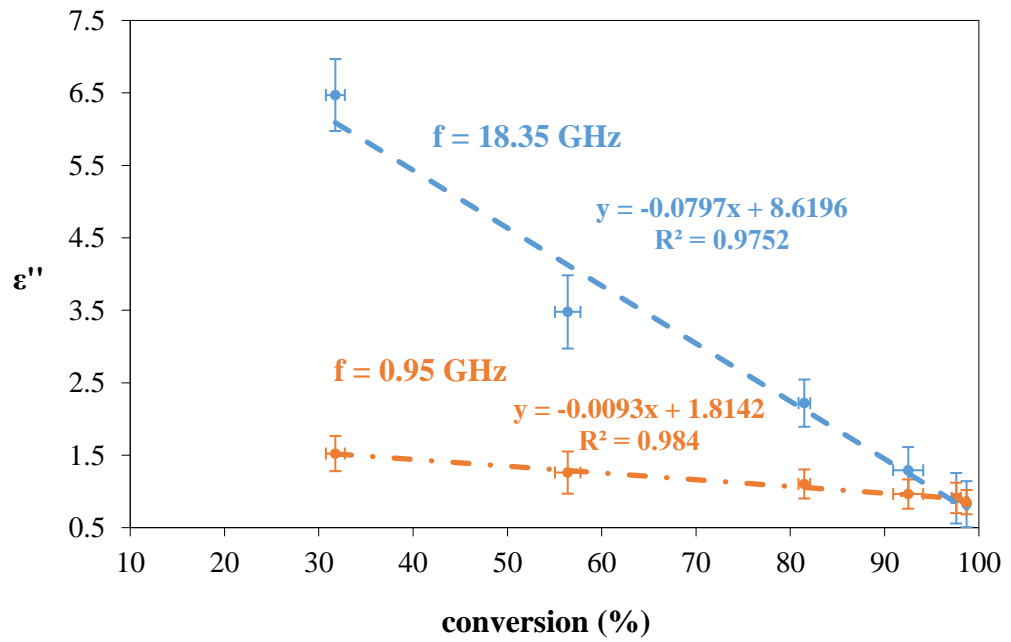


Figure 5.21: Dielectric loss versus conversion for frequency 0.95 GHz and 18.35 GHz

Figures 5.20 and 5.21 demonstrate that both ϵ' and ϵ'' can be linearly related to conversion, as the trend lines exhibit very high coefficient of determination (R^2)

values. Thus, the results obtained in the present study suggest that both ϵ' and ϵ'' could be used to monitor conversion changes based on the appropriate selection of frequency. However, the use of ϵ' is still observed to be more the appropriate, as it offers a larger differential between the monomer and polymer values and therefore better discrimination during the measurement process.

5.5.5 Effect of magnetic stirring compared to mechanical stirring

In this section, the effect of magnetic stirring in the dielectric properties will be investigated. Therefore, a series of ϵ -caprolactone polymerisations were conducted with magnetic and mechanical stirring. All experiments were conducted with a constant [CL]:[Sn(Oct)₂]:[BzOH] molar ratio of 800:1:10. The mixture was heated to the target reaction temperature (160 °C) with the use of a preheated oil bath and the dielectric properties were measured using the coaxial probe. Figure 5.22 shows the dielectric constant and loss of the polymerisation mixture once it reached 160 °C using magnetic and mechanical stirring. The results show that the type of stirring has insignificant effect in the dielectric properties. Similar conclusions on the effect of magnetic stirring were published by Kamaruddin (2012).

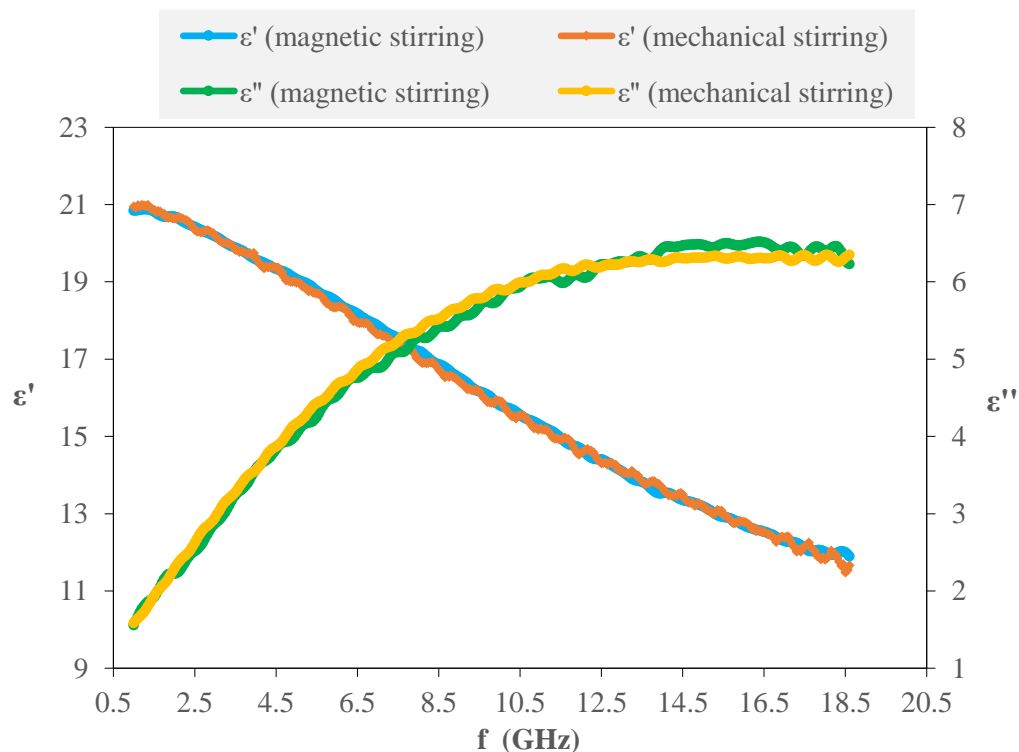


Figure 5.22: Comparison of the influence of magnetic and mechanical stirring in the Dielectric properties of the PCL polymerisation mixture at 160 °C

5.6 Conclusions

This study has presented the online monitoring of the tin octanoate mediated polymerisation of ϵ -caprolactone using an open-ended coaxial line sensor. It was demonstrated that the measurement of the dielectric properties during the progress of the polymerisation can be used to real time follow reaction progress and, with the use of a calibration curve, identify key reaction parameters (e.g., the achieved level of monomer to polymer conversion). Both ϵ' and ϵ'' can be used to follow the progress of the polymerisation. Additionally, a highly controlled polymerisation can be successfully conducted with the probe immersed within the reaction mixture, as the presence of the probe clearly did not affect the quality of the polymerisation. Furthermore, the analysis of the

dielectric data with frequency allowed the identification of the optimum frequencies for the practical operation of the sensor, in terms of linearity and sensitivity. Both ϵ' and ϵ'' decreased during the polymerisation across the frequency range investigated (0.5 GHz - 20 GHz) and the largest scale measurement changes for ϵ' and ϵ'' , which also exhibited the best linearity, were found at frequencies 0.95 GHz and 18.35 GHz respectively. Therefore, a calibration curve was constructed in order to utilise dielectric properties to follow the conversion of ϵ -caprolactone monomer to polycaprolactone in a systematic way. This demonstrated that sensor techniques based on observing the change in dielectric constant or loss using a reflectance method should have broad applicability to many chemical transformations. Additionally, it was confirmed that the presence of magnetic stirring has insignificant effect in the measured dielectric properties.

The application of this method has high potential to improve process control strategies and both, optimise product quality and batch to batch repeatability. For example, by clearly identifying the optimum point to terminate the reaction to prevent formation of by-products due to the onset of transesterification at higher conversion or the ideal point to add a second monomer to synthesise an architectural polymer. Additionally, it can be used to optimise energy usage by minimising the amount of time that the reaction is kept at the elevated temperatures required for polymerisation. On the one hand, the proposed method can be successfully applied in bulk polymerisations as the significant increase in viscosity that was observed over the course of ϵ -caprolactone polymerisation has been shown not to influence the quality of the data obtained which can aid in the development of processes that focus on eliminating the use of solvents. On the

other hand, the application of the technique in bulk polymerisations where there is a big temperature variation within the reaction mixture is challenging due to the temperature dependence of the dielectric properties.

References

Bakeev, K. A. (2010) *Process Analytical Technology: Spectroscopic Tools and Implementation Strategies for the Chemical and Pharmaceutical Industries*. John Wiley & Sons.

Blackham, D. V. and Pollard, R. D. (1997) An improved technique for permittivity measurements using a coaxial probe. *IEEE Transactions on Instrumentation and Measurement* 46(5): pp.1093–1099.

Brown, B. H., Smallwood, R. H., Barber, D. C., Lawford, P. V. and Hose, D. R. (1998) *Medical Physics and Biomedical Engineering*. CRC Press.

Cole, K. S. and Cole, R. H. (1941) Dispersion and Absorption in Dielectrics I. Alternating Current Characteristics. *The Journal of Chemical Physics* 9(4): pp.341–351.

Deng, H., Shen, Z., Li, L., Yin, H. and Chen, J. (2014) Real-time monitoring of ring-opening polymerization of tetrahydrofuran via in situ Fourier Transform Infrared Spectroscopy. *Journal of Applied Polymer Science* 131(15): pp.n/a-n/a.

Destarac, M. (2010) Controlled Radical Polymerization: Industrial Stakes, Obstacles and Achievements. *Macromolecular Reaction Engineering* 4(3–4): pp.165–179.

Dubois, P., Coulembier, O. and Raquez, J.-M. (2009) *Handbook of Ring-Opening Polymerization*. John Wiley & Sons.

Ghavimi, S. A. A., Ebrahimzadeh, M. H., Solati-Hashjin, M. and Osman, N. A. A. (2015) Polycaprolactone/starch composite: Fabrication, structure, properties, and applications. *Journal of Biomedical Materials Research Part A* 103(7): pp.2482–2498.

Gregory, A. P. and Clarke, R. N. (2012) *Tables of the Complex Permittivity of Dielectric Reference Liquids at Frequencies Up to 5 GHz*. National Physical Laboratory.

Gregory, A. P., Clarke, R. N. and Cox, M. G. (2009) Traceable measurement of dielectric reference liquids over the temperature interval 10–50 °C using coaxial-line methods. *Measurement Science and Technology* 20(7): pp.075106.

Gregory, A. P., Clarke, R. N., Hodgetts, T. E. and Symm, G. T. (2008) RF and microwave dielectric measurements upon layered materials using coaxial sensors. NPL. Available at: <http://adsabs.harvard.edu/abs/1993rmdm.rept....G> (Accessed: 21 September 2017).

Gridnev, A. A. and Ittel, S. D. (2001) Catalytic chain transfer in free-radical polymerizations. *Chemical Reviews* 101(12): pp.3611–3660.

Hawker, C. J., Bosman, A. W. and Harth, E. (2001) New Polymer Synthesis by Nitroxide Mediated Living Radical Polymerizations. *Chemical Reviews* 101(12): pp.3661–3688.

Hergeth, W.-D. (2000) On-Line Monitoring of Chemical Reactions. in Ullmann's Encyclopedia of Industrial Chemistry. Wiley-VCH Verlag GmbH & Co. KGaA.

Hill, N. (1969) Dielectric Properties and Molecular Behaviour. London, New York: Van Nostrand Reinhold Inc., U.S.

Jol, H. M. (2008) Ground Penetrating Radar Theory and Applications. Elsevier.

Kamaruddin, J. (2012) Microwave Processing of Bio-degradable Polymers: Ring Opening Polymerisation of ϵ -caprolactone. PhD. The University of Nottingham.

Kamaruddin, M. J., Nguyen, N. T., Dimitrakis, G. A., Harfi, J. E., Binner, E. R., Kingman, S. W., Lester, E., Robinson, J. P. and Irvine, D. J. (2014) Continuous and direct 'in situ' reaction monitoring of chemical reactions via dielectric property measurement: controlled polymerisation. *RSC Advances* 4(11): pp.5709–5717.

Kingston, H. M. and Jassie, L. B. (1988) Introduction to Microwave Sample Preparation: Theory and Practice. American Chemical Society.

Koh, M. L., Konkolewicz, D. and Perrier, S. (2011) A Simple Route to Functional Highly Branched Structures: RAFT Homopolymerization of Divinylbenzene. *Macromolecules* 44(8): pp.2715–2724.

Labet, M. and Thielemans, W. (2009) Synthesis of polycaprolactone: a review. *Chemical Society Reviews* 38(12): pp.3484–3504.

Lewis, I. R. and Edwards, H. (2001) Handbook of Raman Spectroscopy: From the Research Laboratory to the Process Line. CRC Press.

Liao, L. Q., Liu, L. J., Zhang, C., He, F., Zhuo, R. X. and Wan, K. (2002) Microwave-assisted ring-opening polymerization of ϵ -caprolactone. *Journal of Polymer Science Part A: Polymer Chemistry* 40(11): pp.1749–1755.

Mascia, L. (2012) Polymers in Industry from A to Z: A Concise Encyclopedia. John Wiley & Sons.

Metaxas, A. C. and Meredith, R. J. (1905) *Industrial Microwave Heating*. London, UK: The Institution of Engineering and Technology.

Meurant, G. (2012) *Dielectrics in Time-Dependent Fields*. Elsevier.

Misra, D. (1995) On the measurement of the complex permittivity of materials by an open-ended coaxial probe. *IEEE Microwave and Guided Wave Letters* 5(5): pp.161–163.

Mittal, V. (2012) *Characterization Techniques for Polymer Nanocomposites*. John Wiley & Sons.

Nguyen, N. T., Greenhalgh, E., Kamaruddin, M. J., El harfi, J., Carmichael, K., Dimitrakis, G., Kingman, S. W., Robinson, J. P. and Irvine, D. J. (2014) Understanding the acceleration in the ring-opening of lactones delivered by microwave heating. *Tetrahedron* 70(4): pp.996–1003.

Odian, G. (2004) *Principles of Polymerization*. John Wiley & Sons.

Pissis, P., Pandis, C., Maroulas, P., Kyritsis, A. and Kontou, E. (2015) Electrical/Dielectric Measurements for Monitoring Polymerization, Morphology and Mechanical Integrity in Polymer Nanocomposites. *Procedia Engineering*. (ICSI 2015 The 1st International Conference on Structural Integrity Funchal, Madeira, Portugal 1st to 4th September, 2015) 114: pp.598–605.

Santos, A., Cherfi, A., McKenna, T., Seytre, G., L. Lima, E., C. Pinto, J. and Fevotte, G. (2001) Inline Dielectric Monitoring of MMA/BuA Copolymerization Reactions. *CHIMIA International Journal for Chemistry* 55: pp.251–253.

Wang, W., Zheng, Y., Roberts, E., Duxbury, C. J., Ding, L., Irvine, D. J. and Howdle, S. M. (2007) Controlling Chain Growth: A New Strategy to Hyperbranched Materials. *Macromolecules* 40(20): pp.7184–7194.

Wu, K.-J., Wu, C.-S. and Chang, J.-S. (2007) Biodegradability and mechanical properties of polycaprolactone composites encapsulating phosphate-solubilizing bacterium *Bacillus* sp. PG01. *Process Biochemistry* 42(4): pp.669–675.

6 MONITORING OF THE CHEMICAL TRANSFORMATIONS OF SUGARS

6.1 Introduction

Petroleum products are extensively used today and have a major contribution to the economic growth of our modern society. However, their environmental impact is high in terms of life-cycle greenhouse gas emissions and disposal cost (Piemonte and Gironi, 2011). The relation of greenhouse gas emissions with climate change led to the development of policies aimed to reduce carbon emissions (Remuzgo and Trueba, 2017). In 2007, EU leaders set a target to reduce greenhouse gas emissions 20% from 1990 levels by 2020. The development of biobased and biodegradable products can decrease fossil energy consumption in the chemical industry (Díaz, Katsarava and Puiggalí, 2014). Adom *et al.* (2014) reported that sugar-based bioproducts can save 25% to approximately 100% on the life-cycle greenhouse gas emissions compared to their fossil-derived counterparts. The main concern for their extensive use is that the cost of biobased production is usually higher than the cost of petrochemical production. Additionally, the separation of the products from the reaction mixture is challenging and requires the use of bleaching/purification techniques (Oltmanns, Palkovits and Palkovits, 2013)

According to the US Department of Energy, sorbitol is one of the top twelve building block chemicals that can be produced from sugars (Werpy and Petersen, 2014). Isosorbide can be produced by the dehydration reaction of D-sorbitol and has many applications in pharmaceuticals, organic solvents, fuel additives,

monomers and building blocks for biopolymers (Aricò and Tundo, 2016). Isosorbide derivatives, such as dimethyl isosorbide, can replace toxic solvents such as dimethyl sulfoxide, dimethyl formamide and dimethyl acetamide due to its high boiling point (235–237 °C at 760 mm Hg pressure), but has also found applications in personal care and pharmaceutical products (Tundo *et al.*, 2010). However, the production of those products requires either high temperatures and/or extended reaction times to achieve significant product yields (Li *et al.*, 2013). These conditions are detrimental to both the quality of final products and production cost. The long exposure to elevated temperature tends to develop high levels of coloration and/or by-product content, which prevents their direct use in certain commercial applications, such as those in pharmaceuticals and personal care. The current bleaching/purification techniques to refine the quality of final product increase production complexity and costs, reduce overall yield, and generate additional process waste (Oltmanns, Palkovits and Palkovits, 2013). This results in the need for a technique to monitor reaction progress which could help minimise the time that the reaction mixture is kept at the required temperature.

To date, the molecular analysis of sorbitol dehydration in terms of product formation is usually performed using offline techniques such as gas chromatography and high performance liquid chromatography (Giacometti, Milin and Wolf, 1995; Li *et al.*, 2013). These techniques require sample extraction and preparation; thus they cannot be easily adapted to perform measurements on-line within the process and in real time. The development of a direct online method for the real-time monitoring of sorbitol dehydration has high potential to improve process control and both, reduce energy consumption

and waste generation. For example, by identifying the optimum point to terminate the reaction, the amount of time that the reaction is kept at the target temperature can be minimised. Furthermore, the development of a process that can be used in the bulk reaction will eliminate the use of solvents. In chapter 5, the real-time monitoring of the ring opening polymerisation of ϵ -caprolactone through the on-line measurement of the system dielectric properties was presented. It was demonstrated that a technique based on observing the change in the dielectric properties during the progress of a chemical reaction using a coaxial line sensor should have broad applicability to many chemical transformations. The aim of this chapter is to monitor the dehydration of sorbitol to 1,4-sorbitan and isosorbide using the methodology developed in the monitoring of ϵ -caprolactone polymerisation. The dielectric properties of all materials are studied as well as their temperature and frequency dependence. An open-ended coaxial line sensor is used to monitor the dielectric properties during the dehydration of sorbitol to isosorbide in a broad frequency range (1 GHz – 19 GHz). A comparison of the dielectric data at low and high frequencies will highlight the optimum property and frequency range for the online monitoring of the chemical transformation. Finally, the construction of a calibration curve to follow the dehydration by monitoring isosorbide conversion will be discussed in the final section of the chapter.

6.2 Experimental

An open-ended coaxial line sensor utilised to monitor the dehydration of sorbitol to 1,4-sorbitan and isosorbide using para toluene sulfonic acid (pTSA) as a

catalyst under solvent free and atmospheric pressure conditions. The sensor was placed directly into the reaction medium and used to characterise the dielectric properties of the reaction mixture both ‘in-situ’ and with time at frequencies ranging from 1 GHz up to 19 GHz in 50 MHz steps. In addition to measurements obtained by the sensor, samples of the medium were extracted at various time points for off-line molecular analysis, to confirm the level of isosorbide conversion that had been achieved. The experimental results are presented together with their error bars. The maximum standard deviation was used to estimate the error. For results with small deviation, the error bars are omitted for clarity and the measurement error is presented in the label in terms of standard deviation, i.e. $\varepsilon' \pm \sigma(\varepsilon')$, where σ is the maximum standard deviation.

6.2.1 Materials

Sorbitol (D-Glucitol, $\geq 98\%$) and isosorbide (Dianhydro-D-glucitol, 98%) were purchased from Sigma Aldrich. Sorbitan (1,4-Anhydro-D-glucitol, 99%) was purchased from Carbosynth. A desiccator was used to store and maintain the samples in a dry condition.

6.2.2 Dielectric property measurement

The dielectric properties of sugars (sorbitol, 1,4-sorbitan and isosorbide) were studied using the cavity perturbation and coaxial probe techniques.

6.2.2.1 Cavity perturbation method

The cavity perturbation method was selected to measure the dielectric properties of all components prior to the ‘in situ’ study for the following reasons:

- a) As an independent dielectric characterisation method to validate the ‘in situ’ data measured with the coaxial probe method.
- b) It is the preferable method for the measurement of materials' dielectric properties below their melting point. The cavity perturbation technique is more suitable technique for the dielectric characterisation of powdered samples compared to a contact method, such as the coaxial probe, because the sample roughness and air gaps between the probe and a powder sample can affect the accuracy of complex permittivity measurements (Arai, Binner and Cross, 1995; Venkatesh and Raghavan, 2005).
- c) The small amount of sample required for the dielectric characterisation make the technique suitable for samples with low sample availability.

The cavity perturbation technique and apparatus are described in Section 4.2.2. The dielectric properties of sorbitol, 1,4-sorbitan and isosorbide were measured at temperatures from 20 °C to 160 °C with 10 °C step. Each data point represents the average of at least three measurements. The standard deviation was used to estimate the error and is represented by the error bars.

6.2.2.2 Coaxial probe method

The coaxial probe method was used for the dielectric characterisation of individual precursors above their melting point, as well as for the ‘in situ’ monitoring of sorbitol dehydration. The setup consists of an Agilent 85070E

open ended coaxial line sensor and a Keysight N5232A PNA-L Vector Network Analyser (VNA). The coaxial probe technique is detailed in Section 4.2.1 and the setup for ‘in situ’ measurements is described in Section 5.2.3.

6.2.3 Off-line molecular analysis

Samples were extracted at set times during the dehydration of sorbitol to isosorbide for off-line analysis with Nuclear Magnetic Resonance spectroscopy (NMR). ^1H NMR spectra were recorded at 25 °C on a Bruker AVIIIHD 400 (400 MHz) spectrometer, equipped with cryoprobe to prevent further reaction during analysis. The chemical shifts were recorded in δ (ppm) and coupling constants (J) were recorded to the nearest 0.5 Hz. The samples were dissolved in Dimethyl sulfoxide (DMSO) to which the chemical shifts were referenced (2.5 ppm). The conversion of sorbitol into sorbitan and isosorbide and their relative concentrations were determined by comparing the integrations of the methylene resonances for sorbitol (at 3.35 ppm), with those for sorbitan at 3.90 ppm and for isosorbide at 4.05 ppm..

6.3 Dielectric property analysis of sugars

Previous studies reported the dielectric properties of sorbitol in aqueous solutions with sucrose and sodium chloride (Yaghmaee and Durance, 2002), during isothermal crystallization (Minoguchi and Nozaki, 2002), in dry and partially hydrated states (Derbyshire *et al.*, 2003) and at elevated pressure (Casalini and Roland, 2004). However, they have been collected over a limited temperature range and have only focused on sorbitol without considering derivatives such as 1,4-sorbitan and isosorbide. In this section, a study of the

dielectric properties of sugars (sorbitol, 1,4-sorbitan and isosorbide) was performed at a broad temperature (20 °C – 160 °C) and frequency range (1 GHz – 19 GHz) in order to understand the effect of temperature and frequency on the dielectric properties.

6.3.1 Temperature dependence of dielectric properties

In order to study the effect of temperature in the complex permittivity of sugars, the dielectric properties of sorbitol, 1,4-sorbitan, and isosorbide were measured using the cavity perturbation technique at temperatures from 20 °C to 160 °C with 10 °C intervals. Figures 6.1 and 6.2 show the dielectric constant and loss versus temperature at frequency 2470 MHz. Each data point represents the average of three measurements and the error bars show the standard deviation.

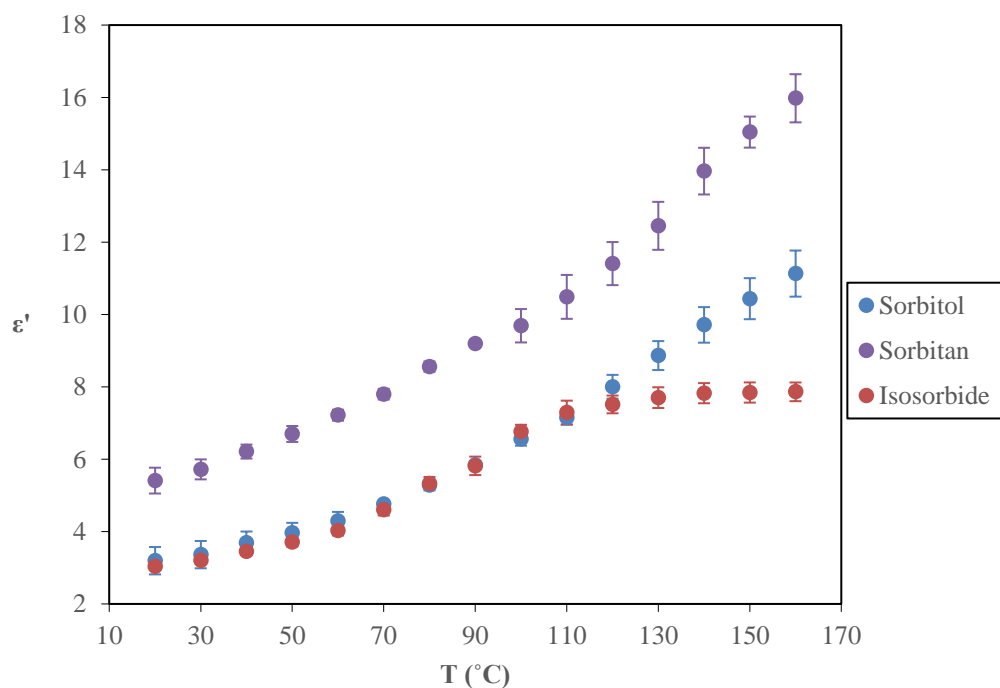


Figure 6.1: Dielectric constant versus temperature at 2470 MHz.

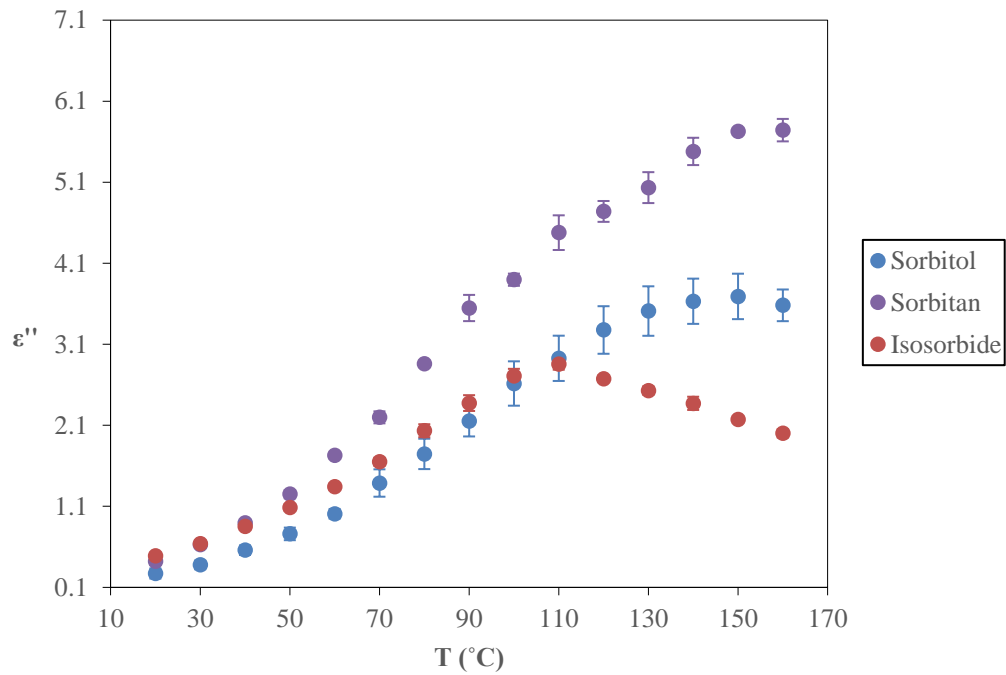


Figure 6.2: Dielectric loss versus temperature at 2470 MHz.

All materials underwent a phase change from solid to liquid during heating. The melting points of sorbitol, 1,4-sorbitan, and isosorbide are 98 – 100 °C, 112 – 113 °C and 60 – 63 °C respectively. Both dielectric constant and loss of all components were found to be strongly and non-linearly dependent with temperature (Figure 6.1). This behaviour could be attributed to the thermally activated conductivity at high temperatures. Additionally, the dipoles of a material in the liquid form have greater degree of freedom to align with the incident electromagnetic field compared to the solid state (Naumann, 2008). The dielectric loss increases with increasing temperature up to a maximum, which corresponds to the relaxation time, and is related with the time required for the dipoles to become oriented with the applied electromagnetic field, as discussed in Section 3.3.3. Loss values above the relaxation peak decreased, as the ability of dipoles to convert electromagnetic energy into heat is reduced at high temperatures (Metaxas and Meredith, 1905).

6.3.2 Frequency dependence of dielectric properties

In order to study the effect of frequency in the complex permittivity, the dielectric properties of sorbitol, and isosorbide were measured at frequencies from 1 GHz to 19 GHz using the coaxial probe technique. Figure 6.3 shows the dielectric constant and loss at temperature 110 °C, which is the target reaction temperature for the dehydration reaction of sorbitol to isosorbide. In Figure 6.3, both ϵ' and ϵ'' decrease as the frequency increases which indicate the reduced ability of the material to store and dissipate energy at high frequencies.

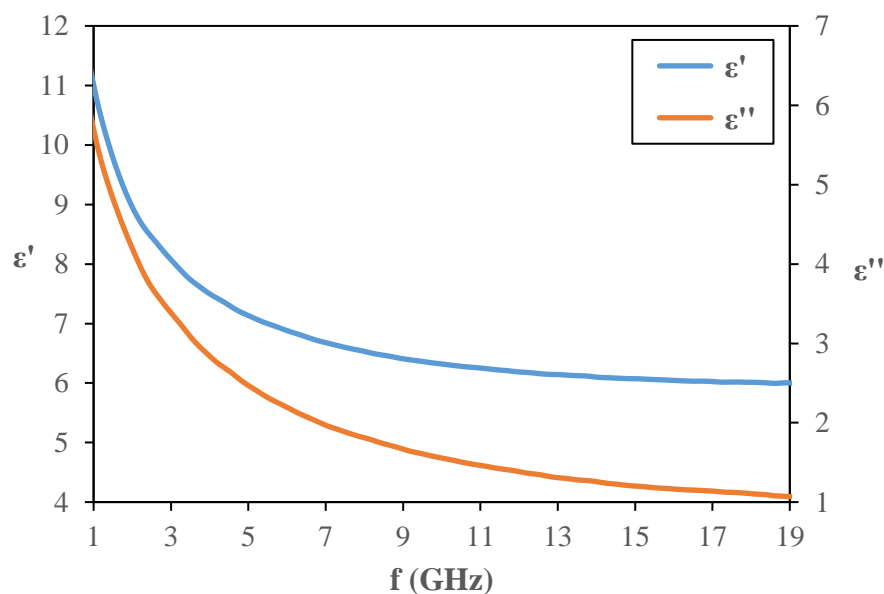


Figure 6.3: Dielectric constant and loss of sorbitol versus frequency at 110 °C. Due to the small deviation, the error bars are indistinguishable. The maximum standard deviations of the measured data are: $[\epsilon' \pm 0.2]$; $[\epsilon'' \pm 0.4]$.

Figure 6.4 shows the dielectric constant and loss versus frequency of isosorbide at frequencies from 1 GHz to 19 GHz. In figure 6.4, ϵ' decreases gradually with increasing frequency, from 10.8 at 1 GHz to 4.8 at 19 GHz. Meanwhile, the ϵ'' increases with frequency from 3.1 at 1 GHz to 3.75 at 2.15 GHz before

decreasing gradually to 0.4 at 19 GHz. This indicates that the relaxation of isosorbide occurs at 2.15 GHz at temperature 110 °C.

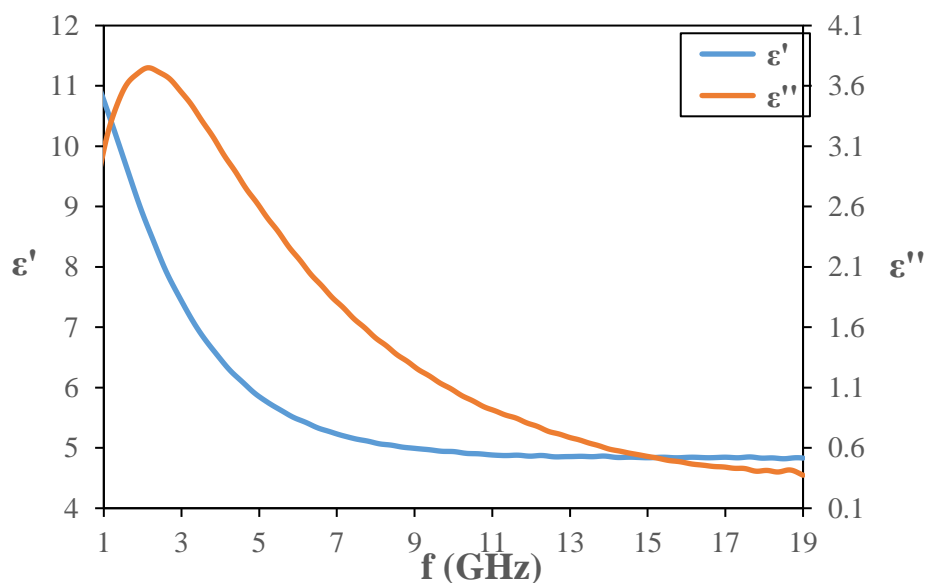


Figure 6.4: Dielectric constant and loss of isosorbide versus frequency at 110 °C. The maximum standard deviations of the measured data are: $[\varepsilon' \pm 0.1]$; $[\varepsilon'' \pm 0.1]$.

6.4 Dehydration of Sorbitol

The dehydration reaction of sorbitol to sorbitan and isosorbide using para toluene sulfonic acid (pTSA) as a catalyst was studied. The dielectric properties of the reaction mixture were monitored “in-situ” and with time with the use of an open-ended coaxial line sensor at microwave frequencies (1 GHz – 19 GHz). Samples were extracted at set times during the progress of dehydration for off-line analysis with ^1H Nuclear Magnetic Resonance spectroscopy. Details of the technique are analysed in Section 6.2.2.

6.4.1 Synthesis of 1,4-sorbitan and isosorbide from D-sorbitol

Sorbitol dehydration experiments were performed with the use of 15 mol% pTSA as a catalyst under solvent free and atmospheric pressure conditions. pTSA used as the preferred catalyst as it can achieve significant product yields (Dusenne *et al.*, 2017). The process involved the following steps:

- 10 g sorbitol (54.89 mmol) and 1.57 g pTSA (8.23 mmol) were introduced into a three neck round bottom flask.
- The mixture was then heated to the target reaction temperature (110 °C) with a heating rate of 5 °C/min with the use of a preheated oil bath. The mixture was mechanically stirred throughout the reaction progress and temperature was monitored using a thermocouple.
- An open-ended coaxial line sensor was used to monitor the dielectric properties.
- At set times during the reaction progress, samples were extracted using a Hamilton syringe and needle for off-line analysis with NMR spectroscopy.
- At the end of the reaction, the flask was removed, and crude product, which was in the in the form of a viscous brown colored oil, was also analysed with NMR without further purification.

The double dehydration of sorbitol, is an acid catalysed reaction, as shown in Figure 6.5. According to Flèche and Huchette (1986), one of the sorbitol's primary hydroxyl groups is preferentially protonated by the catalyst, and defined as C₁ position. After the successful protonation of hydroxyl in C₁ position, a molecule of water is eliminated. This promotes a cyclization between carbon

atoms in C₁ and C₄ positions, which results in the formation of 1,4-sorbitan (in this study, 1,4-sorbitan is referred as sorbitan). Subsequently, this operation is followed by a second protonation of the last primary hydroxyl group at C₆ position, followed by a cyclization with the carbon in C₃ position. This leads to the formation of isosorbide.

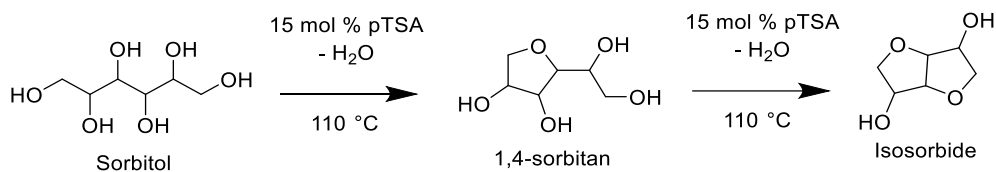


Figure 6.5: Mono- and double-dehydration products of sorbitol catalysed by pTSA.

In Table 6.1, the results of sorbitol dehydration catalysed by 15 mol% pTSA are presented, analysed with ¹H NMR spectroscopy. At 60 min reaction time, 89.28 mol% of sorbitol was converted to sorbitan, which confirms that 1,4-sorbitan is the major first step reaction product. The results showed that after 180 min, 97.41 mol% of sorbitol was converted to sorbitan and isosorbide. Furthermore, it appears that sorbitol dehydrated more quickly to 1,4-sorbitan than the later to isosorbide, which is confirmed from previous studies (Dussenne *et al.*, 2017).

Table 6.1: Results of sorbitol dehydration in bulk, catalysed by 15 mol% pTSA at 110 °C.

Time (min)	Composition (mol %)^a		
	Sorbitol	1,4-sorbitan	Isosorbide
20	36.51	58.57	4.92
60	10.72	78.89	10.39
100	3.18	74.33	22.50
140	3.10	57.26	39.64
180	2.59	40.39	57.02

^a Determined using ¹H NMR (400 MHz, CDCl₃, 25 °C).

6.4.2 Frequency dependence of dielectric properties during the dehydration reaction

The dielectric properties of the reaction mixture were measured over a broad frequency range at set times during the progress of the dehydration. At each time point, a swept frequency signal from 1 GHz up to 19 GHz in 50 MHz steps was transmitted from the Vector Network Analyser into the sample, via the coaxial line, and the dielectric properties were calculated based on the reflection coefficient of the sample, as described in section 4.2.1. Figures 6.6 and 6.7 show how the dielectric constant and loss varied with frequency at selected time points

during the reaction progress. Both dielectric constant and loss drop significantly during the progress of dehydration.

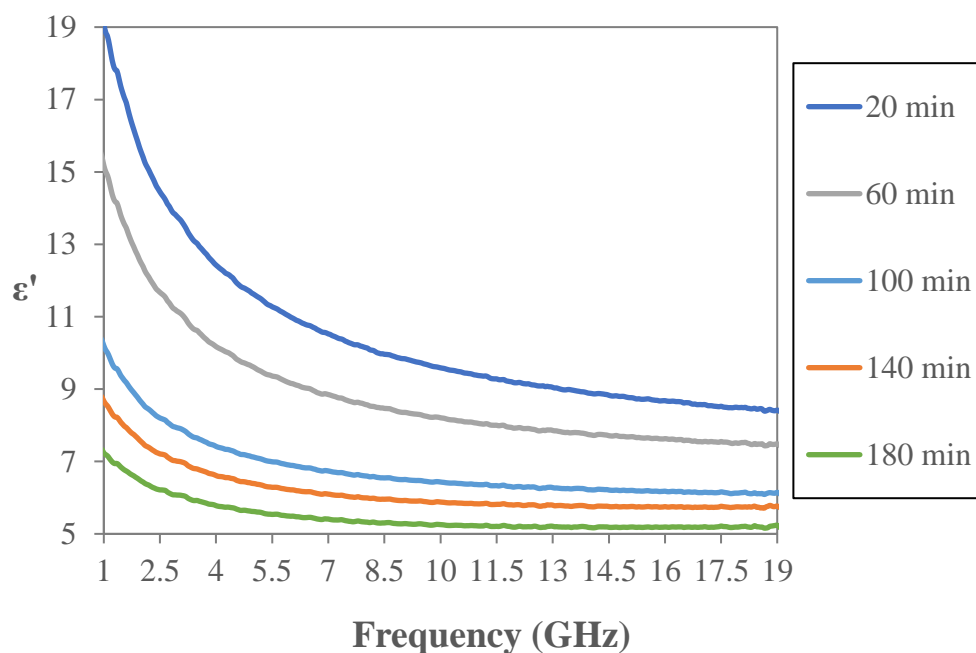


Figure 6.6: Dielectric constant versus frequency (GHz). The maximum standard deviations of the measured data are: 20 min: $[\epsilon' \pm 0.2]$; 60 min: $[\epsilon' \pm 0.4]$; 100 min: $[\epsilon' \pm 0.4]$; 140 min: $[\epsilon' \pm 0.3]$; 180 min: $[\epsilon' \pm 0.2]$.

The comparison of the dielectric data at low and high frequencies will enable the identification of the most suitable frequency for the monitoring of dehydration reaction using the coaxial probe. In Figure 6.7, ϵ' exhibits the largest scale measurement change during the dehydration progress at low frequencies. For example, ϵ' at 1 GHz decreases from 19.1 to 7.2 as the dehydration time increases from 20 min to 180 min, whilst at 19 GHz, a smaller decrease of 8.4 to 5.2 was recorded. In Figure 6.8, ϵ'' values at 19 GHz decreased from 3.6 to 0.5 while at 2.5 GHz decreased from 17 to 2.9. As a result, low frequencies, such as 1 GHz, provide the highest scale measurement change.

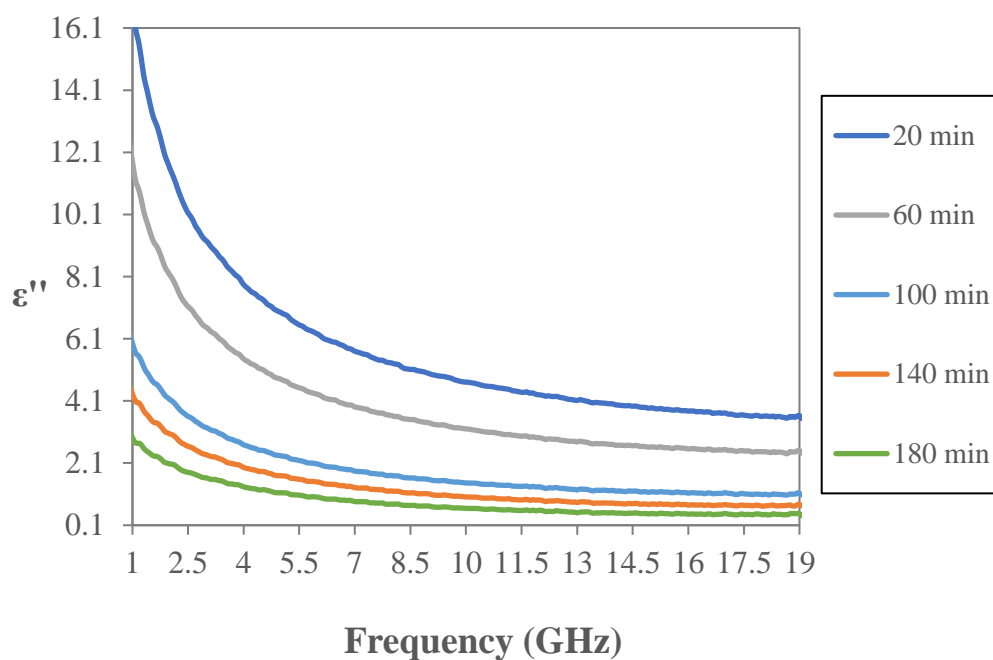


Figure 6.7: Dielectric loss versus frequency (GHz). The maximum standard deviations of the measured data are: 20 min: $[\epsilon'' \pm 0.2]$; 60 min: $[\epsilon'' \pm 0.4]$; 100 min: $[\epsilon'' \pm 0.4]$; 140 min: $[\epsilon'' \pm 0.3]$; 180 min: $[\epsilon'' \pm 0.2]$.

If in Figures 6.8 and 6.9 reaction time was replaced with isosorbide composition, as determined with NMR spectroscopy and detailed in Table 6.1. An additional series is also added with the isosorbide dielectric data, as presented in section 6.3.2.

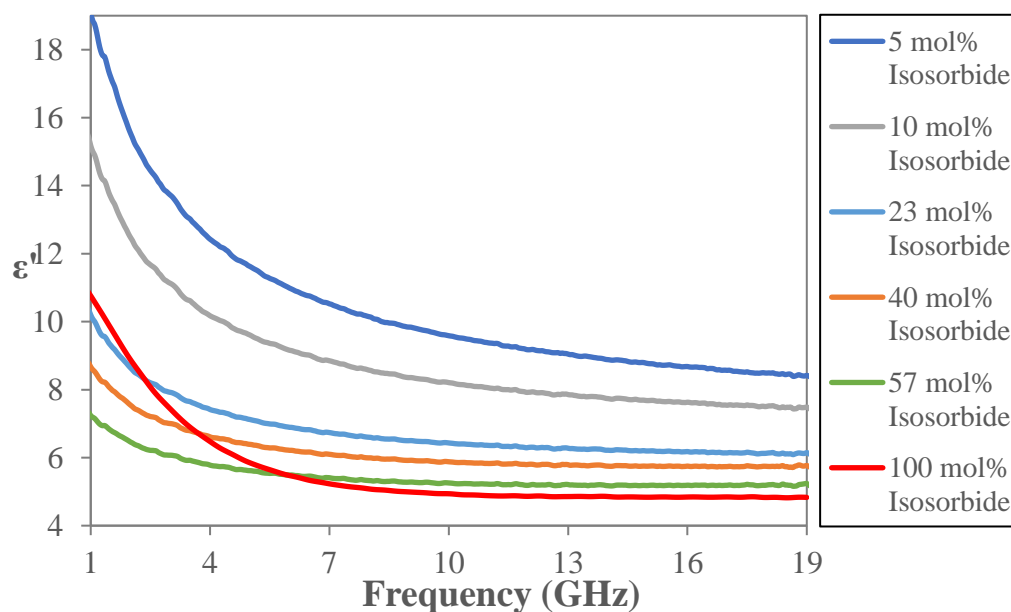


Figure 6.8: Dielectric constant (ϵ') versus frequency (GHz). The maximum standard deviations of the measured data are: 5 mol%: [$\epsilon' \pm 0.2$]; 10 mol%: [$\epsilon' \pm 0.3$]; 23 mol%: [$\epsilon' \pm 0.4$]; 40 mol%: [$\epsilon' \pm 0.4$]; 57 mol%: [$\epsilon' \pm 0.3$]; 100 mol%: [$\epsilon' \pm 0.1$].

In Figure 6.9, isosorbide exhibits a relaxation peak at 2.2 GHz while the reaction mixtures exhibit relaxation at lower frequencies, below the measured frequency range. This behaviour could be explained due to the presence of sorbitan in the reaction mixture, which found to has higher dielectric properties than isosorbide, as described in Section 6.3.1. The selection of the optimum frequency range should consider the dielectric properties of the final product. As a result, low frequencies, while provide the highest scale measurement change at reaction mixtures with low isosorbide composition, they did not provide a clear differentiation in reaction mixtures with high isosorbide composition. However, if dielectric constant is selected as the preferred property for the monitoring of the dehydration reaction, a clear trend in reaction mixtures with high isosorbide composition is observed at frequencies above 6 GHz, as seen in Figure 6.8.

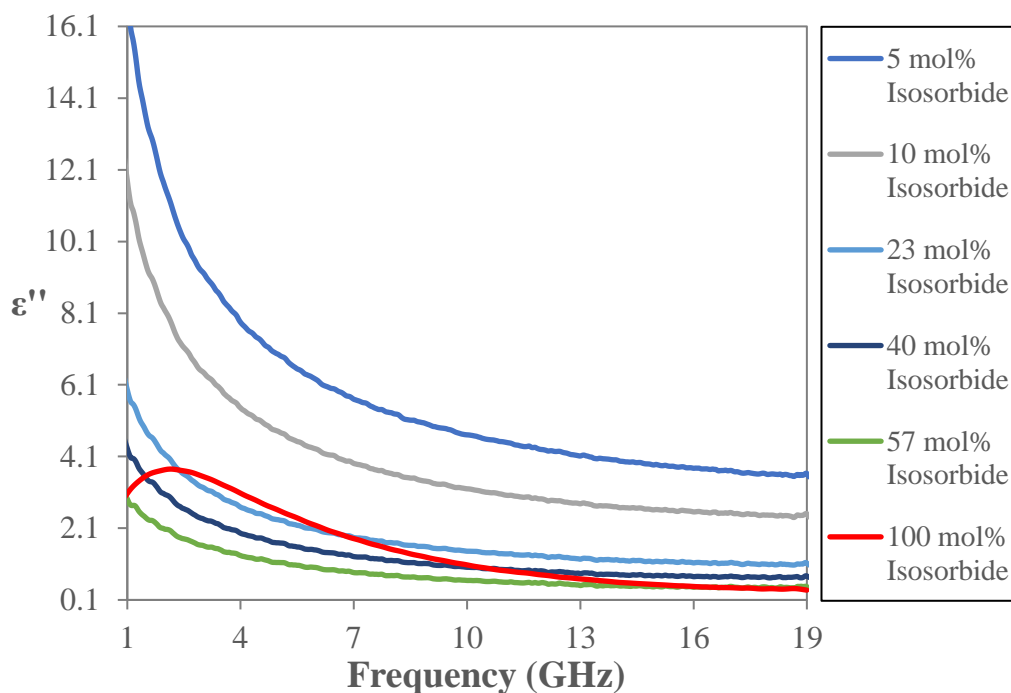


Figure 6.9: Dielectric loss (ϵ'') versus frequency (GHz). The maximum standard deviations of the measured data are: 5 mol%: [$\epsilon'' \pm 0.2$]; 10 mol%: [$\epsilon'' \pm 0.4$]; 23 mol%: [$\epsilon'' \pm 0.4$]; 40 mol%: [$\epsilon'' \pm 0.3$]; 57 mol%: [$\epsilon'' \pm 0.2$]; 100 mol%: [$\epsilon'' \pm 0.1$].

6.4.3 Relationship between the dielectric properties and isosorbide composition

The comparison of the dielectric data at low and high frequencies enables the identification of the most suitable frequencies for the monitoring of sorbitol dehydration to isosorbide. The largest scale measurement change of dielectric data between samples with low and high isosorbide composition is used to identify the sensitivity of the technique to monitor the progress of the reaction. Therefore, in order to utilise dielectric properties to follow the conversion of sorbitol to isosorbide in a systematic way, a calibration curve was constructed using logarithmic fit. The logarithmic fit was selected as the most accurate fit as

it exhibits the highest coefficient of determination values (R^2). In Figures 6.10 and 6.11 the dielectric constant and loss are plotted against mol% isosorbide composition at frequency 6 GHz and 19 GHz respectively.

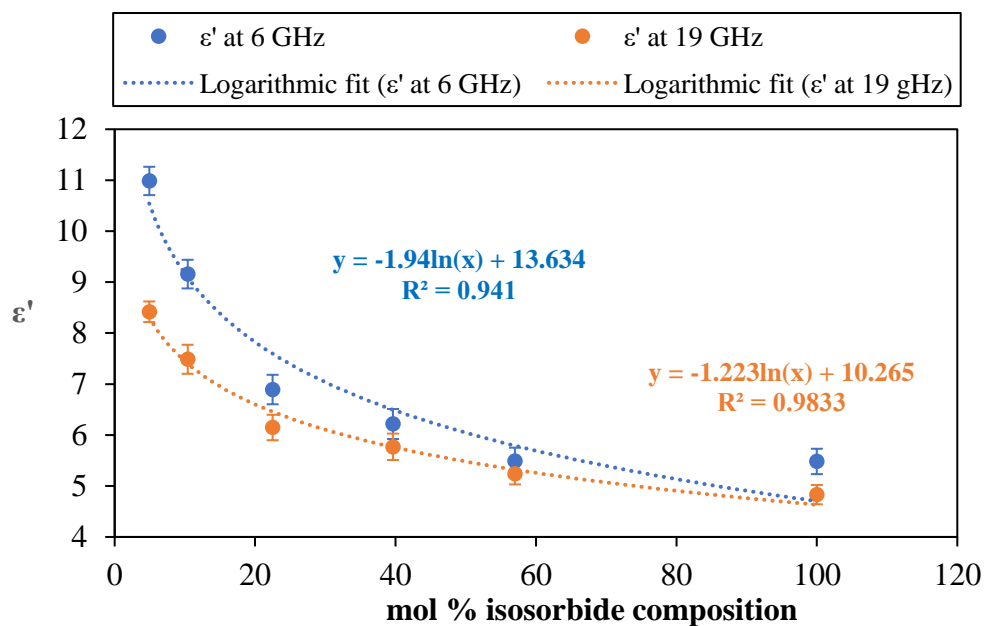


Figure 6.10: Dielectric constant at 6 GHz and 19 GHz versus mol% Isosorbide composition.

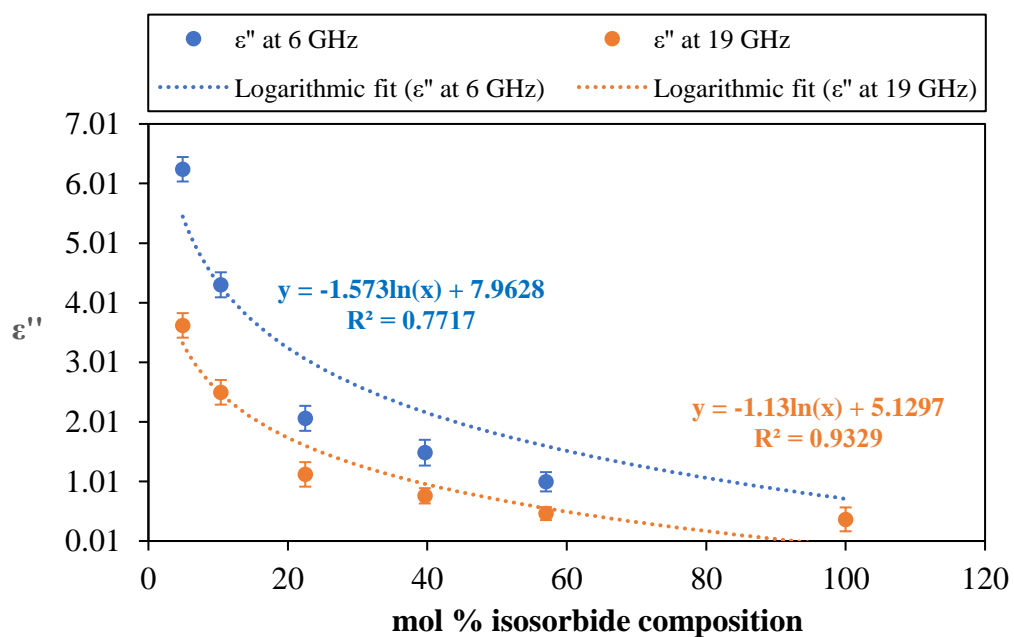


Figure 6.11: Dielectric loss at 6 GHz and 19 GHz versus mol% Isosorbide composition.

In Figure 6.10, low frequencies (e.g., 6 GHz) provide high scale measurement changes at low isosorbide conversion (<60 mol% Isosorbide). However, there is

no significant scale measurement change for isosorbide composition above 60 mol%. During the first cyclization, the amount of water in the reaction increases as the amount of sorbitan increases. For example, at 60 min reaction time, 89.28 mol% of sorbitol was converted to 78.89 mol% sorbitan and 10.39 mol% isosorbide, which confirms that 1,4-sorbitan is the major first step reaction product. At high isosorbide conversion, the subsequent dehydration and cyclization of sorbitan gives rise to isosorbide. At high frequencies, such as 19 GHz, there are small scale measurement changes for isosorbide composition below 60 mol%, but there is a considerable change for isosorbide composition above 60 mol%. For example, ϵ' at 6 GHz decreased from 5.49 to 5.48 as isosorbide composition increased from 57 mol% to 100 mol%, while ϵ' at 19 GHz decreased from 5.24 to 4.83. Dielectric loss was found to have lower sensitivity than the dielectric constant in terms of scale measurement changes for isosorbide composition above 60 mol%. For example, in Figure 6.11, ϵ'' at 19 GHz decreases from 0.5 to 0.4 as isosorbide conversion increases from 57 mol% to 100 mol%. Additionally, the logarithmic fit found to be inaccurate to fit the loss data at low frequencies, such as at 6 GHz, as it exhibits a low coefficient of determination value ($R^2 = 0.77$ at 6 GHz) and clearly cannot be used to fit ϵ'' data. As a result, ϵ' at high frequencies, such as 19 GHz offer high sensitivity to monitor sorbitol dehydration to isosorbide and logarithmic fit is the best fit for the dielectric constant with a high coefficient of determination value ($R^2 = 0.98$ at 19 GHz).

6.5 Conclusions

In this chapter, the dehydration reaction of sorbitol to isosorbide was monitored using dielectric spectroscopy. In detail, a coaxial line sensor was used to monitor the dielectric properties of the reaction mixture, during reaction progress. Additionally, samples of the medium were extracted at selected times for off-line analysis with Nuclear Magnetic Resonance spectroscopy, to confirm the level of conversion that had been achieved. The results demonstrated that the dielectric properties of the reaction medium can be correlated to isosorbide composition. The analysis of the dielectric data with frequency enabled the identification of the optimum property and frequency range to monitor the reaction progress by comparing the dielectric data at low and high frequencies. Dielectric constant at high frequencies, such as 19 GHz, found to be the optimum property to monitor this chemical transformation because it provides high scale measurement changes at high isosorbide composition. Consequently, the experimental data allowed the construction of a calibration curve which could be used to predict the level of isosorbide composition at any given point during the progress of the dehydration.

The application of this method has high potential to improve the synthesis of isosorbide in terms of process control, environmental footprint, and product quality. For example, it can be used to reduce energy usage by eliminating the amount of time that the reaction is kept at the elevated temperatures required to achieve the target level of isosorbide conversion. Additionally, the dehydration of sorbitol was conducted in bulk, with absence of solvent, which enables a potentially viable method to allow these dehydration processes to be transferred from batch to continuous flow.

References

- Adom, F., Dunn, J. B., Han, J. and Sather, N. (2014) Life-Cycle Fossil Energy Consumption and Greenhouse Gas Emissions of Bioderived Chemicals and Their Conventional Counterparts. **Environmental Science & Technology** 48(24): pp.14624–14631.
- Arai, M., Binner, J. G. P. and Cross, T. E. (1995) Estimating errors due to sample surface roughness in microwave complex permittivity measurements obtained using a coaxial probe. **Electronics Letters** 31(2): pp.115–117.
- Aricò, F. and Tundo, P. (2016) Isosorbide and dimethyl carbonate: a green match. **Beilstein Journal of Organic Chemistry** 12(1): pp.2256–2266.
- Casalini, R. and Roland, C. M. (2004) Excess wing in the dielectric loss spectra of propylene glycol oligomers at elevated pressure. **Physical Review B** 69(9): pp.094202.
- Derbyshire, H. M., Grimsey, I. M., Bland, C. R., Broadhead, J., Brocklehurst, K. G., Malone, N. J. and Smith, G. (2003) Properties of saccharides and saccharide derivatives in the dry and partially hydrated states. **Journal of Materials Science** 38(1): pp.57–63.
- Díaz, A., Katsarava, R. and Puiggali, J. (2014) Synthesis, Properties and Applications of Biodegradable Polymers Derived from Diols and Dicarboxylic Acids: From Polyesters to Poly(ester amide)s. **International Journal of Molecular Sciences** 15(5): pp.7064–7123.
- Dussenne, C., Delaunay, T., Wiatz, V., Wyart, H., Suisse, I. and Sauthier, M. (2017) Synthesis of isosorbide: an overview of challenging reactions. **Green Chemistry** 19(22): pp.5332–5344.
- Flèche, G. and Huchette, M. (1986) Isosorbide. Preparation, Properties and Chemistry. **Starch - Stärke** 38(1): pp.26–30.
- Giacometti, J., Milin, Č. and Wolf, N. (1995) Monitoring the esterification of sorbitol and fatty acids by gas chromatography. **Journal of Chromatography A** 704(2): pp.535–539.
- Li, J., Spina, A., Moulijn, J. A. and Makkee, M. (2013) Sorbitol dehydration into isosorbide in a molten salt hydrate medium. **Catalysis Science & Technology** 3(6): pp.1540–1546.
- Metaxas, A. C. and Meredith, R. J. (1995) **Industrial Microwave Heating**. London, UK: The Institution of Engineering and Technology.
- Minoguchi, A. and Nozaki, R. (2002) Broadband complex permittivity measurements of sorbitol during isothermal crystallization. **Journal of Non-Crystalline Solids** 307: pp.246–251.

- Oltmanns, J. U., Palkovits, S. and Palkovits, R. (2013) Kinetic investigation of sorbitol and xylitol dehydration catalyzed by silicotungstic acid in water. **Applied Catalysis A: General** 456: pp.168–173.
- Piemonte, V. and Gironi, F. (2011) Land-use change emissions: How green are the bioplastics? **Environmental Progress & Sustainable Energy** 30(4): pp.685–691.
- Remuzgo, L. and Trueba, C. (2017) Statistical polarization in greenhouse gas emissions: Theory and evidence. **Environmental Pollution** 230: pp.291–301.
- Tundo, P., Aricò, F., Gauthier, G., Rossi, L., Rosamilia, A. E., Bevinakatti, H. S., Sievert, R. L. and Newman, C. P. (2010) Green Synthesis of Dimethyl Isosorbide. **ChemSusChem** 3(5): pp.566–570.
- Venkatesh and Raghavan (2005) An Overview of Dielectric Properties Measuring Techniques. **Canadian Biosystems Engineering / Le Genie des biosystems au Canada** 47(7): pp.15–30.
- Werpy, T. and Petersen, G. (2014) **Top Value Added Chemicals from Biomass. Results of Screening for Potential Candidates from Sugars and Synthesis Gas**. Vol. I. Available at: <http://www.nrel.gov/docs/fy04osti/35523.pdf> (Accessed: 9 June 2017).
- Yaghmaee, P. and Durance, T. d. (2002) Predictive Equations for Dielectric Properties of NaCl, D-sorbitol and Sucrose Solutions and Surimi at 2450 MHz. **Journal of Food Science** 67(6): pp.2207–2211.

7 HYPERBRANCHED POLYMERS

7.1 Introduction

The term “hyperbranched polymers” was first introduced by Kim and Webster to describe a class of macromolecules containing a large number of branchings connected by a short chain resulting in a three-dimensional globular shape with multiple chain end groups and dendritic architecture (Kim and Webster, 1990). In Figure 7.1, a schematic diagram of a hyperbranched polymer is presented next to their dendrimer³ and linear counterparts.

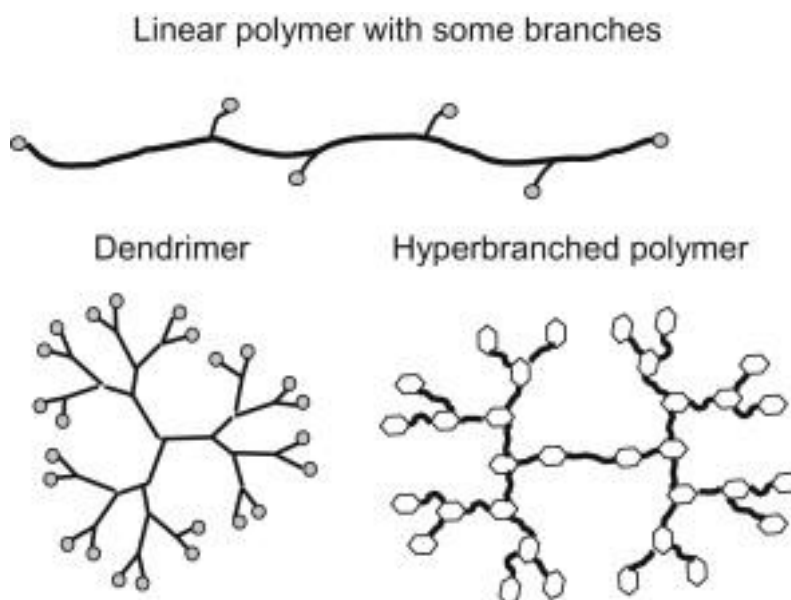


Figure 7.1: Schematic representation of a linear polymer, dendrimer, and a hyperbranched polymer (Biron, 2013).

Branched and hyperbranched polymers offer unique properties compared to their linear counterparts, such as high branching density, that make them amenable for use in a variety of applications (Giussi *et al.*, 2016). Therefore, they have

³ A dendrimer is a macromolecule with a highly arranged structure consisting of tree-like arms or branches that are built around a small molecule or a linear polymer core (Khoee and Khezrian, 2017).

seen an increasing level of interest during the last few decades especially in biomedicine, in drug delivery (Poree *et al.*, 2011), protein purification/detection/delivery, gene transfection and antibacterial/antifouling materials (Zhou *et al.*, 2010). They have also demonstrated considerable potential in energy storage and dielectric applications (Huang and Jiang, 2015) as well as in polymer solar cells (Lv *et al.*, 2013). However, their properties and performance can be negatively affected by side reactions occurred during their preparation which can lead to products with varied molecular structure and branching. The control on molar mass and branching accuracy are the biggest challenges for product and process engineering of hyperbranched polymers (Voit and Lederer, 2009; Gonçalves *et al.*, 2013).

In this project, styrene–divinylbenzene (DVB-co-styrene) copolymers synthesized by catalytic chain transfer polymerisation (CCTP) and nitroxide mediated polymerisation (NMP) were studied using dielectric spectroscopy in order to analyse the polymer architecture and molecular weight. Styrene–divinylbenzene hyperbranched copolymers are extensively used in gas chromatography, gel permeation chromatography (Nakagawa and Tsuge, 1985) and ion-exchange chromatography because of their intractable structure. For example, the development of novel polymer-based anion exchangers make copolymers of divinylbenzene with styrene suitable substrates for obtaining anion exchangers (Uzhel *et al.*, 2016). They have also found applications in inorganic trace analysis for solid-phase extraction preconcentration (Rao, Praveen and Daniel, 2004) and as packing material to evaluate the contamination of groundwater by pesticides (Leandro *et al.*, 2008). In this study, the dielectric properties of styrene–divinylbenzene copolymers with varied hyperbranched

structure were studied with the use of cavity perturbation technique. The aim of this project is to develop a monitoring strategy to optimise the synthesis of hyperbranched polymers by monitoring their molecular architecture and help detect side reactions occurred during their preparation that can affect the properties and performance of the polymer. A detailed analysis of the effect of temperature and molecular weight on the dielectric properties of styrene–divinyl benzene samples with variable DVB ratio was performed in a broad temperature range (20 °C – 180 °C) to highlight their dielectric response and define trends related to their molecular structure.

7.2 Experimental

7.2.1 Materials

Styrene (99%+), Divinylbenzene (80%), Bis[(difluoroboryl)diphenylglyoximato]cobalt(II) (CoPhBF) and 2,2,6,6-tetramethylpiperidine-1-oxyl (TEMPO) were purchased from Sigma Aldrich and used as received without any purification.

7.2.2 Dielectric property measurement

The dielectric properties of materials were studied using the cavity perturbation technique. The cavity perturbation technique is based on the measurements of the shift in the resonant frequency and quality factor when a material is placed inside a resonant cavity, as described in Section 4.2.2. It was selected as the preferred method for the dielectric characterisation of styrene–divinylbenzene samples according to the following criteria:

- It is the preferred method for the dielectric characterisation of low loss materials, such as polymers (Metaxas and Meredith, 1905).
- It is the most suitable method for measuring powders and pulverised samples (Meredith, 1997).
- It is the preferred method for materials in which the total volume of the available sample is too small to be measured with the probe.

The samples were placed into quartz tubes. An empty tube was used for the calibration of the system. The difference between the empty and loaded tube in the quality factor and resonant frequency is used to calculate the dielectric properties, as described in Section 4.2.2.

7.2.3 Gel Permeation Chromatography

Size Exclusion Chromatography (SEC), also called Gel Permeation Chromatography (GPC), is a popular method for determining the whole molar-mass distribution of polymers (Bower, 2002). It is based in measuring the concentration of the polymer dissolved in a solution passing through a column containing a gel with pores having a similar size to the molecular coils in the solution. By measuring the concentration of polymer versus the time it needs to pass the column we can calculate the molar-mass distribution. Calibration of the column can be performed using mono-disperse samples of the polymer with known molar masses (Bower, 2002).

In this study, GPC analysis was performed on an Agilent 1260 infinity series HPLC with an online vacuum degasser, an Agilent online differential refractometer (DRI) and a Wyatt Dawn Heleos II Multi-Angle Light Scattering detector (MALS.) Two Agilent 5 μm PLgel Mixed C columns (7.5 x 300 mm)

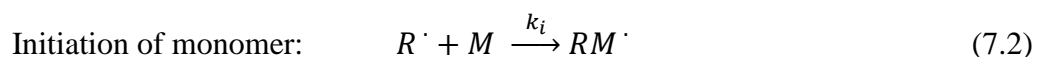
were connected in series with an Agilent PLgel 5 μm Guard column (7.5 x 50 mm.). The column oven, DRI and MALS temperature were set to 35 $^{\circ}\text{C}$ and the flow rate was set to 1 mL per minute. Each sample was dissolved in HPLC grade tetrahydrofuran (THF), at a concentration of 1 mg/mL. DRI calibration was performed using 30 kDa and 200 kDa linear polystyrene narrow dispersity standards dissolved in THF at a concentration of 1 mg/mL. MALS calibration was performed using HPLC grade toluene, filtered through a 0.02 μm PTFE filter and normalisation was performed in THF using a 30 kDa linear polystyrene narrow dispersity GPC calibration standard. The columns were calibrated using narrow dispersity polystyrene standards ranging from 580 Da to 1000 kDa.

7.3 Free radical polymerisation of Styrene–divinylbenzene copolymers

During the last few decades, the development of controlled radical polymerisation (CRP) has made available the synthesis of new polymer structures with controlled architecture. Free radical polymerisation (FRP) is one of the most widely used chain-growth polymerisation processes in the industry, with many commercial applications, such as the production of block copolymers, fluorene end-labelled polymers, and homopolymers with narrow polydispersity (Moad and Solomon, 2005; Tillman, Contrella and Leasure, 2009). The simple underlying mechanism to describe a free radical polymerisation consists of three primary processes: initiation, propagation, and termination.

The initiation involves two steps, as shown in equations 7.1 and 7.2.





The initiator (I) decomposes to give a free radical ($R \cdot$) with a rate constant of decomposition k_d . Then, the free radical adds to the vinyl group of the monomer (M) with a rate constant of initiation k_i , resulting in the initiated monomer. The rate of initiation can be determined from the decomposition of initiator, as described in equation 7.3,

$$R_i = 2k_d f [I] \quad (7.3)$$

where [I] is the concentration of the initiator and f is the initiator efficiency factor. The selection of the appropriate initiator is very important as it can affect the rate of polymerisation, molecular weight, and the structure of the final polymer (Nicolas *et al.*, 2013). Some monomers, such as styrene, have the ability to self-initiate at high temperatures. Although the exact mechanism in which self-initiation takes place is not yet established, the most proposed mechanisms are the Mayo and Flory mechanisms.

According to the Mayo mechanism, radical initiation proceeds by the dimerization of styrene via a Diels – Alder reaction, as described in Figure 7.2. The monoradical initiators $A \cdot$ and $HM \cdot$ are generated through molecule assisted homolyses between the Diels – Alder dimer (AH) and a third styrene.

Flory mechanism proposes that styrene monomers dimerize to form a singlet, 1,4-diradical ($\cdot M_2 \cdot$), as shown in Figure 7.2. Another styrene abstracts a hydrogen atom from the diradical to form the initiators able to start the polymerisation. Even though the exact self-initiation mechanism is yet to be confirmed, the Mayo mechanism is the more favoured as it gains strong support from experimental studies (Khuong *et al.*, 2005).

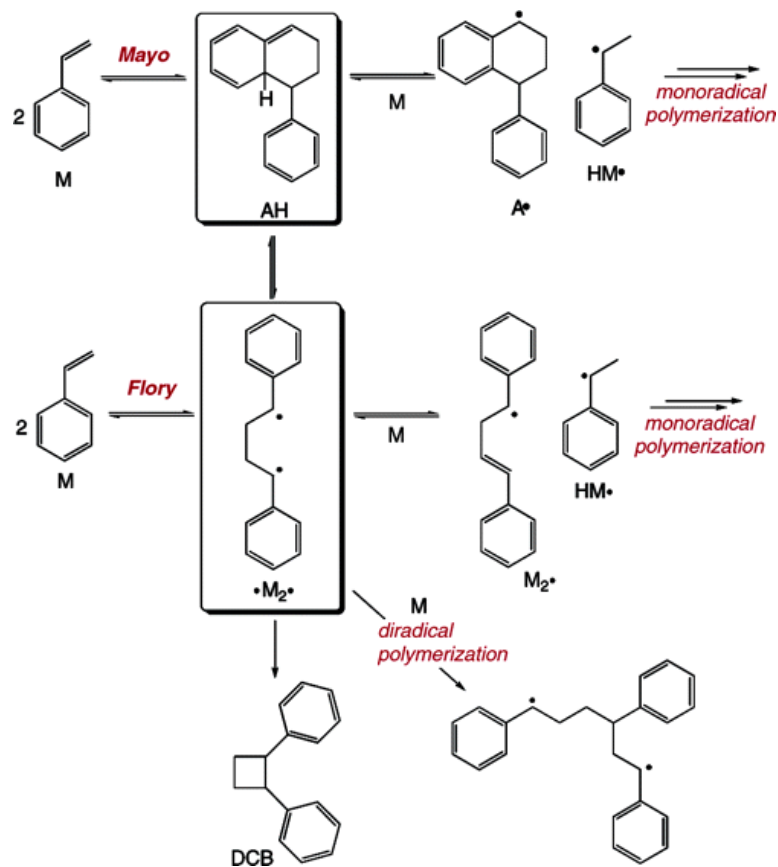


Figure 7.2: Mayo and Flory theory of the self-initiation of styrene (Khuong et al., 2005).

The propagation is a bimolecular reaction in which the free radicals generated in the initiation process react with monomers to produce an initiated monomer, which then reacts with further monomers resulting in a growing polymer chain with a rate constant of propagation k_p .



Finally, the termination reaction occurs by the bimolecular reaction of two propagating polymer radicals. This can occur via radical-radical combination or disproportionation. The rate of termination (R_t) can be influenced by many

factors, such as the temperature, pressure, viscosity, monomer conversion, and can be expressed as in equation 7.5

$$R_t = 2k_t[P']^2 \quad (7.5)$$

where $[P']$ is the concentration of the polymer radicals, and k_t is the rate constant of termination, which is the sum of the rate constants for combination and disproportionation processes. In addition to primary reactions, other reactions occur alongside free radical polymerisation due to inactivity of free radicals, such as chain transfer to monomer (Gridnev and Ittel, 2001).

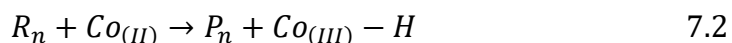
In this study, divinylbenzene was used as a cross-linking agent in the polymerisation of styrene. In order to obtain hyperbranched polymers with high conversion, two copolymerisations of styrene and divinyl benzene were carried out. The first reaction conducted to identify the gelation time. The second polymerisation was identical with the first one, but the sample was quenched five minutes before the gelation time. According to P. J. Flory (1953), gelling will occur when one crosslink per two polymer molecules has formed. The gelation time for the polymerisation of DVB was found to be 45 mins and increased gradually to 156 mins as the percentage of styrene in the copolymerisation increased from 0% to 50%. The increase in the gelation time at samples with high styrene concentration is a result of the decrease in the rate of polymerisation due to the presence of styrene.

7.3.1 Catalytic Chain Transfer Polymerisation

Catalytic chain transfer polymerisation (CCTP) is used to control the free radical polymerisation of multifunctional monomers and has proven to be an efficient method of achieving the controlled synthesis of hyperbranched polymers with a great level of control over the M_w of the final polymer (Barker *et al.*, 2012).

Low-spin Co(II) complexes, such as bis[(difluoroboryl)diphenylglyoximato]cobalt(II) (CoPhBF), have been demonstrated to act as catalytic chain transfer agents (CTAs) and offer improved rates of chain transfer to polymer compared with other CTAs, such as thiols, because of their ability to undergo the termination/reinitiation process many times. As a result, the application of CoPhBF as a catalytic chain transfer control agent offers a way to achieve the targeted M_w , even in polymers with very low M_w , using low CTA concentration. Additionally, it offers enhanced stability against oxidation and hydrolysis (Gridnev and Ittel, 2001; Heuts and Smeets, 2011).

Although a fully consistent mechanism to describe CCT has not yet finalized, the currently most accepted mechanism proposes a two-step process. In the first step, a growing polymer chain (R_n) interacts with the Co(II) complex to form a Co(III) hydride complex and a polymer chain (P_n).



In the second step, the Co(III) hydride complex reacts with the monomer which results in a new radical monomer (R_1) and a Co(II) catalyst (Adlington *et al.*, 2014).

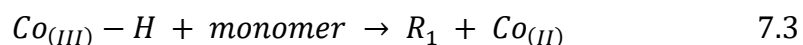


Table 7.1 contains a summary of conditions and reaction time for the catalytic chain transfer polymerisation of DVB. All polymerisation reactions were conducted at 150 °C using conventional heating.

Table 7.1: Styrene–divinylbenzene copolymers synthesis reaction conditions.

No.	DVB (%)	Styrene (%)	Reaction time (CCTP)
1	100	0	40 min
2	90	10	55 min
3	80	20	1 h 2 3min
4	70	30	1 h 41 min
5	60	40	2 h 05 min
6	50	50	2 h 31 min

7.3.2 Nitroxide Mediated Polymerisation

Nitroxide mediated polymerisation (NMP) is one of the most well-established controlled/living radical polymerisation techniques (CLRP). During an ideal CLRP, the key feature of the polymerisation is the establishment of a dynamic equilibrium between the propagating radicals (P') and other dormant species in order to decrease the occurrence of irreversible termination reactions throughout the polymerisation process. The equilibrium can be obtained and maintained through thermal, photochemical, or chemical stimuli, as shown in Figure 7.3 (Nicolas *et al.*, 2013).

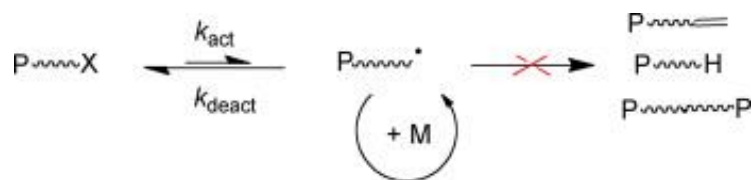


Figure 7.3: Controlled/living radical polymerisation mechanism (Nicolas et al., 2013).

In NMP, propagation is mediated by a persistent oxygen-based radical, such as 2,2,6,6-tetramethylpiperidine-1-oxyl (TEMPO). Nitroxide radicals are used as control agents, and can be used to produce lower molecular weight polymers with narrower polydispersity (Tillman, Contrella and Leasure, 2009). Table 7.2 summarises reaction conditions and reaction time used for the nitroxide mediated polymerisation of DVB.

Table 7.2: Styrene–divinylbenzene copolymers synthesis reaction conditions.
*Sample no.2 gelled before gelation.

No.	DVB (%)	Styrene (%)	Reaction time (NMP)
1	100	0	47 min
2	90	10	*
3	80	20	55 min
4	70	30	1 h 01 min
5	60	40	55 min
6	50	50	1 h 15 min

7.4 Dielectric property assessment of styrene-co-divinylbenzene copolymers

The dielectric properties of poly(styrene-co-divinylbenzene) copolymers have been reported in previous studies. He *et al.* (2017) reported the use of a coaxial waveguide method to measure the complex permittivity of poly(styrene-co-divinyl benzene) copolymers. However, the permittivity of samples was measured over a limited frequency range (1 MHz – 100 MHz), and only at room temperature without considering the effect of temperature, molecular weight and batch to batch repeatability in the dielectric response of the samples. In this work, the dielectric properties of styrene-co-divinylbenzene copolymers were studied over a broad temperature range (20 °C - 180 °C) with a step interval of 10 °C. Cavity perturbation technique was selected for this study as it is the optimum method to meet the criteria determined and discussed in Section 7.2.2.

7.4.1 Temperature dependence of dielectric properties

In order to investigate the effect of temperature on the dielectric properties, a range of DVB-co-styrene solid samples with varied DVB ratio (50%, 60%, 70%, 80%, 90% and 100%) were measured from 20 °C up to 180 °C with 10 °C intervals. A frequency of 2.47 GHz was selected as the preferred frequency for the dielectric characterisation, which can also be used for microwave assisted polymerisation. The results are presented in Figures 7.4 and 7.5. Each sample was measured at least three times and the error bars shows the standard deviation of the measurement.

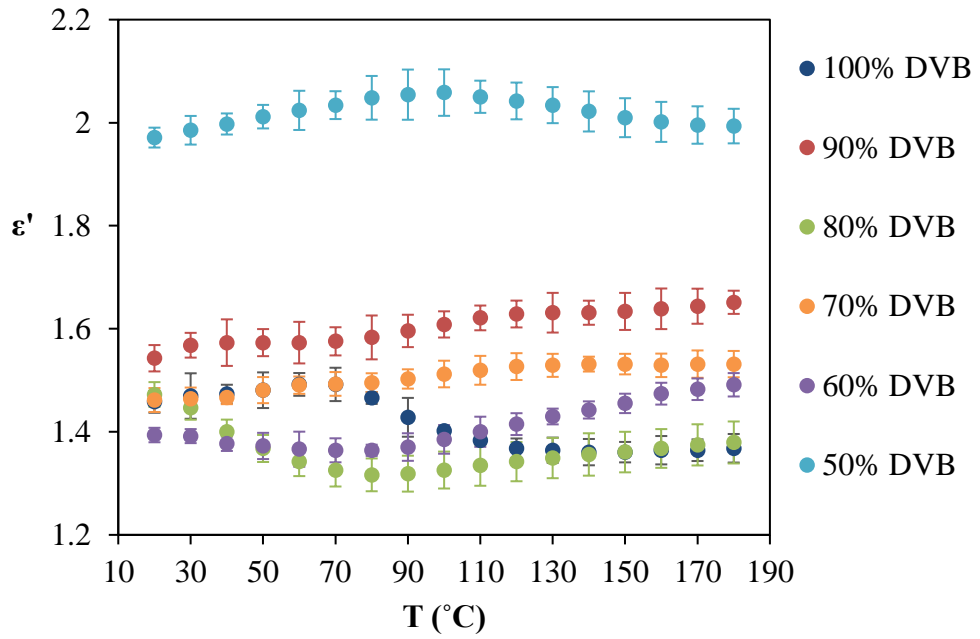


Figure 7.4: Dielectric constant versus temperature at 2470 MHz of DVB:PS powder samples with variable DVB ratio.

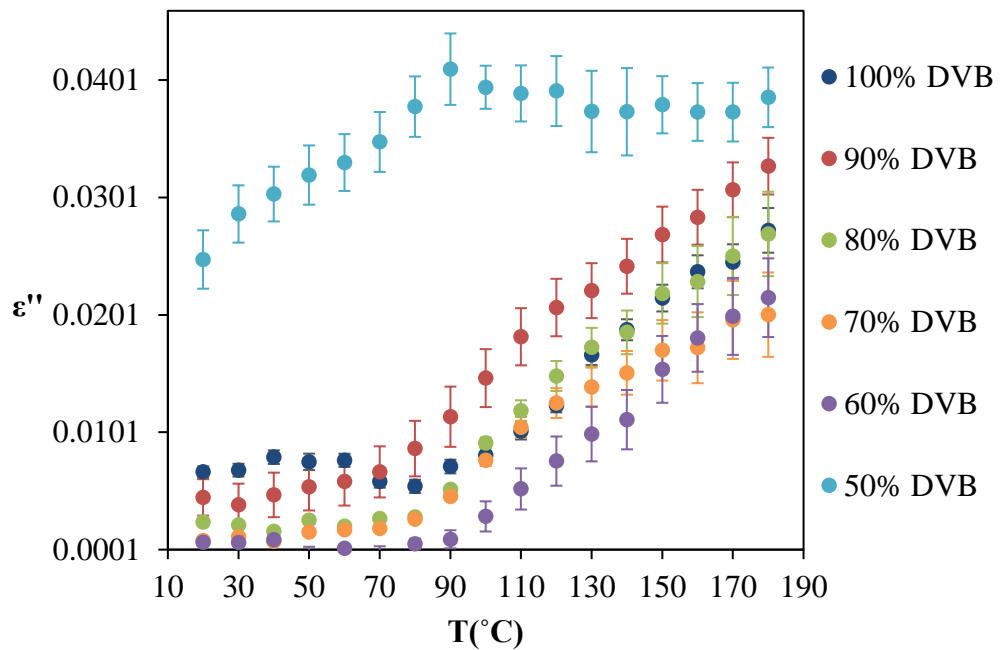


Figure 7.5: Dielectric loss versus temperature at 2470 MHz of DVB:PS powder samples with variable DVB ratio.

Overall the results show that the materials exhibit low dielectric properties and can be categorised as poor microwave receptors. Based on Figure 7.4, the dielectric constant of DVB:PS powder samples was not found to be temperature dependent. The dielectric loss of materials with DVB ratio above 60 % exhibited a linear increase at temperatures from 90 °C up to 180 °C. This could be attributed to the materials' increased liquid physical form at the specified temperature range; a glass transition temperature of 100°C is reported for polystyrene (Rieger, 1996), which is expected to increase with the addition of DVB, as it is linearly proportional to the DVB content (Davankov and Tsyurupa, 2010). When the material is in its liquid form, it allows the induced dipoles to have greater levels of molecular motion (Hild *et al.*, 2016).

7.4.2 Relationship between dielectric properties and hyperbranched polymer structure

In order to relate the dielectric constant to the structure of hyperbranched polymers, the dielectric properties were plotted against the (%) DVB concentration. Figures 7.6 and 7.7 show the dielectric constant and loss at 2.47 GHz versus (%) DVB concentration for samples with 50%, 60%, 70%, 80% 90% and 100% DVB concentration. The samples were measured with the cavity perturbation technique at temperature 150 °C, which is the target reaction temperature for the polymerisation reaction. For each DVB concentration three samples were prepared and measured. The standard deviation was used to calculate the error.

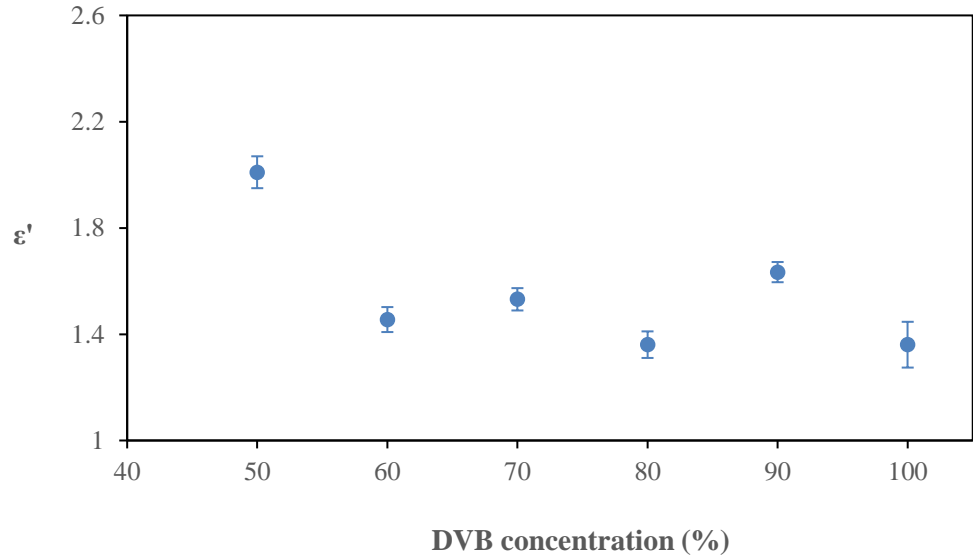


Figure 7.6: Dielectric constant at 2.47 GHz versus DVB concentration at 150 °C.

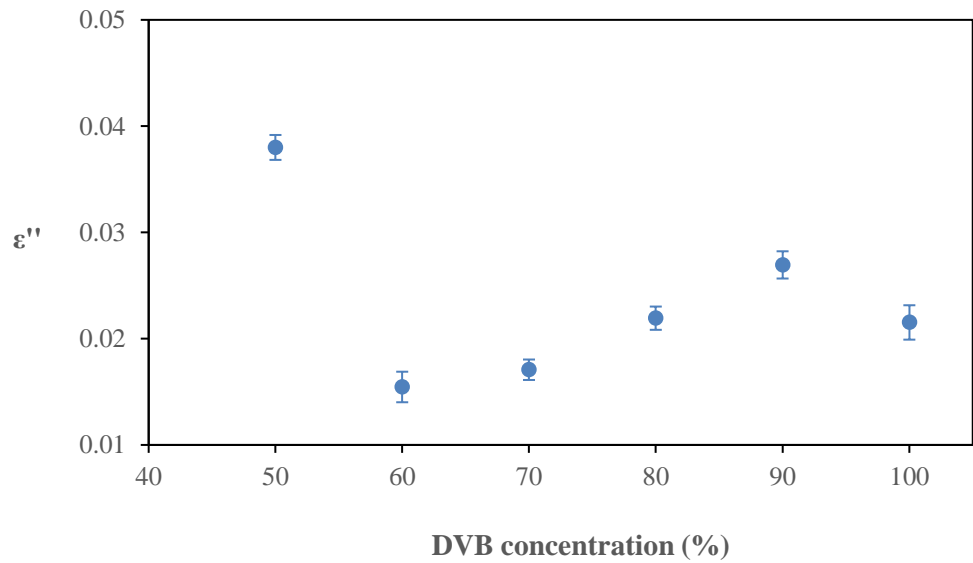


Figure 7.7: Dielectric loss at 2.47 GHz versus DVB concentration at 150 °C.

In Figure 7.6 there is an overall decrease in the dielectric constant with increasing DVB concentration. For example, ϵ' at 2.47 GHz decreases from 2 to 1.36 as the (%) DVB concentration increases from 50% to 100%. This corresponds to the decreasing amount of stored energy at polymers with

increasing branching density. A possible reason to explain this behaviour could be the high rigidity present at polymers with high branching density. He *et al.* (2017), reported the relation of the relative permittivity with the cross-linking density of poly(styrene-co-divinyl benzene) material synthesised via free radical polymerisation. In Figure 7.7, the sample with the highest styrene concentration (50% DVB concentration) exhibits the highest loss value. The addition of styrene increases the mobility of the polymer chain and, as a result, increases the interaction of the material with the incident electromagnetic field.

The absence of a clear trend in the dielectric properties can be related with the physical form of the samples and the dielectric measurement technique. Powdered samples with variable % DVB concentration were packed into a quartz tube to form the sample. The concentration of monomers appears to change the density of the polymer which in turn affect the packing density of the sample. As a result, there was more than one variable present which affect the interaction of the sample with the applied electric field; the amount of polymer in the sample and the concentration of double bonds present in the polymer.

Due to the physical form of the samples (powders) it was observed that the packing density of the sample in the tube can be varied between samples. As a result, the dielectric properties of the sample are affected by the packing density of the sample and, consequently, the comparison of the dielectric properties between samples with varied packing density is not accurate. To overcome this difficulty, a solvent in which the hyperbranched polymers are soluble was selected. Cyclohexanone was selected as the preferred solvent. As it is a polar solvent, their high permittivity is expected to affect the dielectric response of the sample. Figures 7.8 and 7.9 show the dielectric constant and loss versus

frequency of DVB-co-styrene samples with 50%, 60%, 70%, 80% 90% and 100% DVB concentration dissolved in cyclohexanone and measured at room temperature with the cavity perturbation technique resonating in the transverse magnetic modes (TM_{0n0}) occurring at 400 MHz, 912 MHz, 1429 MHz, 1949 MHz and 2470 MHz. For each DVB concentration three samples were prepared by dissolving a fixed amount of polymer into a fixed amount of cyclohexanone. The standard deviation was used to calculate the error of the measurement.

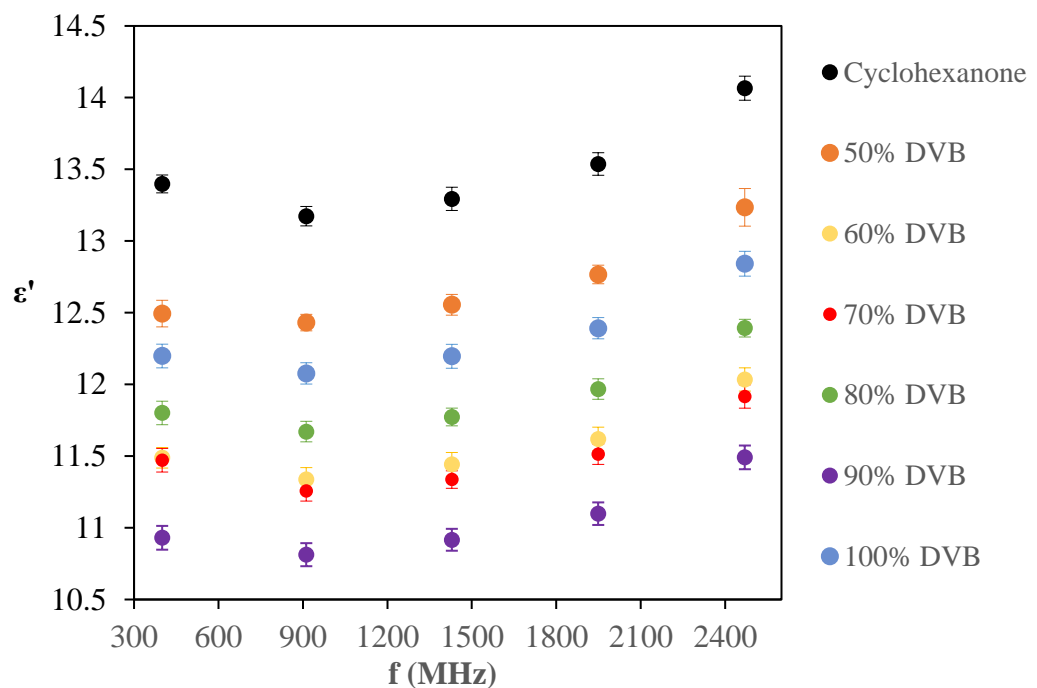


Figure 7.8: Dielectric constant versus frequency of DVB:PS polymers with varied (%) DVB ratio, dissolved in cyclohexanone and measured at room temperature.

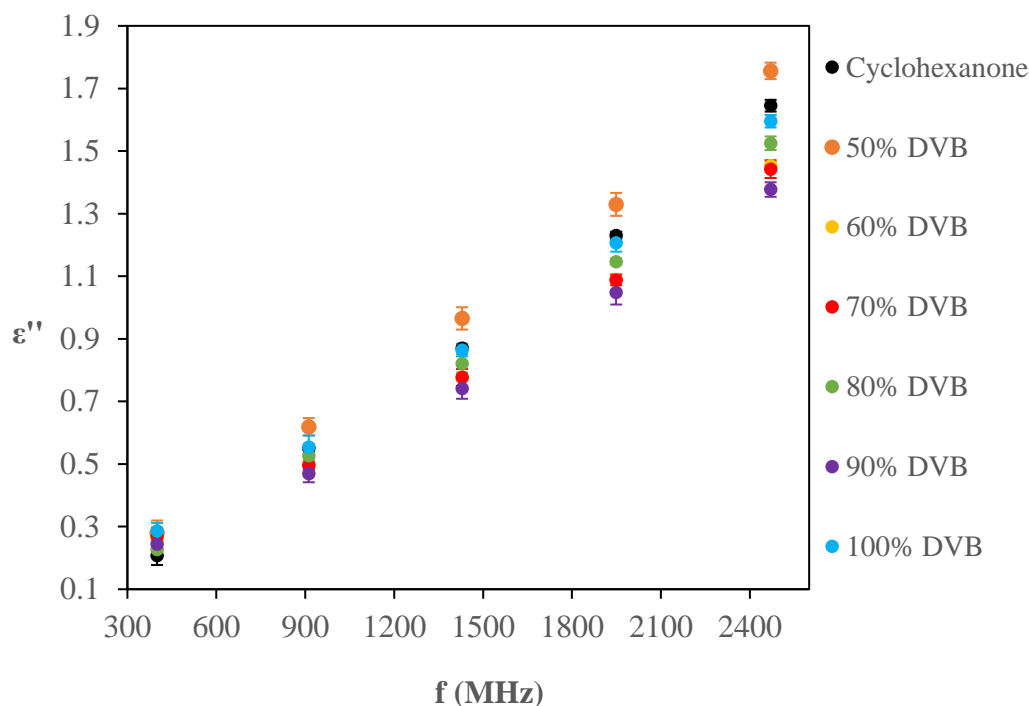


Figure 7.9: Dielectric loss versus frequency of DVB:PS samples with varied (%) DVB ratio, dissolved in cyclohexanone and measured at room temperature.

The dielectric properties of DVB-co-styrene samples dissolved in cyclohexanone were found to be approximately ten times higher than the dielectric properties of the powder polymers. This behaviour can be explained because of the high dielectric properties of cyclohexanone due to the permanent dipole present in the molecule. The dielectric loss values, as shown in Figure 7.9, increase linearly with increasing frequency, which denote the increased ability of the material to dissipate the stored energy into heat as the frequency increases. Even though the use of dielectric spectroscopy to differentiate to differentiate DVB-co-styrene hyperbranched polymers could not be proven, the analysis indicated that the dielectric loss exhibits smaller scale measurement changes than the dielectric constant as the (%) DVB concentration increases, thus the dielectric constant is the most preferred property as it provides higher scale measurement changes than the dielectric loss. Further work is required to

investigate the potential of dielectric spectroscopy in identifying trends in the structure of hyperbranched polymers.

7.4.3 Relationship between polymer molecular weight and dielectric properties

The effect of molecular weight on the dielectric properties has been the subject of extensive studies for many polymers. In detail, S. N. Kolesov (1968) reported the relation of the dielectric properties to the molecular weight of polymer-homologous series of polystyrene and polyvinyl acetate, which are used in the production of electrical insulation. E. O. Forster (1973) evaluated the effect of molecular structure on the dielectric properties of a variety of thermoplastic insulating materials. W. Reddish (2009) studied the relation between the dielectric properties and the chemical constitution of solid polymers. The above referenced studies agreed on the significance of the influence of molecular structure to the physical properties of polymers and especially the permittivity. In this study, the relation of molecular weight with the dielectric properties of two homo-DVB polymer samples, quenched at 25 and 30 minutes polymerisation time was investigated. Their number average molecular weight was measured with gel permeation chromatography, as detailed in Section 7.2.3, and found to be 15.3 kDa and 100.8 kDa. Figures 7.10 and 7.11 show the dielectric constant and loss versus frequency for cyclohexanone, DVB sample quenched at 25 minutes (15.3 kDa) and DVB sample quenched at 30 minutes (100.8 kDa).

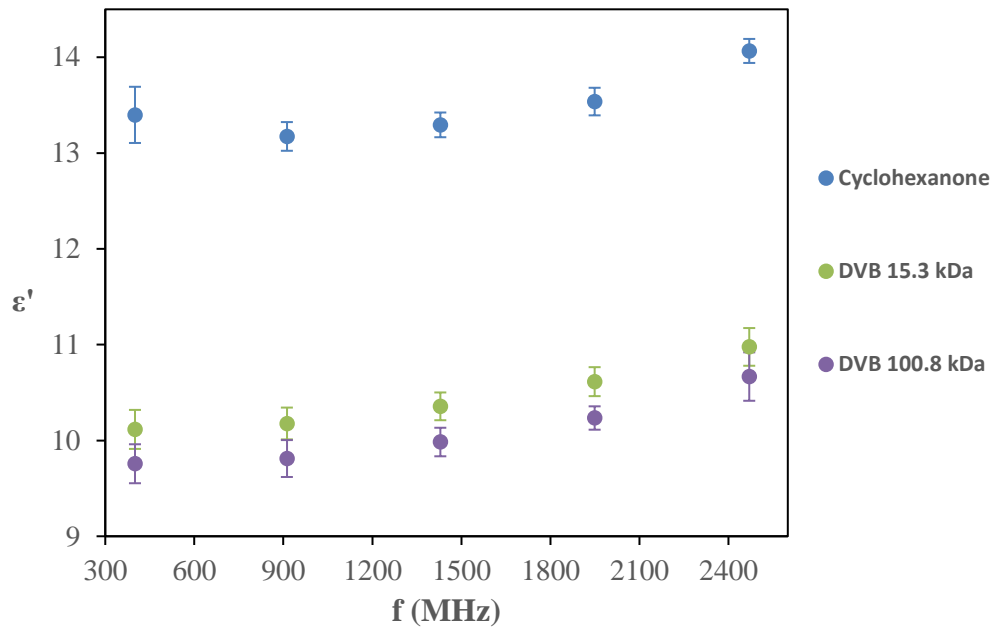


Figure 7.10: Dielectric constant versus frequency (MHz) for cyclohexanone, low and high molecular weight sample.

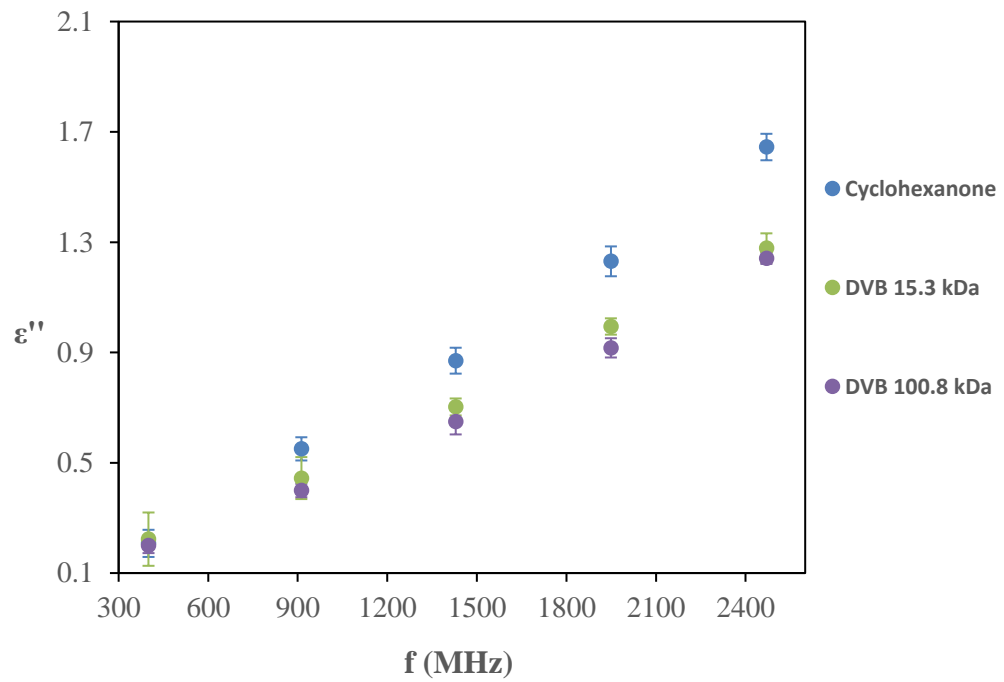


Figure 7.11: Dielectric loss versus frequency (MHz) for cyclohexanone, low and high molecular weight sample.

In Figure 7.10, the dielectric constant of the sample with the highest molecular weight (100.8 kDa) found to be lower than the dielectric constant of the sample with 15.3 kDa molecular weight. In Figure 7.11, the dielectric loss exhibits a small decrease with the increase of molecular weight. However, ϵ' was found to be more sensitive to monitor molecular weight changes; both the differentiation between low and high molecular weight and the signal to error ratios are sufficiently large. Even though a definite statement cannot be made on whether the dielectric spectroscopy is a suitable method to uniquely identify hyperbranched polymers based on their molecular weight, the analysis showed that ϵ' is a more suitable property to differentiate DVB samples with varied molecular weight as it exhibits larger scale measurement changes than ϵ'' .

7.5 Conclusions

In this study, a series of hyperbranched copolymers synthesised *via* catalytic chain transfer polymerisation and nitroxide mediated polymerisation were studied using dielectric spectroscopy. The dielectric properties of styrene–divinylbenzene polymers with varied monomer ratio, e.g., poly(styrene-co-divinylbenzene) copolymers were measured with the use of cavity perturbation technique. The absence of a clear trend was found on the dielectric properties of powder samples with varied DVB concentration, which could be attributed to the physical form and state of the samples during the measurement, i.e. the concentration of monomers appears to change the density of the polymer which in turn affect the packing density of the sample. Consequently, the comparison of the dielectric properties between samples with varied packing density is not accurate. To overcome this difficulty, the polymer samples were dissolved in

cyclohexanone. However, the high dielectric properties of cyclohexanone due to the permanent dipole present in the molecule appear to mask the dielectric properties of polymers. As a result, a clear trend between the dielectric properties and the polymer molecular architecture is not present. The addition of styrene interferes the branching structure of DVB and this results in a more linear structure which increases the flexibility of the dipoles to align with the microwave electromagnetic field. Furthermore, it is noted that as polymerisation time increases, polymer molecular weight increases. Even though the use of dielectric spectroscopy to differentiate the polymer molecular architecture could not be proven, the analysis of the dielectric data showed that the dielectric constant is the most suitable dielectric property to use as it exhibits larger scale measurement changes than the dielectric loss across the frequencies investigated.

A comparison between dielectric spectroscopy, raman spectroscopy, and Gel Permeation Chromatography will allow us to further investigate molecular structure changes and their effect in the dielectric properties. Further work is required to investigate the potential of dielectric spectroscopy in identifying trends in the structure of hyperbranched polymers.

References

- Bower, D. I. (2002) **An Introduction to Polymer Physics**. Cambridge University Press.
- Davankov, V. and Tsyurupa, M. P. (2010) **Hypercrosslinked Polymeric Networks and Adsorbing Materials: Synthesis, Properties, Structure, and Applications**. Elsevier.
- Flory, P. J. (1953) **Principles of Polymer Chemistry**. Cornell University Press.
- Forster, E. O. (1973) Effect of molecular structure on dielectric properties of polymers: I. Thermoplastics. in **Conference on Electrical Insulation Dielectric Phenomena - Annual Report 1973**. *Conference on Electrical Insulation Dielectric Phenomena - Annual Report 1973* pp.447–455.

- Giussi, J. M., Azzaroni, O., Hensel-Bielowka, S., Wojnarowska, Z., Knapik, J. and Paluch, M. (2016) Synthesis, characterization and dielectric relaxation study of hyperbranched polymers with different molecular architecture. **Polymer** 100: pp.227–237.
- Gonçalves, M. A. D., Pinto, V. D., Dias, R. C. S., Costa, M. R. P. F. N., Aguiar, L. G. and Giudici, R. (2013) Gel Formation in Aqueous Suspension Nitroxide-Mediated Radical Co-Polymerization of Styrene/Divinylbenzene. **Macromolecular Reaction Engineering** 7(3–4): pp.155–175.
- Gridnev, A. A. and Ittel, S. D. (2001) Catalytic chain transfer in free-radical polymerizations. **Chemical Reviews** 101(12): pp.3611–3660.
- He, H., Mu, G., Wan, F., Wang, J., Zhu, Q., Li, F. and Wang, M. (2017) Research on cross-linked structure of poly(styrene-co-divinyl benzene) and vacuum flashover characteristics. **IEEE Transactions on Dielectrics and Electrical Insulation** 24(2): pp.1300–1306.
- Heuts, J. P. A. and Smeets, N. M. B. (2011) Catalytic chain transfer and its derived macromonomers. **Polymer Chemistry** 2(11): pp.2407–2423.
- Hild, F., Nguyen, N. T., Deng, E., Katrib, J., Dimitrakis, G., Lau, P.-L. and Irvine, D. J. (2016) Facile Determination of Molecular Structure Trends in Amphiphilic Core Corona Star Polymer Synthesis via Dielectric Property Measurement. **Macromolecular Rapid Communications** 37(15): pp.1295–1299.
- Huang, X. and Jiang, P. (2015) Core–Shell Structured High-k Polymer Nanocomposites for Energy Storage and Dielectric Applications. **Advanced Materials** 27(3): pp.546–554.
- Khoe, S. and Khezrian, S. (2017) Chapter 22 - Applications of aptamers for the diagnosis and therapy of different diseases. in Ficai, D. and Grumezescu, A. M. (eds) **Nanostructures for Novel Therapy**. Elsevier (Micro and Nano Technologies) pp.591–619.
- Khuong, K. S., Jones, W. H., Pryor, W. A. and Houk, K. N. (2005) The Mechanism of the Self-Initiated Thermal Polymerization of Styrene. Theoretical Solution of a Classic Problem. **Journal of the American Chemical Society** 127(4): pp.1265–1277.
- Kim, Y. H. and Webster, O. W. (1990) Water soluble hyperbranched polyphenylene: ‘a unimolecular micelle?’ **Journal of the American Chemical Society** 112(11): pp.4592–4593.
- Kolesov, S. N. (1968) The dependence of the dielectric properties of polymers upon molecular weight. **Polymer Science U.S.S.R.** 9(5): pp.2098–2106.
- Leandro, C., Souza, V., Dores, E. F. G. C. and Ribeiro, M. L. (2008) Determination of pesticides multiresidues in shallow groundwater in a cotton-growing region of Mato Grosso, Brazil. **Journal of the Brazilian Chemical Society** 19(6): pp.1111–1117.

Lv, M., Li, S., Jasieniak, J. J., Hou, J., Zhu, J., Tan, Z., Watkins, S. E., Li, Y. and Chen, X. (2013) A Hyperbranched Conjugated Polymer as the Cathode Interlayer for High-Performance Polymer Solar Cells. **Advanced Materials** 25(47): pp.6889–6894.

Meredith, R. (1997) **Engineers' Handbook of Industrial Microwave Heating**. London: Institution of Engineering and Technology.

Metaxas, A. C. and Meredith, R. J. (1995) **Industrial Microwave Heating**. London, UK: The Institution of Engineering and Technology.

Moad, G. and Solomon, D. H. (2005) **The Chemistry of Radical Polymerization**. Elsevier.

Nakagawa, H. and Tsuge, S. (1985) Characterization of styrene-divinylbenzene copolymers by high-resolution pyrolysis-gas chromatography. **Macromolecules** 18(10): pp.2068–2072.

Nicolas, J., Guillaneuf, Y., Lefay, C., Bertin, D., Gimes, D. and Charleux, B. (2013) Nitroxide-mediated polymerization. **Progress in Polymer Science**. (Topical Issue on Polymer Chemistry) 38(1): pp.63–235.

Poree, D. E., Giles, M. D., Lawson, L. B., He, J. and Grayson, S. M. (2011) Synthesis of Amphiphilic Star Block Copolymers and Their Evaluation as Transdermal Carriers. **Biomacromolecules** 12(4): pp.898–906.

Rao, T. P., Praveen, R. S. and Daniel, S. (2004) Styrene–Divinyl Benzene Copolymers: Synthesis, Characterization, and Their Role in Inorganic Trace Analysis. **Critical Reviews in Analytical Chemistry** 34(3–4): pp.177–193.

Reddish, W. (2009) Chemical structure and dielectric properties of high polymers. **Pure and Applied Chemistry** 5(3–4): pp.723–742.

Rieger, J. (1996) The glass transition temperature of polystyrene. **Journal of thermal analysis** 46(3): pp.965–972.

Tillman, E. S., Contrella, N. D. and Leasure, J. G. (2009) Monitoring the Nitroxide-Mediated Polymerization of Styrene Using Gel Permeation Chromatography and Proton NMR. **Journal of Chemical Education** 86(12): pp.1424.

Uzhel, A. S., Zatirakha, A. V., Shchukina, O. I., Smolenkov, A. D. and Shpigun, O. A. (2016) Covalently-bonded hyperbranched poly(styrene-divinylbenzene)-based anion exchangers for ion chromatography. **Journal of Chromatography. A** 1470: pp.97–103.

Voit, B. I. and Lederer, A. (2009) Hyperbranched and Highly Branched Polymer Architectures—Synthetic Strategies and Major Characterization Aspects. **Chemical Reviews** 109(11): pp.5924–5973.

Zhou, Y., Huang, W., Liu, J., Zhu, X. and Yan, D. (2010) Self-Assembly of Hyperbranched Polymers and Its Biomedical Applications. **Advanced Materials** 22(41): pp.4567–4590.

8 CONCLUSIONS AND FUTURE WORK

An extensive investigation of the application of dielectric spectroscopy to the monitoring of chemical transformations is presented in this thesis. Three systems were studied and the work has been focused on: (a) the analysis of the dielectric properties with temperature and frequency, (b) the relation of dielectric constant (ϵ') and dielectric loss (ϵ'') with key reaction features, such as the level of conversion that has been achieved, and (c) the identification of the optimum frequencies for the practical operation of the sensor, in terms of linearity and sensitivity. Off-line analysis with Nuclear Magnetic Resonance (NMR) spectroscopy and Gel Permeation Chromatography (GPC) was used to calculate key reaction features such as molecular weight and the achieved level of conversion. The systems studied were: (i) the tin octanoate mediated polymerisation of ϵ -caprolactone, (ii) the acid catalyzed dehydration of sorbitol to isosorbide, and (iii) the synthesis of styrene–divinylbenzene (DVB-co-styrene) hyperbranched polymers by catalytic chain transfer polymerisation and nitroxide mediated polymerisation.

This work demonstrated that sensor techniques based on observing the change in dielectric properties have broad applicability to monitor the progress of chemical transformations and can be implemented in most polymerisation reactor geometries as a simple retrofit. The application of this method has high potential to improve process control strategies and both, optimise product quality and batch to batch repeatability; for example, by clearly identifying the optimum point to terminate the reaction to prevent the formation of by-products or the ideal point to add a second monomer to synthesise an architectural polymer.

Additionally, it can be used to optimise energy usage by minimising the amount of time that the reaction is kept at the required temperature.

8.1 ϵ -caprolactone polymerisation

An open-ended coaxial line sensor was used to monitor the progress of the tin octanoate mediated ring-opening polymerisation of ϵ -caprolactone over a broad frequency range (0.5 GHz – 20 GHz). The dielectric properties of the reaction mixture were monitored in real time and samples were extracted at set times for off-line analysis with NMR and GPC. This work investigated the relationship between the change in the dielectric properties and monomer to polymer conversion. Furthermore, the most suitable frequencies across the measured frequency range, in terms of linearity and sensitivity, have been identified to enable the design and operation of sensors capable of monitoring the polymerisation. It was found that both ϵ' and ϵ'' decreased during the polymerisation across the frequency range investigated and the largest scale measurement changes, which also exhibited the best linearity, for ϵ' and ϵ'' were found at frequencies 0.95 GHz and 18.35 GHz respectively. This is an expected behaviour as the monomer consumption is directly proportional to polymer growth. The dielectric properties of the polymerisation mixture are dominated by the polar monomer. The dielectric properties of catalyst and initiator have only minor contribution to the mixture at the target reaction temperature (160 °C) and concentration that they are present in the reaction mixture, i.e. the selected monomer:catalyst:initiator molar ratio (800:1:10). Both ϵ' and ϵ'' can be used to monitor conversion changes based on the appropriate selection of frequency. However, the use of ϵ' was found to be optimal, as it offers a larger

differential between the monomer and polymer values and therefore better discrimination during the measurement process.

This project demonstrated that dielectric property data can be used to follow the reaction progress and identify key reaction parameters, such as the level of monomer to polymer conversion that have been achieved at any time point during the progress of the polymerisation. Furthermore, it was demonstrated that the presence of an open-ended coaxial line sensor immersed within the reaction mixture clearly did not affect the quality of polymerisation as the polymerisation was exhibiting high levels of control i.e. the conversion corrected number average molecular weight (M_n) values were found to be in close agreement with the calculated, theoretical M_n values.

8.2 Dehydration of sorbitol to isosorbide

The method which was developed for the monitoring of the ROP of ϵ -caprolactone was applied to monitor the para toluene sulfonic acid catalysed dehydration of sorbitol to sorbitan and isosorbide. Samples were extracted during the reaction progress for off-line analysis with NMR spectroscopy. It was shown that the dielectric property data recorded during the progress of the dehydration reaction can be correlated to isosorbide conversion. In detail, dielectric constant at high frequencies, such as 19 GHz, is the optimum property to monitor this chemical transformation as it provides high scale measurement changes at high isosorbide conversion. Consequently, a calibration curve was constructed using logarithmic fit which could be used to predict the level of

isorbide conversion in a systematic way at any given point during the reaction progress.

This method has high potential to be applied at industrial scale. A possible application of this method could help reduce the production cost of biobased products. By optimising the amount of time that the reaction is kept at the required temperature, energy usage and waste generation can be minimised.

8.3 Synthesis of DVB-co-styrene hyperbranched polymers

Styrene–divinylbenzene (DVB-co-styrene) copolymers synthesized by Catalytic Chain Transfer Polymerisation and Nitroxide Mediated Polymerisation were studied using dielectric spectroscopy. It was found that a resonant method such as the cavity perturbation technique is capable to differentiate the polymer architecture and molecular weight of DVB-co-styrene hyperbranched polymers with variable DVB ratio. In detail, it was observed that as the concentration of styrene increases, both dielectric constant and loss values increase. This behaviour can be attributed to the hyperbranched polymer molecular architecture. The addition of styrene interferes the branching structure of DVB and this results in a more linear structure which increases the flexibility of the dipoles to align with the electromagnetic field. It was also found that the increase of molecular weight during the progress of the polymerisation has a direct effect on the dielectric properties. In detail, both dielectric constant and loss values reduced as polymerisation time increases.

This study demonstrated that dielectric property data can be used to define structural trends and molecular weight in materials with complex structure such

as hyperbranched polymers. The application of this method will enable the design of a continuous process to improve product quality and batch to batch repeatability of hyperbranched polymers by detecting side reactions occurred during their preparation that can affect the properties and performance of the polymer and identifying the optimum point to terminate the reaction.

8.4 Limitations of the application of dielectric spectroscopy to the monitoring of chemical transformations

This work showed that dielectric spectroscopy can be used “in-situ” to provide process-related information to many chemical transformations. However, the main limitation of the technique is the temperature dependence of dielectric properties which is a direct result of the increased intermolecular interactions with increasing temperature. Additionally, the use of an open-ended coaxial line sensor requires sufficient sample size for accurate measurements. For example, the open-ended coaxial line which was used for the “in-situ” measurements (Agilent 85070E) requires a minimum insertion of 5 mm and a minimum of 5 mm around the tip of the probe. Furthermore, the presence of bubbles found to have a significant effect on the dielectric property measurements. This effect can be minimised with the use of stirring.

8.5 Future work

This thesis revealed that sensor techniques based on observing the change in dielectric properties, such as an open-ended coaxial line sensor, have broad applicability to many chemical transformations. Future work to be conducted in this area could also utilise microwave heating to further improve the sustainability of the monitored process.

A further study of hyperbranched polymers is required to investigate the optimum frequency range, in which the dielectric properties have sufficient scale measurement changes to differentiate polymers with varied structure. The construction of a calibration curve which relates the dielectric properties with hyperbranched structure (e.g., branching density) will enable the monitoring of the polymerisation process.

Future work should also be concentrated in the development of a process control system in order to apply this method at industrial scale. A pilot program could be designed to implement a scaled production system. The use of many open-ended coaxial line sensors fitted in a scaled reaction vessel could be used to better monitor the quality and uniformity of the produced material. Finally, a cleaning system of the sensors before a new batch of material is placed in the vessel should be devised.